Novel Methods for Modelling, Design and Control of Advanced Well Completion Performance

Bona Prakasa

Submitted for the degree of Doctor of Philosophy

Heriot-Watt University
School of Energy Geoscience Infrastructure and Society
Institute of Petroleum Engineering

August, 2018

The copyright in this thesis is owned by the author. Any quotation from the thesis or use of any of the information contained in it must acknowledge this thesis as the source of the quotation or information.

Abstract

This thesis presents new approaches to modelling of reservoir and well flow performance when the wells are completed with Advanced Well Completions (AWC). The particular focus of this research is modelling fluid flow in the reservoir-AWC-well systems using simple, reduced-physics models that do not necessarily require detailed reservoir description yet are comprehensive enough to capture the major trends in the system to achieve the AWC performance evaluation and design objectives. This allows rapid screening and design of the AWC technology that is at the same time less subject to the reservoir uncertainty due to less input on the reservoir geology required. Such models can also complement, e.g. in order to steer or speed-up, the existing AWC modelling and design workflows that involve full reservoir simulation. The outcome aids reliable investigation of expected AWC and reservoir performance derived from the available data in order to perform quick scoping of reservoir management concepts and options prior, or in addition, to detailed modelling. This is particularly important in real field models where the numerical reservoir simulation is often uncertain and computationally expensive, especially when coupled with AWC wellbore models.

The study first introduces three main classes of flow control technologies used in AWCs: passive (realised with Inflow Control Devices - ICDs), the recently introduced autonomous (Autonomous Flow Control Devices - AFCDs) and active (Inflow Control Valves - ICVs). The traditional workflows for AWC performance modelling and design using commercial numerical reservoir simulation for each AWC class are discussed and evaluated. Finally, the novel, rapid AWC modelling methods are developed that can reliably inform reservoir development and management decisions.

The thesis develops the following approaches and modelling methods aimed at analysis and design of AWC flow performance:

1. The model describing the trade-off between the well productivity loss and the improved inflow equalisation in AWCs in well with heel-toe effect and heterogeneous reservoir
2. The technique to estimate the additional, long-term value derived by controlling zonal flow rate (AWC's well) in *pistonlike and non-pistonlike* displacement.
3. The concept relating the various short-term, AWC design methods and their long-term outcomes.

4. Characterisation of inter-well and inter-layer connectivity for waterflooded reservoirs developed with wells completed with zonal gauges and ICV completions.
5. Consequently, the framework for optimal ICV control when the inter-well connectivities are estimated.

This work enables application of rapid AWC design and optimisation. Moreover, integration with the reservoir waterflood monitoring results in a better understanding of the reservoir performance. Practical utility of the proposed methods is illustrated in case studies.

ACADEMIC REGISTRY
Research Thesis Submission

Name*:*	Bona Prakasa		
School:	Energy Geoscience Infrastructure and Society		
Version: *(i.e. First, Resubmission, Final)*	First	Degree Sought:	PhD in Petroleum Engineering

Declaration

In accordance with the appropriate regulations I hereby submit my thesis and I declare that:

1) the thesis embodies the results of my own work and has been composed by myself
2) where appropriate, I have made acknowledgement of the work of others and have made reference to work carried out in collaboration with other persons
3) the thesis is the correct version of the thesis for submission and is the same version as any electronic versions submitted*.
4) my thesis for the award referred to, deposited in the Heriot-Watt University Library, should be made available for loan or photocopying and be available via the Institutional Repository, subject to such conditions as the Librarian may require
5) I understand that as a student of the University I am required to abide by the Regulations of the University and to conform to its discipline.
6) I confirm that the thesis has been verified against plagiarism via an approved plagiarism detection application e.g. Turnitin.

* *Please note that it is the responsibility of the candidate to ensure that the correct version of the thesis is submitted.*

Signature of Candidate*:*		Date:	

Submission

Submitted By *(name in capitals):*	
Signature of Individual Submitting:	
Date Submitted:	

For Completion in the Student Service Centre (SSC)

Received in the SSC by *(name in capitals):*			
1.1 Method of Submission *(Handed in to SSC; posted through internal/external mail):*			
1.2 E-thesis Submitted (**mandatory for final theses)**			
Signature:		Date:	

Table of Contents

List of Figures

List of Tables

List of Publications and Presentations by the Candidate

Prakasa, B., Muradov, K., Davies, D. Rapid Design of an Inflow Control Device Completion in Heterogeneous Clastic Reservoirs Using Type Curves, SPE Offshore Europe, Aberdeen 2015.

Haghighat, M., Prakasa, B., Khalid, E., Davies, D. Guidelines for Flow Control Completion Modelling and Design, Inflow Control Technology Forum, Houston 2015.

Almarri, M., Prakasa, B., Muradov, K., & Davies, D. Identification and Characterization of Thermally Induced Fractures Using Modern Analytical Techniques, SPE Kingdom of Saudi Arabia, Dammam 2017.

Prakasa, B., Shi, Xiang., Muradov, K., Davies, D. Novel Application of Capacitance-Resistance Model for Reservoir characterization of and Zonal, Intelligent Well Control, SPE Asia Pacific, Jakarta 2017.

Muradov, K., Prakasa, B., Davies, D. Analytical Performance of Waterflooding of Non-Communicating Layers by Advanced Wells, Journal of Society of Petroleum Engineering (SPE REE).

I was early taught to work as well as play

My life has been one long, happy holiday

Full of work, and full of play

I dropped the worry on the way

And God was good to me every day.

- *J. D. Rockefeller*

In the midst of winter, I found there was, within me, an

Invincible summer

- *Albert Camus*

Acknowledgement

I owe a special gratitude to my supervisors Dr. Khafiz Muradov and Prof. David Davies who provided a great support and invaluable help during the period of my PhD study.

A big thank you to Dr. Karl Stephen and Prof. Matthew Jackson for agreeing to be my examiners and spending their valuable time in reading this thesis.

I would like to thank all sponsors of VAWE project for the financial support and data provided for my study, as well as valuable discussions and suggestions during the JIP meetings. I am also thankful to Schlumberger, Landmark, Weatherford, and MathWorks for allowing access to their software.

My colleagues in the office: Morteza Highighat, Akindola Dada, Eltazy Khalid, Misfer Almari, Ehsan Nikjoo, Victor Guiterrez and Mojtaba Moradi (Thank you all).

Special thanks to Dr. Junko Hutahaean, (soon-to-be) Dr. Jackson Pola, You both are great buddies!!

Thanks to Edinburgh for being such a great city. I have met and spent times with so many people in this city which I cannot enumerate them. Thank you all.

Finally, most deeply and most patiently, I sincerely thank my mother (Margeretha Nababan), father (Marthin Ritonga), for their relentless prayers. I cannot imagine the world without your love and guidance.

More than academics, I learnt a lot about life in this period, I am a lucky man!!

Chapter 1 – Introduction

Ongoing improvements in drilling and completion technology have moved maximum reservoir contact (MRC) wells (horizontal wells, multilateral wells) from being part of the area of specific expertise to being a standard operation for exploiting hydrocarbons. MRC wells may increase the profitability per dollar invested in well and field developments by maximising the reservoir-well contact, allowing access to otherwise inaccessible reservoir areas/layers, increasing the recovery factor as well as the well flow rates. By doing so, the MRC wells improve well productivity. The extended well length and rock heterogeneity encountered by an MRC well, however, result in a higher variation of the local inflow/outflow rates along the well completion. High flow rates often invite unwanted fluids, for example water and gas to arrive early, thus increasing water cut and reducing recovery. These issues are detrimental to production, and if not mitigated, can turn an initially high-profile MRC well into an uneconomical well after a short period of well production.

Advanced well completion (AWC), a mature and proven technology employs downhole flow control such as inflow control devices (ICDs), interval control valves (ICVs), autonomous flow control devices (AFCDs), and downhole monitoring, such as pressure and temperature gauges (PT gauges). They provide solutions to the production constraints encountered in MRC wells. AWC enables a better-distributed commingled production/injection from/into different reservoir zones/layers by adding a downhole restriction to each device. AWC technology thus addresses the shortcomings of MRC wells and maintains the wells' profitability. There are many examples of AWC technology enabling more efficient field development by improving sweeping efficiency and reducing the number of production/injection wells.

Modelling the AWCs interaction with the reservoir is therefore critical. This is done by coupling the wellbore model, which includes various components of AWC, to the reservoir model. The modelling technique, a grid-based, numerical well/reservoir simulation is highly specialised and computationally expensive. Moreover, the resources/data to feed such model are often not available. Many operators are not aware of this, and instead design and optimise AWC wells using standard, grid-based numerical simulation, techniques that were developed for conventional wells.

1.1 Thesis Motivation

This thesis presents a new approach to model reservoirs with AWC that enables fast design of AWC and complements the operators' existing workflows. The fluid flow through the reservoir-AWC-well system is characterised as a much simpler proxy model (reduced-physics model), that is still comprehensive enough to capture the main characteristic of the reservoir system. It provides a simple model, that is appropriate to the available data, while hence allowing a quick scoping of concepts and options prior, or in addition, to detailed reservoir modelling. Such workflows meet the oil and gas business's preferences for simpler and faster processes.

This thesis provides the first rapid design and optimisation workflow for advanced well technology. A simple, portable toolbox is coded to determine the optimal ICD/AFCD/ICV completion response in various field/fluid conditions within the short time that is available when making a decision. Furthermore, the proposed proxy models could be enrolled as a fast initiation (or quick scoping) prior, or in addition, to detailed modelling enabling a faster work cycle.

1.2 Thesis Outline

Chapter 2 starts by introducing three main categories of AWC: the passive (employing ICDs), the recently introduced autonomous (employing AFCDs), and the active (employing ICVs) completion. Standard modelling techniques for AWC are presented, and their complexity is discussed. The chapter will discuss the definition of the 'restriction strength' provided by the AWC devices that will appear in the subsequent chapters. The primary focus of this chapter is to introduce the need for 'simple' modelling for AWC when making a decision.

Chapter 3 focuses on developing an analytical model for production issues that are mainly encountered when completing the well with ICD completion (uneven flow in the event of the heel-toe effect and a heterogeneous reservoir). The chapter starts with the history of horizontal wells and a literature review of various horizontal wells (with or without incorporating the wellbore friction effect) in homogeneous and heterogeneous reservoirs.

An in-depth explanation of the role of ICDs in mitigating the problems that are mainly encountered in horizontal wells (uneven production/injection due to the heel-toe effect or

a heterogeneous reservoir) is then provided, including the design methodology and the workflow. Then, an analytical model of ICD-completion flow performance is described along with its assumptions. It should be noted that the proposed model in this chapter is an extension of the analytical model of previous studies. The mathematical models are then visualised (or translated into an intuitive graph) as a type-curve that allows the complicated maths to be communicated simply. The practical utility of the proposed model is illustrated through four case studies. The results from the proposed models were verified by conventional, grid-based, numerical simulation for each of the case studies.

Chapter 4 aims to develop a framework that enables to design ICD and AFCD completion for long-term optimisation, i.e. in the 'dynamic' reservoir flow condition. The chapter starts by providing the advantage of having a long-term strategy/outlook when designing the flow control completion. The feasibility of AWC is mainly influenced by the economic parameters, which can only be obtained once we have an outlook on the long-term results from installing the AWC. The developed model is constructed from the combination of classical waterflood displacement equations with a recently developed analytical model of a flow control completion. The idea is then extended for light-oil displacement, which replicates piston-like displacement (an extension of Dykstra-Parsons solution to AWC wells) and medium/heavy-oil displacement, which replicate non-piston like displacement (an extension of Buckley-Leverett & Welge solution to AWC wells). The model was successfully tested and verified using numerical reservoir simulation. The modification of the proposed models is then also made for a horizontal well scenario where the displacement of water is vertical. The resulting workflow is nearly identical to that for a vertical well. The coupling between the type-curve model described in chapter 3 and the proposed models described in this chapter can be used to simplify the decision when designing an AWC.

Chapter 5 explains the novel analytical solution for the capacitance-resistance model (CRM) in the presence of AWC. The new solution is extended for single- and multi-layer reservoirs. The CRM technique, being a data-driven method requires only basic data, such as the production history. It simplifies the complexity of the reservoir model and reduces the required computational time. The CRM derived model is a proxy of the real reservoirs, and can suggest, within a short time period, several critical observations, such as whether there are sealing zones between injector-producer wells or whether there is a significant fracture that could potentially be the source of water breakthrough.

The chapter also discusses the importance of considering the CRM's properties (connectivity and time-storage) as dynamic properties. We investigate a real field case of a thermal-induced-fracture (TIF) reservoir using the principle of a dynamic CRM to estimate the likely TIF growth. When dealing with AWC, the ICV action (closing and opening the valve) would alter the well/zone drainage control. Thus, this provides an opportunity to optimise the waterflood operations, such as reallocating the injection rate by choking ICVs.

The chapter concludes by proposing a new way to optimise the ICV before water breakthrough (proactive optimisation) using the CRM derived parameters "connectivity" and "time-storage". The proposed technique adopts the ideas behind the classic Lorenz plot and translates them into waterflood operations. These new ideas are employed as an intuitive, simple method to design and optimise the AWC.

Chapter 6 summarises the conclusion of this thesis and makes recommendations for future research studies.

Chapter 2 – Introduction to Advanced Well Completion

2.1 Introduction

Advanced well completions (AWCs), also known as intelligent wells systems (IWS), are capable (to some extent) of downhole surveillance and/or providing flexible control of inflow and/or outflow from different zones (Robinson, 2003). This well, in essence, should be capable of doing one of the following:

1. Monitoring and transmitting data to surface the properties of the fluid flowing into and out of the wellbore.
2. Remote action to control the reservoir, zones, and production process.

AWCs enhance the performance of maximum reservoir contact (MRC) wells that would otherwise not produce to the full potential due to the effects like a skewed flow profile due to the heel-toe effect, uneven inflows due to reservoir heterogeneity, or cross-flow between producing zones or sand problems due to resulting water influx. The AWC wells are primarily installed to enhance the delivery of MRC wells (Sefat, 2016) and their aims are to:

1. Reduce the number of wells to be drilled and deliver cost-effective field development.
2. Add value by allowing improved reservoir management and increased hydrocarbon recovery.
3. Increase well profitability and lower operational/maintenance costs by decreasing the required number of well interventions.

2.1.1 The major components of AWCs can be split into:

1) Flow control devices (FCD)

These devices allow on/off or variable control of production or injection of reservoir intervals/layers. There are three types of FCDs: passive, control with inflow control devices (ICDs), active control with inflow control valves (ICVs), and the recently introduced autonomous flow control devices (AFCDs). Section 2.2 explains the characteristics and operation principles of each device.

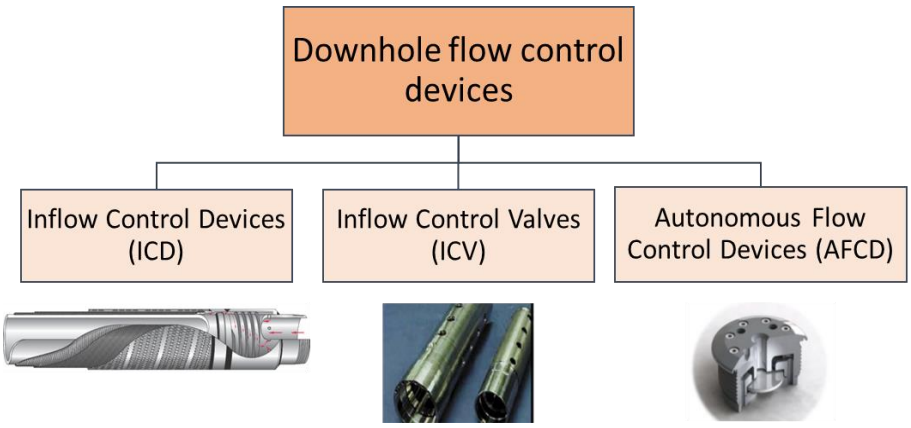

Figure 2-1. AWC main components for flow control

2) Downhole monitoring devices

These devices allow real-time, remote acquisition of reservoir data using modular sensors, for example permanent gauges and quasi-distributed or distributed sensors along the tubing and completions such as distributed temperature and acoustic sensors (DTS and DAS). Various types of measurements (Figure 2-2) are available, though pressure and temperature are the most common parameters measured (Da Silva *et al.*, 2012). Zonal information allows production characeristics to be determined at the level of zone or layer, for example layer production/injection rate and layer water-cut. This information is especially important since most AWCs operate with commingled production/injection. Zonal pressure and rate data are used to conduct layer characterisation of a multi-layer reservoir completed with AWC wells in Chapter 5.

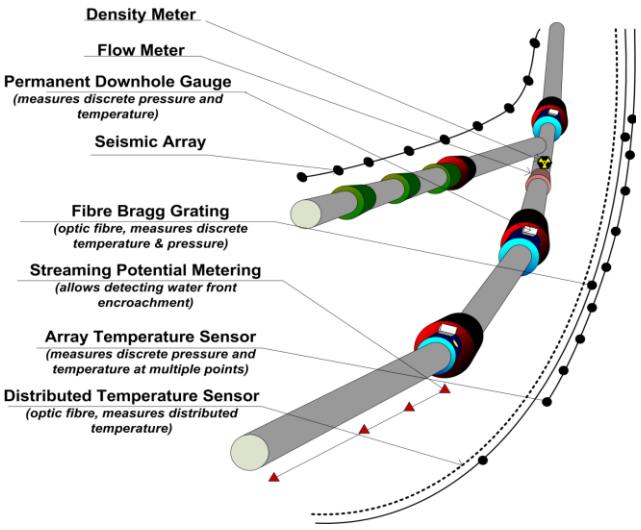

Figure 2-2. AWC main components for downhole monitoring (Da Silva, *et al.*, 2012)

3) Annular flow isolation (AFI) devices

These devices isolate and prevent unwanted fluid flow in the annular space (annular flow) between the tubing and the sand face or cemented/perforated casing. The design of AFI is an important aspect since AWCs often encounter high annular flows rates (Moradidowlatabad *et al.*, 2014), for example, in commingled heterogeneous multi-zones. Furthermore, the performance efficiency of FCD (ICDs, ICVs, and AFCDs) are closely related to the compartmentalisation along the AWC's zones. AFI can be achieved by many types of packers (e.g. Figure 2-3) and by a gravel pack completion in the case of sand-prone wells. Faisal Al-Khelaiwi (2013) detailed the various types of packers used in AWCs. The completion design engineers have to determine the optimum number and placement of packers. Studies for packer placement optimisation have been conducted by Gavioli *et al.* (2012), Moradidowlatabad *et al.* (2014), and Dowlatabad (2015). This thesis will assume that sufficient AFI is installed to ensure negligible annular flow along the length of the wells.

Figure 2-3. Typical external casing packer (Gavioli *et al.*, 2012)

The design of an AWC is dependent on the specific well and geological environment. Examples of an AWCs are an ICD completion in a horizontal well (Figure 2-4), an ICV completion in a vertical well {Figure 2.5a (left). AWC in a vertical well with ICVs and sliding sleeves. Figure 2-5a}, and a combination of multiple downhole control devices installed in a multi-lateral well {Figure 2.5a (left). AWC in a vertical well with ICVs and sliding sleeves. Figure 2-5b}. Further information on the applications of the AWCs can be found in Faisal Al-Khelaiwi (2013).

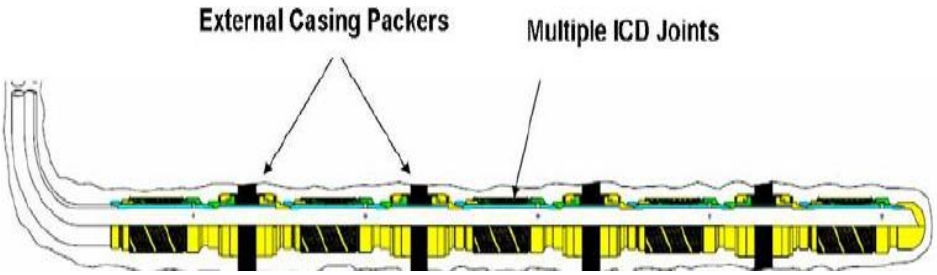

Figure 2-4. AWC completion in a horizontal well with ICDs installed between packers (Henriksen *et al.*, 2006)

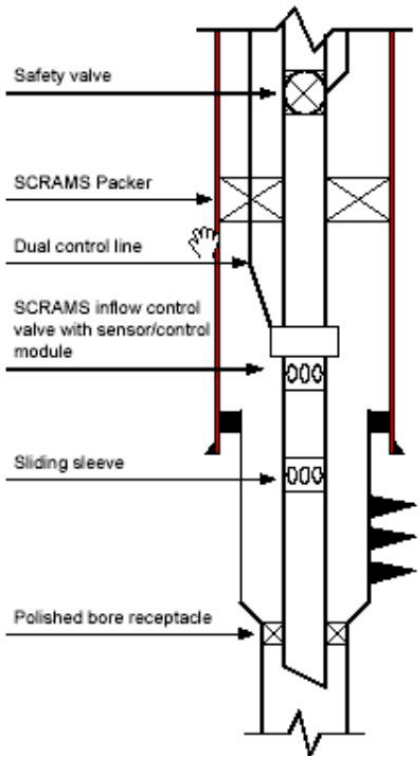

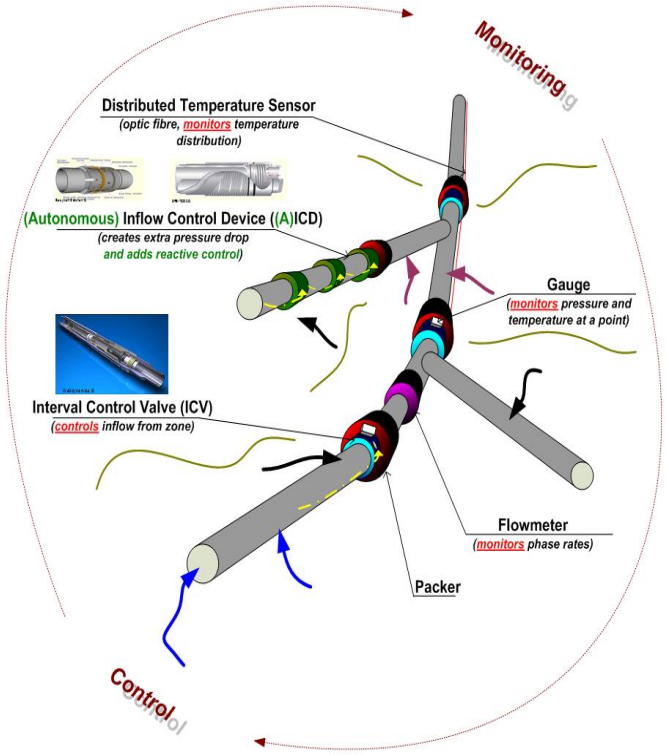

Figure 2.5a (left). AWC in a vertical well with ICVs and sliding sleeves (Courtesy of Sintef).

Figure 2-5b (right). Combination of ICD, AFCD, ICV, multiple packers, and monitoring devices installed in a multi-lateral well (Da Silva, *et al.*, 2012).

2.2 Flow control devices (FCD)

2.2.1 Inflow Control Devices

AWC technology began with the development of the ICD in the early 1990s. ICDs consist of one or more passive flow restrictions mounted on each joint tubing that makes up the well completion (Al-Khelaiwi *et al.*, 2010). The motivation behind the first ICD application was to control the fluid flow path between the reservoir and the well's flow

conduit in order to minimise the inflow imbalance along a long horizontal completion producing light oil from a thin-oil column in a relatively homogeneous, high permeability reservoir bounded by a large gas cap and an active aquifer (Henriksen *et al.*, 2006). The frictional pressure losses along the completion's length resulted in an unbalanced inflow rate between the completion's heel and toe sections. This "heel-toe" effect creates significantly larger reservoir drawdown pressure at the heel section than at the toe, resulting in the early arrival of unwanted fluids (water or gas) at the heel and poorer oil sweep efficiency for the toe section. Brekke and Lien (1994) reported that three completion options were initially being considered:

1. Tubing stinger method
2. Variable perforation density along the length of the completion
3. Inflow Control Tool

All these methods aim to manage/reduce the relatively high inflow rate at the heel section. The inflow control tool, later called the ICD, was chosen as the most cost effective approach. The restrictive force of an ICD is proportional to the square of the flow rate (equation 2-6), added a stronger choking force and performed much better than the other two options. Modelling of an ICD-enabled completion (Figure 2-6) shows a more uniform inflow rate profile along the length of the completion as the ICD has imposed a suitably increased pressure drop between the sandface and the production conduit (base pipe).

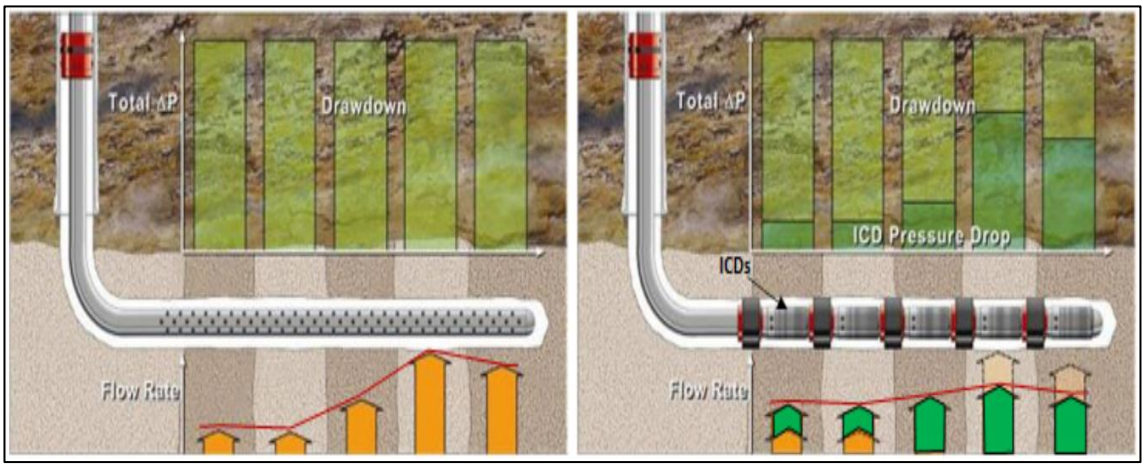

Figure 2-6. Comparison of inflow variation with (right) and without (left) ICDs in a heterogeneous reservoir (Courtesy of WellDynamics).

The original ICD concept was invented by Inventech, a subsidiary of Ziebel, before it was bought by Tejas (Newswire, 2009). The ICD module was installed inside a pre-packed

screen mounted on a solid based pipe and it has a number of labyrinth channels with adjustable lengths and diameters to achieve the required pressure drop, (Figure 2-7) (Brekke and Lien, 1994).

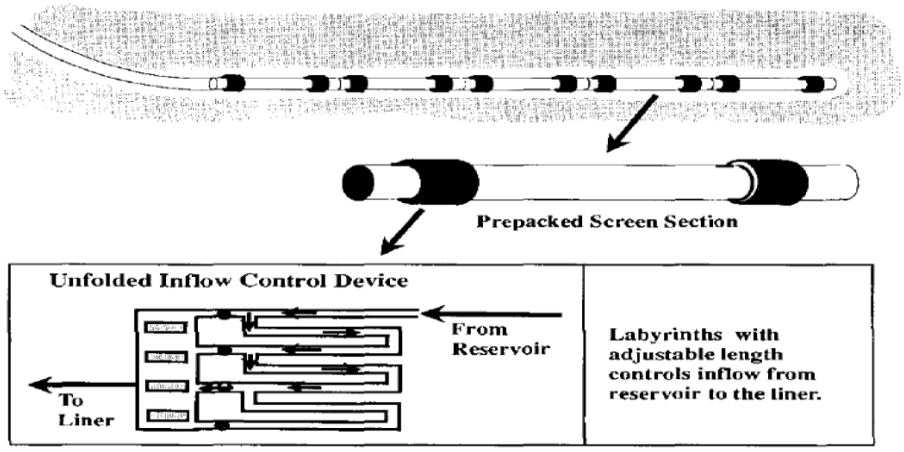

Figure 2-7. Original ICD concept (Courtesy of Inventech)

The ICD market has expanded in the last two decades with new applications being developed. Baker Hughes has installed more than 2 million feet of their helical channel ICDs by mid-2008, while Statoil has installed ICD completion in 120 wells in the North Sea, and Saudi Aramco has more than 200 ICD installations in several fields by 2012 (Al-Khelaiwi, 2013). An ever-increasing market has resulted in service companies offering different ICD types with unique flow resistance mechanisms (table 2-1).

The generic design of the ICD is similar to the original ICD concept depicted in Figure 2-7. The produced fluid passes from the annulus through a debris filter (or screen) and continues along the outer surface of the base pipe before flowing into the ICD module with its special restriction. The fluids would finally exit to the inside of the base pipe, as seen in figure 2-8.

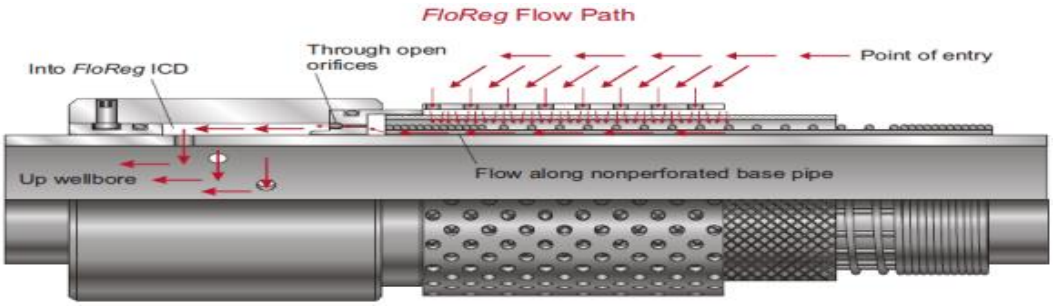

Figure 2-8. The fluid's flow path from reservoir to tubing (courtesy of Weatherford)

Table 2-1. Comparison of commerical ICD types

Type	Diagram	Features	Vendor
Labyrinth	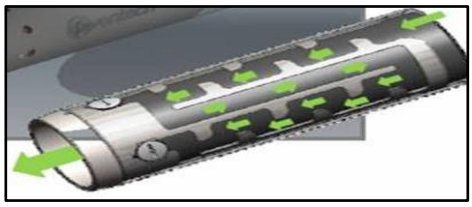	- ΔP is highly dependent on fluid viscosity & velocity. - Less susceptible to erosion. - ΔP is strongly influenced by emulsion.	Tejas
Helical-slot	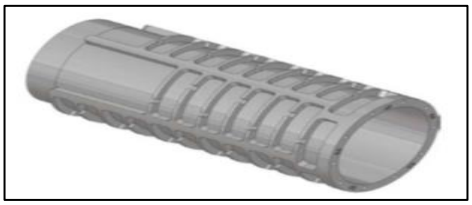	- A modification of the helical channel. - Minimises the influence of fluid viscosity on ΔP.	Baker Hughes
Helical channel		Six flow resistance rating achieved by altering the diameter, length, and number of channels.	Baker Hughes
Tube	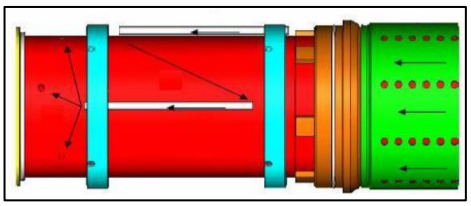	Combines a flow restriction and a straight tube to create ΔP.	Easy Well
Nozzle	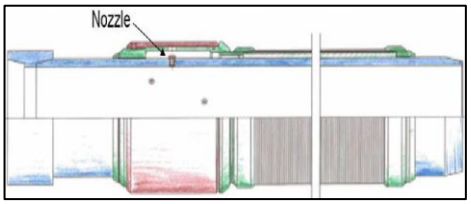	Erosion resistance material required for high fluid velocity flow with sand production,	- Reslink - Flotech
Orifice	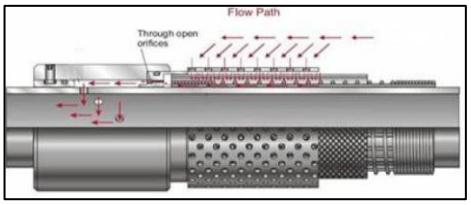	Multiple orifices produce flow equalisation. Can be modified on the well site easily by un/plugging the orifices.	- Weatherford - Schlumberger

2.2.2 Inflow Control Valves

The first ICVs together with the monitoring system were installed as the first intelligent well system in 1997, in the Snorre Fields located in the Norwegian part of the North Sea

(Gao *et al.*, 2007). The installed ICVs at the time, were limited to only four discrete positions: fully-open, closed, and two intermediate chokes (Williamson *et al.*, 2000). Skarsholt *et al.* (2005) reported that seven years production experience proved the value of ICVs in this field despite several challenges that need to be addressed for their future application. The main challenges are:

1. Equipment reliability

   Only 41 wells were still functional in 2004 out of the 55 wells completed with IWS in Snorre Fields,, indicating a 25% failure rate (Skarsholt *et al.*, 2005). Failures were mainly due to the low reliability of the lower completion (Skarsholt *et al.*, 2005; Gao *et al.*, 2007) where the downhole monitoring and downhole control system are located. Note that these failure statistics include failure of other completion components, such as cement or packer failures, as well as the ICVs.

   Equipment reliability is a vital consideration in AWCs. This idea holds true for all drilling and completion practices but is especially vital when considering installing a new technology. With the rapid growth of advanced well completion all over the world, the reliability issues of AWC have been significantly improved. WellDynamics/Halliburton reported that the success of AWC has increased to 95% (Grebenkin and Davies, 2012).

2. Data modelling/data overload

   AWCs can be installed with multiple sensors transmitting information ranging from real-time pressure data, temperature, and acoustics (Da Silva *et al.*, 2012). These measurements have the potential to be very informative as they indicate both the reservoir's and the well's performance. However, available models are not always able to simulate the reservoir or well profile correctly (Muradov and Davies, 2013).

   A fully functional AWC system would be able to incorporate a workflow with predictive modelling or data management system to take advantage of all available measurements and make informed production/injection optimisation decisions. There have been significant efforts to develop such systems including the publications reported by Burda *et al.*, (2007), Berg *et al.* (2010), and Cheung *et al.* (2015).

The first deployment of ICVs with only four-positions were considered inadequate to cover all the desirable control positions (each position represents a different flow area that is chosen based on desired flow rate and pressure drop). Since then, ICVs have been developed, and now ICVs can be put into three categories based on control position (or flow area) options. The complexity of the application became the criteria for choosing the level of control flexibility for the ICV. ICV type 1 is the simplest while type 3 is the most complex.

1. *On/Off ICV*. The ICV is either a fully-open or fully-closed.
2. *Discrete ICV*. The ICV has a limited number of positions (typically up to 10, including the fully-open and fully-closed positions).
3. *Infinitely Variable ICVs:* Provides continuous control between the fully-open and fully-closed positions.

Their control-line connects the downhole valve to the surface, and ICVs can also be categorised based on how they are powered and controlled. Potiani, Eduardo, and Hughes (2014) compared the hydraulics system, electric-hydraulics, and the all-electric system.

1. Hydraulic systems

   The valves in ICV are actuated by a hydraulic line. This ICV type would require feed-through packers and a feed-through wellhead for the hydraulics lines to go through. Being the oldest, most widely used control system for downhole equipment, it has the advantage of familiarity and reliability. However, each valve requires a dedicated control line to operate. This system is constrained to wellhead feed-through capability {the maximum number of hydraulic lines that can be installed in a standard well is 5, (Al-Khelaiwi *et al.*, 2010)}. n+1 control lines are required for n valves. This would limit the segments/zonation length of the completed interval and the ICV performance. The summary of concerns are:

   - Installation depth of the ICV
   - Operating pressure of the ICV
   - Limited number of penetrations possible in subsea wellheads.
   - Control line fluid degradations/contamination
   - Control line damage when running through the Multi-Lateral (ML) junction or the horizontal sections.

2. Electric-hydraulics systems (2 hydraulic lines, and 1 electrical cable)

This ICV type uses electrical measurement and transmission of data to the surface while hydraulic power operates the valves. This reduces the number of control lines (hydraulics and electrics) since two control lines can operate several valves. The concerns for this ICV type is the same with those for type 1 ICVs.

3. All-electric systems

   The developments in ICVs enabled a single electric downhole cable to control up to 20 valves. This type practically eliminates many of the concerns mentioned in other ICV types. Potiani, Eduardo, and Hughes (2014) concluded that all-electric systems are as reliable as the other two with some all-electric system have been still fully functional 10 years after installations.

2.2.3 Autonomous flow control devices

The recently introduced autonomous inflow control device (AICD) and autonomous inflow control valve (AICV) react to unwanted fluid phases, such as free gas and water, by restricting the in-situ flow rate and hopefully improving oil recovery. For simplicity, we will combine AICDs and AICVs as AFCDs where their distinction is not explicitly required in this thesis. AFCDs are the latest versions of ICDs since they replace the passive or fixed restriction with a self-adjusting restriction. This feature is advantageous in a reservoir with high uncertainty, where the location of producing layers that will experience early breakthrough is unknown.

The first reported installation of AFCD technology was in 2008, in Troll Field (Halvorsen, *et al.*, 2012). The AFCD was deployed to control gas production in a multi-lateral well. The well had two laterals completed with different downhole control devices, lateral 1 was an ICD completion, and lateral 2 was an AFCD completion. These two laterals were completed in similar geology and they were drilled parallel with a spacing of only 191 metres (fig. 2.9a and 2.9b), hence allowing a realistic, real-field comparison between ICD and AFCD completion performance.

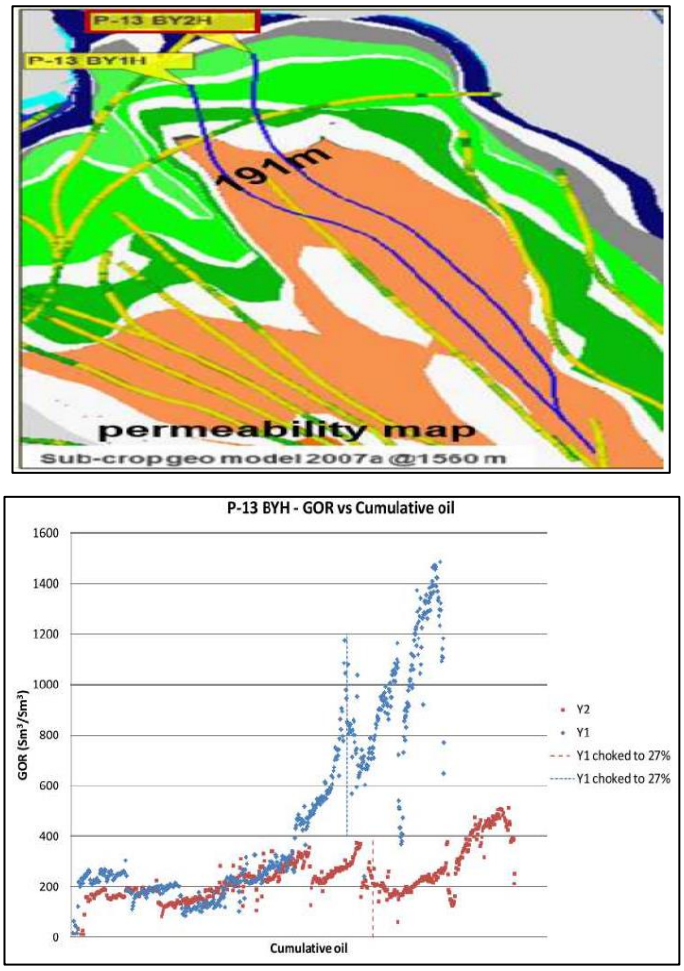

Figure 2-9a. (upper). Permeability map for Troll Field around well P-13. Figure 2.9b. (below). GOR vs. cumulative oil production performance of laterals one and two. (Halvorsen, Elseth and Nævdal, 2012)

The performance of these two laterals were compared after 2 years of production. Lateral two (completed with AFCD) produced approximately 20% more oil than the lateral one (Halvorsen *et al.*, 2012). There is an indication of a significant and increasing gas breakthrough in lateral one, while there is only a moderate Gas Oil Ratio (GOR) increase in the lateral two. The report concluded that AFCD completion successfully outperformed the ICD completion by producing a higher oil rate for an extended period before the gas breakthrough and continued producing after initial breakthrough at a lower GOR. Note that oil production in the Troll field is limited by the production facility's gas handling capacity.

Various AFCD design concepts have been developed with differing response to change in the properties of the produced fluids. More on the AFCDs/AICVs can be found in Eltaher (2017).

2.3 Modelling of Advanced Wells

Modelling of an AWC completion requires incorporation of the various components to its completion system. These vary the pressure losses along the well completion; a parameter that was considered constant in a standard well completion. The complexity is exacerbated by the need of the new approach to also account for the connection between the well components and reservoir grid, as well as capturing the essential physics of fluid flow through the annulus and new FCDs.

In general an AWC consists of five, main flow paths. Eltaher (2017) illustrated the production flow paths (Figure 2-10). Note that the flow path for an injector well will be reversed.

1. Flow from the reservoir towards the well's sandface

   E.g. in the case of liquid flow there may be assumed a linear relationship between the flow velocity and the pressure drop (Darcy's law).
2. Flow along the annulus

   Annular flow along the area between the tubing's outer diameter and the formation sandface (for AWCs completed in open-hole). Such modelling must account for the friction and any turbulence flow along the annulus. The study in this thesis, however, assumes perfect AFI, i.e. annular flow losses are sufficiently small that that do not affect the findings in this thesis.
3. Flow across the FCD

   Flow across the FCD is characterised by a flow regime within a non-linear velocity/pressure drop relationship. Characterisation of the flow relationship of each device is typically evaluated in flow- testing, with the results of flow rate versus pressure drop performance data curves for single-phase oil, water, and occasionally gas flow. The performance data is then expressed as a mathematical correlation or as tables based on this empirical data.
4. Flow along the production tubing

   The flowing wellbore pressure is generally defined as the pressure at the mid-point of the completion interval. It is assumed to be constant over the entire interval. This approach is no longer valid for many MRC well since pressure losses occur along the wellbore length (due to friction, acceleration, hydrostatics, and phase changes). Chapter 3 of this thesis discusses this topic in more detail.
5. Flow along the downstream completion

The fluids will flow through any other components of lower completion on their way to the surface, such as a stinger or a polished bore receptacle.

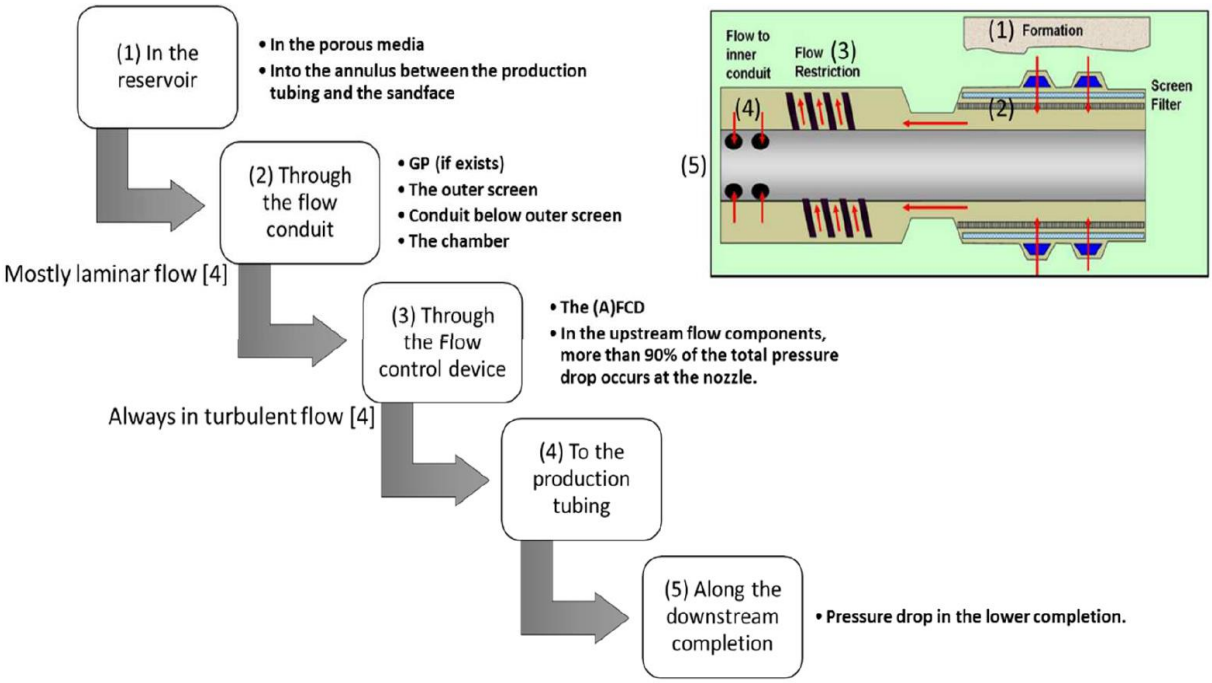

Figure 2-10. Illustration of flow path from the reservoir to the tubing in AWCs

The pressure loss that occurs in these sequences is accounted for by discretising the well model into multiple segments, where each segment is defined by four independent variables: fluid pressure, total flow rate, water fraction and gas fraction. This approach is known as the multi-segment well model (Holmes *et al.*, 1998) and is available in several commercial simulators. An advanced well is modelled as a collection of segments arranged in a gathering tree topology where each segment is made up of nodes and flow path (Schlumberger, 2014).

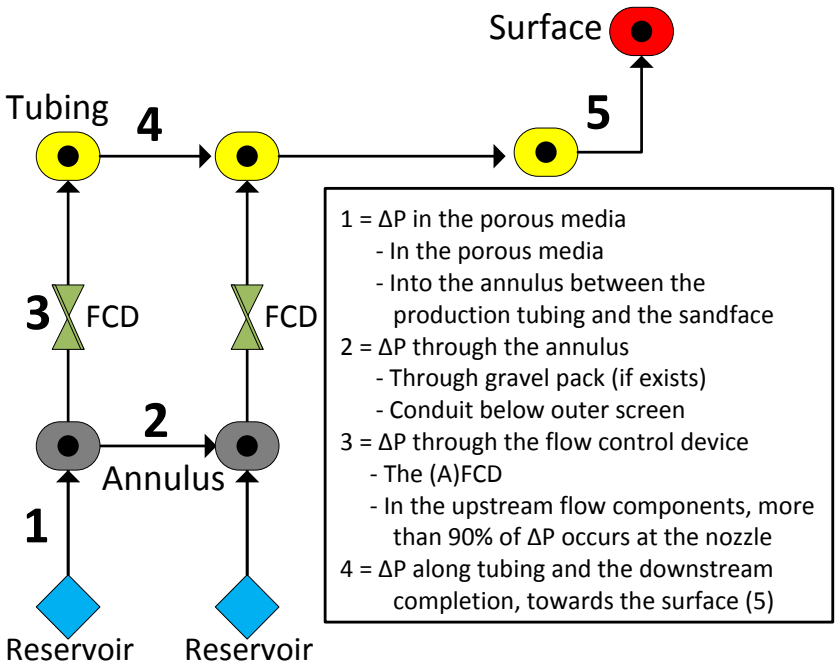

Figure 2-11. Schematic of the multi-segment well model

The pressure drops across each segment can be calculated by several methods depending on the multi-phase flow regime and the available information. The homogeneous flow is the most frequently used model. This approach assumes all phases flow at the same velocity (the no-slip assumption) and flow together. The assumption is reasonable when the effect of free gas or phase segregation on the flow in the segments is negligible. The drift-flux model should be used when two or more phases are flowing at different in-situ velocities and a slip is occurring between the phases.

Total pressure drop is calculated as the sum of all the pressure drop components.

$$\Delta P = \Delta P_h + \Delta P_f + \Delta P_a \tag{2-1}$$

Where:

$$\Delta P_h = \rho\, g\, L_p . \sin(\theta) \tag{2-2}$$

$$\Delta P_f = 2f\, \frac{L_p}{D_p} \rho\, v^2 \tag{2-3}$$

$$\Delta P_a = H_{v,out} - H_{v,in} \tag{2-4}$$

ΔP_h is the pressure loss (or gain) due to hydrostatic pressure.

ρ is the mixture density.

g is the gravity acceleration.

L_p is the segment length.

θ is the segment angle against the horizontal plane.

ΔP_f is the frictional pressure drop.

f is the fanning friction factor.

D_p is the pipe diameter.

v is the fluid velocity.

ΔP_a is the acceleration pressure loss.

$H_{v,out}$ is the outlet velocity head.

$H_{v,in}$ is the inlet velocity head.

2.3.1 Models for specific flow control devices

The calculation of total pressure drops (or gain) can be simplified for segments where a flow control device is installed. E.g. since the length and elevation difference between the inlet and outlet of a nozzle-type FCD is small (compared to the segment's properties), ΔP_h and ΔP_f are negligible {see WSEGVALVE keyword in (Schlumberger, 2014)}. The total pressure drop across the FCD largely depends on the pressure drop due to acceleration (equation 2-5).

$$\Delta P = \Delta P_a = \Delta P_{FCD} \quad (2\text{-}5)$$

The pressure drop across an FCD is calculated based on the flow performance data that measured by each manufacturer. Figure 2.12 to 2.14 are examples of published flow performance data.

ICD flow-performances

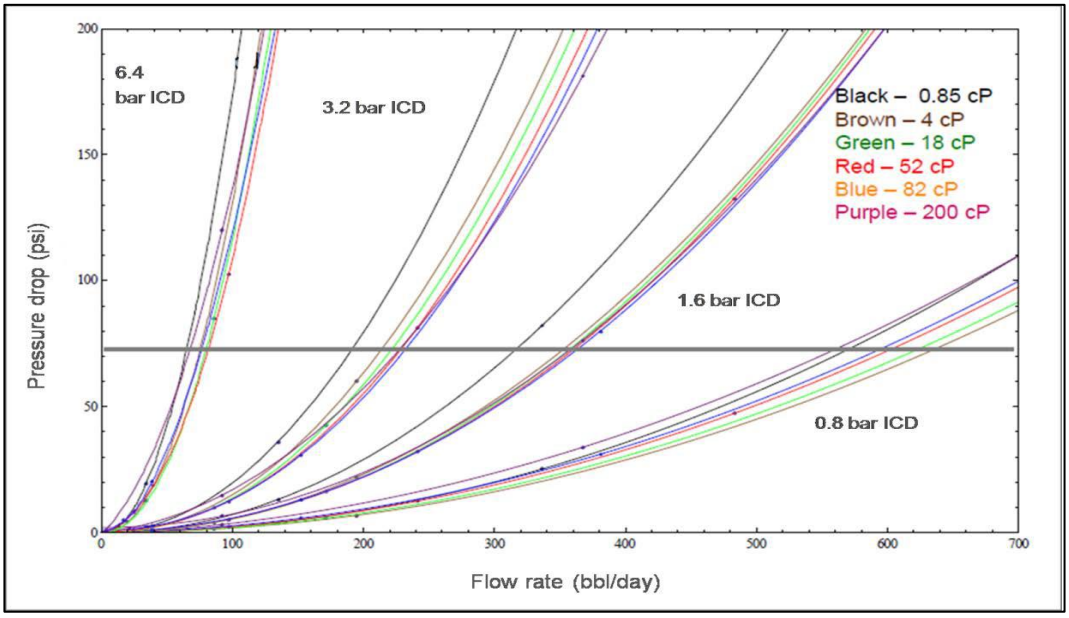

Figure 2-12. Example of flow performance of adjustable slot-type ICDs (Al-Khelaiwi, 2013)

ICV flow-performances

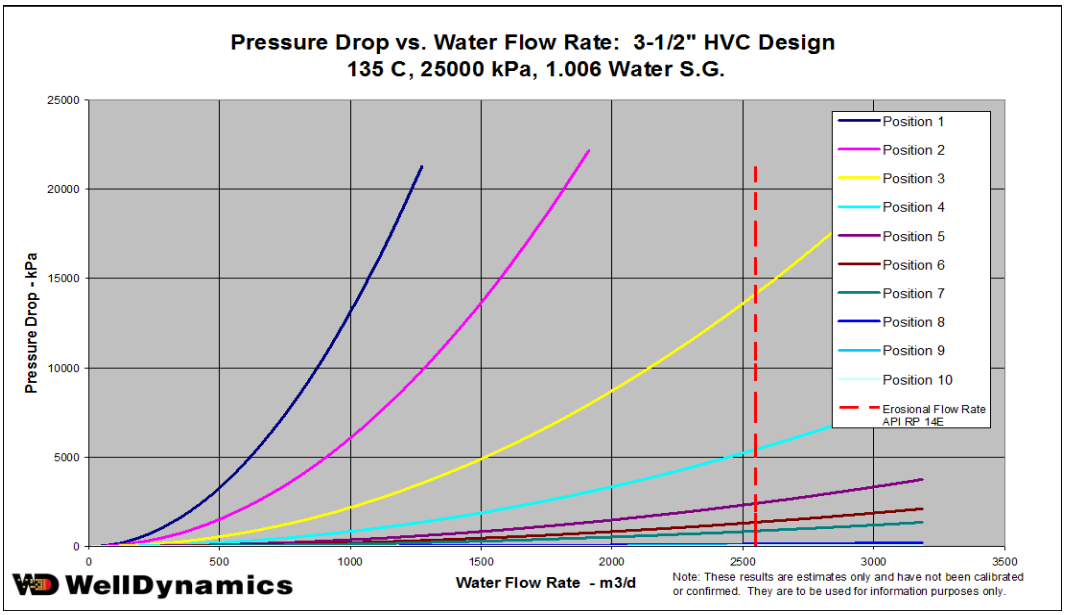

Figure 2-13. Example of flow performance of discrete position ICV (Al-Khelaiwi, 2013)

AFCD flow-performance

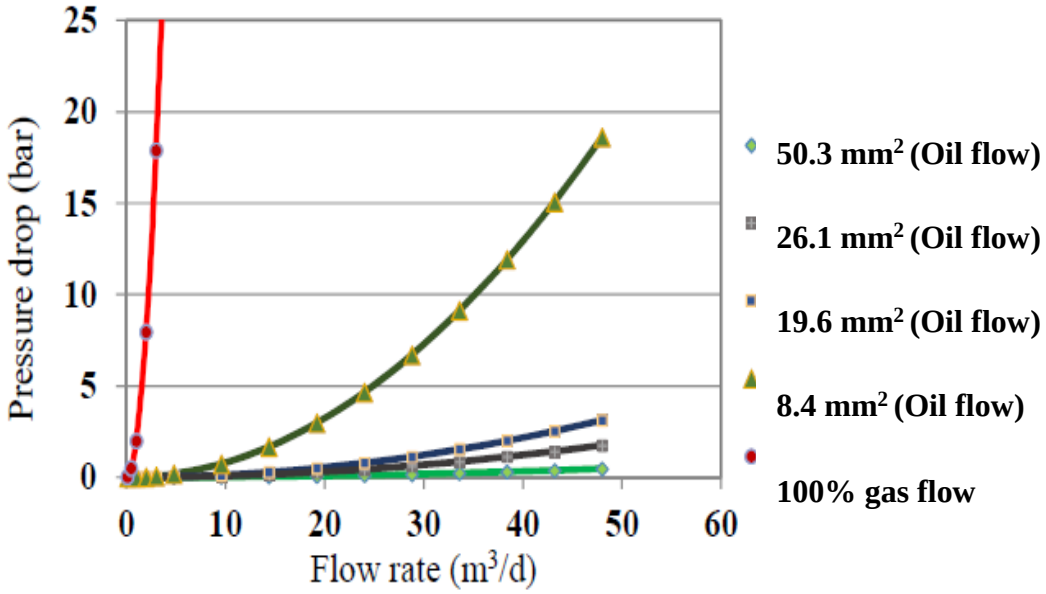

Figure 2-14. Example of flow performance of a single-phase AFCD (Eltaher, 2017)

The performance of these FCDs can be represented with the help of a simple empirical constant, called the segment's FCD strength (a), and the segment flow rate (Q).

$$\Delta P_{FCD} = a\, Q^2 \qquad (2\text{-}6)$$

Note that parameters in equation 2-6 are measured on a segment basis that is a section between two adjacent packers. The completion may have multiple FCDs installed in a segment. The FCD strength (a), in equation 2-6 is an upscaled FCD strength, which represents the performance of (n) devices. Note also that a (FCD strength) in this equation is different from the specific a(l) used in Birchenko *et al.*, (2010).

$$a = \frac{a(l)}{{L_p}^2} \qquad (2\text{-}7)$$

Where $a(l)$ is the FCD strength per unit length, and L_p is the segment length.

The way this generated pressure drop is independent on the device's manufacturer:

1) ICD

a. *An ICD that uses frictional pressure drop developed by flow through one or more small conduits.* The restriction strength can be calculated from Poiseuille's law (equation 2-8) to describe the (frictional) performance of this type of ICD. Examples are: the helical channel design that uses one or more flow channels wrapped around a base pipe and the labyrinth design using a tortuous pathway to impose abrupt alterations in the fluid's flow direction. Unfortunately, this type of ICD, being relatively viscosity dependent, encourages (less viscous) water production after water breakthrough.

$$a = \frac{C_u \rho B^2}{C_d^2 d^4} \tag{2-8}$$

b. *An ICD that works as a local restriction.* Strength derived from Bernoulli's law (equation 2-9) estimates the pressure loss across the nozzles and orifices of this type of ICD restriction, though the design does make it more sensitive to abrasion and plugging.

$$a = \frac{(\rho_{cal}\, \mu)^{\frac{1}{4}}}{(\rho\, \mu_{cal})} \frac{\rho}{\rho_{cal}} B^2\, a_{channel} \tag{2-9}$$

Where a is the restriction strength of a single ICD device, ρ_{cal} is the density of the calibration fluids, ρ is the density of mixed fluids, μ_{cal} is the viscosity of the calibration fluids, μ is the viscosity of mixed fluids. B is the formation volume factor, $a_{channel}$ is the channel ICD strength, d is the ICD nozzle diameter, C_d is the discharge coefficient for the nozzle or orifice, and C_u is a unit conversion factors: {$8/\pi^2$ for SI units, $1.0858.10^{-15}$ for metric units, and $7.3668.10^{-13}$ in field units}.

2) AFCD

AFCD adds an extra restriction to the flow of unwanted fluids by autonomously reacting when there is an unwanted change in fluid properties by altering the flow geometry within the device. The AICD/AICV performance (Figure 2-14) is described separately for single-phase oil flow and for single-phase water or gas flow since the

performance curves differ significantly. However, in both cases their single-phase flow performance can be acceptably matched by equation 2-10. {The AICD/AICV multiphase flow performance is difficult to model accurately and frequently only single-phase flow performance data is available. Modelling techniques for AFCDs are thoroughly discussed in Eltaher (2017)}. Commercial reservoir simulators (Halliburton, 2012; Schlumberger, 2014) use the empirically fitted equations formulated by Halvorsen *et al.*, 2012; Mathiesen *et al.*, 2014:

$$a = \left(\frac{\rho_{mix}^2}{\rho_{cal}}\right)\left(\frac{\mu_{cal}}{\mu_{mix}}\right)^y a_{aicd} \quad (2\text{-}10)$$

ρ_{cal} is the density of the calibration fluids, ρ_{mix} is the density of mixed fluids, μ_{cal} is the viscosity of the calibration fluids, μ_{mix} is the viscosity of mixed fluids. a_{aicd} is the device strength parameter, and y is a fitting input constant.

3) ICV

Flow through the ICV is sub-critical for most ICV applications. It can be modelled using a simpler version of surface chokes flow performance, where flow through the ICV is sub-critical. Commercial simulators (Halliburton, 2012; Schlumberger, 2014) model the choke strength of ICV (Figure 2-13) as :

$$a = \frac{8C_u\rho_{mix}}{\pi C_d^2 d_V^4} \quad (2\text{-}11)$$

C_u is a unit conversion factors: {$8/\pi^2$ for SI units, $1.0858.10^{-15}$ for metric units, and $7.3668.\ 10^{-13}$ in field units}, ρ_{mix} is the density of mixed fluids, C_d is a (dimensionless) discharge coefficient based on the valve position, and d_v is the ICV restriction diameter.

2.4 Problems with MRC wells reduced by ICD and AFCD installation

Ongoing improvements in drilling technology have maximised the reservoir contact with horizontal well designs becoming more sophisticated (multi-lateral, snake-wells). An MRC well, with higher productivity index, enables a lower drawdown to achieve the target production rate compared to a conventional well. However, greater reservoir contact results in higher inflow variation for more heterogeneous reservoirs encountered along the length of the completion (Figure 2-15 and Figure 2-16). The details of the magnitude of the observed changes in hydrocarbon saturation, formation permeability,

and reservoir pressure can rarely be predicted along the length of the completion in advance of drilling the well. Further, increasing the wellbore length yields a higher drawdown being observed at the heel location. This is due to the heel-toe effect (Figure 2-17). MRC wells may also be completed across several reservoir blocks with different reservoir and fluid properties. For example, the Troll oil field has a gas cap thickness that varies between 0 and 150 metres due to reservoir compartmentalisation (Figure 2-18). The timing of the arrival at different well location will vary greatly.

These issues lead to the premature arrival of unwanted fluids (water or gas) that impair the well's productivity and reduce reservoir recovery. Furthermore, the arrival of unwanted fluids could also adversely affect the well's performance due to related issues such as sand problems, and after water coning, and liquid-loading in gas well from excessive water production. ICD and AFCD type AWC's are installed to overcome these issues by adding local restrictions to the zones with a higher production rate. The local choking will increase the tubing intake pressure, resulting in a (relatively) higher, local reservoir drawdown in the previously low-producing zones (e.g. well's toe section, and/or lower productivity zones).

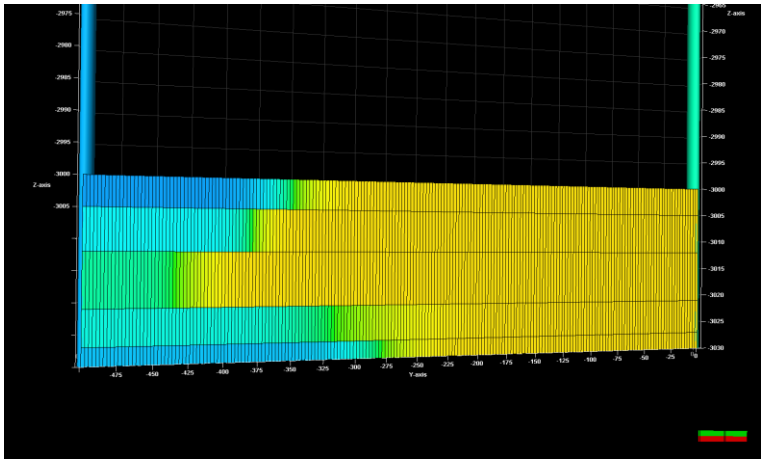

Figure 2-15. An AWC completion in a vertical well illustrating different water propagation in different layers due to reservoir heterogeneity.

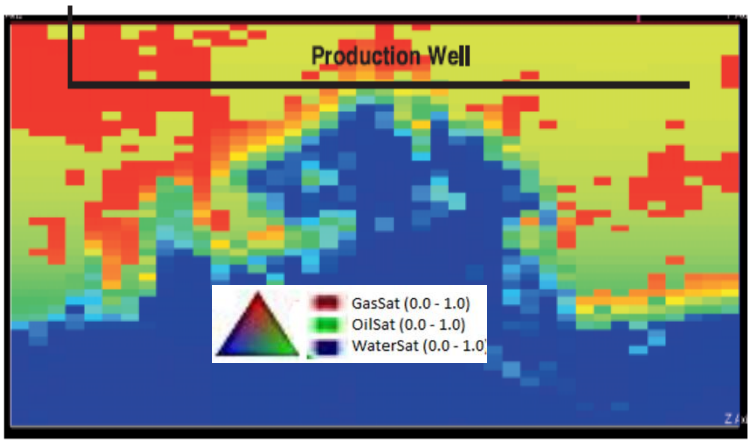

Figure 2-16. AWC completion in horizontal well with flow variation.

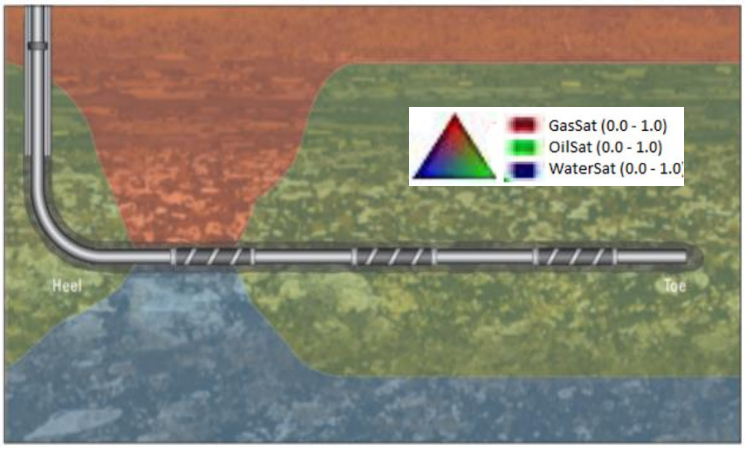

Figure 2-17. An AWC completion in horizontal well illustrating the heel-to-toe effect.

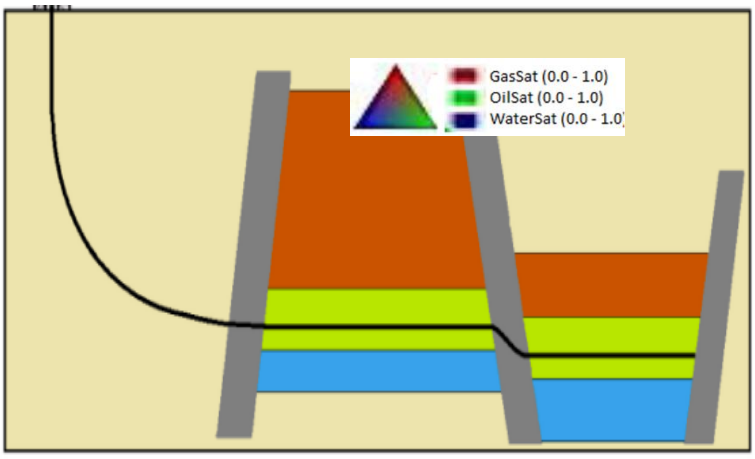

Figure 2-18. An AWC completion in horizontal well in a compartmentalised reservoir.

2.5 Problems with AWCs completed with monitoring system and ICVs

Wells equipped with a downhole monitoring system reveal more information about the performance of the wells and reservoirs. Integrating active control devices (ICVs) with monitoring technology in AWC systems can significantly improve hydrocarbon recovery (Grebenkin and Davies, 2010). Specific downhole information is now available to allow well management to achieve specified objectives by controlling the ICVs (Denney, 2012). The critical necessities here are that:

1. The wells have sufficient and appropriate measurement sensor.
2. Data analysis and interpretation techniques should reliably and consistently extract the desired information from the given measurements. These two requirements represent a fit-to-purpose intelligent well.

The data derived from these intepreted measurement are used to update the reservoir model or ensemble of models to reduce uncertainty in the reservoir description. It hence allows better, more informed reservoir management decisions (Prakasa *et al.*, 2017).

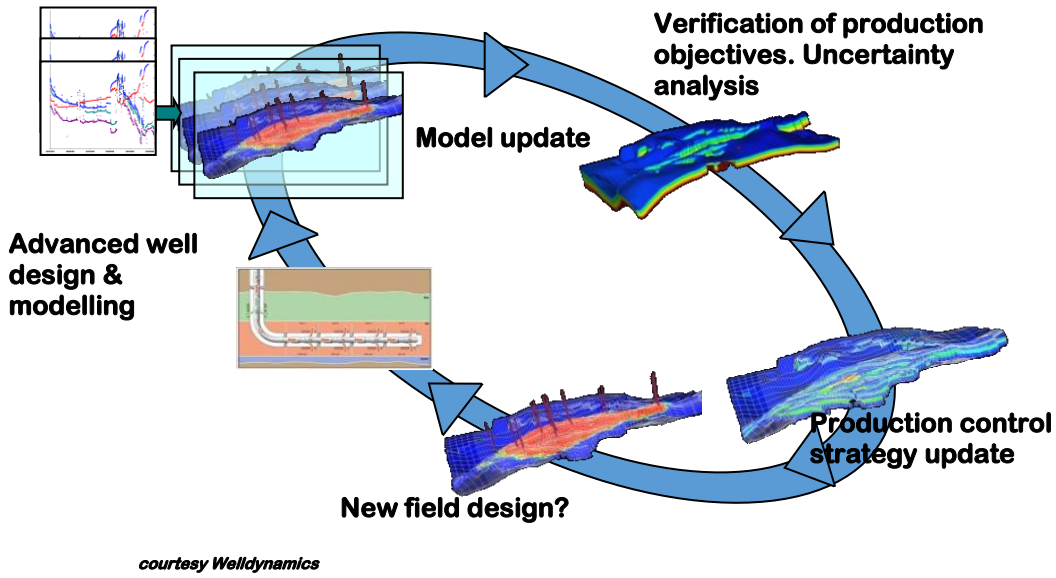

Figure 2-19. The cycle of closed-loop reservoir optimisation

Brouwer and Jansen (2004) introduced a systematic approach for optimal control of the downhole flow control device based on the optimal control theory. They evaluate which control scenario that maximises standard Net Present Value (NPV). Since then, there was a significant number of studies devoted to the development of the methodologies for optimising production and injection parameters during the different stage of production.

Many authors (Yeten *et al.*, 2005; Ajayi and Konopczynski, 2007; Addiego-Guevara, Jackson *et al*., 2008; Alhuthali, Datta-Gupta *et al.*, 2008; Birchenko, Demyanov *et al.*, 2008; Hasan, Ciaurri *et al.*, 2009; Alghareeb *et al.*, 2009; Almeida *et al.*, 2010; Cullick and Sukkestad, 2010; Dilib and Jackson, 2012; Pinto *et al.*, 2012, Sefat *et al.*, 2015), compare the added values of intelligent completions against conventional well by comparing the mean value of oil production, the recovery factor or NPV and their distribution for both IW and conventional scenarios. These studies can be classified into two approaches:

1. Reactive Optimisation (Grebenkin and Davies, 2012)

   The settings of the valves in the ICV are specified in response to arrival or near arrival of unwanted fluids in the well. The objective of this approach is mainly determined by the current condition of the well and its short-term objectives.
2. Proactive Optimisation (Alghareeb *et al.*, 2009; Almeida *et al.*, 2010; Sefat *et al.*, 2015).

   The settings of the valves in the ICV are specified in response to the flow behaviour forecast. The control is initiated at rather an early stage of the production. The objective of this approach is to mitigate future adverse issues (long-term objectives).

In wells with active flow control (ICVs), a feedback loop between measurement and production optimisation can be developed, that is, a closed-loop feedback control (Dilib *et al.*, 2013). ICVs provide real-time, adjustable, zonal flow control which allows implementation approach to increase the economic viability of the field while honouring the defined constraints by the equipment operator. This is in contrast to ICDs and AFCDs, whose fixed design can only be optimised in the installation stage. The inherent flexibility and the extra level of control provided by ICVs, when compared to conventional wells, allow better management of the field development delivering a reduced level of geological production uncertainty. This is done by identifying any mismatch of reservoir properties with the current reservoir model, the model is then updated based on the real-time information from the multiple sensors which are installed in AWC. The new setting of the valves is specified based the updated model and once a control strategy is applied to the wells, the behaviour of the flow system is re-monitored to update the reservoir models and the process is continuously repeated.

Optimisation under reservoir uncertainty, i.e. robust optimisation approach was firstly introduced by Yeten *et al.* (2003) for finding optimal well location, Bailey and Couet (2005) for maximising asset value in a gas field and Van Essen *et al.* (2013) for production injection optimisation in conventional wells. Birchenko et all (Birchenko, Demyanov et al. 2008) showed that well completed with ICVs could reduce the production uncertainty by 50%. Addiego-Guevara *et al.* 2008 found that even a simple reactive control strategy may significantly reduce the risk and provide insurance against reservoir uncertainty. Sefat *et al.* (2014) investigate the performance of the mean-variance approach on pro-active optimisation of AWC, while the uncertainty is represented by a small number of realisations selected based on a developed framework. The primary challenge of pro-active optimisation is the complexity when determining the optimal response of ICVs which requires expensive computational resources, and since the strategy is generally optimised under reservoir uncertainty, the complexity is even more exaggerated (Sefat *et al.*, 2015).

2.6 The needs for simple AWC modelling

The design and optimisation of AWCs is usually carried out using numerical well and reservoir simulators, and calculations are redone based on the modelling approach described in section 2.3. AWC modelling demands a comprehensive information on the entire production system. Detailed information for each segment should ensure that the simulation is as near perfect as possible representation of reality. However, in practice, this information is not readily available, and the completion has to be designed with an incomplete understanding of the future AWC's production performance.

Karim *et al.* (2010) reported that the main challenge to installation of an ICD type AWC in the SS field, offshore east Malaysia was to obtain real-time updates and calibration of the pre-designed ICD model with revised geological information obtained from the logging-while-drilling (LWD) real-time data. Once the drill-bit reached the target depth (TD), there was only a 24-hour time-window (between reaching the TD and the running-in-hole of the completion") to fine-tune the ICD design to the latest reservoir information. This operation required a model with fast computing time, hence, a commercial static modelling tool, NETool (Halliburton, 2012), was used to design and fine-tune the ICDs' sizes. The report also emphasised the impracticality of running dynamic reservoir modelling with the numerical grid-based simulator due to its tedious procedures and heavy-duty computing and simulation time.

NETool is the most widely used simulator when designing an AWC completion. It is a static modelling tool that allows quick multiple sensitivities of various parameters. This platform, however, still requires the output of a reservoir simulator to provide a snapshot of the reservoir performance, where the completion is designed. When the latest information from the open-hole log's latest information is used to update the accurate workflow (with revised reservoir properties) and run a new base-case dynamic numerical reservoir simulator before engineers run any sensitivities in NETool. This sequence is the ideal standard practice. However, it is often not followed due to operational constraints (Karim *et al.*, 2010), resulting in the design of the FCD completion not being based on the latest information.

The challenge when designing AWCs is to find the right balance (or trade-off) between well productivity loss (due to added restrictions) and improved added values, obtained by re-distributing/balancing the flow variation (Birchenko *et al.*, 2011; Al-Khelaiwi, 2013). The static modelling tool, being very simple, is only able to capture the short-term added value of the candidate well's inflow performance immediately after installing the AWC completion based on a "snapshot" in time of the well's performance. Such short-term evaluation, being simple and intuitive; has been widely used by production and completion engineers. However, it cannot capture future reservoir behaviour and ultimate project economics of such a completion. The long-term evaluation task is appropriate for a grid-based numerical simulator. However, using this approach is labour intensive and requires extensive reservoir simulation skills.

The computational power available to solve complex numerical simulations has increased over the years. However, the industry still lacks a model that has the capability to evaluate AWC performance in various scenarios (short-term and long-term evaluations) without adding too much complexity. Therefore, a simple analytical design tool capturing the important physics of the wellbore and reservoir will allow engineers to perform (Birchenko *et al.*, 2011):

- Quick assessments of the AWC's performance (screening AWC candidates).
- Verification of numerical simulation results.
- Communicating best practice in a non-product specific manner.

Moreover, due to with the uncertainty inherent in the many assumptions made for the geological, petrophysical, and fluid properties, the results of detailed full-physics

numerical simulation modelling is innately inaccurate. The Top-Down Reservoir Modelling (TDRM) (Williams *et al.*, 2004) philosophy is starts by investigating the simplest possible model appropriate to the available data and business decisions to be made; further details are added later as required. Hence, an analytical model is suitable as the pre-cursor before initiating detailed modelling (Figure 2-20).

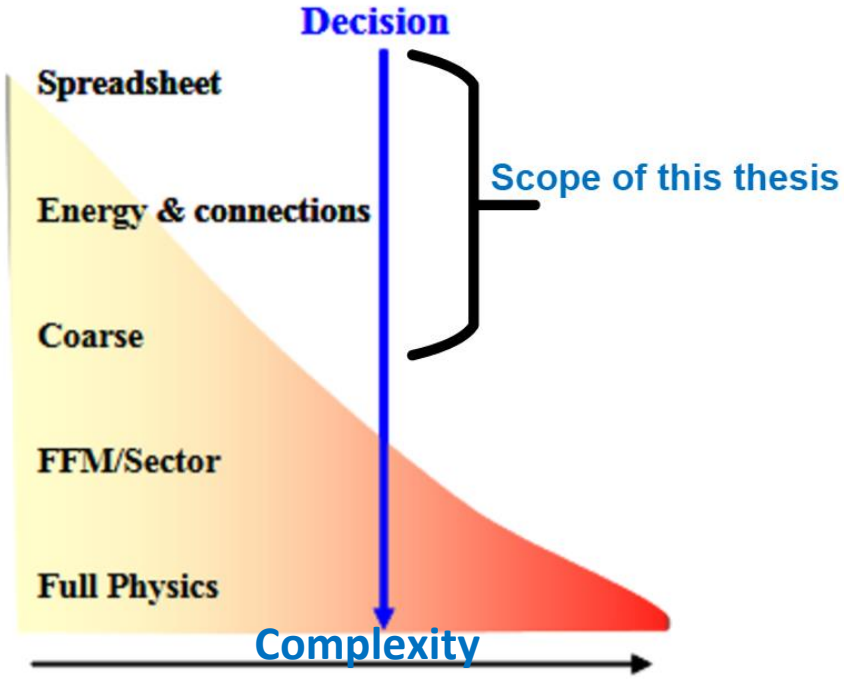

Figure 2-20. Decision focus by a top-down approach. The scope of this thesis covers the spreadsheet, the energy and connections, and the coarse model

This philosophy is also applicable to reservoir monitoring and optimisation (Hird *et al.*, 2011; Jahangiri *et al.*, 2014; Prakasa *et al.*, 2017). The significant development of a downhole monitoring system gathers an enormous amount of data from a real-time surveillance system when the well is producing. Therefore, a practical model that could capture the reservoir overview and link it to the specified valve settings is highly desirable.

The primary objective of this thesis is to devise a diagnostic tool or platform that practising engineers can use to do quick AWC designs and/or leverage day-to-day production data for monitoring and optimisation. A simple, portable toolbox is coded to determine optimal-ICD/AFCD/ICV completion responses in various field/fluid conditions. The practical utility of the proposed method will be illustrated through synthetic and real-field reservoir case studies.

Chapter 3 - Design of Flow Control Completion in Static Condition

3.1 Brief Introduction of horizontal well

Ever since Edwin Drake drilled the first ever commercial oil well (vertical) in Pennsylvania, vertical wells have been widely used to produce the hydrocarbon from underground rocks. The vertical (or moderately deviated) wells are relatively cheap to drill, and to this day, they are still preferred in many field. Vertical wells, however, have a lower productivity and covers smaller drainage areas than a horizontal well. The latter can have a higher reservoir-well contact and often provide a better sweep efficiency. A typical horizontal well schematic is illustrated in Figure 3-1.

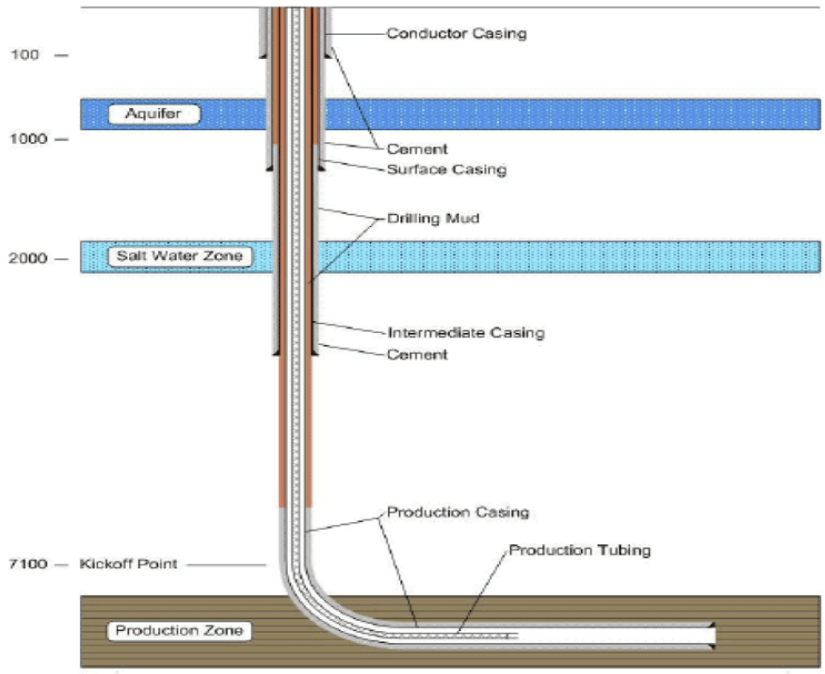

Figure 3-1. Schematic of Horizontal well (courtesy of RigZone)

Horizontal well technology advances and has become widely available since 1990, with as ever-increasing number of horizontal wells being drilled (Figure 3-2). The technology has achieved commercial success with costs reducing by 300% compared to the early experimental well. In past 5 years, due to shale revolution nearly all the high-production U.S. oil wells, i.e. those with producing at least 400 barrels of oil equivalent (BOE) per day, were horizontal (Figure 3-3). Horizontal wells have moved from being an area of niche technology to being standard practice both for oil producers and water injectors.

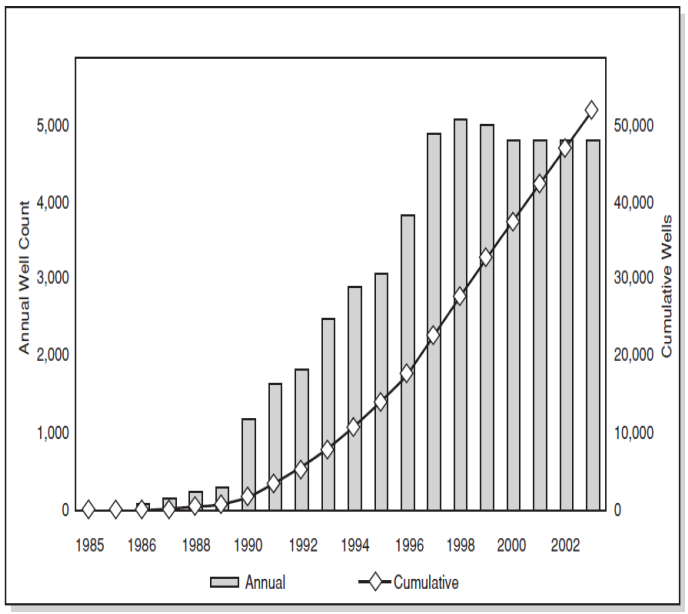

Figure 3-2. Increasing trend of horizontal wells (Davies, 2012)

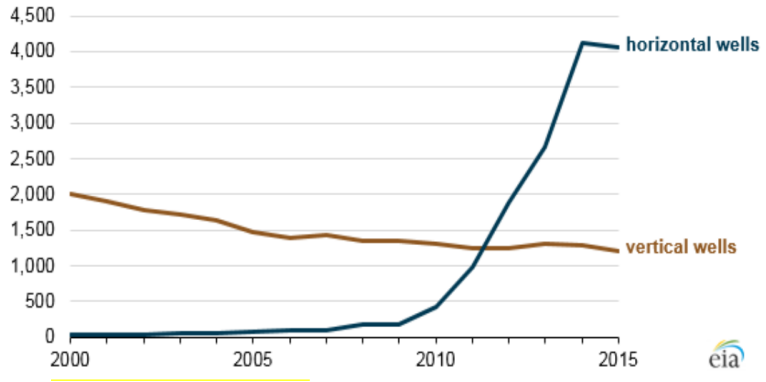

Figure 3-3. Count of oil wells in US, producing at least 400 boe/day between 2000-2015. (U.S Energy Information Administration, 2016)

The main components of a horizontal well normally consist of the vertical or deviated section, the build-up, and the horizontal section. The horizontal section is normally the section between the entry points into the reservoir (heel), to the end point of the well (toe). This section is typically drilled parallel to the fluid contact like water oil contact (WOC) or gas oil contact (GOC), or the reservoir/non-reservoir rock contrast. The vertical distance between the well and the oil-water contact is called the standoff. See Figure 3-4 for an illustration.

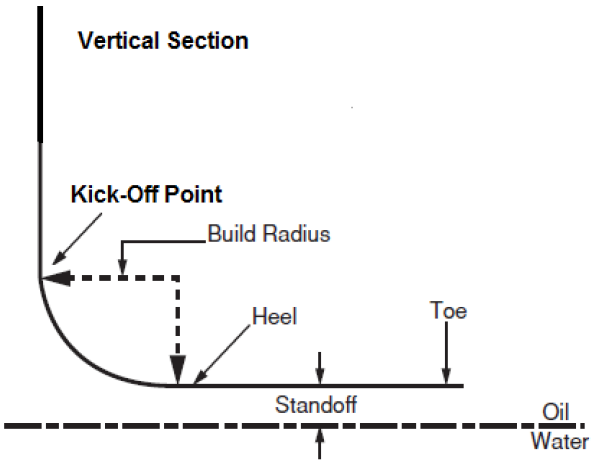

Figure 3-4. Horizontal well nomenclature (Davies, 2012)

Many operators may now drill wells with more than 6,000 ft of horizontal section. One of the longest horizontal section ever recorded, measuring 35,770 ft. MDRT was completed in May 2008 by Maersk Oil and Qatar Petroleum. The longest total horizontal well was measuring 15,000-m, drilled by ExxonMobil in November 2017 in the Sea of Okhotsk.

This work investigates the impact of flow control completions on horizontal well performance, so at first, we will dedicate several sections to generally describing the horizontal well technology and its widespread modelling routines. We will also briefly cover the well and reservoir flow description concepts and statistical terms as they will be used in our novel methods described later.

3.2 Development of Horizontal Wells Modelling

The initial studies (Borisov, 1984; Giger, 1984; Joshi, 1988; Renard *et al.*, 1991) derived different mathematical solutions, depending on the boundary conditions (Table 3-1), to calculate the well Productivity Index (PI) or J (terms used by production engineers and reservoir engineers respectively). This parameter is a commonly measured well property, defining the well potential or the ability to produce per given drawdown pressure.

$$J = \frac{Q_w}{(P_{avg} - P_{wf})} \quad (3\text{-}1)$$

Where Q is the hydrocarbon Production rate at standard conditions, P_{avg} is the average reservoir pressure (sometimes can be P_e or external pressure) and P_{wf} is the bottom-hole flowing pressure.

Drilling a horizontal well is significantly costlier than drilling a conventional vertical well. On top of that, a horizontal well is technically more challenging and prone to potential drilling failures. All this prompts the question: What is the benefit of drilling such well?

There are various parameters used to justify drilling a horizontal well. The most informative way, according to (Levitan *et al.,* 2001) is to evaluate the performance of a well with the Productivity Improvement Factor (PIF) or the ratio of horizontal well's PI to vertical well's PI, equation 3-2

$$PIF = \frac{J_H}{J_V} \quad (3\text{-}2)$$

Where PIF describes the Productivity Improvement Factor, J_H is the horizontal well's PI and J_V describes the vertical well's PI.

The term Productivity Index (PI) or *J* was used because other parameters such as rate or drawdown pressure are interrelated, i.e. rate depends on the pressure drawdown and vice versa (Beliveau, 1995).

3.2.1 Infinite Conductivity Wellbore Models

Numerous solutions for J_h have been published in the literature. The model for reservoir operating under steady-state (SS) condition was the subject of the earlier publications due to its simplicity and yielded the most widely used solutions. In this chapter, only the SS solutions that have been verified in real case studies are going to be discussed. The first ever published solution was from (Borisov, 1984), where the analytical solution is derived for single-phase incompressible fluids in a homogenous reservoir. The model assumes that the well is placed in the centre of the formation with elliptical drainage area. The analytical model assumed that the horizontal well is acting like fracture with infinite conductivity, i.e. there is constant wellbore pressure along the well. In the same year (Giger, 1984) also developed the analytical solution for single-phase, slightly

compressible fluids, homogeneous reservoir. To account for the anisotropic properties of the reservoir, the equivalent parameter B which is the square root of horizontal and vertical permeability ratio, is assigned to account for the differing horizontal and vertical permeability. (Joshi, 1988) also developed the new equation for single phase, slightly compressible fluids, in a homogeneous, anisotropic reservoir. His model did not necessitate the well to be in the centre of the drainage area. Joshi's equation is the most widely-used equations used for predicting horizontal-well performance. (Renard *et al.*, 1991) extending Joshi's equation for circular, ellipsoidal or rectangular drainage shape and later (Elgaghah *et al.*, 1996) proposed a new model for a more complex drainage area, whereby now the reservoir can be considered as a stacked series of semicircles and rectangles. (Furui *et al.*, 2005) developed a new model which accounts for the axial direction of flow, i.e. along the well, and assumes that fluids flow horizontally from the boundaries and radially in the vicinity of the well.

The essence of these approach to these problems is the reduction of the three-dimensional problem into a two-dimensional problem: vertical and horizontal flow (Anklam and Wiggins, 2005). The solution can then be derived based on different drainage area shapes, e.g. elliptical, rectangular, that affecting the flow regimes.

Table 3-1. Comparison of the early horizontal well inflow analytical equations

Authors	**Equations (Field Units)**	**Assumptions**
Borisov	$J_h = \frac{0.00708\, k_h h}{\mu_o B_o \left[ln\left(\frac{4\, r_e}{L}\right) + \left(\frac{h}{L}\right) ln\left(\frac{h}{2\pi\, r_w}\right)\right]}$	• Single-phase flow • Incompressible fluid • Isotropic • Homogenous reservoir (no-skin) • Centered within the formation thickness • Elliptical drainage area

Giger, et al.	$J_h = \frac{0.00708\, k_h L}{\mu_o\, B_o \left[\frac{L}{h} ln\left(\frac{1+\sqrt{1-\left(L/2r_e\right)^2}}{L/2r_e}\right) + ln\left(\frac{h}{2\pi\, r_w}\right)\right]}$	• Single-phase flow • Incompressible fluid • Anisotropic • Homogenous reservoir (no-skin) • Centered within the formation thickness • Elliptical drainage area
Joshi	$J_h = \frac{0.00708\, k_h h}{\mu_o\, B_o \left[ln\left(\frac{a+\sqrt{a^2-\left(L/2\right)^2}}{L/2}\right) + \left(\frac{h}{L}\right) ln\left(\frac{h}{2r_w}\right)\right]}$ $where\ a = L/2\left(0.5+\sqrt{0.25+\left(2r_e/L\right)^4}\right)^2$	• Single-phase flow • Incompressible fluid • Anisotropic • Homogenous reservoir (no-skin) • Elliptical drainage area
Renard & Dupey	$J_h = \frac{0.00708\, h\, k_h}{\mu_o\, B_o \left[Cos^{-1}(X) + ln\left(\frac{h}{2\pi \widehat{r_w}}\right)\right]}$ $where\ X = \left(0.5+\sqrt{0.25+\left(2r_e/L\right)^4}\right)^2$ $\widehat{r_w} = \frac{\left(1+\sqrt{\frac{k_h}{k_v}}\right)}{\left(2\sqrt{\frac{k_h}{k_v}}\right)} r_w$	• Single-phase flow • Incompressible fluid • Homogenous reservoir (no-skin) • Circular, elliptical and rectangular geometry

J_h : Horizontal's well PI (stbd/psi)	Bo : Oil formation volume factor
h : Payzone thickness (ft)	r_e : Drainage radius (ft)
k_h : Horizontal Permeability (mD)	r_w : Wellbore radius (ft)
μ_o : Viscosity Oil (cP)	L : Horizontal well length (ft)

Joshi (1991) evaluated the benefit of drilling a horizontal well against a vertical well using the equations presented in Table 3-1 are used to calculate the well's productivity (j_h) and the Productivity improvement factor (PIF). The required parameters are given in Table 3-2.

On a side note, practising engineers know very well that in reality, information such as in Table 3-2 is not readily available. They often must use field experience and make assumptions for those parameters.

Table 3-2. Well data used by (Joshi, 1991), example 3-1

Horizontal Well properties		
Payzone thickness (h):	**160**	ft
Horizontal permeability 1 (k_x):	**75**	md
Horizontal permeability 2 (k_y):	**75**	md
Oil viscosity (μo):	**0.62**	cp
Formation volume factor of oil (B):	**1.34**	
Drainage area (A):	**80**	Acre
Wellbore radius (r_w):	**0.365**	ft
Skin factor (S):	**0**	
Horizontal wellbore length (L)	**900**	ft
Vertical Permeability (k_v)	**75**	md
Effective horizontal permeability (k_h)	**75**	md
Drainage radius (r_e)	**1053.5**	ft
Vertical well drainage area	**40**	Acre

Results of this case are plotted in Figure 3-5. We can observe from the result that the horizontal well will improve the well productivity when compared to the vertical well. Figure 3-5 also suggests that having longer reservoir contact (i.e. increased horizontal well length) increases the PIF.

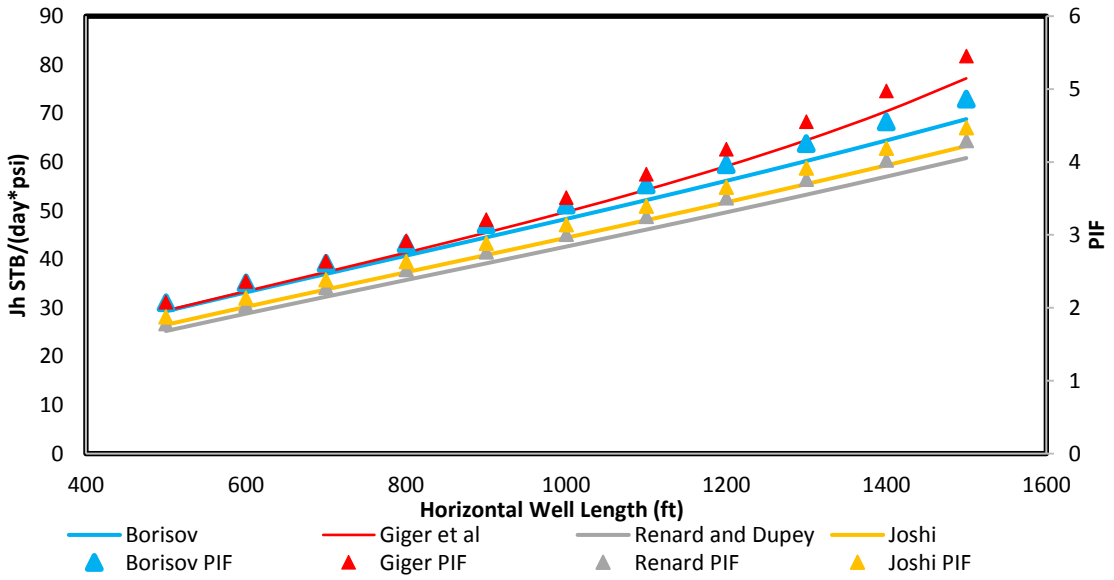

Figure 3-5. Productivity and PIF for different analytical solutions

One conclusion from this result could be that the maximum horizontal well length will always show maximum gain. This is practically not true with many field histories reporting poor performance of long horizontal wells. Surveys in the 1990s (Levitan *et al.*, 2001) reported project with proper implementation of drilling technique ensuring the success ratio of drilling a horizontal well of 95%. The objective of drilling long horizontal wells without operational problems was achieved, but it came with an ever-increasing cost per feet with longer horizontal sections. An increased production rate (from having greater reservoir contact) were expected to offset this cost. However this was not the case. It was reported only about 50% of horizontal wells that were economically justified.

The reported case indicated an essential element was not being accounted for by the equations in Table 3-1. This element is the frictional pressure loss in the wellbore. The above solutions (and many other equations) assumed pressure drop along the well length is negligible, i.e. an infinitely-conductive well. This is an acceptable assumption for a short horizontal well with small flow rate. However, many wells today have an extensive horizontal section and operates with large flowing rate. For those wells, the effect of friction pressure along the well is no longer trivial, and a single value of pressure is insufficient to represent the whole horizontal section. (Babu and Odeh, 1989) are ones of the first initiators of horizontal well modelling, looked into this problem. Their model still assumed a uniform flux with infinite conductivity, but they did point out the inaccuracy of assuming constant pressure along the entire length of the horizontal section.

This issue is illustrated in Figure 3-6. Continuous fluid flow along the horizontal well requires a certain amount of pressure drop between the toe and heel section, or $P_{Toe} - P_{Heel}$ (ΔP_{HT}**)** > 0. The heel-toe effect reduces the potential drawdown, particularly at the toe section. The drawdown for this section is overestimated by traditional models, resulting in the predicted well rates also being overestimated. The extra pressure drop depreciated by tubing outflow due, for example, to the well being completed with a too small diameter of tubing, will have a similar effect on the rate predictions as the heel-toe effect. Note that the analysis of this chapter assumes a perfectly horizontal well where the pressure loss between heel and toe is dominated by the friction effect, and hydrostatic head differences are (relatively) negligible.

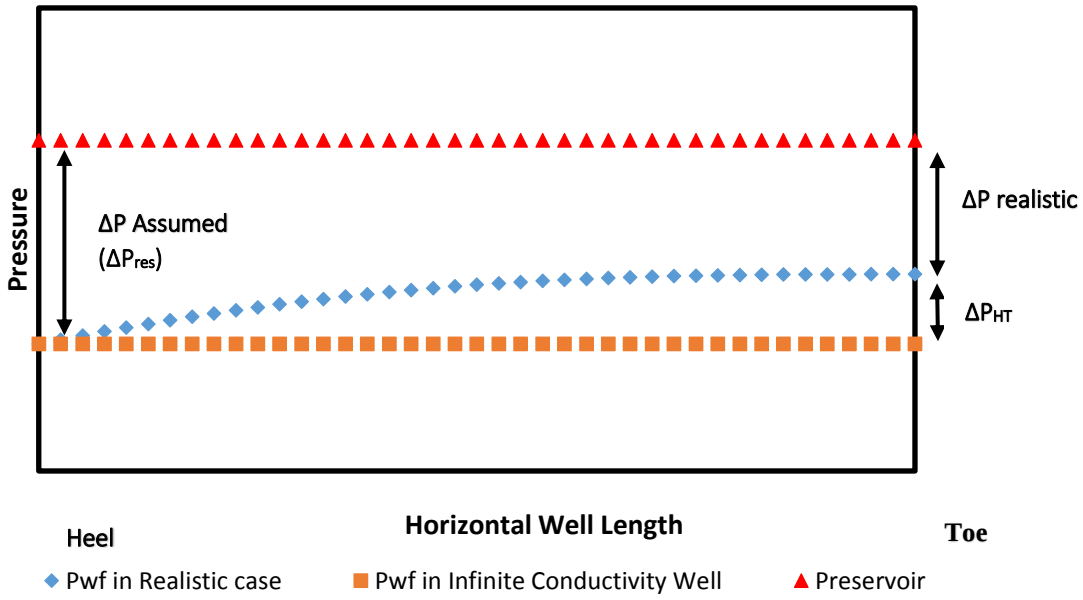

Figure 3-6. Pressure loss models in the horizontal well section

3.2.2 Finite Conductivity Wellbore Model

Equation describing horizontal well performance should incorporate wellbore hydraulics. The new model is required to couple the physics of flow from the reservoir (Darcy law) and the flow along the well (wellbore hydraulics) in the well sections. Specific productivity index was introduced that discretised the PI from a well to unit length of the well.

$$q_s(l) = J_s(l)[P_e - P_w(l)] \qquad (3\text{-}3)$$

Where $q_s(l)$ is the inflow rate from the reservoir to wellbore per unit length of the well at location l, $J_s(l)$ is Specific PI at location l, P_e is Constant Pressure at the boundary condition, and $P_w(l)$ is the wellbore pressure at location l.

Equation 3-3 can be solved with the following assumptions:

1. Flow in the reservoir follows Darcy's law.
2. The inflow from the reservoir to the well can be described by the steady- or pseudo-state condition.
3. The boundary of the reservoir is parallel to the well and/or the distance between well and the reservoir boundary is significantly longer than the well length.

(Cho and Shah, 2002) illustrated this as shown in Figure 3-7.

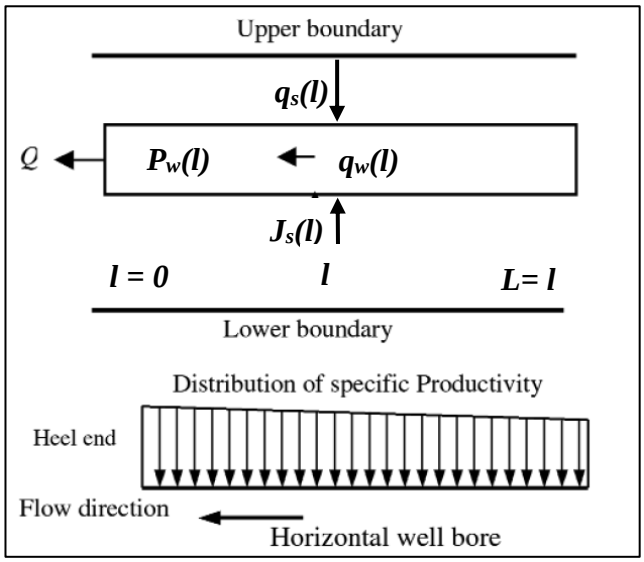

Figure 3-7. Simple horizontal well flow model with Js (Cho and Shah, 2002)

The first published mathematical analysis of the pressure drop along the wellbore was from (Dikken, 1990). He introduced the link between specific productivity index, $J_s(l)$, and the specific inflow rate, denoted by $q_w(l)$.

$$\frac{dq_w(l)}{dl} = -q_s(l) = J_s(l)[P_e - P_w(l)] \tag{3-4}$$

With constant J_s and constant P_e, differentiation over l results in:

$$\frac{d^2q_w(l)}{dl^2} = J_s(l)\frac{dP_w(l)}{dl} \tag{3-5}$$

The problem is then solved with the following boundary conditions:

$$\begin{cases} \left[\frac{dq_w(l)}{dl}\right]_{l=0} = J_s(l)[P_e - P_w(0)] = J_s(l)\Delta P_{heel} \\ [q_w(l)]_{l=L} = 0 \end{cases} \tag{3-6}$$

Dikken used Blasius turbulent friction factor correlations to describe pressure gradient along the well. He presented the semi-analytical solution to calculate the rate at location l, $q_w(l)$ for laminar and turbulent flow cases.

(Joshi, 1991) suggested a quick evaluation to check the importance of the pressure drop in the completion. He applied a standard pipe flow correlation, calculate the friction factor, f_m, based on Reynold's number and assumed all fluids enter the wellbore at the toe. The locations where there is maximum drawdown difference: in the heel and toe,

Joshi used in a parameter called *drawdown ratio*, or the ratio of drawdown in toe and heel, Rd. This parameter is used in the horizontal well performance evaluation as well as in the selection of the completion size and material.

$$R_d = \frac{\Delta P_{Toe}}{\Delta P_{Heel}} \tag{3-7}$$

The method significantly overestimates the calculated pressure loss, but is a very useful as a quick-look tool for assessing whether a more robust analysis is necessary. (Hill and Zhu, 2008) extended Joshi's approach by developing an upgraded quick-look evaluation of the relative importance of the pressure drop along the well. The difference is that they used half of the total flow rate (which is then equivalent to Joshi's pressure loss divided by 4).

(Seines *et al.*, 1993) observed that the dependence of friction factor on Reynold's number is less significant for highly turbulent flow. The study proposed to normalise the specific flow rate, $q_w(l)$ over the well length along with the friction factor and the PI_s. The normalized flow rate, u, then appears in the second-order non-linear ordinary differential equation (ODE). The equation was solved analytically for infinite well length and numerically for finite well length. They also noticed that the pressure gradient along the well was dependent on several wellbore and reservoir properties, hence they introduced l*, a new dimensionless variable, to normalize L (the well length) incorporating the effect of these properties.

$$l^* = \sqrt[3]{\frac{12D^5}{J_s^2 C_f \rho f_a B^2 \Delta P_w}} \tag{3-8}$$

Where l^* is the dimensionless length of the well, D is the inside diameter of the wellbore, J_s is the specific PI, C_f is the conversion factor, ρ is the fluid density, f_a is the friction factor, B is the formation volume factor, ΔP_w is the drawdown in the heel section. (Halvorsen, G., 1994) reviewed the work of Seines's and observed that the accuracy of solutions for a finite well has increases when expressed with a Weierstrass elliptic function. Halverson's method is not explicit and required iteration to resolve the implicit relationship between parameters. (Penmatcha, Arbabi and Aziz, 1999) proposed a semi-analytical model similar to the one suggested by Seines. They proposed a new parameter to calculate the error in the well productivity calculation when frictional pressure drop along the well is not considered.

$$E_p = \frac{(q_{nofriction} - q_w)}{q_{nofriction}} \quad (3\text{-}9)$$

With Ep is the productivity error, $q_{nofriction}$ is the well's rate when friction effect is deactivated, and q_w is the well's rate when the friction effect is incorporated.

Ep is analogue to equation 3-2, PIF. The deviation of the productivity improvement factor(PIF), friction-affected well, from the original PI is explicitly quantified by Ep. Engineers can now execute a simple analysis, as exemplified by Halvorsen's paper which provided an extensive sensitivity analysis of the effect of the various well and reservoir parameters.

(Birchenko, Usnich and Davies, 2010) proposed a more simple and robust method to model the horizontal well flow. Combining Seines, Halvorsen, and Penmatcha methods together with the Darcy-Weisbach equation, the definition of friction factor was solved by using the Weierstrass elliptic function. Birchenko's explicit model assumes an average friction factor along the well. This solution adopted Seines' dimensionless number, comprising various physical well and reservoir parameters, allowing the extensive analysis for each parameter, such as that reported by Penmatcha, to be simplified to only one parameter, the horizontal number.

$$\begin{cases} H_q = \frac{C_f \rho f_a B^2 J_s L^2 q_w}{D^5} \ (for\ Rate\ Constraint) \\ H_p = \frac{C_f \rho f_a B^2 J_s L^3 \Delta P_w}{D^5} \ (for\ Pressure\ Constraint) \end{cases} \quad (3\text{-}10)$$

The description of these parameters is identical to those described below equation 3-8.

The horizontal number can be interpreted as the ratio between the reservoir and wellbore flow conductivity. In long horizontal wells where the wellbore throughput is much smaller than the reservoir supply (e.g. in extended reach wells completed with big-bore completion) the horizontal number will be high, and conversely, when the reservoir conductivity is smaller, the horizontal number will be small.

The solution was derived explicitly, even allowing the horizontal numbers to be plotted against the drawdown ratio (Rd) and Productivity Error (Ep). The motivation of Birchenko's model is to compose a quick, simple tool for feasibility studies as well as a confirmation of the results for numerical simulation (similar to the objectives of Joshi and Hill and Zhu).

Dimensionless numbers allow the dynamics of a system to be analysed as a type curve (TC). A TC describes the relationship between the reservoir and well's physical properties and the well's flow rate. The dimensionless parameters enable scaling of the system to the actual conditions. Modelling horizontal well performance using dimensionless numbers has been widely practised (Joshi, 1991). Birchenko nicely demonstrated the performance of horizontal well modelling using type-curves.

Flow rate constraint

For example: For the flow rate constrained well flow case (a.k.a. 'rate constraint') the TC (Figure 3-8) shows that when e.g. Hq = 1, for Ep = 0.19 the Rd = 0.75. These numbers indicate that the well's productivity is reduced by 19% from the no-friction PI case and the drawdown value at the toe is 75% of the drawdown at the heel of the well.

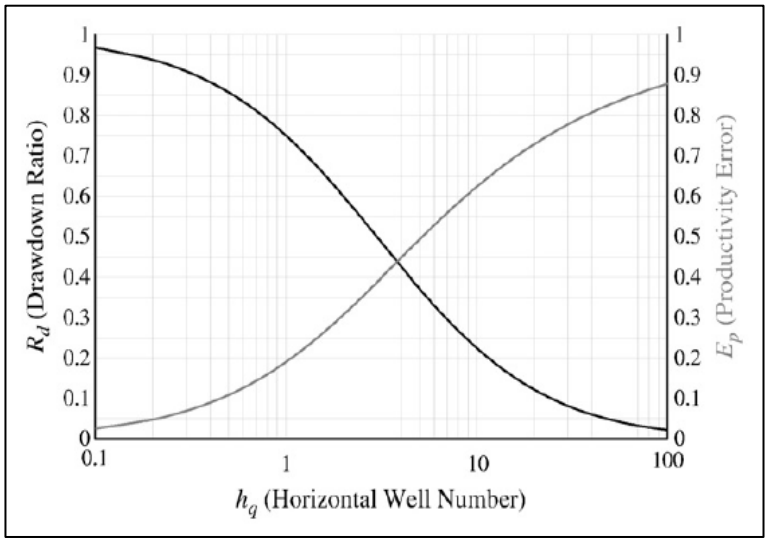

Figure 3-8. Horizontal well Type-Curve for rate constrained case

Pressure constraint

For the bottomhole pressure constrained well flow case (a.k.a. 'pressure constraint') TC, Figure 3-9, when e.g. Hp = 30 for the Ep = 0.68 the Rd = 0.21. These numbers indicate that the well's productivity is reduced by 68% from the no-friction PI case and the drawdown value at the toe is about 21% of the drawdown at the heel of the well.

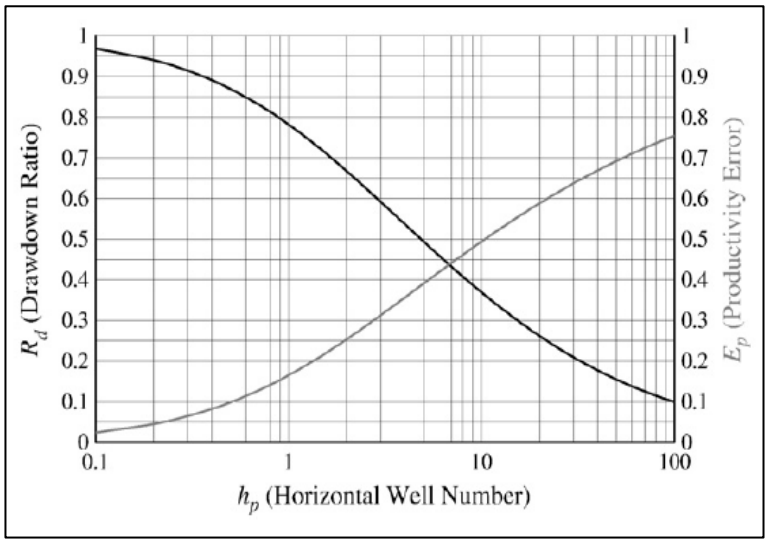

Figure 3-9. Horizontal well Type-Curve for pressure constrained case

3.3 Horizontal Well flow performance in heterogeneous reservoirs

A typical horizontal well drilling plan is to penetrate the reservoir parallel to the bedding plane, preferably the reservoir with the same geological facies. It is standard practice because it allows easier drilling operation. It also allows engineers to assume constant reservoir properties along the well and simplify the well performance calculation. However, depending on the geological environment, the well may intersect multiple payzones. The motivation is simply to improve the well performances. The well having more contact with the reservoir would have improved productivity because it is a direct function of the reservoir-well contact. This strategy is adopted despite the riskier drilling operation in order to meet the project's plateau rates with the reduced number of wells.

3.3.1 Geological structures and horizontal wells in heterogeneous reservoirs

A horizontal well (or a highly deviated well) in a heterogeneous reservoir is commonly preferred in a geological structure such as Channel point bars and Shale drape (Figure 3-10). The lateral accretion within fluvial streams results in the reservoir two configurations that often impede the lateral flow to the vertical wellbore. If the orientation of the point bar can be determined, a horizontal well can be directed to penetrate multiple sand wedges

which are isolated from the wellbore by this shale drapes (Aguilera, 1991).

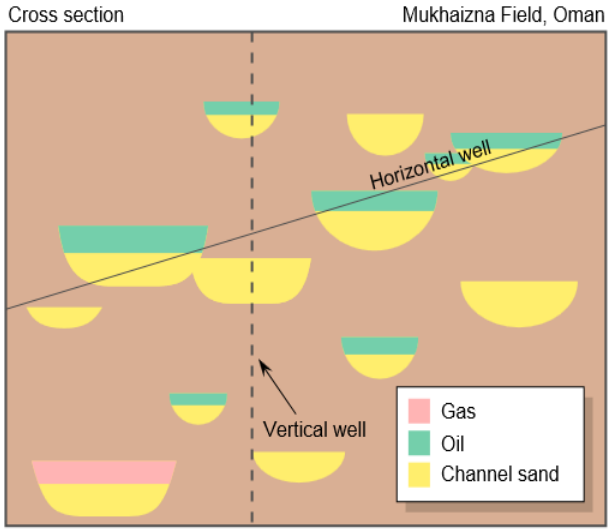

Figure 3-10. A Horizontal (or highly deviated) well in channel sands

Braided stream systems. One of the products of braided stream systems is pods or finer sediments which contain low permeability lenses. The horizontal wells in such systems are typically oriented with the long axis parallel to the stream direction (Aguilera, 1991). The fluid will generally flow along the primary axis of the stream system. In this case, a vertical well could only produce from a long narrow section of the reservoir, with less contribution from channel sands located adjacent to the wellbore, but in a direction normal to the stream's direction of flow.

Carbonate and fractured systems (Figure 3-11). A horizontal well is aimed to connect areas of high permeability rock that are compartmentalised by low permeability sections. Commonly the carbonate systems have a natural fracture system that can significantly enhances the production of the well by providing the additional fluid flow path. A horizontal well is capable of increasing the probability to intercept a fracture system and reduce the risk of having a dry hole. However, the water production can be detrimental when a fracture system is connected to the aquifer, (Aguilera, 1991).

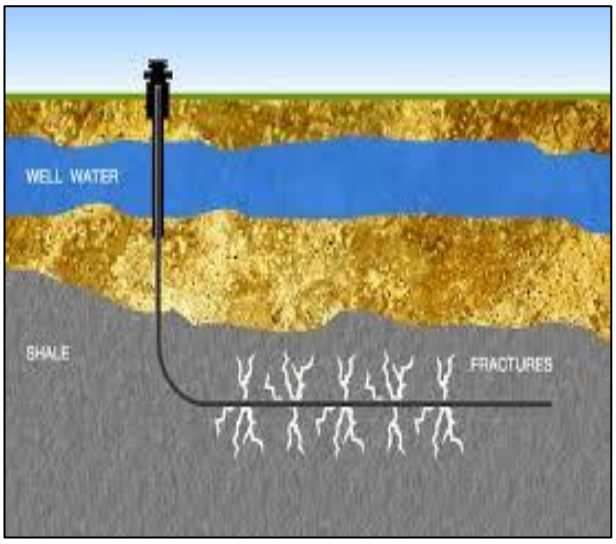

Figure 3-11. Horizontal well in fracture system

3.3.2 Measures of reservoir heterogeneity

Heterogeneity, or the spatial variation in reservoir properties, is common and significantly impacts the fluid flow (Lake and Jensen, 1989) Heterogeneity types often dictate the likely recovery process and flow performance. An assessment of the reservoir heterogeneity is required to evaluate whether a reservoir is economically feasible to develop or not. Petroleum engineers often use simple statistics to characterise the geological heterogeneity without the need of detailed extensive data sets. The three commonly used measurement of heterogeneity are:

1. Coefficient of Variation (Cv) (Jensen, 2000).

$$\mathrm{Cv} = \frac{SD}{\overline{K}} = \frac{\sqrt{\sum_{i=1}^{N} \frac{(k_i - \overline{k})^2}{N-1}}}{\overline{K}} \qquad (3\text{-}11)$$

Where S_D is the standard deviation, measuring the positive square root of the variance of the permeability sets, from sample i to N, and $\overline{K}$ is the arithmetic average of the permeability. Cv is a measure of normalised standard deviations which is used to delineate the levels of heterogeneity.

0.0 < Cv < 0.5	Homogenous
0.5 < Cv < 1.0	Heterogeneous
1.0 < Cv	Very Heterogeneous

In past decades, Cv gained popularity as a parameter to describe the layered reservoir especially since probe permeameter studies have become popular.

2. Dykstra-Parsons Coefficient (Jensen, 2000).

Dykstra-Parsons Coefficient is the most widely used heterogeneity measure. This parameter was uniquely developed in the petroleum industry. It can also be called "the variance", or "the variation". It assumed a log-normally distributed reservoir permeability:

$$V_{DP} = \frac{K_m - K_1}{K_m} \qquad (3\text{-}12)$$

Where $\boldsymbol{K_1}$ is the value of permeability at one standard deviation below the median permeability ($\boldsymbol{K_m}$). The value is determined by plotting a probability plot for log (k) and read off the values from 1 standard deviation from the mean value, which is the 50th and the 84th percentiles. This is illustrated in Figure 3-12.

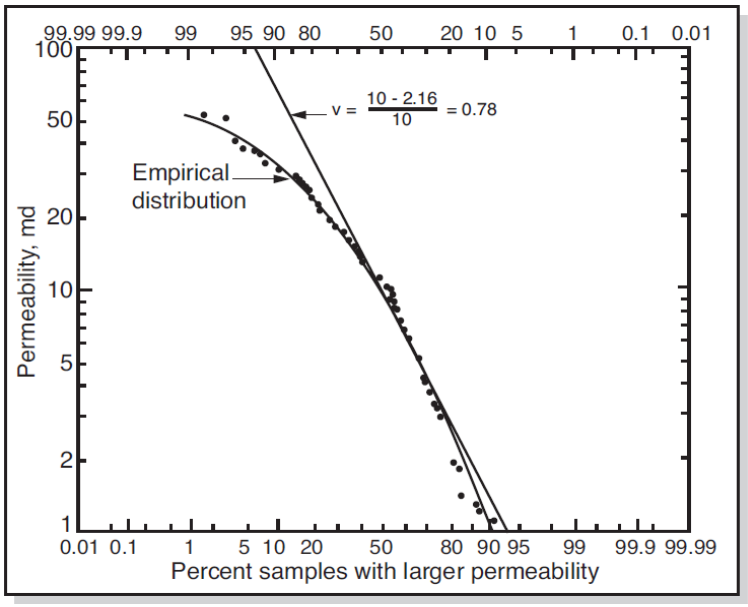

Figure 3-12. Illustration of measuring heterogeneity using Dykstra-Parson coefficient (Corbett, 2012)

One of the most common assumptions regarding the permeability distribution in reservoirs is that it is (more often than not) log-normally distributed. One explanation for this is given in the theory of breakage (Jensen *et al, 2000*):

Suppose we start with a grain of diameter $D_{po,}$ which fragments to a smaller grain in

proportion f_0 yield a grain of $D_{p1.}$ Repeating this process obviously leads to an immense tree of possibility for the ultimate grain diameter. However, if we follow one branch of this tree, its grain diameter D_{p1} will yields an additive process upon taking a logarithm. Therefore, we should expect ln D_{p1} to be normally distributed from the *Central Limit Theorem*. Since permeability is proportional to the grain size squared (e.g. in Kozeny-Carman equation), it is also log-normally distributed.

The main advantage of using this parameter, V_{DP}, is that it has been the subject of numerous studies in the petroleum industry. Different correlations have been built relating the V_{DP} to the other parameters such as recovery factor, injection volume, water cut, dimensionless time, etc (Johnson, 1956; Jensen and Currie, 1990; El-khatib, 2011).

3. Lorenz coefficient (Lake and Jensen, 1989)

The Lorenz Coefficient (Lc) (Or Gini Index) is the particular area within Lorenz Plot, a plot which illustrated the relationship between total reservoir porosity and permeability. The Lorenz plot constitutes two parameters:

$$\begin{cases} \mathrm{F}_J = \frac{\sum_{j=1}^{J} k_\mathrm{j} h_\mathrm{j}}{\sum_{i=1}^{I} k_\mathrm{j} h_\mathrm{j}} \\ \mathrm{C}_J = \frac{\sum_{j=1}^{J} \Phi_\mathrm{j} h_\mathrm{j}}{\sum_{i=1}^{I} \Phi_\mathrm{j} h_\mathrm{j}} \end{cases} \tag{3-13}$$

Where J is the index of data points, with maximum I. F_J, is the flow capacity and Cj is the storage capacity (Figure 3-13.). These capacities, ordered from smallest to largest, are plotted on a linear plot (red line). The Lorenz Coefficient is the ration between the (grey) area bounded by the line of equality (Y = X line, black line in Figure 3-13.) and the Lorenz curve (red line in Figure 3-13.), and the triangle (blue) area between the line of equality and the Cartesian plot (blue line if Figure 3-13.). Since the triangle area is always 0.5, hence the Lorenz coefficient (Lc) can be calculated as twice the shaded area and is in the range from 0 to 1. As a reference, the full uniformity or homogeneity is identified by the black diagonal line and it has Lc = 0. More about the Lorenz coefficient will be discussed in chapter 5.

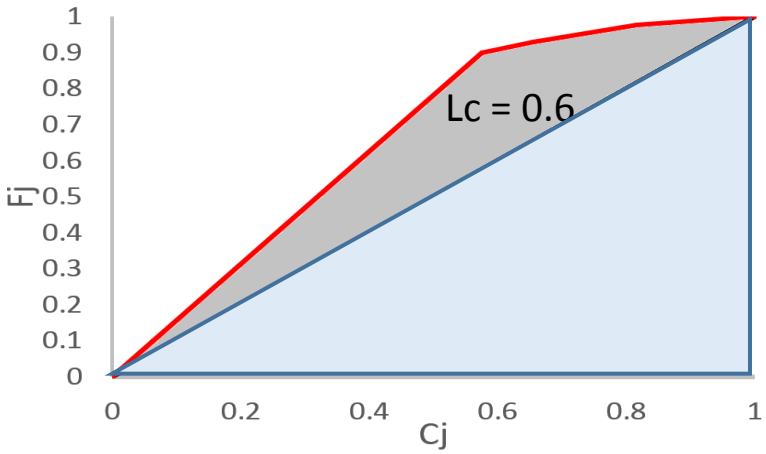

Figure 3-13. Illustration of measuring heterogeneity using Lorenz Plot

3.3.3 Model of flow in a horizontal well in a heterogeneous reservoir

Horizontal wells can be exposed to multiple pay zones, produce hydrocarbons from multiple geological facies with different properties. The total production comes from various payzones. In this case, the wellbore pressure drop due to friction and acceleration can often be assumed negligible compared to the flow variation due to the reservoir heterogeneity. The range of validity of this assumption was thoroughly discussed by (Dikken, 1990; Birchenko, Usnich and Davies, 2010). This assumption implies constant bottom-hole flowing pressure throughout the completion length, i.e. infinitely conductive wellbore. Further, assuming the reservoir pressure is uniform (at least initially), the ΔP_W or $(P_e(l) - P_l(l)$ is also constant, and the flow is:

$$q_W = \sum_{i=1}^{N} q_i = \sum_{i=1}^{N} (j_i \Delta P_W) \quad (3\text{-}14)$$

With q_W is well production, j_i is specific productivity index and N is the total number heterogeneous layers.

3.4 Role of ICDs in Horizontal Wells

3.4.1 ICD completion in wells with dominating heel-toe effect

Increasing horizontal length increases the inflow and thus the friction pressure drop along the well, with the flowing pressure in the toe section being higher than the pressure in the heel section as was depicted in Figure 3-6 and Figure 3-7. This is the previously discussed Heel-Toe Effect (HTE). The resulting drawdown difference between the heel and the toe was referred to as the Drawdown ratio (R_d). A larger Rd leads to higher influx in the heel

section and can result in early water and/or breakthrough in this section (Figure 3-14).

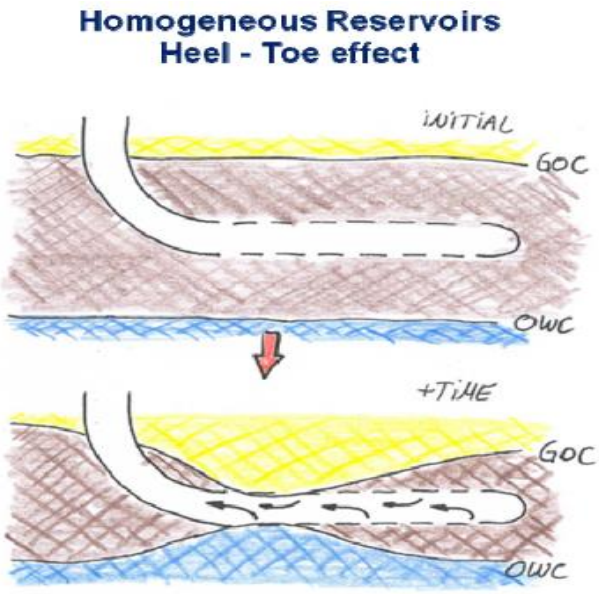

Figure 3-14. Homogeneous reservoir flow affected by strong Heel-Toe Effect (Vela et al., 2011).

ICD technology is designated to modify the inflow rate variation by adding larger pressure drop in the layers with higher production rates. Figure 3-15 illustrated how the ICDs reduce the heel-toe effect in a horizontal well in a homogeneous reservoir. Notice how the inflow distribution after installing ICD (green, Figure 3-15 right) is evened compared to the screen completion (orange, Figure 3-15 left).

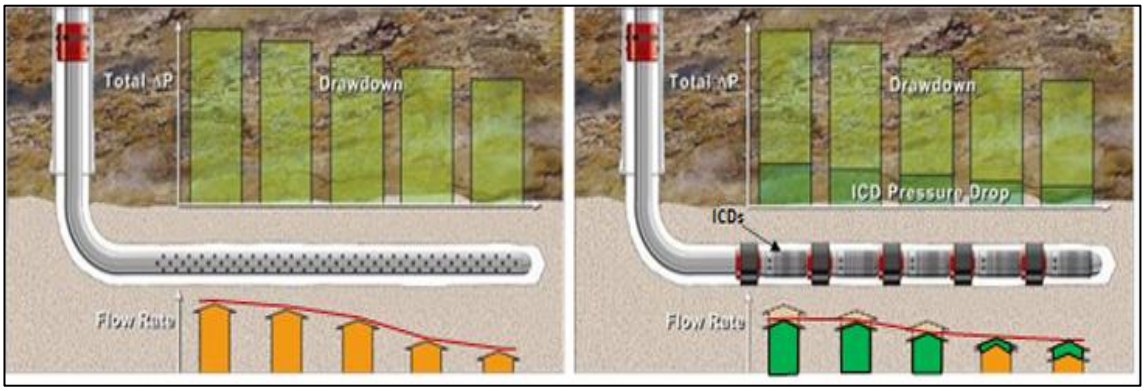

Figure 3-15. Comparison of inflow variation with and without ICDs in a homogeneous reservoir in a well with a strong heel-toe effect. (Courtesy of WellDynamics).

3.4.2 ICD completion in heterogeneous reservoirs

Increasing the reservoir-well contact improves the well productivity, but also results in the greater variation in the reservoir properties being observed along the length of the completion. The details of the magnitude of the observed changes in hydrocarbon saturation, formation permeability, reservoir pressure, etc. can rarely be predicted along the length of the completion in advance of drilling the well. Experience shows that the more productive completion zones often experience earlier water or gas breakthrough, resulting in the well's oil recovery being reduced due to this rapid increase in the level of unwanted fluid produced. Figure 3-16 illustrates how large volumes of unrecovered oil can remain in the poorer producing zones. Varying specific well productivity along the length of the completion can also result in crossflows between the annulus and tubing or high flow rate along the annulus. Inflow rate variation can thus reduce the well's added value expected from the extra reservoir-well contact. The expected well performance can be compromised but this can be addressed by changing the design of the completion.

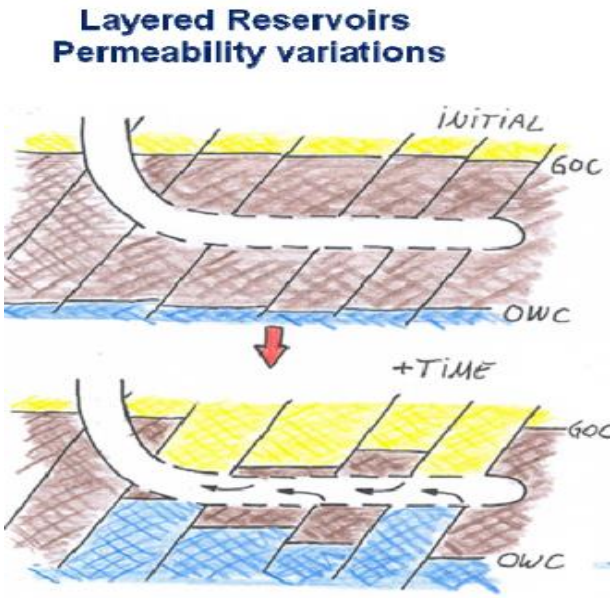

Figure 3-16. Heterogeneous reservoir flow affected by the inflow variation in the well (Vela et al., 2011).

A better-balanced water/gas flood front results in a higher sweep efficiency and improved well and reservoir performance. The extra pressure drops generated by the ICD completion suppresses the effect of the reservoir heterogeneity by reducing the flow rate from the more productive layers and increases the recovery from the less productive zones/layers (Figure 2-6).

An ICD completion can have the additional advantage (F. Al-Khelaiwi *et al.*, 2010b) of being more effective than Inflow Control Valves when rapid changes in the local inflow rate are observed along the length of the completion due to the potentially finer discretisation of the flow control zones by installing more ICDs and annular flow isolation (packers).

3.5 ICD design objectives and options

ICD design aims to redistribute inflow/outflow along the well length, i.e. inflow profile alteration (Al-Khelaiwi *et al.*, 2010a). The idea is to regulate the flow, to some extent, to obtain the flow profile which will give desirable results, e.g. higher recovery, lower water cut, etc., (Daneshy *et al.*, 2012). The problem is to guess what kind of flow profile that should be. The two ideal (though rarely achievable), expected profiles reported are the flat (uniform inflow) profile and the U-flow (U-shaped, uniform coning) profile. This section will describe the profile selection methods for the heel-toe dominated profile case. Similar approaches can be applied to a well with inflow variation due to a heterogeneous reservoir.

1. Uniform Flow (U-Flow) design objective

   The objective is to achieve a uniform inflow along the well, by modifying drawdown with additional, completion pressure selectively along the well, at least at the start of the production. This approach is intuitive, reliable and currently the most popular ICD design method when the varying ICD size along the completion is allowed {which is less common compared to the constant size (or 'strength') ICD designs}. The idea is that every part of the well should give an equal flow contribution. For example, in a well with HTE problem, the heel section that is exposed to larger drawdown is completed with ICDs having stronger restriction, while the toe section is completed with weaker ICDs (figure 3-17 left). The flow distribution when well is completed with such designed ICD completion should look like a flat line as if the well has no heel-toe effect (figure 3-17 right). This method is reported in various publications (Garcia *et al.*, 2009; Marzooqi *et al.*, 2010; Zadeh *et al.*, 2012; Akbari *et al.*, 2014).

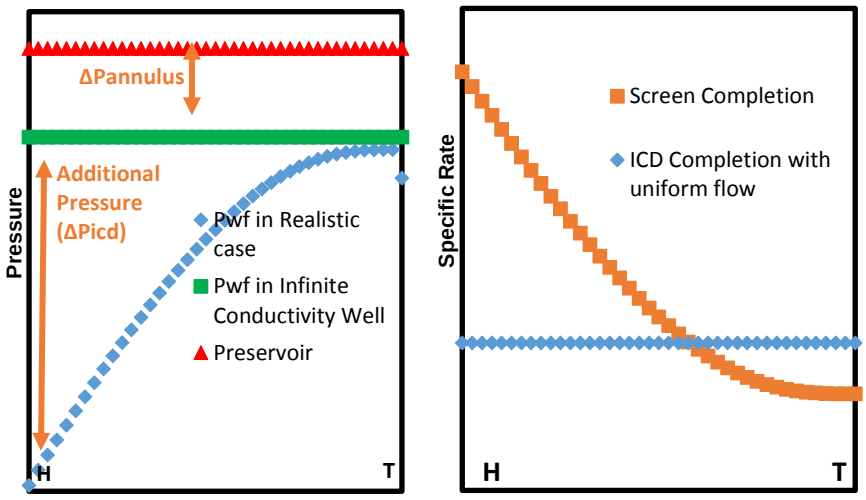

Figure 3-17 (left). Required additional pressure to create a uniform inflow profile in a well with a dominating heel-toe effect. The HTE is translated to pressure drop required across the ICDs. Figure 3-18 (right). Heel-Toe inflow profile (orange) is evened with this ICD completion (blue).

2. U-flow design objective

When the horizontal well is completed there is an edge effect: the flanks are exposed to larger drainage areas and governed by elliptical flow (Daneshy *et al.*, 2012). This effect will make the flow potential of the heel and toe section greater than the other sections (Shi *et al.*, 2016) and (Daneshy *et al.*, 2012). In these cases, applying the uniform flow ICD design would limit the real potential of those flank sections (Lim, 2017). On the contrary, the required additional pressure drop across the ICDs should allow, to some extent, flow irregularity in the flanks sections, since higher flow contributions in flanks are expected (figure 3-18 left). The required ICD pressure drop would be designed to deal with such U-shape flow distribution (figure 3-18 right).

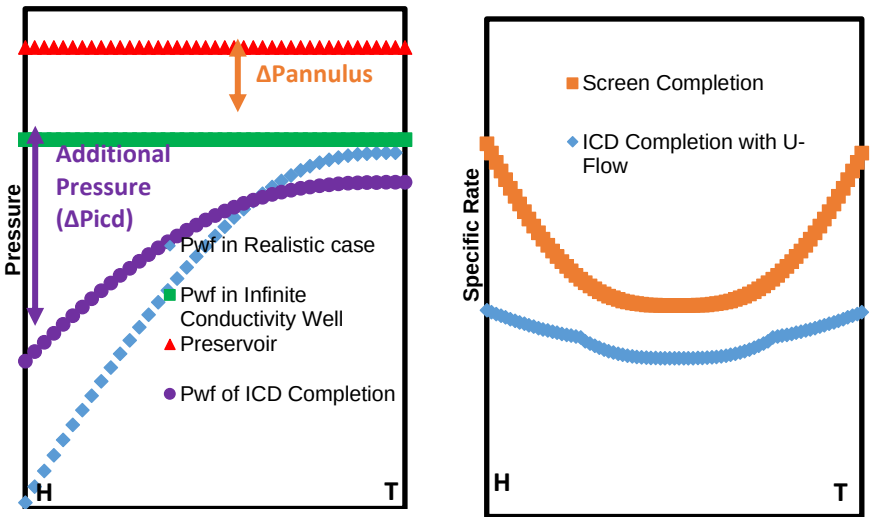

Figure 3-18 (left). Required additional pressure to create a U-low profile in well is translated to pressure drop required across the ICDs. Figure 3-18 (right). U-flow inflow profile (orange) is reduced (controlled) with the ICD completion (blue).

Calculation of the required, additional ICD pressure is key when adjusting the original flow profile to the desired one. This extra pressure loss is then translated to the ICD size.

As mentioned, there are two approaches to selecting the ICD sizes in a given well.

1. Constant size of ICDs installed along the length of the completion interval

   This is the most widely used method due to design and operational simplicity. This method suits the well when there is a lack of geological information and/or the well has a high reservoir uncertainty (Henriksen *et al.*, 2006; Birchenko *et al.*, 2011b; Lim, 2017). It also mitigates the risk of the completion not being run to target depths and ICDs not being set across the correct intervals.

   When completing all segments with constant ICD size (Figure 3-19) the section with higher influx will automatically have higher restriction/pressure drop. This is beneficial since such completion would act as self-regulating when the exact position of high productivity layers is unknown or can change. On the other hand, this method also causes unwanted (though lower) restriction across the low-influx zones.

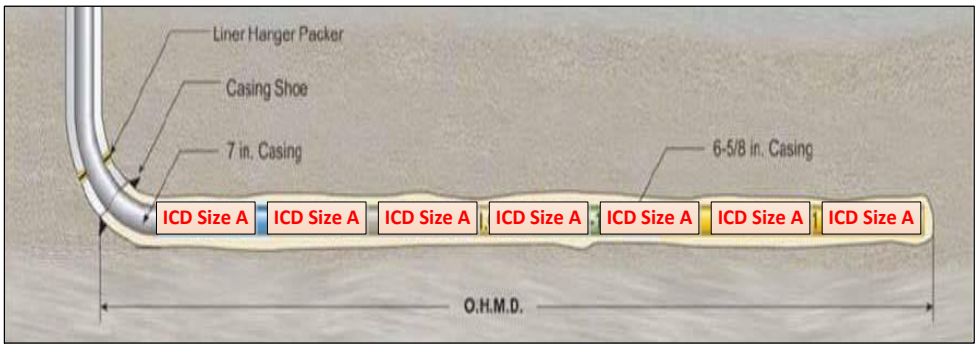

Figure 3-19. Illustration of constant ICD size completion

2. Variable ICD size along the length of the wellbore

   This method uses different ICD size, optimised for different well sections Figure 3-20). Compared to the constant size approach, this method is more efficient since the zones with lower influx (and/or the ones that do not pose a risk of early breakthrough) are completed with low or no restriction ICD strength (El-fattah *et al.*, 2013; Fu *et al.*, 2014). By contrary, an aggressive restriction will be located across the zones with high influx. This can achieve better equalisation with a lower PI reduction. This method, however, requires accurate reservoir information, and the room for error is small. This method requires more complex execution and completion placement at the wellsite.

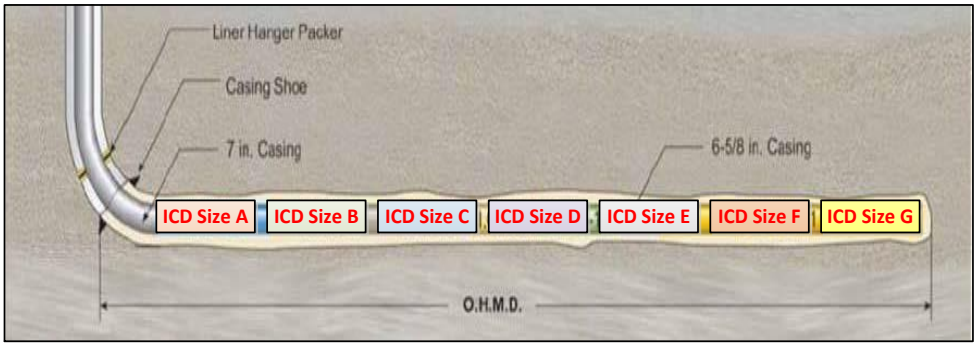

Figure 3-20. Illustration of the variable ICD size in all segments.

Finally, the workflow to calculate the right ICD size depends on which of these completion methods is selected. Below we discuss several available ICD sizing methods.

1. Design of Variable strength ICD completion to achieve uniform inflow from a homogeneous reservoir

   The workflow is as follows: the original drawdown (i.e. assuming open-hole

completion) in each segment, $\left(\overline{\mathrm{P}} - \mathrm{Pwf}_{(\mathrm{x})}\right)_{\mathrm{screen}}$ is calculated. Then the ICD size is designed with the objective to create an equal drawdown along the well (to achieve equal flow assuming the reservoir pressure is uniform) at the start of the production. The toe section is used as the reference point as it experiences the lowest drawdown, i.e. the target specific inflow rate is calculated for the toe first. This is done by assigning the target well rate and/or its operating BHP. Finally, the selection of ICD size is commenced from the heel, which is the section with largest original drawdown.

$$\Delta Picd_{Heel} = (\bar{P} - Pwf_{Heel}) - J_s(x)(\bar{P} - Pwf_{Toe}) \qquad (3\text{-}15)$$

Where $\Delta Picd_{Heel}$ is the ICD pressure drop at the heel section, $\bar{P}$ is the average reservoir pressure, $Pwf_{Heel}\ and\ Pwf_{toe}$ are the flowing bottom-hole pressure at the heel and toe section respectively.

After the heel the next adjacent segment is now considered, and the required pressure drop for the section is calculated with equation 3-15. This process is repeated for the rest of the wellbore until the flow in every segment is the same. Once the ICDs are installed then the overall well's rate is reduced – this is the price for unform inflow. Finally, the resulting well's Productivity Index is evaluated (In this study the BHP refers to the pressure inside the tubing at the heel, and so the well PI accounts for the pressure drop across the ICD completion), thus if it is unsatisfactory, the workflow can be repeated by assuming a higher rate or larger drawdown. This workflow is illustrated in Figure 3-21. More about this workflow is explained in Al-Khelaiwi (2013).

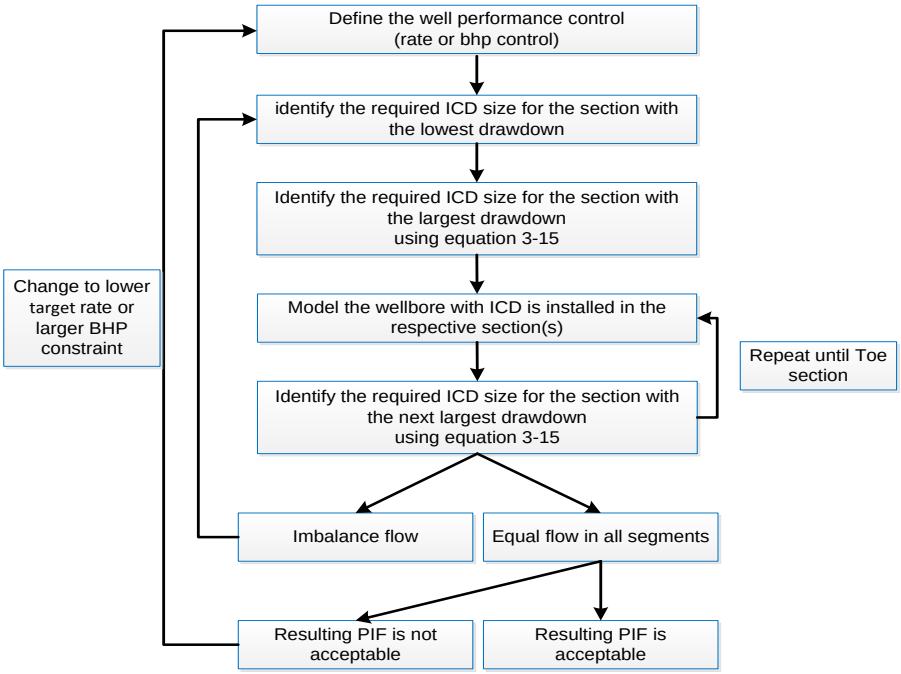

Figure 3-21. Workflow to achieve uniform inflow with variable strength ICDs

2. Design of variable strength ICD completion to achieve U-Flow

   The process is similar to the uniform flow method, whereby ΔP_{ICD} is calculated sequentially for each segment. The main differences are:

   - The specific PI along the well is not constant. The part of the well with higher influx is termed as H, and part with low-influx is termed as L.
   - The objective is to achieve a controlled U-flow (termed as U) along the well.

   The workflow follows the same steps as in Figure 3-21, estimating the desired influx from the lowest production interval, and then instead of starting from the heel section, this method initiates by calculating the ICD size in the higher influx section, Q_H, which could be either in the heel or in the toe. It follows sequentially towards the section with the lowest influx. The exact shape of the desired U-profile can be based on various parameters, such as the ones related to the semi-radial flow in the flank sections, breakthrough time, or drainage area (Daneshy *et al.*, 2012; Lim, 2017)

3. Design of constant strength ICD completion to promote a more even flow

   In this method the calculation of $\Delta Picd$ per segment is not required anymore, reducing the complexity of the workflow. The workflow is basically an iteration

process from the weakest to the strongest restriction strength, whereby the level of flow equalization is evaluated for each iteration. If the resulting PIF is unsatisfactory, the process is repeated again with reduced target flow rate or a larger operating drawdown. The workflow is shown in Figure 3-22. More about this workflow is explained in Al-Khelaiwi (2013), Lim, (2017).

4. Design of constant strength ICD completion to promote U-Flow

   The method is similar to the above but requires that in each iteration the resulting flow equalisation creates a better U-flow than the original U-flow distribution. This implies that there is a desired level of U-flow that gives lower WC, higher recovery, etc. More about this workflow is explained in Daneshy *et al.*, (2012), Al-Khelaiwi (2013), Lim, (2017).

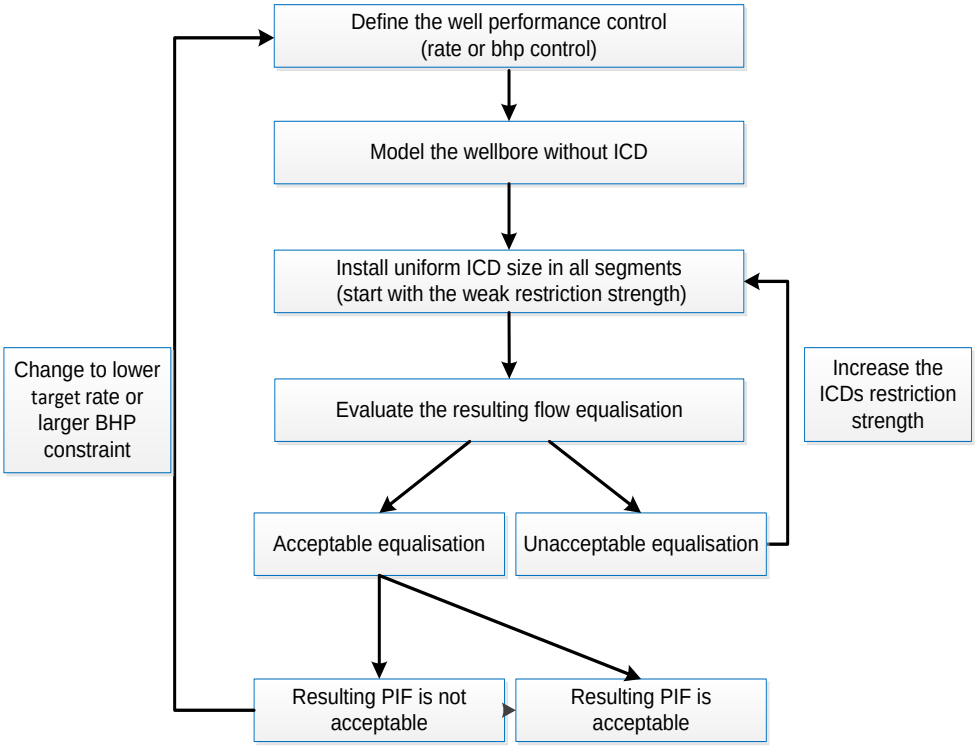

Figure 3-22. Workflow to achieve a more uniform flow with constant strength ICDs

These workflows (Figure 3-21 and Figure 3-22) ideally should consider calculation of flow in the tubing, annulus and the well/reservoir interface. This task is typically performed in a numerical wellbore simulator, such as NETool (Halliburton, 2012) that use a network modelling approach to model well flow performance.

An ICD design workflow should find a compromise between the benefits and the drawbacks of an ICD completion. On one hand, the ICD completion improves the inflow rate distribution, but on the other it reduces the well's Productivity Index (PI) by adding an extra pressure drop. The design's challenge is to manage this additional pressure drop without excessively reducing the well's PI. This relationship requires a reliable method of estimation. It also needs to be able to answer questions like:

- When can the ICD completion add value or is feasibility?
- What is the performance forecast of the ICD completed well?
- Is there a quick tool or simple rules available for completion redesign to accommodate for potential operational issues, such as alternative design if the logging tool revealed a different reservoir permeability or severe loss of circulation in an interval, etc.?
- How to perform verification of numerical simulation results?
- How to produce an initial guess design before going to a more details analysis?

Below in this chapter we present an integration of analytical modelling of wells with ICDs and the type-curve methodology that can be used to design and optimise the ICD completion. This workflow is simple, requires minimum computational power to analyse and make the necessary ICD size adjustment based on the latest, more accurate information from the open-hole logging. The objective follows those suggested by previous studies (Joshi, 1991; Hill and Zhu, 2008; Birchenko, Usnich and Davies, 2010) suggested to compose a quick-look analysis of an ICD completion performance.

The proposed methodology will be further evaluated by the wellbore numerical simulator, NETool, the most widely used platform in the industry for wellbore modelling of an ICD completed well (Halliburton, 2017). The presented methods will be thoroughly explained and summarised in a workflow that provides a rapid decision-making tool. The application of the workflow will be illustrated on a synthetic oil-rim reservoir mimicking a larger North-Sea oil field. Several scenarios illustrate the range of studies that can be possible carried out without running a reservoir simulator. A comparison will be made between the proposed simplified design workflow and the comprehensive results from a NETool numerical simulation to support this new workflow.

3.6 Analytical Modelling of Flow in Wells with ICDs

The full analytical derivation of inflow performance in ICD completions is provided in (Birchenko, 2010). Illustrated by figure 3-23, It extends the equation 3-3 with the non-linear pressure drop across the ICDs. For a unit length of a well, the pressure drops across reservoir and ICDs can be expressed via the specific inflow rate (U) and specific ICD strength a:

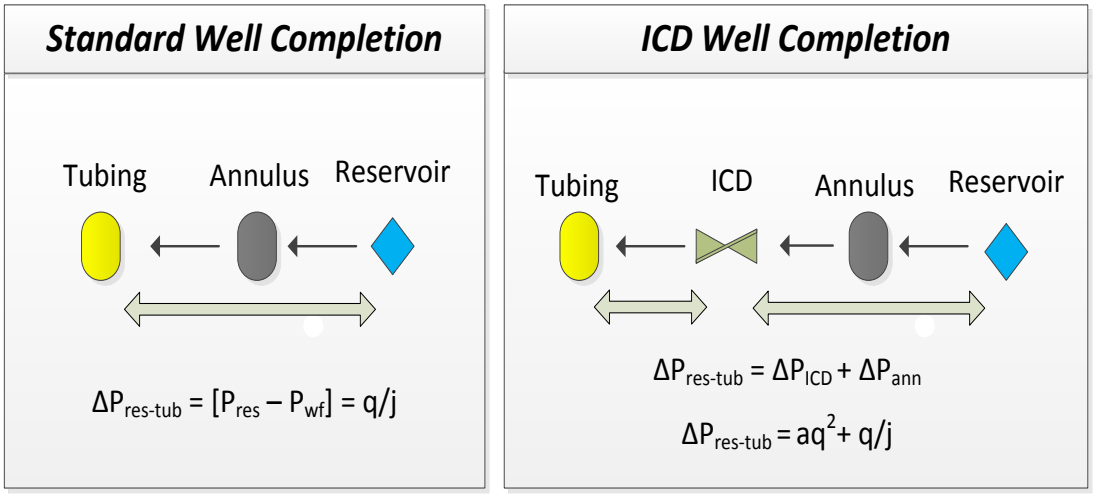

Figure 3-23. Nodal pressure analysis for a standard well (left) and an ICD well completion (right). The ICD's pressure drop is not linearly related to the flow velocity

$$\Delta P(l) = \Delta P_{icd}(l) + \Delta P_{ann}(l) = a(l)U^2(l) + \frac{U(l)}{J(l)} \qquad (3\text{-}16)$$

Where $\Delta P_{ICD}(l)$ is the pressure drop across the ICDs, $\Delta P_{ann}(l)$ is drawdown pressure between the reservoir and the annulus, a is the specific ICD strength, U(l) is the specific inflow rate, and ΔP (l) is the total drawdown pressure between reservoir and the tubing.

Note that the specific parameters above are measured per unit length.

Equation 3-16 is a quadratic equation describing the specific flow rate, U(l), with two real roots. Since the negative roots has no physical meaning in this well problem, the solution for U(l) is taken as the positive root:

$$U(l) = \frac{-1+\sqrt{1+4.\Delta P(l).a(l).j(l)^2}}{2.a(l).j(l)} \qquad (3\text{-}17)$$

Several assumptions have been made:

1. The Productivity Index (j) equation describes a linear flow from the reservoir to the sandface
2. The well is completed with a uniform ICD strength completion.
3. The produced fluid is incompressible.
4. There is no flow in the annulus or in the reservoir parallel to the well (perfect annular flow isolation and negligible axial flow in the reservoir).

The total production rate q_w is a summation of specific inflow, $U(x)$ over well length (L):

$$q_w = \int_0^L \frac{-1+\sqrt{1+4.\Delta P.a(l).j(l)^2}}{2.a(l).j(l)} \tag{3-18}$$

(Birchenko, Muradov and Davies, 2010) extended this formulation to quantify the reduction of the heel-toe effect by ICDs in homogeneous reservoirs (i.e. assuming uniform j distribution, no U-flow effects). The new analytical model adopts equation 3-10, to parameterize the level of heel-toe effect with ICD installation, named ICD number. This new dimensionless number is derived for production cases with two well production constraints: the well rate constraint, and the BHP constraint.

$$\begin{cases} I_q = \frac{C_f \rho f B^2 j L^2 q_w}{\left(2aj q_w/_L + 1\right) D^5} \ (for\ Rate\ Constraint) \\ I_p = \frac{C_f \rho f B^2 j^2 L^3 \Delta P_{ann}^{heel}}{\left(2aj^2 \Delta P_{ann}^{heel} + 1\right) D^5} \ (for\ Pressure\ Constraint) \end{cases} \tag{3-19}$$

The important solutions from this model is summarised in the following table:

Table 3-3. Summary of the solutions for ICD performance in wells with dominating heel-to effect.

	Rate constraint	**Pressure constraint (annulus drawdown)**
Boundary condition counterpart	$\Delta P_w = \Delta P_{ann}^{heel} = aU^2(heel) + \frac{U(heel)}{J(heel)}$	$q_w = J\Delta P_{ann}^{heel}\sqrt{\frac{1.5}{(1+I_p)}}$

Segment rate	$U(l) = \frac{q_w}{L}\sqrt{\frac{2I_q}{3}\left(\frac{q(l)}{q_w}\right)^3 + G_q}$ Where : $G_q \approx \left(1 + 0.1647I_q + 0.001793\left(I_q\right)^2\right)^{-1}$	$U(l) = j\Delta P_{ann}^{heel}\sqrt{(1-G_p)\left(\frac{l}{L}\right)^3 + G_p}$ Where : $C_q \approx \left(1 - \frac{H_p}{(1.5 + I_p)}\right)$

Where l is the length of the well from the heel, D is the tubing inside diameter, J_s is the specific sandface PI, C_f is the conversion factor, ρ is the fluid density, f_a is the average friction factor, B is the formation volume factor, ΔP_w is the drawdown in the heel section, a is the ICD strength. As previously equations these equations are defined per unit length of the well.

Birchenko also derived a solution for ICD completion performance in a heterogeneous reservoir. His solution required one more assumption.

5. The bottom hole pressure $\{P_{wf}(l)\}$ is constant across the production interval since we assumed that the frictional pressure losses (heel-toe effect) can be neglected compared to the variable influx effect from a medium-to-high heterogeneous reservoir.

The expression of a production rate in a well completed with ICDs in a heterogeneous reservoir is the same as above, except ΔP_w is now independent of the location:

$$q_w = \int_0^L \frac{-1+\sqrt{1+4.\Delta P_w.a.j^2}}{2.a.j}\,dl \qquad (3\text{-}20)$$

Equation 3-20 needs to be integrated over the spatial permeability distribution. The solution for this integration is mathematically complicated. It is easier to describe the spatial permeability distribution using the statistical distribution (η) and then since the integration is an additive operation where the order of the integrated parts does not matter, the production rate of well completed in heterogeneous reservoir can be calculated as:

$$q_w = L\int_{j1}^{j2}\left\{\frac{-1+\sqrt{1+4.\Delta P_w.a.j^2}}{2.a.j}\right\}\eta(j).dj \qquad (3\text{-}21)$$

Where j_2 and j_1 represent the maximum and minimum j of the j distribution along the well in question.

3.7 Proposed method for ICD completion design in a homogenous reservoir

This solution uses the assumptions listed in section 3.6, together with several parameters that have been explained earlier:

1. Horizontal number. H_p and H_q

Hp and Hq describe the level of Heel-Toe-Effect due to friction {equation (3-10)}. This parameter explains the condition of well before ICD has been installed, e.g. when a non-restrictive, screen or open-hole completion was used.

2. ICD number. I_p and I_q

Ip and Iq describe the reduction of Heel-Toe effect after installing ICD completion. When the ICD strength is negligible such as e.g. in the screen completion, the ICD well number has the same value as the horizontal number. Birchenko *et al.* (2010) derived solutions for two production constraints: constrained well flow rate and constrained pressure. New, equivalent solutions that Birchenko derived are:

Rate constrained production:

The ICD number is described in equation 19a. Since we are interested in finding the required ICD size, we'd like to find the explicit expression for a (the ICD strength) before converting this number into the ICD equipment design parameter of the nozzle diameter or the channel strength.

One can invert the equation 3-19a such that:

$$a = \frac{\left(C_f \rho f B^2 j L^3 q_w / I_q D^5 - L\right)}{2 j q_w} \; (for\ Rate\ Constraint) \qquad (3\text{-}22)$$

Pressure constrained production:

Birchenko *et al.,* (2010) derived solutions for the pressure constrained production case, where the boundary condition is the given drawdown in **the annulus at the heel** (ΔP_{ann}^{heel}), which reflects for example sand production-related limit.

In this thesis we use a similar approach to the above but uses a different boundary condition that is more commonly practiced by production engineers, that is to set the

minimum wellbore flowing pressure in the tubing (Pwf) at the heel as the boundary condition. For example, this is needed in order to be able to lift the fluids to surface. **One novelty of this chapter is that the well will now be constrained by the total drawdown between the reservoir pressure and the tubing flowing pressure, ΔP_w.**

A solution for this condition is derived as follows:

- Recall the ICD number for pressure constrained well described in equation 19b
- Substitute ΔP_{ann}^{heel} with equation 3-16 & 3-17:

$$\Delta P_{ann}^{heel} = \Delta P_w - \frac{\left(\sqrt{1+\alpha\Delta P_w}-1\right)^2}{\alpha} \tag{3-23}$$

We can now write the new ICD number for the tubing pressure constrained well:

$$I_p = \frac{C_f \rho f B^2 j^2 L^3 \left(\Delta P_w - \frac{\left(\sqrt{1+\alpha\Delta P_w}-1\right)^2}{\alpha}\right)}{\sqrt{1+\alpha\Delta P_w}\, D^5} \tag{3-24}$$

Where $\alpha = 4aj^2$

The relationship between the ICD strength (a) and ICD number in the pressure constraint scenario (Ip) is non-linear and requires simplification. This was not required for the rate constrained solutions.

Equation 3-19b can be modified such that:

$$\beta \equiv 2\left(a + \frac{1}{2j^2\Delta P_{ann}^{heel}}\right)$$

Where the $\beta = \frac{C_f \rho f B^2 L^3}{I_p D^5}$

We can now write equation 3-19b as:

$$\beta \equiv \frac{2a\sqrt{1+4aj^2\Delta P_w}}{\left(\sqrt{1+4aj^2\Delta P_w}-1\right)}$$

The solution can be simplified and formed as a cubic equation:

$$(16j^2\Delta P_w)a^3 + (4 - 16j^2\Delta P_w\beta)a^2 + (4j^2\Delta P_w\alpha^2 - 4\beta)a = 0$$

The physical solution for the above cubic equation above is:

$$a = \frac{\left(4j^2\Delta P_w\beta - \sqrt{8j^2\Delta P_w\beta + 1}\right) - 1}{8j^2\Delta P_w} \; (for\ Pressure\ Constraint) \qquad (3\text{-}25)$$

With this solution, the specific ICD strength a is now expressed as an explicit function of ΔP_w. The full derivation is explained in Appendix A.

3. Productivity Error, E_p

This parameter had been already explained in section 3.2.2. It quantifies the mismatch between the infinitely conductive wellbore production rate and the one where frictional pressure drop along the well is considered. Recall equation 3-9:

$$Ep = \frac{(q_{nofriction} - q_w)}{q_{nofriction}}$$

This parameter describes the reduction in productivity due to both friction and the additional pressure drop across the ICDs when applied to an ICD completed well.

4. Drawdown Ratio. R_d

The parameter has been described in section 3.2.2. It designates the ratio of drawdown between the heel and toe sections. (Equation 3-7).

$$Rd = \frac{\Delta P_{Toe}}{\Delta P_{Heel}}$$

Joshi and Hill and Zhu thoroughly explained the meaning of the drawdown ratio parameter. The friction effect will cause the drawdown ratio to be lower than 1. This means a higher influx at the heel in homogeneous reservoir, earlier water breakthrough, higher water cut, lower recovery. Rd is improved when the well is completed with ICDs. Rd is thus a representative of the **inflow uniformity**.

The relationship between these 4 parameters was plotted for several different production cases in homogeneous reservoirs. The reservoir-well configurations can be simplified into the dimensionless parameters Iq (equation 19a) and Ip (Equation 24). These dimensionless parameters are used to represent the friction effect in a well.

This relationship is illustrated in Figure 3-24 to Figure 3-27. The ICD completion is

installed in each scenario to reduce the HTE (and consequently to reduce the Horizontal/ICD number). The sensitivity to various ICD strengths is presented with different values of Rd and Ep (equations 3-7 and 3-9). They are based on pressure drawdown constraint, where flow rates are calculated based on table 3-5 top-right. The numerical modelling was performed with the numerical simulation (NETool wellbore simulator) to validate the analytical prediction.

We showed that HTE in a long horizontal well installed with small production tubing diameter ('long-small') is not necessarily high, but depends on the reservoir permeability (case 3 and 4 in table 3-4). On the contrary, a short-length, big-diameter ('short-big') wellbore when completed in a low permeability reservoir it requires high reservoir drawdown to produce at a given rate resulting in a high friction horizontal number (case 1 and case 2 in table 3-4).

Table 3-4. Homogeneous reservoir properties for validation

			Case 1	Case 2	Case 3	Case 4
Specific PI	J	*Sm3/day/bar/m*	**1**	**1**	**10**	**10**
Well's length	L	*m*	**100**	**1000**	**100**	**1000**
Well's PI	j	*Sm3/day/bar*	**100**	**1000**	**1000**	**10000**
Completion internal diameter	D	*inch*	**8.85**	**5.9**	**8.85**	**5.9**
Absolute Roughness	e	*mm*	**5**	**5**	**5**	**5**
Reservoir Drawdown	ΔP	*bar*	**575**	**2.3**	**500**	**0.22**
Hp			**0.75**	**8.4**	**23.9**	**75**

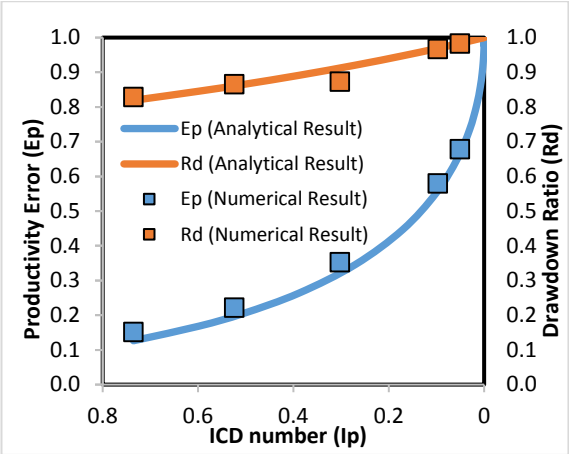

Figure 3-24. Case 1. Short–big bore completion in a low permeability reservoir. Hp = 0.75

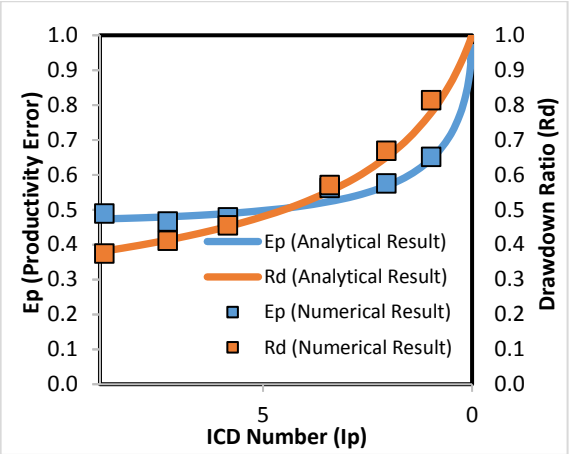

Figure 3-25. Case 2. Long–small bore completion in low permeability reservoir. Hp = 8.8

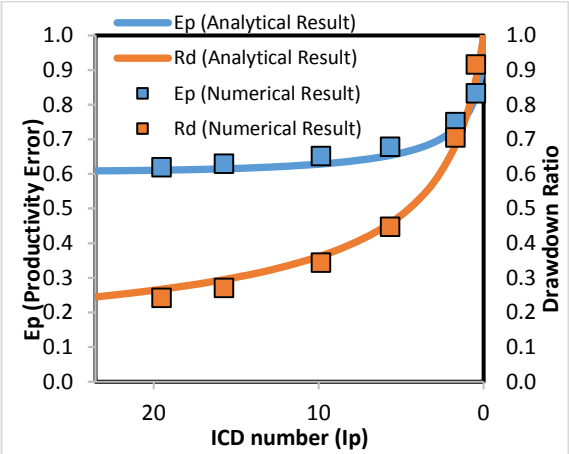

Figure 3-26. Case 3. Short–big bore completion in high permeability reservoir. Hp = 23.9

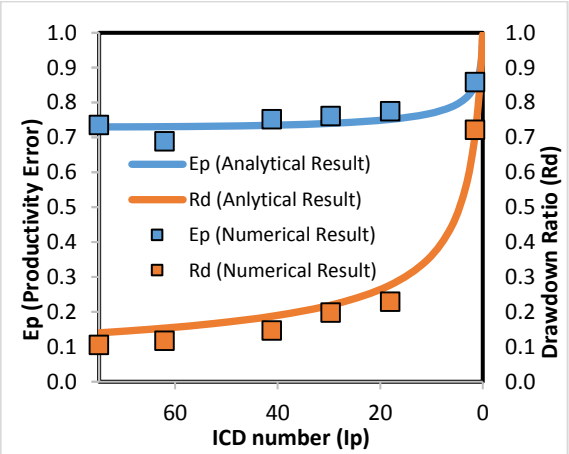

Figure 3-27. Case 4. Long–small bore completion in high permeability reservoir. Hp = 75

Heterogeneous reservoir properties.			
Reservoir Heterogeneity	*IVoh*	**0.39**	
Permeability Distribution		**Log-normal**	
Well length (Original plan)	*L*	**1000**	m
Completion internal diameter	*D*	**0.15**	m
Well's min PI	*J1*	**0.016**	Sm^3/day/bar
Well's average PI	*Jm*	**0.026**	Sm^3/day/bar

Well's max PI	*J2*	**0.036**	Sm^3/day/bar
Segment Length	l_{icd}	**25**	m
In-situ fluid density	ρ	**840**	kg/m^3
In-situ fluid viscosity	μ	**2.3**	Cp
Formation volume factor	*B*	**1.2**	Rm^3/Sm^3

The reduction of HTE after installing ICDs (the higher the strength the smaller is the ICD number) can be clearly seen in the above figures: the smaller the ICD strength gets the closer the drawdown ratio approaches 1 – uniform inflow. The productivity error also increases, showing a higher deviation between the open-hole production rate and the ICD-completed one as the strength increases. A well with an infinitely high ICD restriction (corresponds to the ICD number of 0) would be perfectly equalised (with Rd = 1), but the well's PI is reduced to a very low value and essentially the well will not flow (Ep = 1). In other words, a constant ICD size completion can only achieve absolutely uniform inflow when the inflow is muted. In practice, the inflow uniformity level is subject to how much well productivity can be sacrificed. The results for these 4 cases are all re-plotted in one semi-log graph in Figure 3-28.

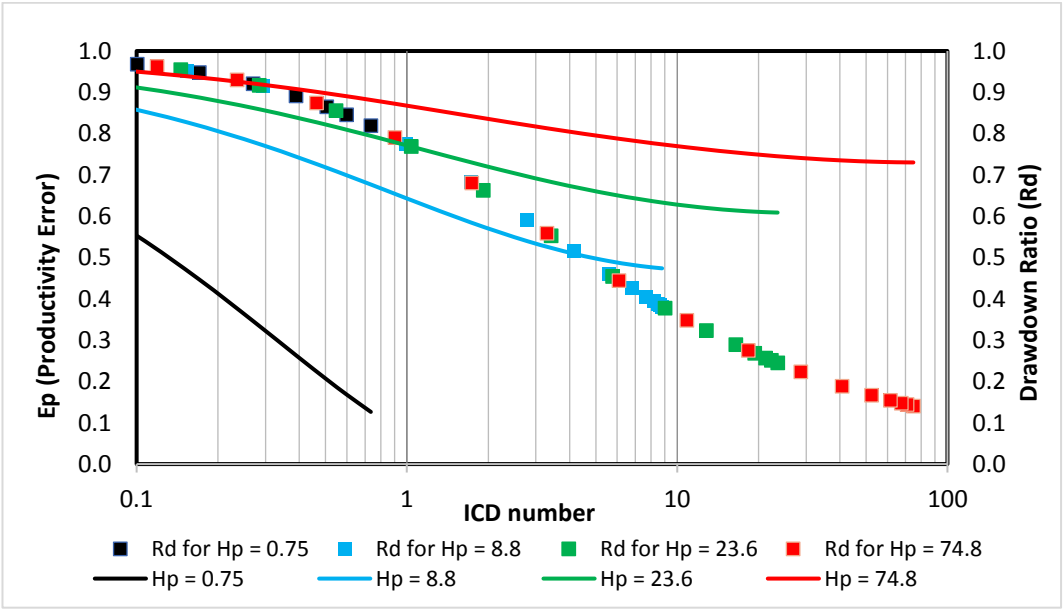

Figure 3-28. Comparison for different cases of ICD completion performance in homogeneous reservoirs, covering the range low HTE to high HTE. The solid lines show Ep for various cases.

It is observed further that relationship of some of these 4 parameters, e.g. Rd vs Ip, is universal. A universal type curve to represent the ICD completion performance in a

homogeneous reservoir can be drawn (figure 3-29 and 3-30) for a pressure constrained and rate constrained well production respectively.

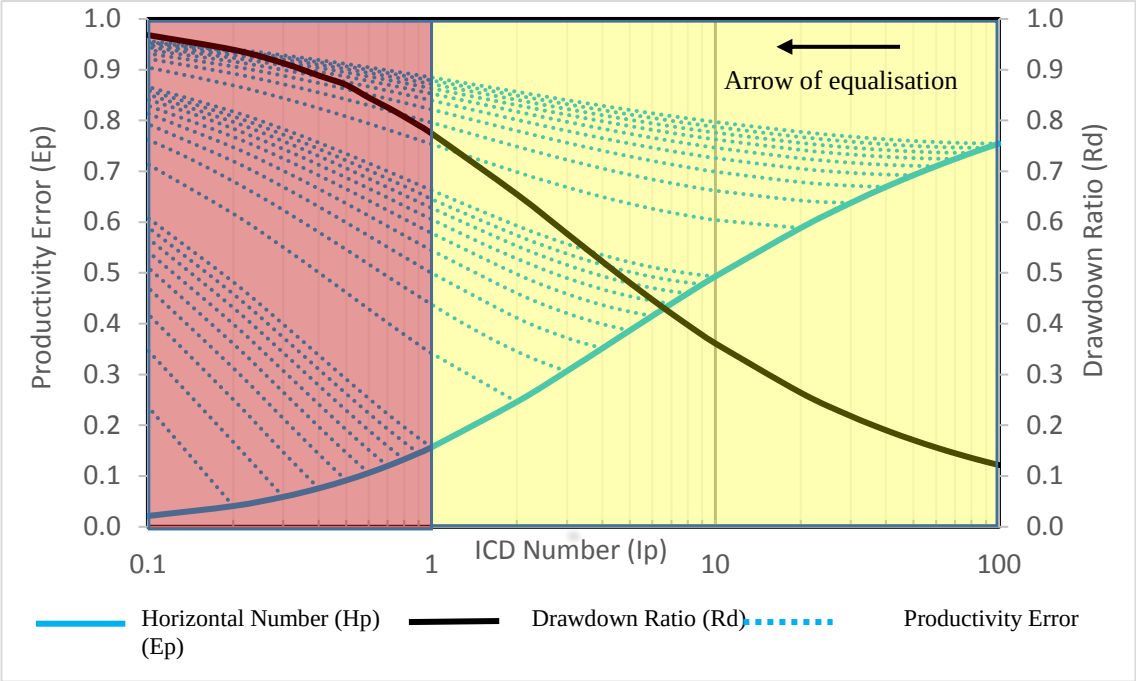

Figure 3-29. Type Curves of ICD completion performance for a pressure constrained well in a homogeneous reservoir.

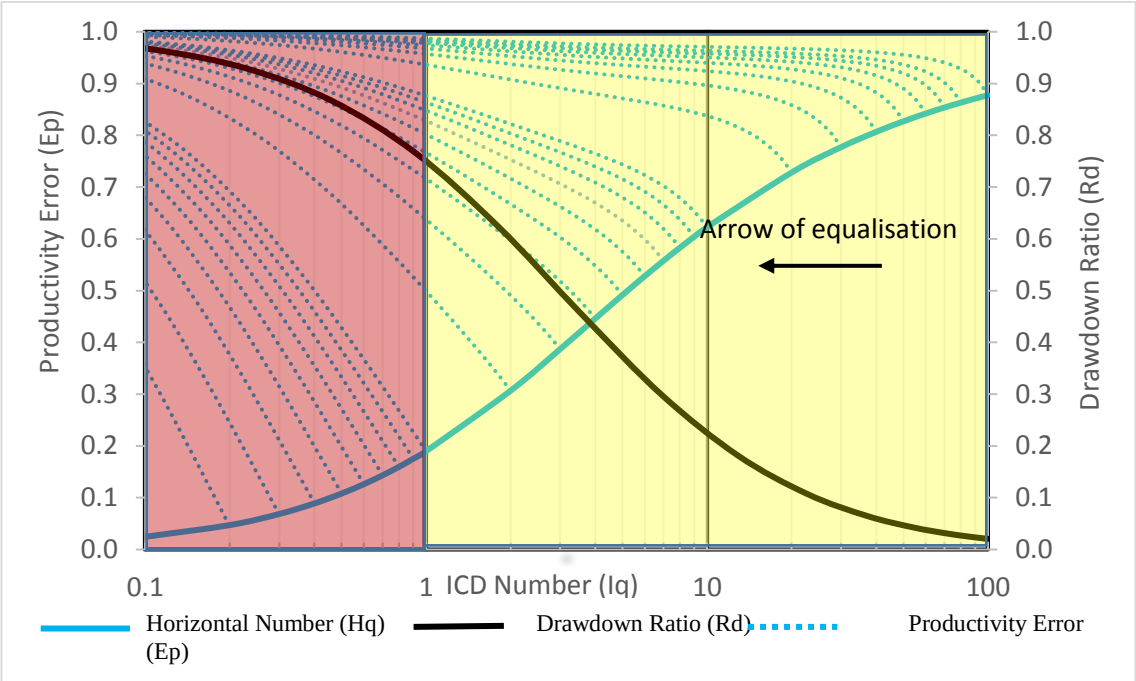

Figure 3-30. Type Curves of ICD completion performance fora production rate constrained well in a homogeneous reservoir

It can be seen that:

1. The relationship between the ICD completion strength and the reduced productivity is specific for each heel-toe case. This is reflected by the specific Ep vs Ip curves for a specific Hp (or Ip when ICD strength (a) = 0, i.e. screen or open-hole completion) value.
2. The relationship between the ICD completion strength and the reduction in inflow non-uniformity is universal. This is reflected by the same curve of Rd vs Ip for all Hp (or Ip when ICD strength (a) = 0, i.e. screen or open-hole completion) values.

Table 3-5. Summary of parameters informed by type-curve analysis to design ICD completion performance in wells with the dominating heel-toe effect such that Hp or Hq >5.

	Rate constrained	**Pressure constrained**
	$\Delta P_w = aU^2(heel) + \frac{U(heel)}{J}$	$q_w = J\Delta P_w - \frac{\left(\sqrt{1+\alpha\Delta P_w}-1\right)^2}{\alpha}\sqrt{\frac{1.5}{(1+H_P^{ICD})}}$
Horizontal number	$H_q = \frac{C_f \rho f_a B^2 J_s L^2 q_w}{D^5}$	$H_p = \frac{C_f \rho f_a B^2 J_s L^3 \Delta P_w}{D^5}$
ICD number	$I_q = \frac{C_f \rho f B^2 j L^2 q_w}{\left({}^{2ajq_w}/_{L} + 1\right) D^5}$	$I_p = \frac{C_f \rho f B^2 j^2 L^3 \left(\Delta P_w - \frac{\left(\sqrt{1+\alpha\Delta P_w}-1\right)^2}{\alpha}\right)}{\sqrt{1+\alpha\Delta P_w}\, D^5}$ *Where* $\alpha = 4aj^2$
Drawdown Ratio	$R_d = \frac{\Delta P_{Toe}}{\Delta P_{Heel}}$	
Productivity Error	$E_p = 1 - \frac{PI_{ICD}}{PI_{nofriction}}$	
Required ICD Strength	$a = \frac{\left({}^{C_f \rho f B^2 j L^3 q_w}/_{I_q D^5} - L\right)}{2jq_w}$	$a = \frac{\left(4j^2\Delta P_w\beta - \sqrt{8j^2\Delta P_w\beta + 1}\right) - 1}{8j^2\Delta P_w}$

		$Where\ \beta = \frac{C_f \rho f B^2 L^3}{I_p D^5}$
ICD size	$a_{channel} = \frac{(\rho\ \mu_{cal})^{\frac{1}{4}}}{(\rho_{cal}\ \mu)} \frac{\rho_{cal}}{\rho} \sqrt{l_{ICD} B} \Big/ a$ (ICD Channel type) $Nozzle\ diameter = \sqrt[4]{\frac{C_u \rho l_{ICD}^2 B^2}{C_d^2 a}}$ (ICD Nozzle type)	

The procedure to use these type-curves for a well completion design is:

1. Calculate the open-hole heel-toe effect dependant horizontal number {Hp and Hq when ICD strength (a) = 0}.
2. Find the desired ICD size using curves (Ip, Iq) vs. the target inflow equalisation (Rd) and reduced productivity (Ep) than can be afforded for the properties of the reservoir and the tubing size.

Alternatively, (Birchenko, Muradov and Davies, 2010) proposed the "rule-of-thumb" for ICD size selection. He suggested that the pressure drop across the ICDs should be of the same order of magnitude as the drawdown to make effect:

$$\Delta P_{ICD} \approx \mathrm{n}\Delta P_{ann}^{heel} \tag{3-26}$$

$$a \approx \frac{\mathrm{nL}^2}{\Delta P_{ann}^{heel} J^2} \tag{3-27}$$

$$\text{Where n} \approx \left(1/Rd\right)_{noICD} - 1 \tag{3-28}$$

They did not provide a comprehensive justification supporting this recommendation. The type-curve approach developed here is more comprehensive and clear. These type-curves can be readily used to account for the behaviour of ICD completion in the context of reducing the heel-toe effect.

As mentioned above, the procedure of using the type-curve analysis is started by identifying the HTE level for a given horizontal well (Hp or Ip when a = 0, Hq or Iq when a = 0). The selected Hp/q will correspond to a certain value of Rd (depicted as the bold, blue curve) and Ep (the bold, black curve) in figures 3-28 and 3-29. The (black) 'arrow of equalisation' in these figures is a realistic physical description of the ICD-completion impact on the well performance, showing that installing ICD should reduce the HTE, while the largest HTE values (Hp/q) are achieved when the well is completed open-hole.

Once the Rd and Ep intersection points have been established, one should follow the curve of Rd and dashed blue curve of Ep for the given Hp/q to evaluate the trade-off between the inflow equalisation and the reduction in the well's PI due to installing ICDs. *Note that the dashed-blue curves of Ep are unique for different Hp/q values (every Hp/q has its signature Ep curve) while the bold-black curve of Rd is universal for all Hp/q values.* This type-curve allows one to perform analysis needed for ICD completion design optimisation.

Take a look at the yellow region in figure 3-28:

- Take the slope of Rd curve, that is Rd value after installing ICD (Rd_{ICD}), {or the intersection point of the Rd (bolded-black) curve against the ICD number (Ip/q)} minus the original Rd value in the open-hole well (Rd_{OH}) {or the intersection point of the Rd (bolded-black) curve against the Horizontal number (Hp/q), or ICD number when a = 0}.
- Take the slope of Ep curve, that is Ep value after installing ICD (Ep_{ICD}) {or the intersection point of the Ep_{ICD} (dashed-blue Curve) against the ICD number (Ip/q)} minus the original Ep value in the open-hole well (Ep_{OH}) {the intersection point of the bolded-blue curve (Ep Curve) against the Horizontal number or ICD number when a = 0 (Hp/q)}.
- We define that efficient flow equalisation is when the long-term gain, indicated by the flow distribution improvement represented by an increasing Rd, can offset its short-term cost, indicated by the reduction of well's PI represented by an increased Ep. That is: $(Rd_{ICD} - Rd_{OH)} \geq (Ep_{ICD} - Ep_{OH})$. Efficient equalisation is covered within this yellow-shaded area.

Take a look at the red region in figure 3-28:

- In this region, the slope of Rd curve is (generally) smaller than the slope of the Ep curve. In other words, the long-term gain indicated by the reduction of Ep is obtained in the expense of larger reduction of well's PI (or increased Ep). $(Rd_{ICD} - Rd_{OH)} < (Ep_{ICD} - Ep_{OH})$. Inefficient equalisation region is shown by this red-shaded area.
- Note that the threshold value for (In)efficient equalisation, Ip = 1 is chosen as a practical purpose to ease the use of this type-curve. More accurate calculation can be obtained by solving the mathematical models presented in appendix A.

The ICDs with moderate strength, e.g. for the cases with Hp>5 this means the curves in the yellow shaded area (Hp >1) in the figure 3-29 and figure 3-30, is when ICDs are efficient in reducing HTE (or increasing Rd for that matter), but also in reducing the Ep (or loosing productivity). This is reflected by the steep slope of Rd vs Ip and Ep vs Ip curves in figure 3-29 (or vs Iq in figure 3-30). Conversely, the ICD design in the red shaded area (Hp <1) for these cases will excessively reduce the PI without much improvement in inflow uniformity. This now allows a better understanding of the ICD-completion performance from the type-curves, followed by e.g. a recommendation to install ICD completion that results to Ip number close to 1 for the cases of Hp or Hq > 5. The resulting equations for ICD sizing are summarised in Table 3-5. The practical use of these type-curves will be explained in a case study in section 3.10

3.8 Proposed method for ICD completion design in heterogeneous reservoirs

This solution uses the assumptions listed in section 3.6. It is also necessary to introduce or extend the definition of several parameters:

1. Productivity Error. Ep

The parameter Ep is adopted from equation 3-9.

$$E_p = \frac{(q_{OH} - q_{ICD})}{q_{OH}} = 1 - \frac{<U>_{ICD}}{<U>_{OH}} = 1 - \frac{<U>_{ICD}}{<J>\,\Delta P} \qquad (3\text{-}29)$$

Where $<U>_{ICD}$ is the average inflow per unit length of the ICD completion, and $<U>_{OH}$ is the average inflow per unit length of the open-hole (OH) completion. Ep carries similar meaning as before: to quantify the change of well's PI completed with ICD, when compared to the original well's PI completed with a non-restricting completion, e.g. open hole or screen completion. (See red and blue dashed lines in Figure 3-31).

Note that $<U>_{OH} = <J>\,\Delta P$ where <J> is the average specific OH well PI. Ep is a measure of the reduction in well's capacity potential: Ep = 0 when the well is an OH completion and Ep = 1 when well completion imposes such a large pressure loss that the well is unable to flow.

2. Inflow variation. IV

IV is a measure of the variation of specific inflow rate along the length of the completion. (See Figure 3-31, IV is the measure of variation of the blue and red lines).

$$IV = \frac{(U_m - U_1)}{U_m} \quad (3\text{-}30)$$

Where U_1 is value of specific inflow rate at one standard deviation below the median value of specific inflow rate (U_m) The value is determined by plotting a probability plot for log (U) and read off the values 1 standard deviation from the mean value, 50^{th} and 84^{th} percentiles. They are similar to the Dykstra-Parsons coefficient that is discussed in section 3.3.2. A low IV coefficient implies that the degree of the reservoir inflow variation is low (a uniform reservoir) while a high IV coefficient indicates that the well is completed across a highly heterogeneous reservoir(s).

Note that IV reflects the dynamic properties (flow) instead of the static properties (e.g. permeability) of the reservoir. This is important since the typical measurements of permeability e.g. MRI log and Porosity log that are followed by correlation of poro-perm, are often unable to indicate the properties beyond the near wellbore reservoir properties due to the limitation of the logging tools. The near wellbore permeability can be misleading to reflect the true potential of a zone/layer, e.g. when there is a high-permeability zone behind the near wellbore region. The flow measurement is thus more reliable to indicate the productivity of zones.

3. Inflow Equalisation. IE

IE is the ratio of "inflow variation with ICD completion" to "OH inflow variation".

$$IE = \frac{IV_{ICD}}{IV_{OH}} \quad (3\text{-}31)$$

The IE = 1 is when the well is completed OH (i.e. the well has the 'original', uncontrolled inflow profile), while IE = 0 when the well is completed with an infinitely strong ICD completion (i.e. a completion with a uniform (though non-existent) inflow profile along its length).

The Ep – IE relationship is displayed in Figure 3-31:

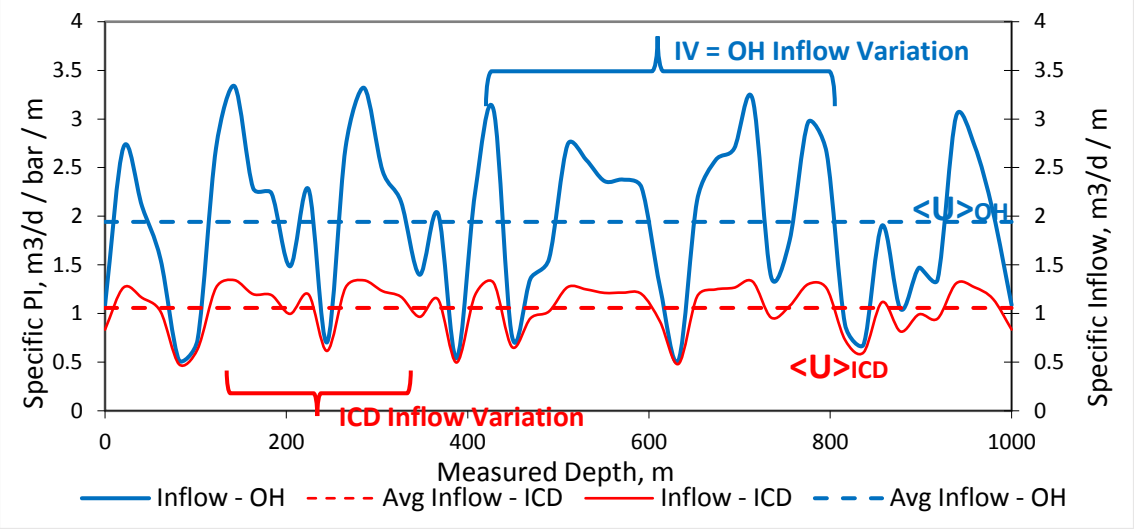

Figure 3-31. Illustration of Inflow Variation (IV) and Inflow equalisation (IE) Birchenko *et al.* (2010)

The relationship between these 3 parameters was plotted for different heterogeneous reservoirs. First, the 3D reservoir box model was built using the PETREL RE platform. The dimension was 500m x 1000m x 70m, and the reservoir was completed in the middle of the x axis, with a 1000 meter horizontal well along the y axis, with an analytical bottom-up aquifer below the reservoir. The rock properties, i.e. permeability values for each grid were assigned and distributed by *Petrophysical Modelling* module in PETREL RE. Using this module, we can perform sensitivity analysis of different permeability distribution along the wells, for example, see figure 3-32 to figure 3-33.

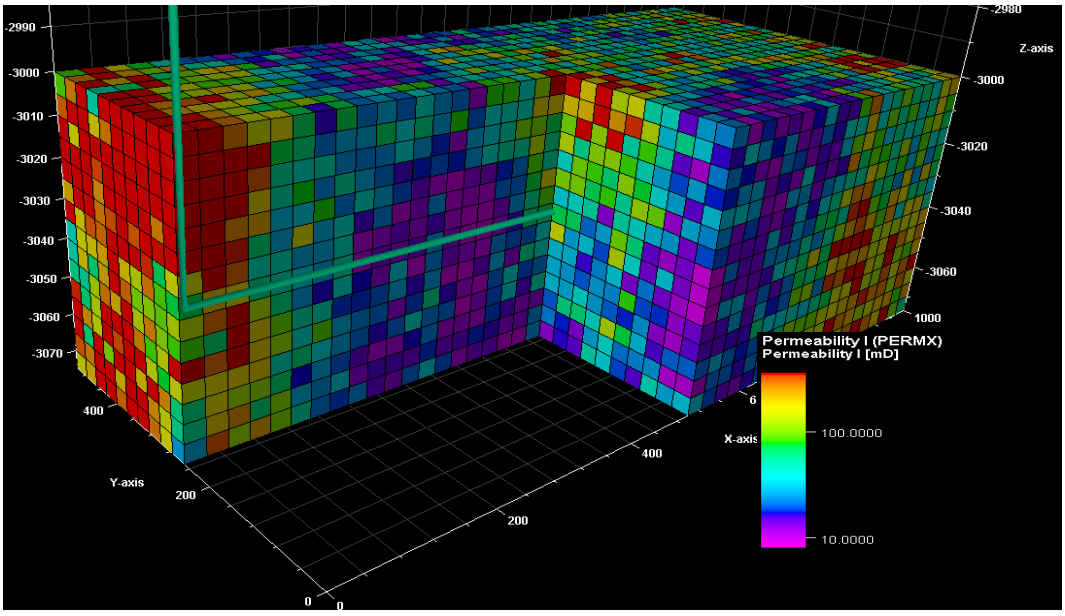

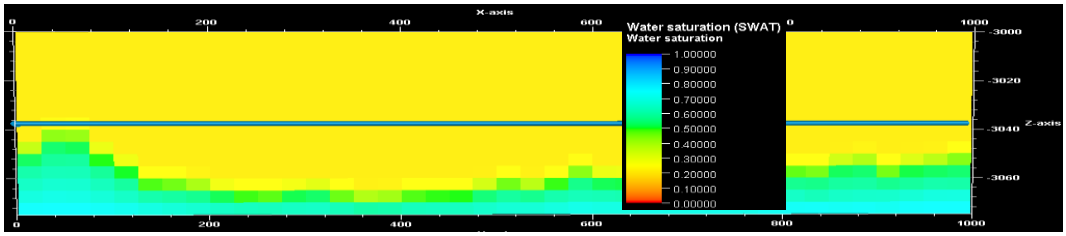

Figure 3-32. The reservoir is heterogeneous (top), resulting in early breakthrough in several layers leaving the other layers unswept (bottom).

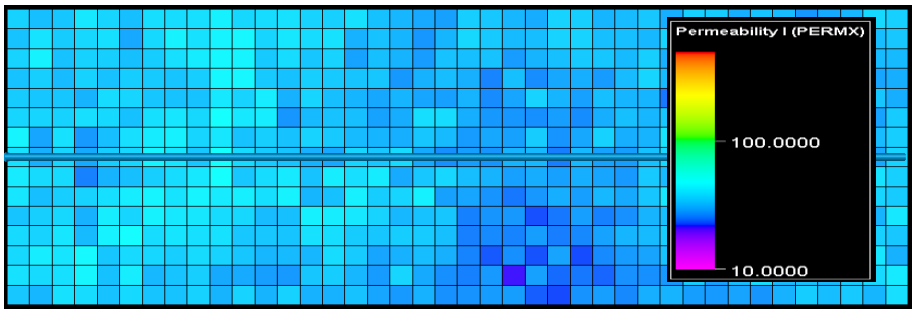

Figure 3-33. Highly homogenous Reservoir. Cv_{OH} = 0.13; IV_{OH} = 0.12.

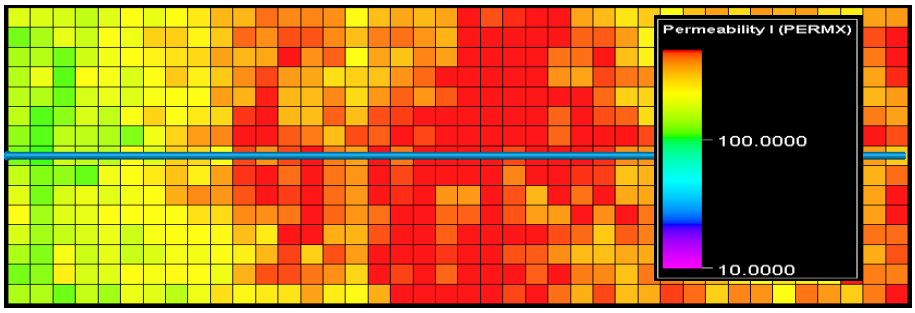

Figure 3-34. Homogenous Reservoir. Cv_{OH} = 0.36; IV_{OH} = 0.34

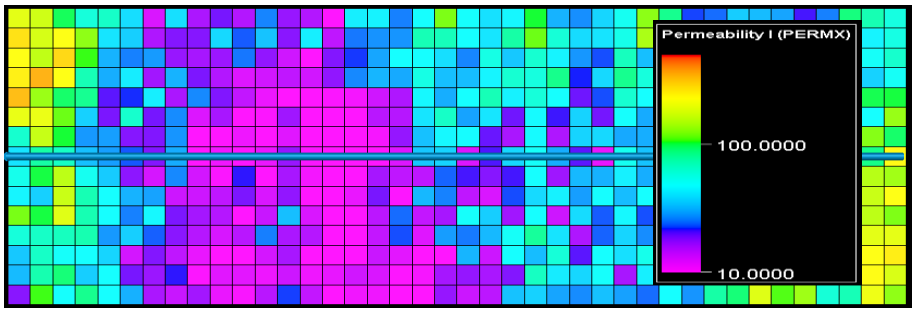

Figure 3-35. Heterogeneous Reservoir. Cv_{OH} = 0.74; IV_{OH} = 0.48

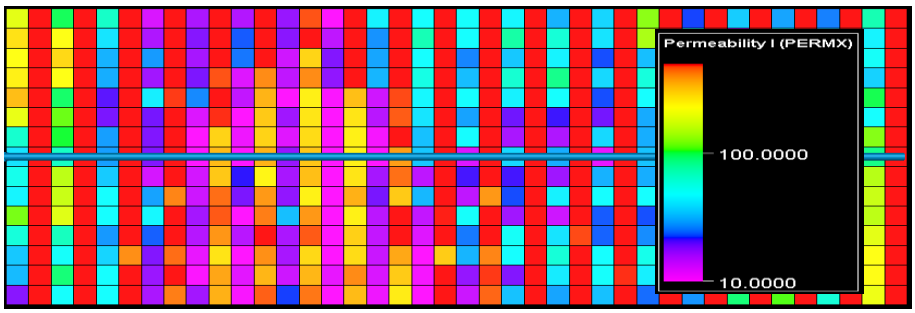

Figure 3-36. Highly heterogeneous reservoir. Cv_{OH} = 1.26; IV_{OH} = 0.72

Coefficient of Variation (Cv) is widely used when comparing geological heterogeneities (Corbett, 2012). Conventionally, a homogeneous reservoir is defined by Cv < 0.5; a heterogeneous reservoir is defined as the reservoir with Cv value is between 0.5 to 1.0 (0.5 < Cv < 1.0); and a highly heterogeneous reservoir has Cv above 1.0 (Cv >1.0). The Cv is calculated from the permeability distribution. Analogous to the comparison between the Inflow Variation and the Dykstra-parson explained in the above sections, the dynamic (inflow) parameter is preferred in this work. We use the inflow-distribution based CoV instead of the static (permeability-based) CoV. The examples in figures 3-32 to 3-35 represent cases of increasing reservoir heterogeneity (up to figure 3-35). Each example is also translated to the Inflow Variation (IV) terms since in this thesis we are interested to build a model using IV. Note that CoV is subscripted with OH, to emphasize that this (dynamic) flow distribution was measured in the open-hole completion, and once completion is equipped with ICDs, the CoV_{ICD} value will be reduced.

Increasing Heterogeneity →

k=constant	Cv ⩽ 0.5	0.5 < Cv < 1.0	Cv ⩾ 1
"Uniform"	"Homogeneous"	"Heterogeneous"	"Very Heterogeneous"

Figure 3-37. Definition of reservoir heterogeneity (Corbett, 2012).

Our workflow is based on the existence of a series of universal curves of IE versus Ep for each case of the OH reservoir heterogeneity quantified by the IV coefficient. These universal curves were developed after analyzing modelling results from reservoir illustrated by figure 3-33 to 3-36. These reservoirs represent different spatial permeability variation level from homogeneous to very heterogeneous (figure 3-35). We build relationship between Ep – IE as displayed in Figure 3-31. The analytical results are

validated with NETool numerical simulator. Note that since these type curves are based on dimensionless variables, they can cover wide ranges of design cases.

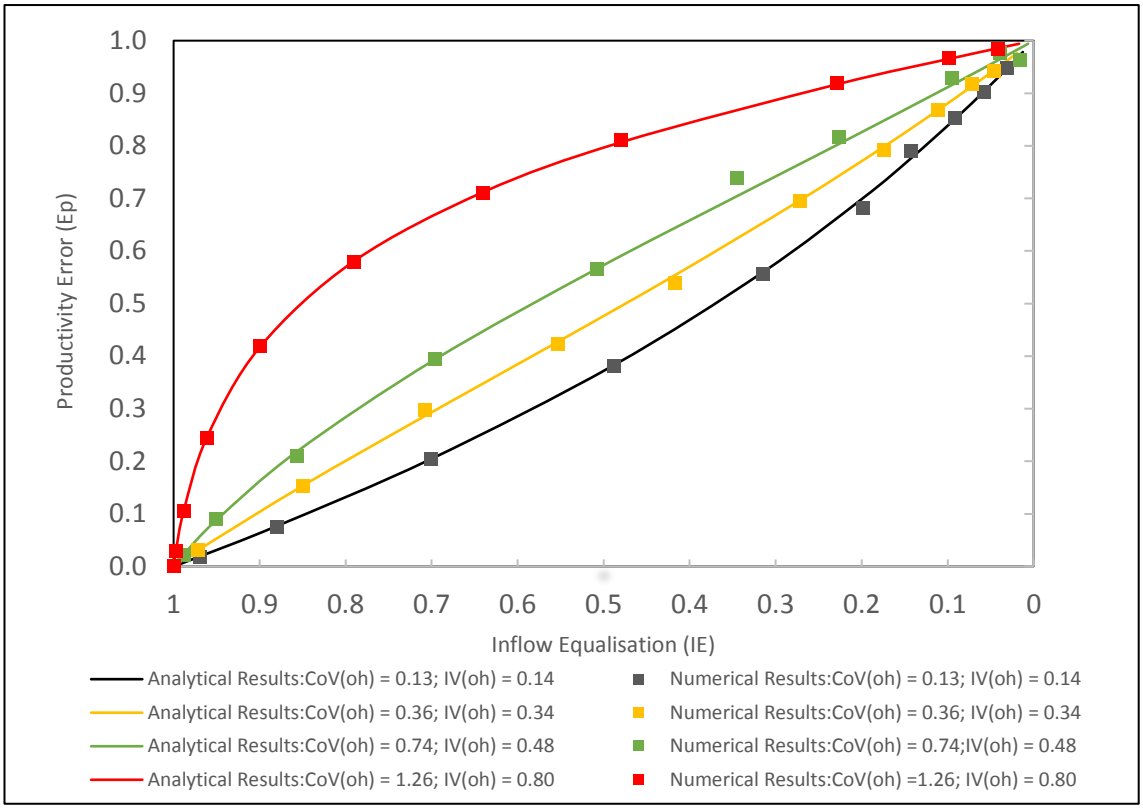

Figure 3-38. Universal type curves of Inflow Equalisation and well Productivity Error for various heterogeneity scenarios represented by the Dykstra-Parsons coefficient

Figure 3-32 illustrated that achieving a given degree of inflow uniformity requires a bigger reduction in the production potential for a more heterogeneous reservoir. Furthermore, we have built the Ep-IV type curves (Figure 3-38) for reservoirs ranging from very homogeneous to very heterogeneous. The universality of the Ep-IV type curves has been validated on a range of numerical simulations.

The reduction of inflow variation is specific for a given inflow heterogeneity level (measured by the 'initial', or open-hole inflow variation, IV_{OH}). These type curves offer a tool to the ICD's design by calculating the required ICD strength for a specified combination of affordable Ep and desired IV_{ICD}. Hence, the procedure to use these type-curves for a well completion design is similar to that of the heel-toe effect:

1. Calculate the level of Inflow variation (IVoh) of the (initial) openhole well before the well is completed with ICD i.e. select the IVoh value on the X axis.

2. Select the desired IVicd value and translate this value into the desired ICD size (using equation 3-32 and 3-33) that can be afforded for the properties of the reservoir and the tubing size. Note that a unique (IVicd) curve is associated to each IVoh value.

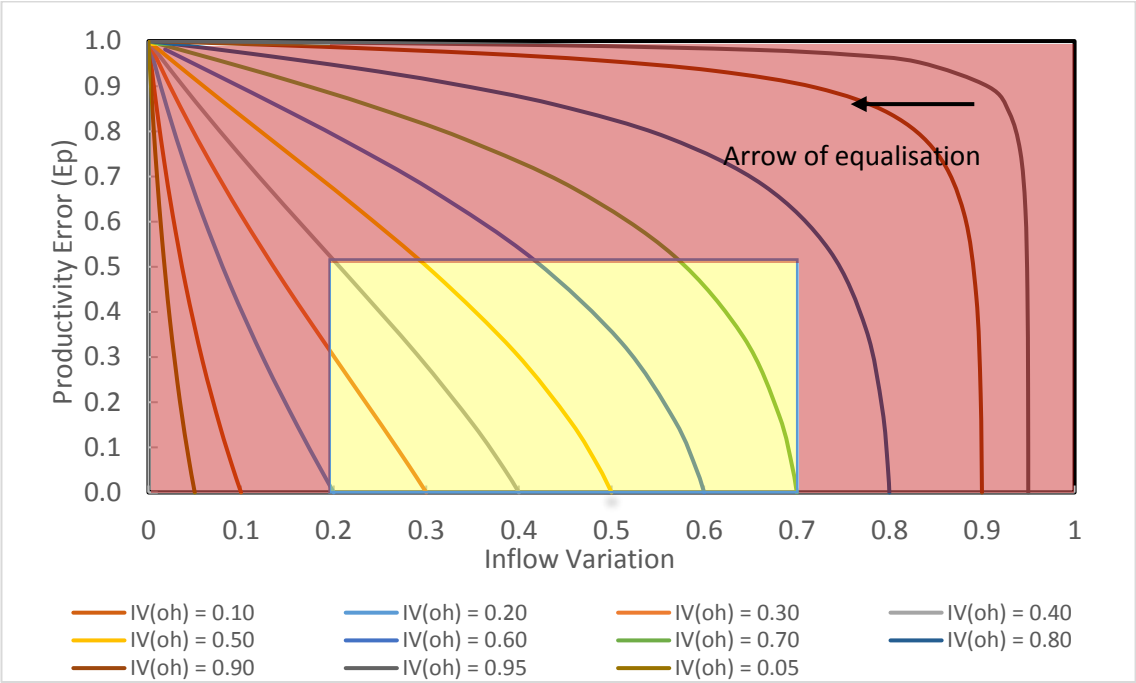

Figure 3-39. Type Curve for an ICD completion performance in a heterogeneous reservoir

The short-term constraints: production rate and the associated drawdown are related to the Ep while the inflow uniformity-affected reservoir sweep efficiency and thus the long-term constraints e.g. cumulative fluid production, are related to the IV. The optimum ICD strength is thus a trade-off between these two parameters.

Similar to the HTE scenario, efficient equalisation for ICD completion in heterogeneous reservoir is when the ratio of long-term gain (or the flow distribution improvement, represented by IV reduction) to that of its short-term cost (or the reduction of well's PI represented by an increased Ep) is at its highest. That is: efficient equalisation = maximum$\frac{(IV_{ICD}-IV_{OH})}{Ep}$. In practices, few engineers may not agree with sacrificing more than 50% of their original well's PI, hence the efficient equalisation can be observed for the yellow-shaded area. Conversely, inefficient equalisation is when the reduction of well productivity is much greater than the flow distribution improvement. Inefficient

equalisation is represented by the red-shaded area where the slope of the Rd curve is much smaller than the slope of the Ep curve.

For a given range of heterogeneity representative IV_{OH} values, the corresponding type curve plot can be divided into two areas. E.g. for wells with IV_{OH} values of 0.6-0.7 (very heterogeneous inflow) the yellow shaded area in Figure 3-39 is when the ICD completion is considered to perform efficiently, that is when the reduction of inflow variation is steep while the well's productivity's loss is slow. The red shaded area below IV_{ICD} = 0.2 is when the reduction of inflow variation results in excessive productivity reduction. The red shaded area above IV = 0.7 shows the ICD completion performance rapidly reducing the well productivity but not yet affecting the inflow uniformity much.

Note that as far as the highly heterogeneous reservoirs are concerned (high IV_{OH} number), the modelled reservoir's very permeable layers (or fractures, channels) that, though present in small numbers, have a significant effect on the total well inflow performance. A more logical method would be to install varying-size ICDs with a very aggressive restriction across the highly permeable layers, or if required, to fully shut those prominent layers with blank pipe, while installing lower strength ICDs across the layers with lower permeability.

The procedure to use this type-curves analysis is similar to the one developed for homogeneous reservoirs. The first step is to calculate the level of open-hole inflow variation, (IV_{OH}). The next step is the selection of the desired ICD inflow variation (IV_{ICD}), against the reduced well's PI (Ep), or vice versa.

Further, the found IV_{ICD} value actually depends on a unique combination of the drawdown ΔPw (for pressure constrained production) or rate Q (for rate constrained production) values, as well as on the specific ICD strength (a) in a given case. We thus need to find the formula that relates the specific a (ICD strength) to IV_{ICD} (Inflow Variation ICD) in a given case.

The resulting ICD strength for pressure constrained production is:

$$a = \frac{\left(\frac{(\Omega . Jm^2 - J1^2)}{(\Omega - 1)} - Jm^2\right)}{\left(\frac{(J1^2 - \Omega^2 . Jm^2)}{\Omega(\Omega - 1)}\right)^2 \Delta Pw} \qquad (3\text{-}32)$$

Or for a rate constrained well:

$$a = \frac{\left(\frac{(\Omega.Jm^2 - J1^2)}{(\Omega-1)} - Jm^2\right) < J > L(1-E_p)}{\left(\frac{(J1^2 - \Omega^2.Jm^2)}{\Omega(\Omega-1)}\right)^2 q_w} \quad (3\text{-}33)$$

Where $\Omega = \frac{J1}{Jm}(1 - IV_{ICD})$

This solution for the desired ICD strength is an explicit function of IV_{ICD} and IV_{OH} constituents. Vice versa, this formulation allows calculating Ep as a function of a for a given IV_{OH}. The full derivation is explained in Appendix B.

The above formulae have been tested for various reservoir scenarios with different heterogeneity levels. The resulting prediction was then validated with the numerical simulator (NETool), as displayed below in figure 3-40 to 3-43. The input data are tested for different reservoir heterogeneity levels as shown in figure 3-33 to figure 3-36. The analytical model is in agreement with the numerical results. The equations used are summarised in Table 3-6.

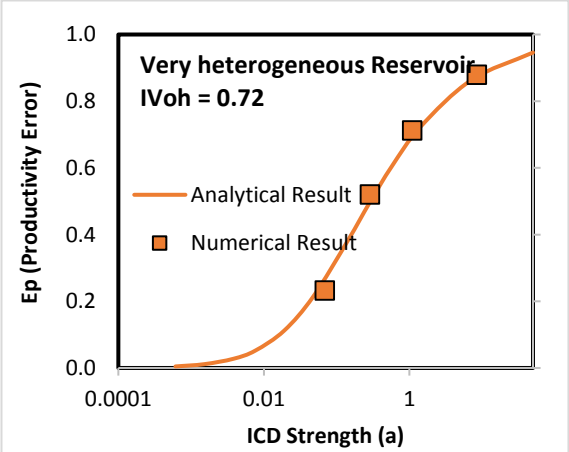

Figure 3-40. ICD completion performance in a highly heterogeneous reservoir. IV_{OH} = 0.72.

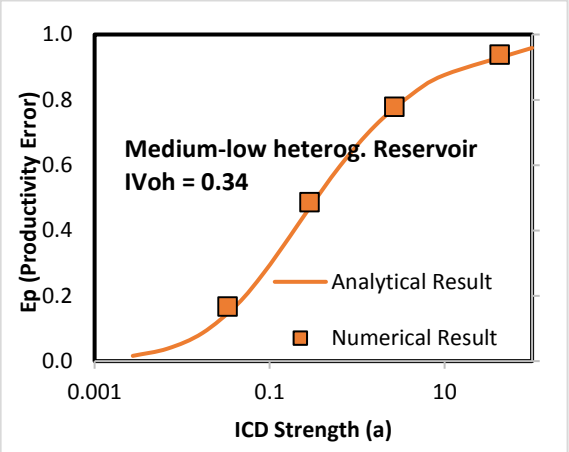

Figure 3-41. ICD completion performance in a medium-low heterogeneous reservoir. IV_{OH} = 0.34

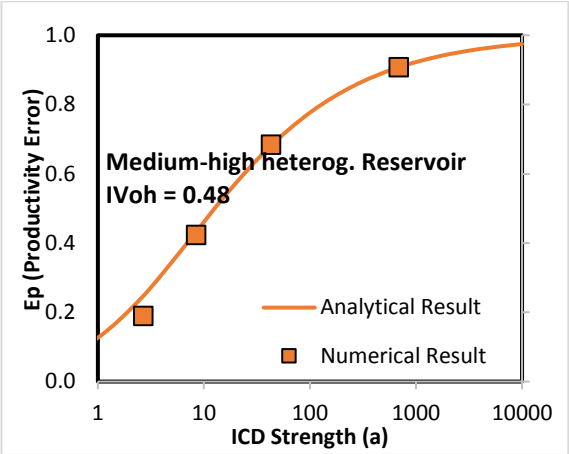

Figure 3-42. ICD completion performance in a medium-high heterogeneity reservoir. IV_{OH} = 0.48

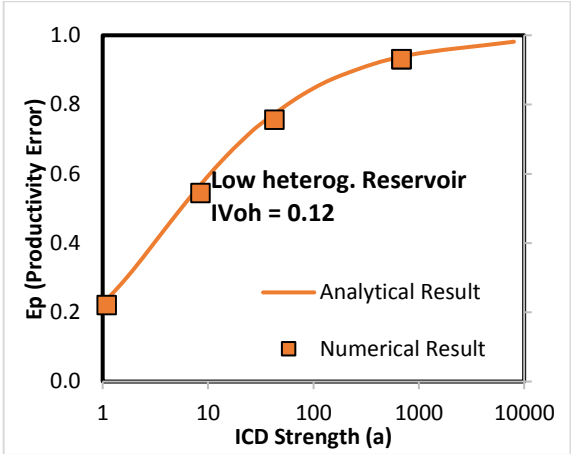

Figure 3-43. ICD completion performance in a low heterogeneity reservoir. IV_{OH} = 0.12

Table 3-6. Summary of parameters used in type-curve- informed ICD completion performance design in heterogeneous reservoirs.

Production ->	**Rate constrained**	**Pressure constrained**
	$\Delta P_w = \frac{q_w}{< J > L} \frac{1}{(1 - E_p)}$	$q_w = (1 - E_p) < J > \Delta P_w \, L$
Inflow Variation	$IV = \frac{(U_m - U_1)}{U_m}$	
Inflow Equalisation	$IE = \frac{IV_{ICD}}{IV_{OH}}$	
Productivity Error	$E_p = 1 - \frac{< U >_{ICD}}{< U >_{OH}}$	
Required ICD Strength	$a = \frac{\left(\frac{(\Omega . Jm^2 - J1^2)}{(\Omega - 1)} - Jm^2\right) < J > L(1 - E_p)}{\left(\frac{(J1^2 - \Omega^2 . Jm^2)}{\Omega(\Omega - 1)}\right)^2 q_w}$ *Where* $\Omega = \frac{J1}{Jm}(1 - IV_{ICD})$	$a = \frac{\left(\frac{(\Omega . Jm^2 - J1^2)}{(\Omega - 1)} - Jm^2\right)}{\left(\frac{(J1^2 - \Omega^2 . Jm^2)}{\Omega(\Omega - 1)}\right)^2 \Delta P}$ *Where* $\Omega = \frac{J1}{Jm}(1 - IV_{ICD})$

ICD size – strength relationship	$a_{channel} = \frac{(\rho\ \mu_{cal})^{\frac{1}{4}}}{(\rho_{cal}\ \mu)} \frac{\rho_{cal}}{\rho} \sqrt{l_{ICD} B} \Big/ a$	(ICD Channel type)
	$Nozzle\ diameter = \sqrt[4]{\frac{C_u \rho l_{ICD}^2 B^2}{C_d^2 a}}$	(ICD Nozzle type)

3.9 The type-curve based ICD design workflow

The above type-curves can form the basis of a fast workflow to design a uniform-strength ICD completion. They provide the insight to the ICD's design parameters and aid calculating the required ICD strength for a specified combination of either Hp, Ip, Ep, and Rd (for homogeneous reservoirs); or IV_{ICD}, $IV_{OH,}$ and Ep (for heterogeneous reservoirs).

An ICD completion design can be driven by **long-term objectives** (increased cumulative oil, delayed breakthrough time, improved sweep efficiency, etc.). These parameters are related to the inflow uniformity represented by **Rd or IV_{ICD}**. A more uniform inflow rate distribution along the length of the completion is likely to enhance these long-term objectives (e.g. El-Khatib, 2012 showed that the breakthrough time, fractional recovery and water cut of a heterogeneous reservoir are all a function of the IV value of an OH well.).

An ICD completion design can also be driven by **short-term objectives** (increased production rate and/or drawdown at a specific time). The production rate and the associated well drawdown (i.e. the short-term objectives) are related to the **Ep**. The ICD strength required to achieve the objectives selected from the type curves is calculated using the analytical solutions as was shown above. Figure 3-44 and Figure 3-45 show the ICD design workflow that was coded into a standard Engineering worksheet in Excel with the results further validated by comparison with numerical simulation software (NETool^{TM}, 2012).

The ICD completion's design varies depending on whether the design objective is a:

Long-term production strategy

Homogeneous reservoir: use figure 3-29 & figure 3-30 to select the Ep value corresponding to the best combination of I(p/q) and Rd, followed by calculating the flow rate, drawdown and the required ICD strength using equations 3-22 & 3-25.

Heterogeneous reservoir: use Figure 3-38 to select the Ep value corresponding to the desired IV value (IV_{ICD}), followed by calculating the flow rate, drawdown and the required ICD strength using equations 3-31 & 3-32.

Short-term production strategy

Homogeneous reservoir: In this case the target flow rate or the drawdown is specified, and the type curves (figure 3-29 & figure 3-30) are used to calculate the resulting Ep value. The corresponding I(p/q) allows calculating the required ICD strength using equations 3-22 & 3-25.

Heterogeneous reservoir: The target flow rate or the reservoir drawdown is specified, and the type curves (Figure 3-38) are used to calculate the resulting Ep. The corresponding IV_{ICD} allows calculating the required ICD strength using equation 3-32 & 3-33.

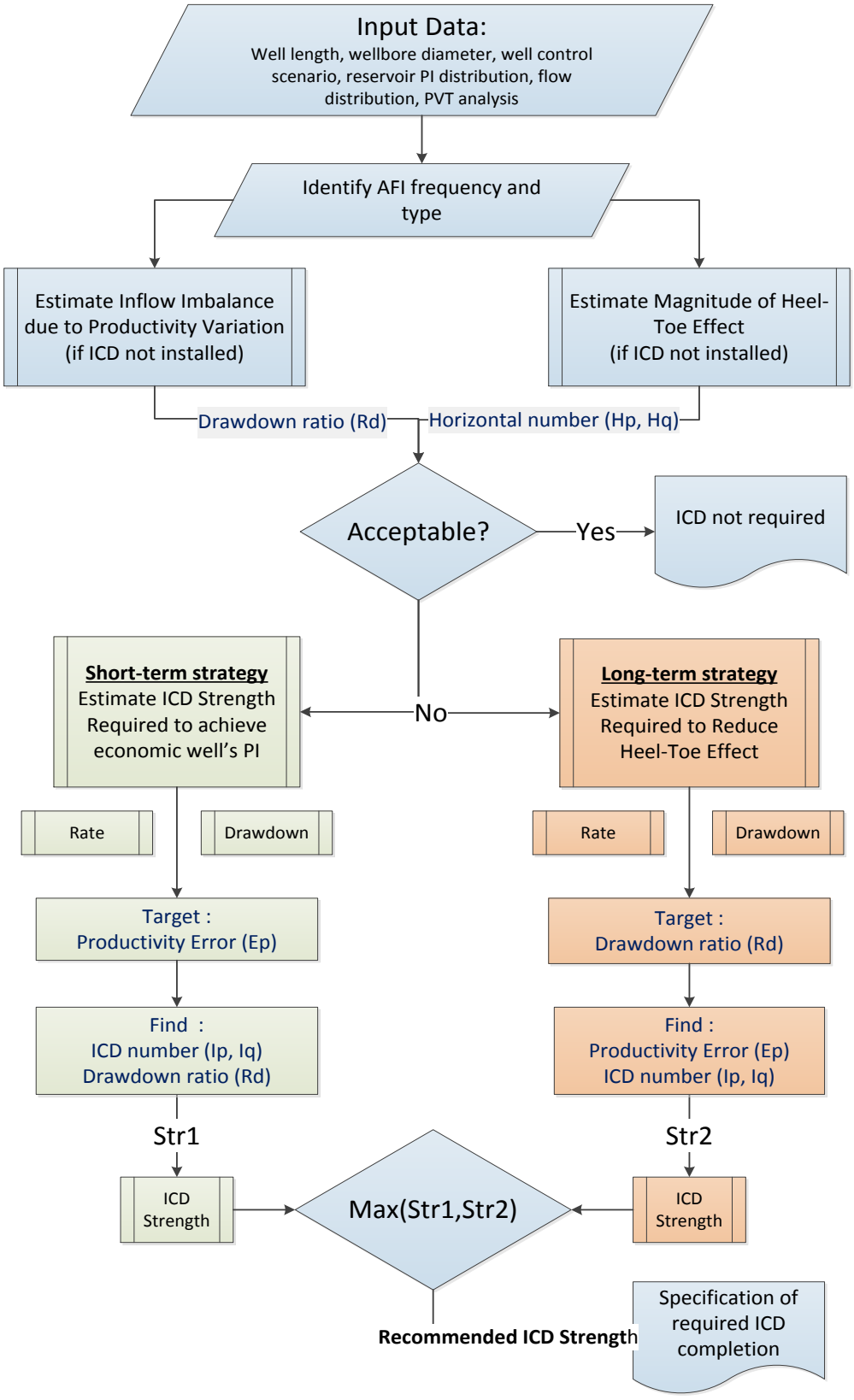

Figure 3-44. Workflow for ICD completion design in homogenous reservoirs.

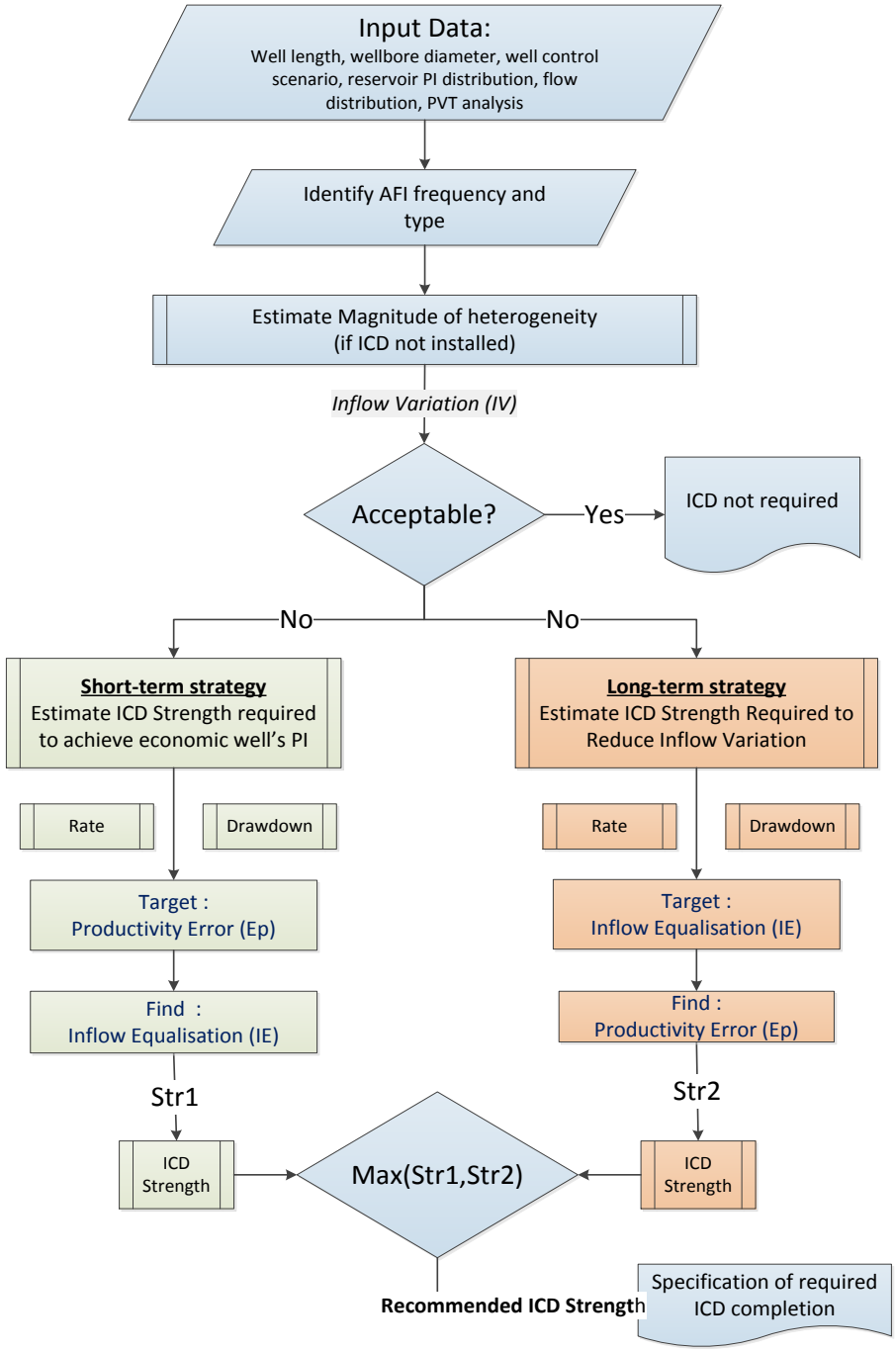

Figure 3-45. Workflow for ICD completion design in heterogeneous reservoirs.

3.10 Case Studies

We illustrate the application of these new workflows to four synthetic in homogeneous & heterogeneous reservoirs scenario. They show the range of situations that often need solving when sufficed time or resources are not available for running a numerical simulator.

3.10.1 Homogenous reservoir scenario

Case 1a evaluates the ICD size that was recommended by (Birchenko, *et al.* 2010) and (Henriksen, Gule and Augustine, 2006) for a well in an oil-rim reservoir (Figure 3-46), a permeable homogenous sandstone with the initial reservoir pressure close to the bubble point pressure (Table 3-7). The 3D reservoir box model was built using the PETREL RE platform. The dimension was 750m x 2500m x 15m, and the reservoir was completed in the middle of the x axis, with 2500 meter horizontal well along the y axis, with an analytical bottom-up aquifer below the reservoir.

The production is constrained by the allowable drawdown. The recommendation by both studies was to assign ICD pressure drop with the *n* times magnitude of the annulus drawdown at the heel, ΔP_{ann}^{heel}. The type-curve method is now used in this thesis to evaluate Birchenko's method in the context of reduction of inflow inequality against the well's performance. Our workflow is tested and compared to Birchenko's recommendations.

Case 1b also used the data outlined in table 3-6, however, in this case, the pre-completion ICD design should be revised at the well site against the new geological information (it appears the reservoir has lower permeability than expected) obtained after drilling the well (e.g. open-hole well log), prior to completion. This case study exemplifies the usefulness of rapid workflow to evaluate the various combinations of well completion selection with a limited time for analysis.

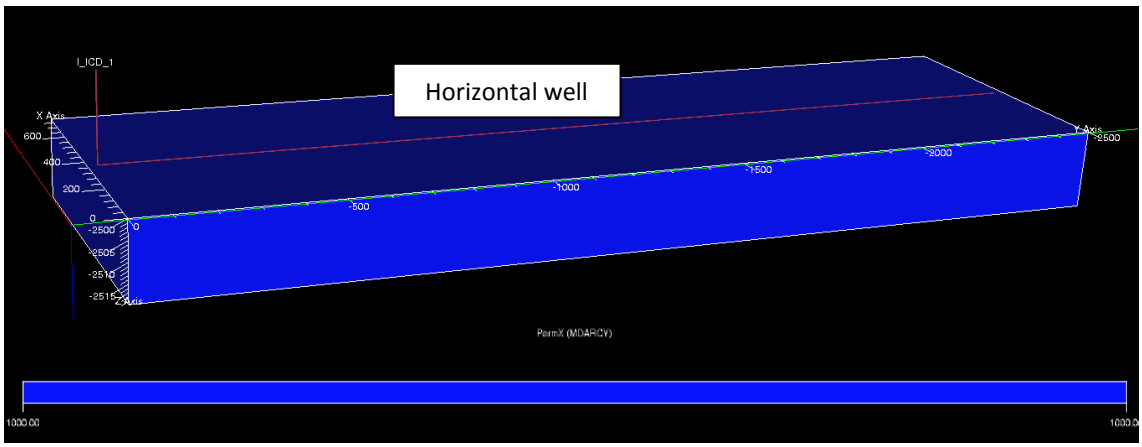

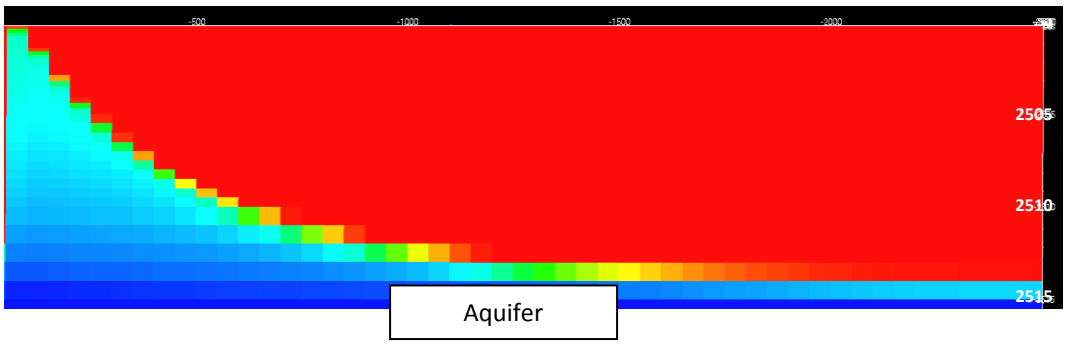

Figure 3-46. The reservoir is homogeneous (top). When producing the water influx is higher in the heel section leaving most of the layer unswept (bottom).

Table 3-7. Reservoir oil column data properties (Birchenko, Muradov and Davies, 2010).

Homogenous reservoir data.			
(Total) Drawdown at the heel	ΔPw	**1.2**	bar
Well length	L	**2500**	M
Completion internal diameter	D	**0.15**	M
Stand-off to aquifer	H	**15**	M
Well's PI estimate (neglecting friction)	J	**5000**	Sm^3/day/bar
Well's PI no friction for case 1b	J	**1500**	Sm^3/day/bar
In-situ fluid density	ρ	**800**	kg/m^3
In-situ fluid viscosity	μ	**1.7**	cp
Formation volume factor	B	**1.2**	Rm^3/Sm^3
Absolute roughness of base pipe	e	**0.05**	mm

Homogenous reservoir case study

Case study 1a – Evaluation of recommended ICD strength

Well and reservoir parameters of this scenario are listed in Table 3-7. Using equation 3-24, the screen/open hole completion, (i.e. ICD strength = 0) well's Ip = 23.6. The corresponding drawdown ratio (Rd) is 0.25, and the productivity error (Ep) is 0.60. (See red node in Figure 3-50). The Ep value indicates that the well's productivity is reduced by 60% from the anticipated PI for the no-friction PI case, and the Rd value indicate that the drawdown value at the toe is about a quarter of the drawdown at the heel of the well.

Applying Birchenko's rule of thumb (equation 3-28) the ICD completion pressure drop

should be n = $\left({}^{1}/_{\mathrm{Rd}}\right)_{\mathrm{noICD}} - 1 = 3$ times higher than the open hole drawdown. This suggests installing ICD with the strength (equations 3-27) of 0.63 bar.day^2/Sm^4 or when translated to a typical 12.5 m length ICD specific product-type, this is equivalent to $a_{icd} \approx$ 0.003 bar/(Rm^3/day)^2 in each segments for channel ICD strength, which for nozzle type ICDs with 1ea nozzle per segment, equals the ICD nozzle diameter ≈ 4.1 mm. This value is in a good agreement with the actual value of the ICD size installed in the real field (Henriksen, Gule and Augustine, 2006). When these ICDs are installed, the new Ip from equation 3-24 (a = 0.63 bar.day^2/Sm^4) is 2.8. The new drawdown ratio (Rd) using this ICD size will be improved from 0.25 to 0.60, and it is achieved with small PI reduction, Ep_{OH} (productivity error for OH completion) = 0.60 → Ep_{ICD} (productivity error for ICD completion) = 0.70 See yellow node in Figure 3-50.

The performance of ICD completion following Birchenko's rule-of-thumb in this case makes sense. However, we can still improve the performance of this completion by following our workflow, in this case by trying to obtain the ICD number (Ip) =1. Such (Ip = 1) improves the drawdown ratio from Rd_{OH} (drawdown ratio for open-hole completion) = 0.25 to Rd_{ICD} (drawdown ratio for ICD completion) = 0.77, while the PI reduction is still relatively low, Ep_{OH} = 0.60 → Ep_{ICD} = 0.74 (see the purple node in Figure 3-50). From equation 3-25, the required ICD strength is 2.05 bar.day2/Sm^4 or equivalent to $a_{icd} \approx$ 0.001 bar/(Rm^3/day)^2 for each of channel ICD segments or d ≈ 3.1 mm for each of nozzle/orifice ICD. The results in case 1a are validated against a numerical simulator, Figure 3-47 and Figure 3-48.

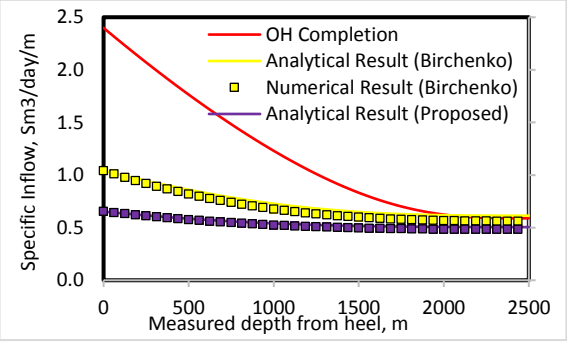

Figure 3-47. Flow profile of case 1a. Comparison between analytical & numerical results.

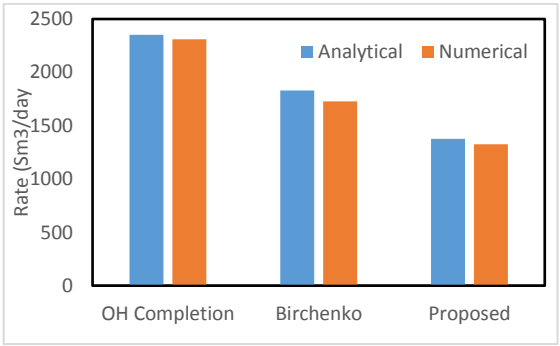

Figure 3-48. Well's rate in case 1a. Comparison between analytical & numerical result

In case 1a, the new recommendation would weigh on the long-term strategy more than

the short-term strategy. As can be seen on the figure 3-46, the proposed ICD size initially produces less than what Birchenko's recommendation was (1300 Sm^3/day vs. 1700 Sm^3/day). The proposed strategy would be more favourable in long-term e.g. resulting in a lower cumulative water production, hence cheaper water treatment cost.

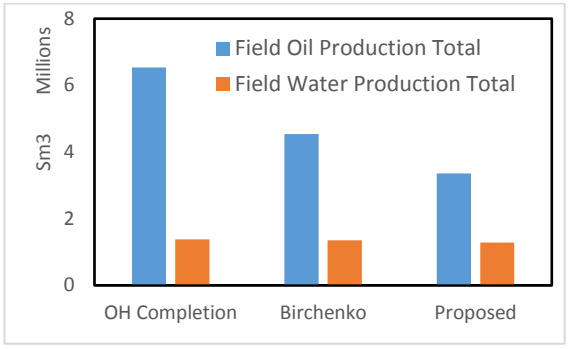

Figure 3-49. Cumulative production of case 1a after 10 years of production.

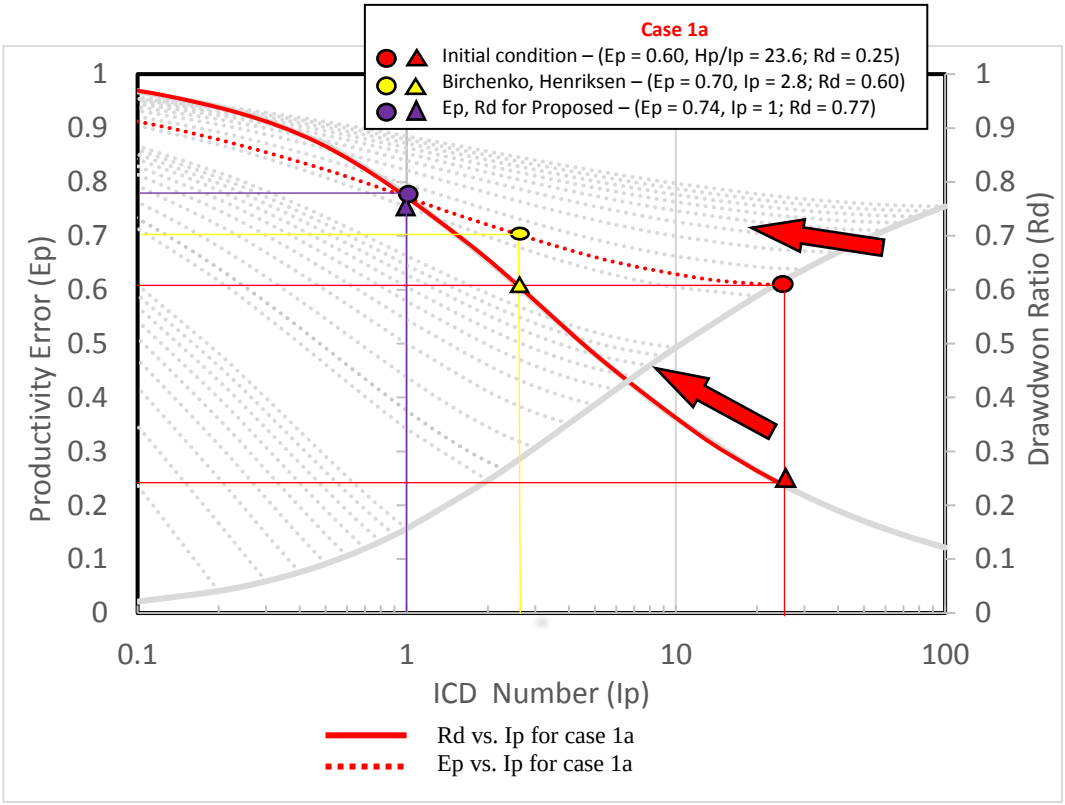

Figure 3-50. Illustration of case 1a design options plotted as points on the type curves.

Case study 1b – Completion re-design to adjust for the updated (lower permeability) geological information

The open-hole well log run after drilling the well reveals the reservoir is less permeable than what was expected. The actual well's PI is 1500 Sm^3/day/bar. Consequently, this well will also have different heel-toe effect. A quick calculation is needed to find the new ICD configuration and adjust it on site. Given the limited time between logging and running the completion string.

First, we can directly quantify the new heel-toe effect using equation 3-24. New Ip will be 2.3, and from the type-curve, the corresponding Rd = 0.62. Ep= 0.26 (see blue node in Figure 3-54). If we were to follow the Birchenko's rule-of-thumb, the new ICD strength (equations 3-27 and 3-28) a ≈ 9.0 bar.day^2/Sm^4 or when translated to a typical 12.5 m length ICD specific product-type, this is equivalent to $a_{icd} \approx 0.033$ bar/$(Rm^3/day)^2$ in each segments for channel ICD strength, which for nozzle type ICDs with 1ea nozzle per segment, equals the ICD nozzle diameter ≈ 2.16 mm. The new completion configuration is Hp = 0.23, Rd = 0.93. Ep= 0.62 (see green node in Figure 3-54).

Unlike the scenario in case 1a, following Birchenko's rule-of-thumb case 1b will result in poor ICD performance. The improvement of drawdown ratio, from Rd_{OH} = 0.62 → Rd_{ICD} = 0.92, is penalized with severed well's productivity loss, from Ep_{OH} = 0.26 → Ep_{ICD} = 0.62. With this configuration: (Rd_{ICD} - Rd_{OH}) < (Ep_{ICD} - Ep_{OH}) hence the reduction of well's PI with this rule-of-thumb is not worth it.

Earlier it was suggested that for a certain range of Hp values the reduction of heel-toe effect is efficient until ICD number, Ip = 1 (See brown node in Figure 3-54). This is obtained by installing ICDs with the strength (equations 3-27) of 1.60 bar.day^2/Sm^4 or when translated to a typical 12.5 m length ICD specific product-type, this is equivalent to $a_{icd} \approx 0.006$ bar/$(Rm^3/day)^2$ in each segments for channel ICD strength, which for nozzle type ICDs with 1ea nozzle per segment, equals the ICD nozzle diameter ≈ 3.32 mm. This way the drawdown ratio will be improved, Rd_{OH} = 0.62 → Rd_{ICD} = 0.77 with lower PI's reduction, Ep_{OH} = 0.26 → Ep_{ICD} = 0.38. i.e. (Rd_{ICD} - Rd_{OH}) > (Ep_{ICD} - Ep_{OH}). The results of this case are validated by the numerical simulator as depicted in Figure 3-51 &Figure 3-52.

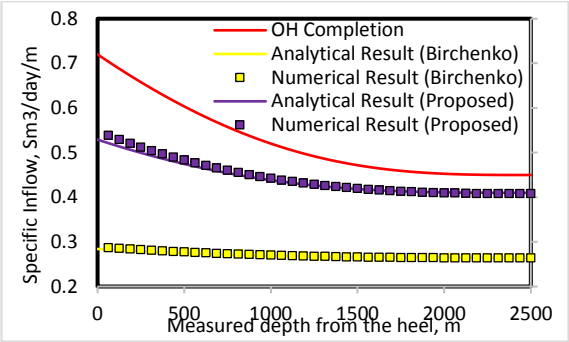

Figure 3-51. Flow profile in case 1b. Comparison between analytical & numerical results.

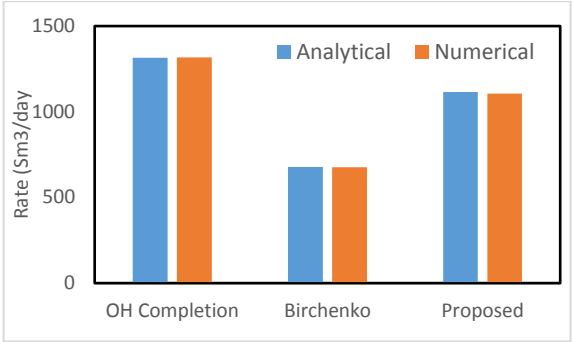

Figure 3-52. Well's rate in case 1b. Comparison between analytical & numerical result

In case 1b, the new recommendation puts more weight on the short-term strategy than on the long-term one. As can be seen on the figure 3-50, the proposed ICD size would initially produce more than Birchenko's recommendation (1100 Sm^3/day vs. 675 Sm^3/day), however it results in larger cumulative water production. See figure 3-51 for comparison of cumulative oil and water after 10 years of production.

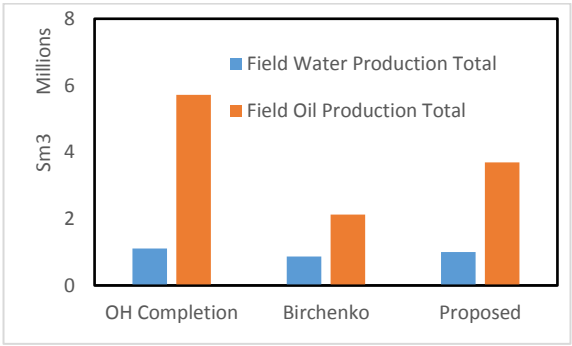

Figure 3-53. Cumulative production of case 1b after 10 years of production.

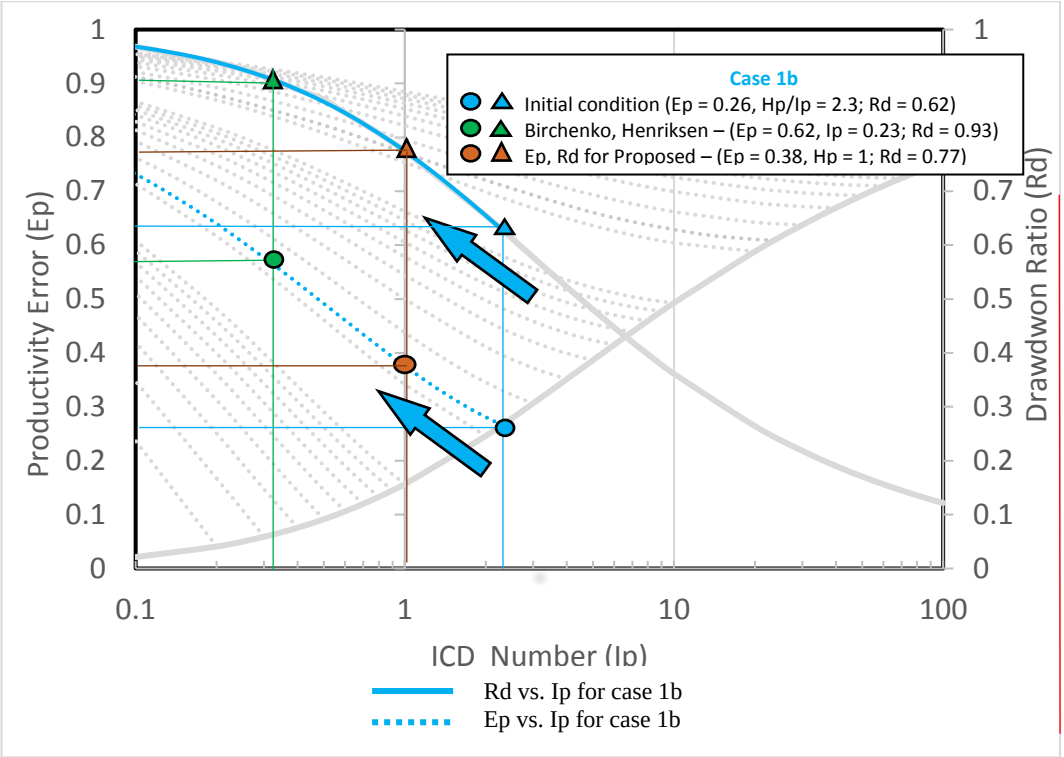

Figure 3-54. Illustration of case 1b design options plotted as points on the type curves.

3.10.2 Heterogeneous reservoir case study

Case 2a explores the rapid ICD completion design in a heterogeneous reservoir (see details in figure 3-32, table 3-8). For instance, assume that an adjustment to an ICD completion design is needed when drilling problems result in reduction of the length of the horizontal completion compared to the planned length. Case 2a pursues short-term objectives: the well completion is constrained by the need to achieve at least the minimum (economic) production rate at a given (e.g. the maximum allowable) drawdown. This completion requires higher flow rate per layer (or specific inflow <U>) to offset the shorter producing length. Increase in the drawdown is not allowed (e.g. due to the sand problem), hence a lower Ep value is required for this completion corresponding to the reduction in the ICD strength. The final IV_{ICD} is resultant from this new Ep value design.

Table 3-8. Heterogeneous reservoir properties (Birchenko, Muradov and Davies, 2010)

Heterogeneous reservoir properties.		
Reservoir Heterogeneity	*IVoh*	**0.39**

Permeability Distribution		**Log-normal**	
Well length (Original plan)	L	**1000**	m
Completion internal diameter	D	**0.15**	m
Well's min PI	$J1$	**0.016**	Sm^3/day/bar
Well's average PI	Jm	**0.026**	Sm^3/day/bar
Well's max PI	$J2$	**0.036**	Sm^3/day/bar
Segment Length	l_{icd}	**25**	M
In-situ fluid density	ρ	**840**	kg/m^3
In-situ fluid viscosity	μ	**2.3**	Cp
Formation volume factor	B	**1.2**	Rm^3/Sm^3

Case 2b evaluates the impact of the reservoir permeability profile being more heterogeneous than expected. Case 2b uses the long-term objectives-oriented workflow since the aim here is to achieve a specific value of inflow uniformity (IV_{ICD}). The original ICD completion will no longer modify the inflow profile sufficiently. An alternative ICD completion design with an increased ICD strength to achieve the desired IV_{ICD} is required, the latter being possible as case 2b is not constrained by the drawdown.

Heterogeneous reservoir case study

Case study 2a – Completion re-design following a drilling problem

Assume a 1,000 m long horizontal well is planned to be in drilled the middle of an oil-saturated zone. The initial ICD completion was designed to deliver the initial target rate of 300 Sm^3/day with a reservoir drawdown of 25 bar and the equipment has been designed and delivered on this specification. A "quick-look" engineering review of the completion is unexpectedly required because drilling issues problems have limited the completion length of 500 m.

The original completion was designed based on the expectation that a fairly heterogeneous reservoir with the heterogeneity index (IV_{OH}) value of 0.39 would be encountered (equation 3-31). The expected ICD completion performance follows the red curve in Figure 3-57, and the target completion was specified to achieve IV_{ICD} of 0.20, hence intersects the Ep value of 0.51 (i.e. the well retains 49% of the original productivity). The required ICD strength (equation 3-32) was 105 $bar/day^2/Sm^4$. This ICD strength is equivalent to an ICD with a single nozzle of 1.6 mm diameter in each 25 m-

long joints (equation 2-6 and 2-8 assuming an ICD with one nozzle for each joint). This 'initial' design is represented by the red node in Figure 3-57 (IV_{ICD} = 0.39; Ep = 0.51).

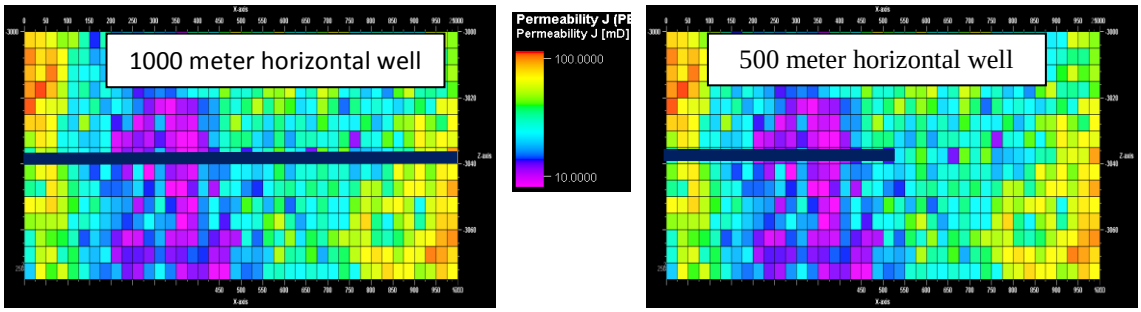

Figure 3-55. Shorter (500m instead of 1000 m) horizontal length (right) after the originally planned 1000 m horizontal length length) was cut short due to drilling problems.

The reduced horizontal well length of 500 m with the original ICD completion requires a drawdown of 67 bar to produce 315 Sm^3/day (the minimum production rate); more than twice the maximum allowed drawdown of 25 bar. This is because using this completion to produce the minimum target rate would exacerbate the reduction of PI from Ep_{OH} = 0.48 to Ep_{OH} = 0.63 (yellow node in Figure 3-57).

After the completion re-design the well produces (initially) 308 Sm^3/day of oil while respecting the maximum allowable drawdown of 25 bar. The modified ICD strength of 4.5 bar.day^2/Sm^4 was calculated using equation 3-32. The new completion requires the enlarged ICD nozzle of 3.5 mm diameter (Equation. 2-8, assuming an ICD with one nozzle for each 25 m tubing joint). This can be achieved with the ICD equipment on site by either adjusting the ICD strength, if this option is available, or by varying the density of ICDs, e.g. in this case installing/opening four 1.6mm pre-ordered ICDs per joint instead of one to achieve a similar specific flow area across the completion. However, the new design honouring the combination of rate, drawdown and available ICD strength reduces the target inflow uniformity value IV_{ICD} from 0.20 to 0.35 (see the purple node in Figure 3-57).

All these results were validated by numerical simulation in Figure 3-56.

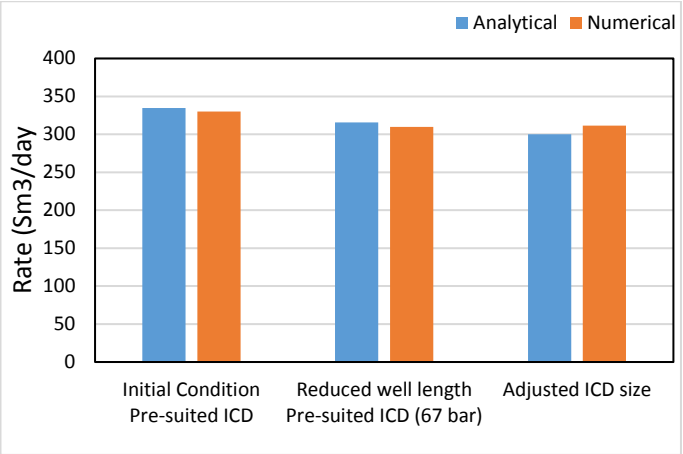

Figure 3-56. Well's rate in case 2a. Comparison between analytical & numerical results for three different options in this scenario.

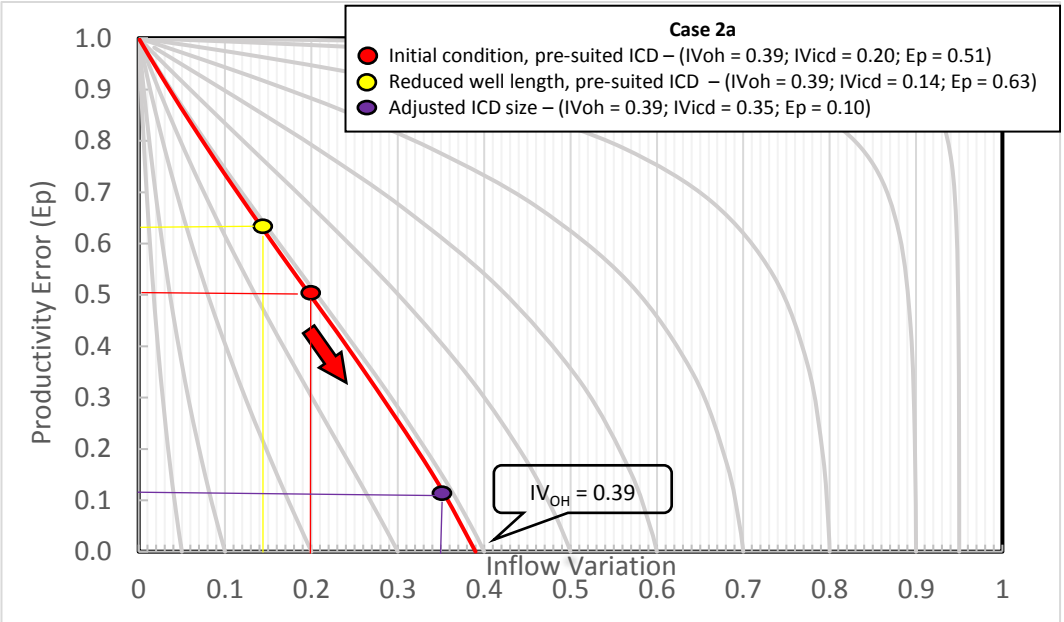

Figure 3-57. Type curves for case 2a: ICD completion designs for the expected and the actual inflow rate distributions.

Case study 2b – Adjusted completion design to account for the more heterogeneous geological configuration

Second 1000 m long horizontal completion is planned in the same field as above (Figure 3-58, left). The production constraints and the planned completion are as per case 1. However, the analysis of the drilled well's log data (Figure 3-58, right) indicates that the reservoir is actually more heterogeneous than expected. The IV_{OH} value is now 0.49, higher than the expected value of 0.39. The ICD completion performance is shifted from

the one following the red curve (design assuming initial heterogeneity, IV_{OH} = 0.39) to the one shown by the blue curve (IV_{OH} = 0.49) in Figure 3-60.

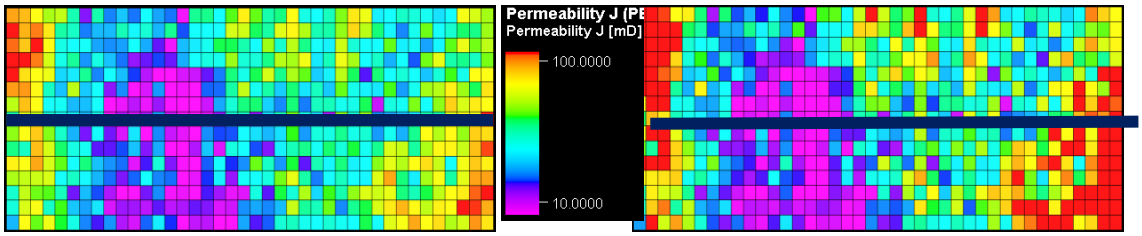

Figure 3-58. Expected and actual permeability distribution of the case 2 horizontal completion.

Producing the well with the original ICD completion would result in IV_{ICD} value of 0.27 (equation 3-30). This scenario is represented by the blue node in the type curve plot 2-50 (IV_{OH}= 0.49; Ep = 0.53; IV_{ICD}= 0.27). The Ep value of 0.53 indicates that the well's productivity index with the planned ICD completion is 47% of the openhole value. However, IV_{ICD} = 0.27 may be judged to result in a lower ultimate recovery than the one for the originally specified 0.20 value of IV_{ICD}. The brown node representing the new ICD design is shifted vertically (follow the blue arrow in Figure 3-60) to the original desired value IV_{ICD} = 0.20. The required ICD strength for this adjustment is 205 $bar.day^2/Sm^4$ (equation 3-32), equivalent to one ICD per tubing joint with a single nozzle of 1.35 mm in diameter. This change results in a reduced productivity: the new Ep_{ICD} value is 0.66. This scenario is represented by the green node in Figure 3-60 with IV_{OH} = 0.49; IV_{ICD} = 0.20 and Ep = 0.66. The modified ICD completion design has suppressed the greater inflow heterogeneity to the originally specified target of 0.20 IV_{ICD} at the cost of increasing the sacrificed well productivity index from 53% to 66% of the OH well Productivity Index. These results have also been validated by numerical simulator in Figure 3-59.

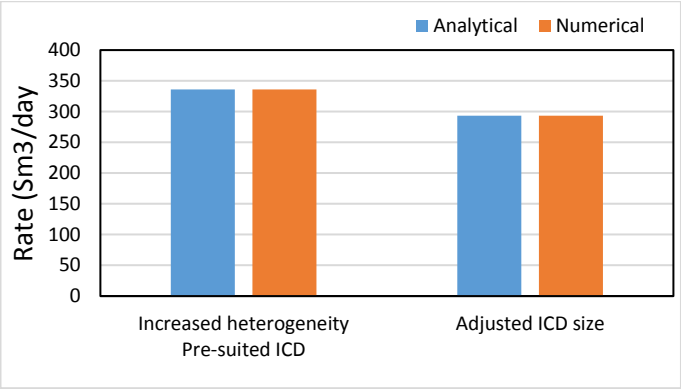

Figure 3-59. Flow rate forecasts in Case 2.

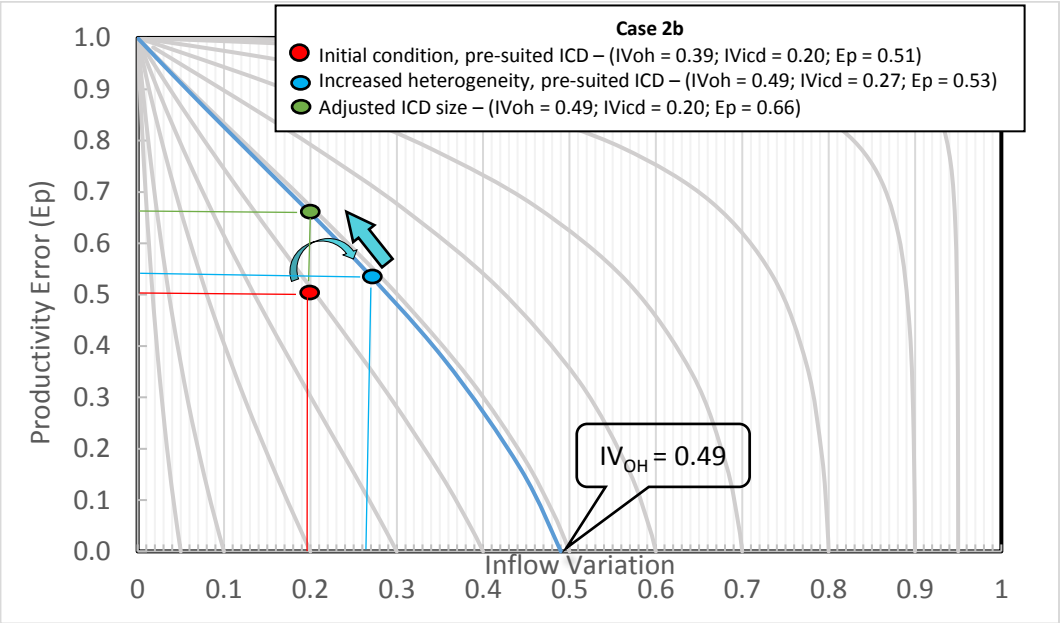

Figure 3-60. Type curves for case 2b: ICD completion designs for the expected and the actual inflow rate distributions.

3.11 Discussion & Conclusion

ICD completion performance type-curves have been developed in this work for rapid evaluating the loss in well productivity versus the reduction in the inflow variation along the length of the completion. Such type-curve analysis reduces the complexity of the ICD completion design aimed at reducing the following inflow/outflow problems:

- Non-uniform inflow profile due to mainly the frictional pressure loss along the completion (Heel-to-Toe effect), or
- Inflow rate variation caused mainly by the reservoir heterogeneity.

This study extends the available, analytical, ICD completion modelling and design methods by proposing a visual, type-curve based approach to select completion nearest ICD strength that meets the well's objectives. This method provides immediate insight into the relationship between the long-term and short-term objectives-related aspects of such completion. The type curves based on dimensionless variables can be employed to analyse a broad range of ICD completion design cases.

Explicit formulae to calculate the required ICD strength and size for the selected "inflow rate variation" / "loss in well productivity trade-off" scenario are also derived. Finally, the type curves' accuracy has been verified by a commercially simulator in a broad range of reservoir and well models.

The type curves can also be treated to aid the selection of the initial design of the completion, before optimising it further with numerical simulation, e.g. with the full numerical reservoir modelling. The benefit is particularly useful when optimising the required ICD size against the desired well performance in order to e.g. reduce the "search space" of the reservoir optimisation workflow.

The workflow was tested by coding it as MS Excel spreadsheet. It is a portable, rapid calculation tool to aid real-time well completion decisions. This allows wellsite crew to take advantage of the latest advance in ICD technology by simply changing the ICD installation density or size of the built-in adjustable restriction, the completion specialist can thus modify the completion designs using the most recent reservoir information. Such real-time decision making can improve the well's performance, as well as reduce the uncertainty, being based on the latest, more accurate reservoir measurements. Our workflow has been illustrated by four scenarios which consider typical field situations. The results were confirmed via comparative, commercial simulator studies.

It is important to recognise that the overall well performance model in this study is developed for "initial or before breakthrough" condition. This does limit the applicability of the proposed methods as far as the long-term production objectives are concerned, as was explained. Strictly speaking, the flow profile modification referred in this study can be considered as the "near-wellbore" one. The long-term objectives-related parameters used in this study rather refer to the inflow heterogeneity or Inflow Variation, with measures developed by petroleum geologist. These parameters are assumed to be related to the ultimate reservoir recovery or water breakthrough time. The solid link between the

instantaneous production optimisation and the long-term production objectives will be additionally developed in the subsequent chapter of this thesis.

At this moment, choking or reducing the layer's or zonal flow is the one and only available control action. For instance, equalising inflow can be achieved by the means of reducing inflow in all layers until it is the same as the worst flowing layer. This is shown in our type-curve to cause excess loss of productivity (curve shapes in Fig 3-37). In the future, efforts should be pursued to develop an AWC system that can improve the productivity/permeability of each layer being completed, e.g. creating local layer's stimulation, or performing layer's fracturing.

3.12 Summary

The focus of this chapter is investigating the benefit of ICD completion to the "cost" of achieving a more uniform inflow profile caused by either a dominant heel-toe effect (in homogeneous reservoirs) or by reservoir heterogeneity. The case histories illustrate how the solution between these two, that is the between the better inflow profile and the loss in productivity, is not an either-or option, instead it is a compromise to find results that are acceptable. The process of finding this optimum solution is normally done using a numerical simulator. We have presented a new approach to design such advanced well completion by combining analytical solutions and graphical plots. Complex effects like HTE or reservoir heterogeneity are presented as simple, dimensionless parameters. The other key element here is that the workflow communicates the modelled results clearly, so that the ICD completion performance and impact can be immediately, intuitively understood by looking at the graphs. The goal is to draw a mental picture of the ICD completion performance when reducing inflow variation.

This chapter has presented:

- An overview of the horizontal well technology.
- A review of several horizontal well completion design analytical solutions and the importance of THE in them.
- A review of horizontal well technology application to heterogeneous reservoirs and measures used to quantify reservoir heterogeneity.
- The role of ICD completion in HTE control and heterogeneous reservoir inflow control.

- A review of Analytical modelling of ICD completions.
- The development of type-curves based method to design ICD completion to suppress HTE, and its application workflow.
- A new analytical model for reduction of HTE by ICD completion in the flowing pressure- constrained wells.
- A new guideline for choosing the ICD size in such wells.
- The development of a type-curve method to design ICD completion in heterogeneous reservoirs and its application workflow.
- An explicit solutions to relate ICD strength to IV_{OH} and IV_{ICD}.
- Examples of application of the developed, type-curves based methods for ICD completion design.

3.13 Nomenclature

J – Productivity Index (PI)	P - Pressure
$\bar{P}$ – Average reservoir pressure	L – Total well horizontal length
Q – Production rate	D – Inside diameter of the well
l – length measured from heel	l^* – Dimensionless length of the well
C_f – unit conversion factor: $2.956 \cdot 10^{-12}$ in field units and $4.343 \cdot 10^{-15}$ in metric	B – Formation Volume Factor
ρ – Fluids Density (produced or injected fluid)	f_a – Average value of Fanning friction factor along the completion interval (Birchenko, Usnich and Davies, 2010)
SD – Standard Deviation	$\overline{K}$ – Average (arithmetic) permeability
K – Permeability value	N – Sample number
U – Specific inflow	F – Flow Capacity
C – Storage Capacity	L – Lorenz Coefficient
ΔP – Pressure drop (Drawdown)	a – ICD strength per unit length
η – Probability density of the specific productivity index	I – ICD number
H – Horizontal number	$a_{channel}$ – ICD strength for channel type
$\langle \quad \rangle$ - Angled brackets are used to denote average values of variables	C_d - Discharge coefficient for nozzle or orifice
$\Omega = \frac{J1}{Jm}(1 - IV_{ICD})$	n - Exponent

$\alpha = 4aj^2$	$\beta = \frac{C_f \rho f B^2 L^3}{I_p D^5}$
h – Payzone thickness	r - radius
G – Auxiliary index	

3.13.1 Subscripts

w – well	H – Horizontal well
v – vertical well	Heel – heel section in horizontal well
wf – well flow	Toe – toe section in horizontal well
avg – average	No friction – No friction condition
e – External boundary	Friction –friction condition
ICD – Inflow Control Devices	OH – Open-hole
q – rate constrained	p – pressure constrained
1 – one standard deviation below median values	ICD – Inflow Control Devices
s - segment	
m –median values	2 – one standard deviation above median values

3.13.2 Abbreviations

AFCD	Autonomous Flow Control Devices (a class of FCDs)
AWC	Advanced well completion: an arbitrary combination of FCDs in a well or a well's zone
BOE	Barrel of Oil Equivalent
Cv	Coefficient of Variation
DP Coefficient	Dykstra-Parsons coefficient
Ep	Productivity Error
FCC	Flow Control Completion. Same as AWC
FCD	(any) Flow Control Device
HTE	Heel-Toe effect
ICD	Inflow control device (a class of FCDs)
ICV	Inflow control valve (a class of FCDs)
IE	Inflow Equalisation
IV	Inflow Variation

MDRT	Measured Depth from Rotary Table
Rd	Drawdown Ratio
PI	Productivity Index
PIF	Productivity Improvement Factor
WOC	Water Oil Contact
GOC	Gas Oil Contact

Chapter 4 – Rigorous Design of Flow Control Completion for Long-term Production Objectives

4.1 Brief Introduction to Coupled Wellbore-Reservoir Modelling

One of the advanced well completion technology's major objectives is improve the inflow distribution along its length, typically to make it more uniform. This is expected to result in delayed water breakthrough, reduced sand production, improved sweep efficiency and enhanced recovery. However, the downhole restriction in the AWCs can only be tolerated as long as the minimum Productivity Index (PI) of the well is achieved. The corresponding, allowed pressure drop across the AWC is important to estimate when calculating the optimal AWC design.

Such calculation is typically performed using a numerical, nodal analysis, wellbore simulator (e.g. NETool). The process ideally explores a wide range of completion types and details along with the associated pressure drops in the well and reservoir (Halliburton, 2012). Prediction of AWC's performance using the software NETool has been widely used and has become standard, being employed by almost every company that uses AWCs (*source: personal communication*).

NETool is a steady-state wellbore simulator, modelling the well performance at a given time in the well's life (a.k.a. snapshot modelling). However, the well and reservoir performance changes with time. This prompts an essential question whether such a 'snapshot' completion design (essentially a short-term strategy), is optimum over the long-term of the well's productive life time.

Latter objective requires incorporating the full reservoir simulation into the completion selection workflow (Figure 4-1 and Figure 4-2). First, the reservoir simulation computes the impact of completing a well with an open-hole completion (or a sand screen) on the full field reservoir recovery. The simulation generates results for the wells' inflow performance at different time steps. These results, representative of different periods in the well's life, are exported to a static wellbore flow simulator. NETool is usually chosen for this. The study starts at the initial time-step (t = 0 days) and a completion optimisation process is followed, that obeys any short-term constraints and objectives, e.g. maximum oil production rate, or allowable drawdown at that timestep. Next, the reservoir simulator

is run for the new full-field scenario with thus revised well design. *Please note that the selected completion design may or may not be available for modelling in the commercial reservoir simulators. Also, there are several cases where the elements of wellbore modelling in a commercial simulator have not been fully verified (Eltaher, 2017).*

The nodal-analysis based static wellbore flow simulation evaluates the short-term parameters, e.g. production rate, flowing pressures. While the reservoir simulation evaluates the long-term strategy parameters, e.g. the cumulative water, oil recovery. The workflow, and completion design is iterated until both the short-term and long-term objectives are met if either evaluation shows unsatisfactory performance.

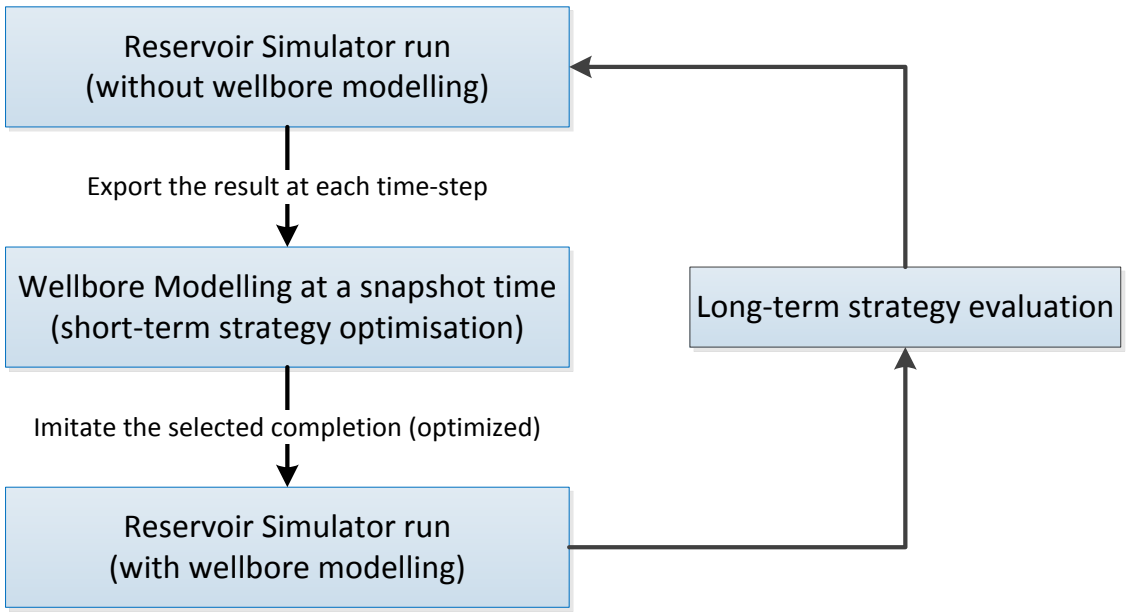

Figure 4-1. Workflow coupling wellbore and reservoir simulators when optimising advanced well completions

The challenge presented by the completion optimisation requires a clear understanding of the time-dependent inflow and outflow performance of the well in question (Livescu *et al.*, 2010). The selected completion designed based on the steady-state model often becomes ineffective in the later life of the well (Livescu *et al.*, 2010). This challenge inspired the development of the coupled completion and reservoir simulation. Several commercial simulators can perform wellbore modelling along within the reservoir simulation, by coupling the two components (Figure 4-1, Figure 4-2).

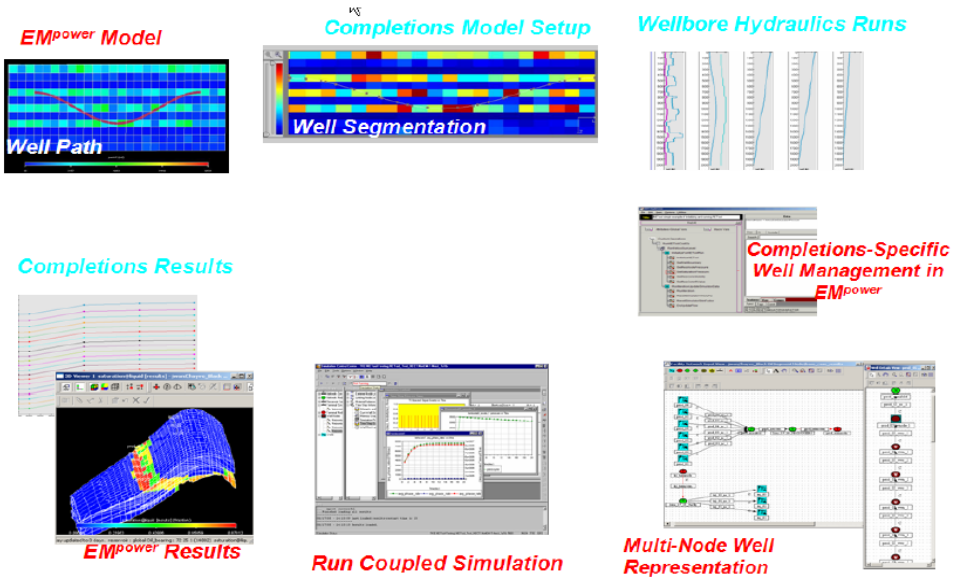

Figure 4-2. Em[power] workflow model (Wan *et al.*, 2008)

The importance of coupling the wellbore and reservoir simulations was recognised by many operators. For example, ExxonMobil (Grubert *et al.*, 2009) applied the Three-Tier methodology to introduce three degrees of coupling into their proprietary software, EM[power]. The basic one, Tier-3, is similar to the nodal-analysis simulation described earlier. It performs static completion optimisation at a particular time (i.e. snapshot optimisation). The computing time is small, but this method is only appropriate for a few reservoir conditions. The Tier-2 method provides a one-way, dynamic coupling scheme of that reservoir and wellbore. The reservoir simulator runs the wellbore hydraulics simulation at each time step, but without feedback to the reservoir simulator. Tier-2 thus does not give the correct prediction of the completion performance over time. The Tier-1 method is the fully-coupled simulation of for an accurate model of the reservoir and the wells completion which includes the AWC completions. Each component within the well is considered as a set of nodes and connections. This method results in the high level of accuracy, however, it required substantial time and hardware resources.

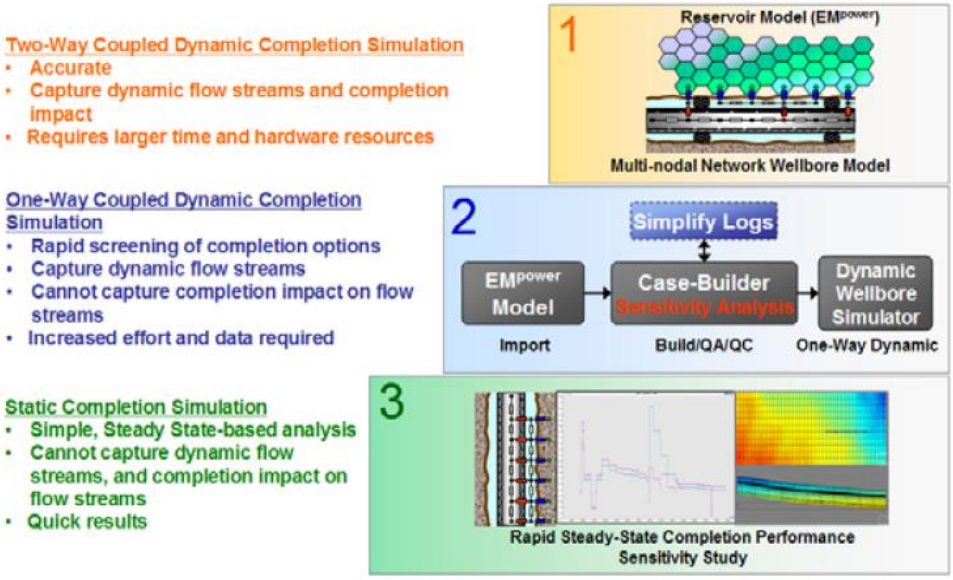

Figure 4-3. Workflow for coupling wellbore and reservoir simulators (Grubert et al., 2009)

The fully coupled approach requires more computing power and engineering time. This however, is often not the case; plus sufficient input information, such a detailed geological model is also often not available (Williams *et al.*, 2004). Modelling an Advanced Well Completion (AWC) adds complexity to the wellbore model, increasing even more the required computing time and resources compared to a typical reservoir simulation. The complex physics of the flow devices necessitates multiple model iterations, while and the simulation may require even more resources for the new generation of flow control devices (AICV, AFCD).

As an example, Heriot-Watt's *Joint Industry Project (JIP)* did an early, full-field feasibility study of wells with autonomous flow control devices for an offshore, viscous oil field (Haghighat, *et al* 2015). The objective of the study was to find the best completion (type and size) for the oil reservoir completed with 3 multi-lateral wells in the presence of a large aquifer. The primary challenge of the study was that the full-field simulation time exceeded 24 hours for completing a single run (Figure 4-4). The simulation time almost doubled when flow control devices were introduced into the well models (the green and red lines in Figure 4-4). More than 500 sensitivity runs were required to find the optimum completion design. A method to reduce computing time is thus much needed.

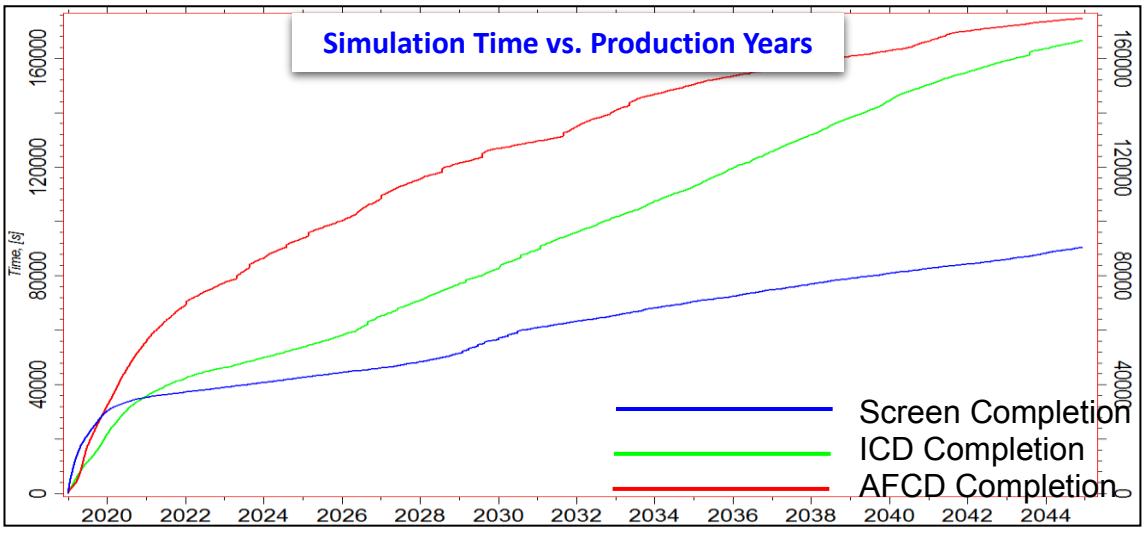

Figure 4-4. Simulation time for a viscous oil field runs

The remainder of this chapter explains a fast and transparent approach to link the short-term and long-term evaluation of an advanced well completion equipped with flow control devices. The work extends the classical methods of a waterflooded well's performance to a well with an AWC. The proposed model can be implemented as an analytical model to evaluate the well performances. It provides a simple means of estimating the long-term value derived by controlling the zonal flow rate using AWCs or any other means (e.g. a well workover). The accuracy of the prediction have been verified by comparison with the results from a numerical reservoir simulator. Several examples illustrate the proposed model's performance and value, while its limitations will also be discussed. (I thank my supervisor, Dr. Khafiz Muradov, for his contribution to development of the analytical model presented in the next section).

4.2 Simplified Methods for Waterflood Analysis

Waterflood is the most commonly used oil recovery mechanism; hence its analysis and way to prepare a well's performance forecast has been a popular topic of research since the 1940s. Simplified analysis methods offer (semi-) analytical solutions and type curves were used to understand and reasonable accurately forecast the waterflood performance for a range of geological environments, flood patterns and well control situations. These simplified analysis methods are still routinely used to robustly evaluate the expected oil recovery, waterflood efficiency, impact of the flood pattern, even though the numerical reservoir simulators are widely available nowadays.

The oil recovery factor is the product of the efficiency of oil displacement by water (on

the pore level) and the volumetric sweep efficiency (the extent of the water front on the reservoir level). The latter is the product of the areal and vertical sweep efficiencies. The areal sweep efficiency is very much the function of the flood pattern, geological discontinuities, mobility ratio, etc. The vertical sweep efficiency at any given time is the fraction of the cross-section between e.g. an injection and a production well that is flooded by water. This efficiency, inter alia, strongly depends on the reservoir heterogeneity: more permeable layers are flooded faster distorting the water front.

Prediction and analysis of the vertical sweep (or horizontal sweep for horizontal well) efficiency will be the main topic of this chapter since generally the AWCs are designed to deal with the non-even flood front propagation in heterogeneous reservoirs. The areal sweep efficiency and oil displacement efficiency can be found by other means: mathematical models, e.g. Dyes et al., 1954 or core flooding experiments respectively.

Analytical solutions for vertical sweep efficiency in heterogeneous reservoirs require number of assumptions, such as the level of inter-layer communication. Two situations must be assumed: the layers can either be non-communicating or are perfectly communicating (i.e. instantaneous, vertical, pressure equilibrium).

The case of non-communicating layers with arbitrary properties was well analysed by Dykstra and Parsons, 1950. They derived analytical solutions (called here the "DP method") which applied when on a layer-by-layer basis, provide estimates of the recovery efficiency, the fractional flow curve, with regard to the injected water volume. They also used these analytical solutions to derive general formulae and type curves for a reservoir with a vertical, log-normal, permeability distribution. Later, major contributions in this area include the works by Muscat, 1950, who derived expressions for other types of permeability distribution; while the situations with other-than-one water-oil ratios were analysed by Johnson, 1956. The model prediction w.r.t injected volumes were translated into the time domain by Reznik et al., 1984, and El-Khatib, 1985. Osman and Tiab, 1981, extended the model to the case of composite layers (i.e. were permeability vary laterally).

The frontal displacement theory describing the two-phase, immiscible displacement in linear system was developed by Buckley and Leverett, 1942. This solution will be called the BL method. Frontal displacement theory establishes a relationship between the average water saturation as a function of either cumulative water injected, or of the injection time. Welge, 1952, presented a new method to obtain the average saturation

behind the water front, a very useful method for determining the oil recovery. Snyder and Ramey, 1967 used these theories to predict the analysis of non-pistonlike displacement during a waterflood.

Warren, 1964, and Goddin et al., 1966 considered the effect of crossflow between layers. During waterflooding solutions in communicating layers were presented by Hiatt, 1958 with later, major extensions to the cases of variable layer properties (El-Khatib, 1985); reservoirs with log-normally distributed, vertical permeability (El-Khatib, 1999); and even included the effect of gravity-driven cross-flow (El-Khatib, 2003), including inclined reservoirs (El-Khatib, 2012).

This thesis extends the DP and BL methods for stratified reservoirs with non-communicating layers to the case of wells with AWCs. A simple and quick approach to predict waterflood performance is offered to allow estimation of the long-term value of an AWC. This method will be verified against the predictions of a reservoir numerical simulation model. Reasons why a similar approach is unlikely to be found for both the case of communicating layers and for the above permeability distributions will also be discussed.

The chapter will describe the development of the model, as follows:

- *Modelling AWC with piston-like displacement in a vertical well*. The original DP method will be briefly described, followed by the extension to include the AWC performance. Further, the algorithm to implement the extended DP method workflow is presented. The method's performance will be compared against a numerical reservoir simulation using a synthetic reservoir model. This will also illustrate how the method can be used to design and evaluate the long-term AWC value.
- *Modelling an AWC with non-piston like displacement in a vertical well*. The original BL method will be briefly described, followed by the extension to include the AWC performance. Further, a new method to predict the average water saturation behind the front, extending the Welge model is also described. The effect of AWC on the frontal displacement for heavy, medium and light oil reservoirs will be explained. The method will be validated against the numerical reservoir simulation.
- *Modelling AWC in a horizontal well in a heterogeneous reservoir*. The above methods of modelling an AWC during waterflooding analysis are extended to the case of a water front rising from the aquifer below, as opposed to the injector-producer pair

dominated waterflood discussed above. The mathematical derivation will be explained and its predictions validated against a numerical simulation. The results of the cases studies with this model will be further coupled to the type-curve AWC analysis described in chapter 2. This closes the loop for the rapid, of ICD completion design workflow for wells in heterogeneous reservoirs.

4.3 Modelling the performance of a waterflood with vertical AWC wells using modified DP method

4.3.1 DP method for a non-communicating, layered reservoir with piston-like displacement

The DP method is traditionally used for vertical wells. It can also be used for predicting the performance of a waterflood with deviated or horizontal wells (in the latter case the layers must be tilted and/or contain channels), as long as the assumptions listed below are satisfied. This justifies our extension of the method to AWCs that are not vertical. *Note that the equivalent methods for a communicating layered reservoir also exist. But since they assume perfect vertical pressure equilibrium for all layers (i.e. the local pressure derivative at a given distance from the well is the same for every layer), they are impractical for wells with flow control completion whose sole purpose is to create significantly different pressure drops across each layer.*

The original DP method (Dykstra and Parsons, 1950) assumes non-communicating layers. This is normally expressed by the stronger assumption $k_v = 0$; stressing the fact that the gravity forces' layer-by-layer impact on the oil displacement front is minor compared to the overall lateral flow. This holds true for numbers of heterogeneous reservoirs. This method and its modifications are still extensively used for estimating vertical sweep efficiency – an integral part of estimating the field's recovery factor at its design stage. A brief derivation of the original DP method for the conventional wells provided below:

Figure 4-5 is an injector-producer pair, separated by distance L, in a heterogeneous reservoir.

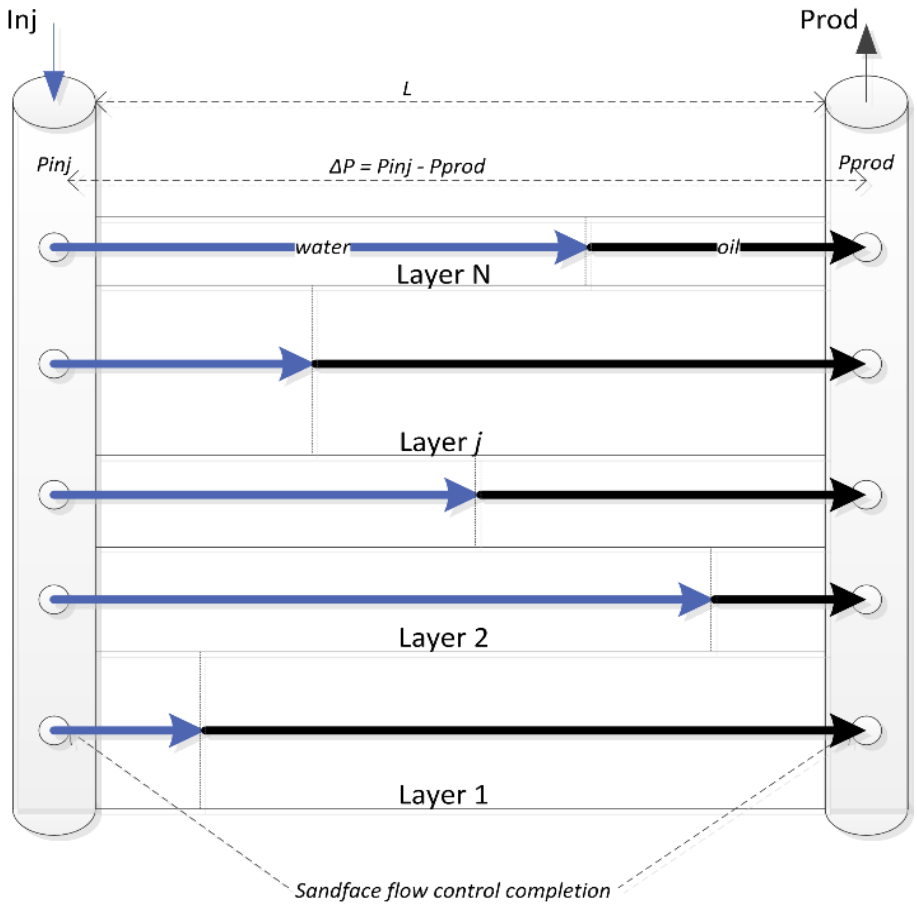

Figure 4-5. Schematic view of oil displacement from an injector to a producer at some time in a heterogeneous reservoir

Each layer has its own properties: height h, effective cross-sectional area A, porosity φ, horizontal permeability k, end-point saturations S_{wi} and S_{or}, end-point mobilities $\lambda_w^{'} \equiv k_{rw}^{'}/\mu_w$ and $\lambda_o^{'} \equiv k_{ro}^{'}/\mu_o$, and end-point mobility ratio $M^{'} \equiv \lambda_w^{'}/\lambda_o$,. The effective cross-sectional area is the area that is actually being flooded, i.e. this area (in a given layer) multiplied by the water flow velocity in a layer should give the injection flow rate for this layer. The method assumes:

1. *Diffuse flow, non-vertical equilibrium.* The displacement take place under the diffuse flow condition. It requires uniform distribution of fluid saturations at any point in the linear displacement path with respect to thickness. Diffuse flow can occurs either in of two extremes: the non- or perfectly vertical equilibrium. Our method covers the first condition (non-vertical equilibrium). This is when the injection rates are high or when the capillary and gravity forces' layer-by-layer impact on the oil displacement front is minor compared to the overall lateral flow,

hence the communication between layers are minimal. This is normally expressed by setting $P_c = 0$ and $k_v = 0$.

2. *Incompressible fluids*. This implies our analysis is applicable to analysis of oil displacement by water, or when the effect of gas compressibility is negligible on the overall displacement efficiency.
3. *Piston-like displacement in each given layer*. This expresses the fact that the lateral water front variation within a given layer is minor compared to the overall front variation caused by the reservoir heterogeneity. This holds true for a vast number of heterogeneous reservoirs.
4. *The pressure drop between the injection and production wells is constant.* More specifically in this paper: the pressure drop between their sandface or bottom hole pressures. This is reasonable since the injection and production wells are often controlled by pressure for the most of their production life. Besides, 100% voidage ratio is traditionally assumed in displacement models – the injection rate for each layer matches its production rate and the liquids and rock are assumed to be incompressible. Section 4.3.3 will show how the method can also be extended to the constant production rate cases.

All the volumes and rates are discussed at reservoir conditions.

Consider layer *j* where water front has travelled to coordinate x_j (Figure 4-6):

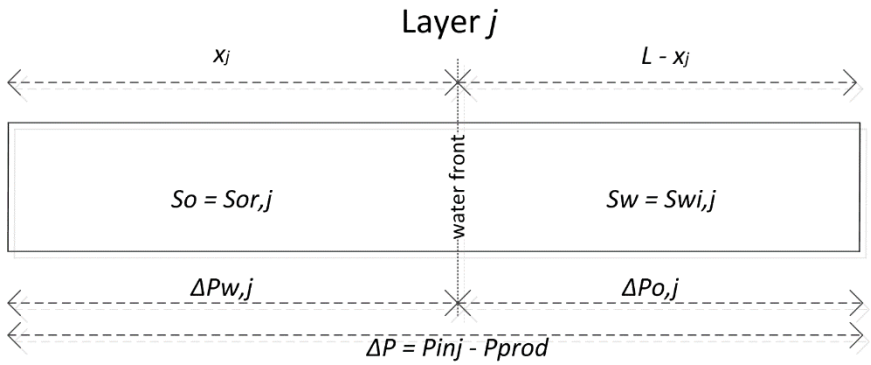

Figure 4-6. Saturation profile in Layer j

Darcy's equation states that in oil and water regions the flow velocities are, respectively:

$$u_o = -\frac{k\lambda_o^{'}\Delta P_o}{L-x} \tag{4-1}$$

$$u_w = -\frac{k\lambda_w^{'}\Delta P_w}{x} \tag{4-2}$$

Fluids are assumed incompressible, so these velocities are equal to each other, i.e. $u_o=u_w=u$.

Noticing that $\Delta P=\Delta P_o+\Delta P_w$, and combining this equation with equation 4-1 and 4-2, the front velocity $\frac{dx}{dt}$ (here equal to the flow velocity u divided by the movable pore volume fraction) for Layer j can be found as:

$$\frac{dx_j}{dt}=\frac{u_j}{\Delta S_j\phi_j}=-\frac{k_j\lambda'_{w,j}}{\Delta S_j\phi_j L}\cdot\frac{\Delta P}{x_j^*+M_j(1-x_j^*)} \tag{4-3}$$

Where the dimensionless front distance x^* is defined as $x_j^*\equiv x_j/L$ and the movable saturation ΔS defined as $\Delta S=1-S_{wi}-S_{or.}$

It is now clear that the production or injection rate q is a function of the water front distance:

$$q_j=u_jA_j=\frac{k_j\lambda'_{w,j}A_j}{L}\cdot\frac{\Delta P}{x_j^*+M_j(1-x_j^*)} \tag{4-4}$$

The time-independent, oil recovery efficiency vs. injected volume curves for oil displacement analysis can be constructed by eliminating time from the equations and focusing on the relative front positions. The ratio of the front velocities in layer j and in the (reference) layer R, are:

$$\frac{dx_j}{dt}\Big/\frac{dx_R}{dt}=\frac{dx_i}{dx_R}=F_{j,R}\frac{x_R^*+M_R(1-x_R^*)}{x_j^*+M_j(1-x_j^*)} \tag{4-5}$$

Where $F_{j,R}$ is defined as $F_{j,R}\equiv\frac{k_j\lambda'_{w,j}}{\Delta S_j\phi_j}\cdot\frac{\Delta S_R\phi_R}{k_R\lambda'_{w,R}}$

The original DP derivation workflow then integrates equation (4-6) to find an analytical solution for the water front position x in Layer j at the exact time when Layer R is experiencing water breakthrough (i.e. when $x^*_R=1$ so Layer R is flooded).

$$\int_0^{x_j^*}\left[x_j^* + M_j(1-x_j^*)\right]dx_j^* = F_{j,R}\int_0^1\left[x_R^* + M_R(1-x_R^*)\right]dx_R^* \qquad (4\text{-}6)$$

Further, the integral solution can then be expressed explicitly for x_j as:

$$x_j^* = \frac{M_j - \sqrt{M_j^2 + F_{j,R}(1-M_j)(1+M_R)}}{M_j - 1} \qquad (4\text{-}7)$$

(Except for the case $M_j=1$ when the integral solution yields $x_j^* = \frac{F_{j,R}(1+M_R)}{2}$).

(It is also possible to find the imaginary distance (and hence the injected volume) of the water front in a layer after it has been flooded by changing the integration limits.)

The front distances in the remaining layers are calculated by taking the first layer to experience breakthrough as a reference layer. This allows calculation of both the overall reservoir saturation and the injected volumes at this time. The production rates of oil and (in the reference layer) water are calculated using equation 4-4. This allows calculation of the production well's fractional flow f_w (or water cut WC).

The curve of reservoir water saturation or injected volume vs. WC is constructed by repeating this this step for each subsequent layer in the order that they experience water breakthrough. This allows analysing the waterflooding dynamics, efficiency and the estimated recovery factor, hence the main objective of the method is achieved.

The formation permeabilities can be corrected if the layers are differentially depleted, as proposed in Dake, 2001.

Time can be re-introduced into the model if required. This may be important when the actual production/injection forecast is needed, e.g. for economic field evaluation. Time can be introduced accurately by integrating the analytical solution for x_j (Reznik et al., 1984, El-Khatib, 1985). Alternatively, time can be *approximately* introduced by matching the injection rates and injected volumes, i.e. $t_{bt,R} \approx \left.\frac{WI_R}{q_R}\right|_{at\ x_R^*=1}$. This is an *approximate* answer because the injection rate changes with time though not significantly until water breaks through. Section 4.3.2 will follow the same workflow while introducing the extended solutions that incorporates the impact of an arbitrary sandface, flow control

completion in wells.

4.3.2 Extension of the DP method to the case of wells with AWC

In general, a Flow Control Completion (FCC) imposes a pressure drop that is quadratically proportional to the flow rate:

$$\Delta P_{FCC} = a_{flowing\ phase} q^2 \tag{4-8}$$

The coefficient *a* (FCC strength) is a function of the FCC strength, the number of FCDs per zone in question, and the flowing fluid properties. Various formulae explaining how to calculate it for a given FCC type or for a completion zone containing multiple FCCs are presented in (Al-Khelaiwi, 2013). In this study for simplicity, we will refer to it simply as a_w for water flow and a_o for oil flow. The total pressure drop across a layer is now a function of both the reservoir and FCC pressure drops:

$$\Delta P = \Delta P_{FCC,injector} + \Delta P_{layer} + \Delta P_{FCC,producer} = \left(a_{inj} + a_{prod}\right) q^2 + \Delta P_{layer} = a^* q^2 + \Delta P_{layer} \tag{4-9}$$

Where a^* for a given layer equals $a^* \equiv a_{bbt}{}^* = a_{w,inj} + a_{o,prod}$ before water breaks through this layer; and $a^* \equiv a^*_{abt} = a_{w,inj} + a_{w,prod}$ after water breakthrough. It is possible to model any arbitrary FCC performance or well workover action for any given layer by changing the coefficients *a* for this layer. The following FCC examples illustrate what can be modelled:

- ICD, ICV, AFCD, AICV completion (with any arbitrary number of devices per layer) when the *a* coefficients are selected to match the FCC's number/layer and the single phase flow performance curves
- When a conventional completion is installed, i.e. when a = 0
- Closure of the zone by e.g. an autonomous water shut-in response of the FCC, or closure of an ICD/ICV, zonal isolation by a well workover, etc. by taking either $a_{w,prod} = \infty$ or simply $q_{abt}=0$.
- Any other arbitrary flow control action for each layer.

This allows modelling any FCC performance.

The original DP method is any valid for the reservoir-only flow, i.e. for an openhole completion where the impact of FCC is absent, and the sandface pressures are calculated. This sandface-to-sandface pressure drop (ΔP) across any layer can be found by rearranging equation 4-9 as:

$$\Delta P_{layer} = \Delta P - a^* q^2 \tag{4-10}$$

Changing ΔP to ΔPlayer in equation 4-4 results in $q_j = \frac{k_j \lambda_{w,j}^{'} A_j}{L} \cdot \frac{\Delta P - a_j^{*} q_j^{2}}{x_j^* + M_j(1-x_j^*)}$, and expressing this quadratic equation for *u=q/A* yields:

$$u_j = \frac{-B_j + \sqrt{B_j^{2} + 4a_j^{*} A_j^{2} C_j^{2} \Delta P}}{2a_j^{*} A_j^{2} C_j} \tag{4-11}$$

Where coefficients B and C are defined as:

$$B_j \equiv x_j^* + M_j(1-x_j^*) \tag{4-12}$$

$$C_j \equiv \frac{k_j \lambda_{w,j}^{'}}{L} \tag{4-13}$$

Note that in the AWC case, the effective cross-sectional area is introduced immediately since it affects the reservoir pressure drop. This differs from the original method where this area only appears later in the method, when calculating the flow rates and watercuts. This new approach demands that the effective cross-sectional area be reliably estimated, by taking into account the areal sweep efficiency, flood patterns, faults, etc.

The integral (equation 4-14) is solved by following the same logic that led to equation 4-6 in the original method:

$$\int_0^{x_j^*} \frac{\Delta S_j \phi_j}{u_j} dx_j^* = \int_0^{x_R^*} \frac{\Delta S_R \phi_R}{u_R} dx_R^* \tag{4-14}$$

The general analytic solution for integral 4-14 for arbitrary limits is:

$$\int_{x^*_{j,\min}}^{x^*_j} \frac{\Delta S_j \phi_j}{u_j} dx^*_j = \frac{\Delta S_j \phi_j}{4(1-M_j)C_j \Delta P} \left[\begin{array}{l} B_j \left(\sqrt{B_j^2 + 4a_j^* A_j^2 C_j^2 \Delta P} + B_j \right) + \\ +4a_j^* A_j^2 C_j^2 \Delta P \ln\left(\sqrt{B_j^2 + 4a_j^* A_j^2 C_j^2 \Delta P} + B_j \right) \end{array} \right]_{x^*_{j,\min}}^{x^*_j} \quad (4\text{-}15)$$

Particular limits will be considered in Section 4.3.3, which describes the complete application workflow.

4.3.3 Workflow AWC with piston like displacement in vertical well

Consider an injector-producer pair, separated by distance L, in a heterogeneous reservoir. Each layer has its own height *h*, effective cross-sectional area *A*, porosity φ, horizontal permeability *k*, end point saturation S_{wi} and S_{or}, end-point mobilities $\lambda_w^{'} \equiv k_{rw}^{'} / \mu_w$ and $\lambda_o^{'} \equiv k_{ro}^{'} / \mu_o$, and mobility ratio $M \equiv \lambda_w / \lambda_o$. One or both of the injector and producer completion can have a FCC, the impact on each layer's flow is described by the a^* coefficient defined by equation 4-8. Note that a^* can vary, e.g. a^*_{bbt} before breakthrough and a^*_{abt} after breakthrough.

The following steps, the original DP method, use the equations derived in Section 4.3.2, that describe how the waterflood analysis can be carried out:

Step 1. Order the layers by breakthrough time, approximately estimated as the inter-well distance divided by the front velocity calculated at the time when $x_j^*=0.5$, derived using equations 4-11, 4-12, 4-13.

$$t_{bt,j} \approx \frac{L}{\left. \frac{dx_j}{dt} \right|_{x_j=0.5L}} = L \frac{\Delta S_j \phi_j}{u_j(x^*_j = 0.5)} = \frac{L \Delta S_j \phi_j}{2a_{j,bbt}^* A_j^2 C_j} \left(-\left[0.5 + M_j(1-0.5) \right] + \sqrt{\left[0.5 + M_j(1-0.5) \right]^2 + 4a_{j,bbt}^* A_j^2 C_j^2 \Delta P} \right) \quad (4\text{-}16)$$

Step 2. Take the first layer to experience breakthrough as the reference layer. Find the water front positions in the other layers when the reference layer experiences water breakthrough (i.e. when $x^*_R=1$). This is done by equating the solutions described by equation 4-15 as follows:

$$\int_0^{x^*_j} \frac{\Delta S_j \phi_j}{u_j} dx^*_j = \int_0^1 \frac{\Delta S_R \phi_R}{u_R} dx^*_R$$

Which yields:

$$\frac{\Delta S_j \phi_j}{(1-M_j)C_j}\left[\begin{array}{l}\left(x_j^*+M_j(1-x_j^*)\right)\left(\sqrt{\left(x_j^*+M_j(1-x_j^*)\right)^2+4a_{j,bbt}{}^*A_j{}^2C_j{}^2\Delta P}+\left(x_j^*+M_j(1-x_j^*)\right)\right)-M_j\left(\sqrt{M_j{}^2+4a_{j,bbt}{}^*A_j{}^2C_j{}^2\Delta P}+M_j\right)+\\ +4a_{j,bbt}{}^*A_j{}^2C_j{}^2\Delta P\ln\left(\dfrac{\sqrt{\left(x_j^*+M_j(1-x_j^*)\right)^2+4a_{j,bbt}{}^*A_j{}^2C_j{}^2\Delta P}+\left(x_j^*+M_j(1-x_j^*)\right)}{\sqrt{M_j{}^2+4a_{j,bbt}{}^*A_j{}^2C_j{}^2\Delta P}+M_j}\right)\end{array}\right]=$$

$$=\frac{\Delta S_R \phi_R}{(1-M_R)C_R}\left[\begin{array}{l}\left(\sqrt{1+4a_{R,bbt}{}^*A_j{}^2C_R{}^2\Delta P}+1\right)-M_R\left(\sqrt{M_R{}^2+4a_{R,bbt}{}^*A_R{}^2C_R{}^2\Delta P}+M_R\right)+\\ +4a_{R,bbt}{}^*A_R{}^2C_R{}^2\Delta P\ln\left(\dfrac{\sqrt{1+4a_{R,bbt}{}^*A_R{}^2C_R{}^2\Delta P}+1}{\sqrt{M_R{}^2+4a_{R,bbt}{}^*A_R{}^2C_R{}^2\Delta P}+M_R}\right)\end{array}\right] \tag{4-17}$$

The validity of the derivation can be tested by setting the FCC coefficients a in equation 4-17 to zero. The result should now match the original, (no-FCC) solution described by equation 4-7

Note that x_j can no longer be expressed explicitly as in the original method (equation 4-7). It must be solved numerically. We solve such equation with gradient-based, non-linear solver (available in MS Excel) in a fraction of a second.

Step 3. These front positions can be used to calculate the injected water volume in S.I units (WI) or in reservoir pore volumes (WI*), as well as the reservoir oil recovery efficiency (RE) as follows:

$$WI=\sum_{j=1}^{N}A_j\Delta S_j\phi_j x_j^*L \tag{4-18}$$

$$WI^*=\frac{\sum_{j=1}^{N}A_j\Delta S_j\phi_j x_j^*L}{\sum_{j=1}^{N}A_j\phi_j L} \tag{4-19}$$

$$RE=\left.\frac{\sum_{j=1}^{N}A_j\Delta S_{wi,j}\phi_j x_j^*L}{\sum_{j=1}^{N}A_j\phi_j L(1-S_{wi,j})}\right|_{if\ x_j^*\geq 1 then\ x_j^*=1} \tag{4-20}$$

Note that x_j in equation 4-20, equals 1 if $x_j>=1$ for the layers that had previously

experienced breakthrough when a subsequent reference layer is used.

Step 4. The production flow rates for each layer at the time of water breakthrough into layer R are calculated as $q_j = u_j A_j$ where u_j is calculated using equations 4-11, 4-12, 4-13. The reference layer is producing water while the other layers are still producing oil. The fractional flow rate of water f_w is thus calculated as:

$$f_w = \frac{\sum_{j=1}^{N}\left(q_j \cdot \begin{Bmatrix} 1 if\ x_j^* \geq 1 \\ 0 if\ x_j^* < 1 \end{Bmatrix} \right)}{\sum_{j=1}^{N}\left(q_j \cdot \begin{Bmatrix} 1 if\ x_j^* \geq 1 \\ 1 if\ x_j^* < 1 \end{Bmatrix} \right)} \tag{4-21}$$

(if watercut is preferred instead of fraction flow, "*1 if* x_j**<1*" should be changed to "*1/*b_o *if* x_j**<1*" where b_o is the oil formation volume factor).

Step 5. Select the next layer to experience water breakthrough as the reference layer, and repeat Steps 2, 3, and 4. Continue until all layers have experienced breakthrough.

Step 2a. For a given reference layer the layers that had experienced water breakthrough earlier have been producing water for some time. The original method describes how this can be taken into account when calculating WI. Namely: an imaginary water front position, propagating beyond *x*=1*, is calculated and used to calculate the volume of water injected into an already flooded layer. Assume the reference Layer R is experiencing water breakthrough, while Layer k had experienced breakthrough earlier and had been producing water. To calculate the relative front positions in this case use:

$$\int_0^1 \frac{\Delta S_k \phi_k}{u_k} dx_k^* \Big|_{a^*=a^*_{bbt}} + \int_1^{x_k^*} \frac{\Delta S_k \phi_k}{u_k} dx_k^* \Big|_{a^*=a^*_{abt}} = \int_0^1 \frac{\Delta S_R \phi_R}{u_R} dx_R^* \tag{4-22}$$

The integral's solution is given in equation (5-17) where the integral limits should be taken form the equation 4-22 above.

The second integral on the right-hand side in equation 4-22 describes the imaginary propagation of the water front beyond the production well. Since layer k is producing water after water breakthrough, the FCC across this layer in the production well is now responding to the water production. *Note that this step can also be removed altogether if*

zonal water shut-in upon breakthrough is assumed by, e.g. ICV reactive control, water-restrictive AFCD, ICD sliding sleeve closure, well workover operation, etc.

An example of the application of this workflow, and the excellent match of its results with those of a comprehensive, numerical reservoir simulation model prediction, is shown in the next section. This workflow was realized as an Excel spreadsheet and that is solved using gradient-based, non-linear solver in Excel in a fraction of a second for arbitrary boundary conditions and FCC set-ups

Finally, since time can be introduced into the production forecast, the method can be modified to model a constant production rate case (as opposed to the constant pressure drop case discussed in the calculations above):

A. **Introducing time.**

   The traditional, accurate methods of translating the injected volume into time by integrating the injection rate over front position x are not applicable here since there is no explicit analytical solution for x. Instead, equation 4-16 is used to find the approximate time of each breakthrough, allowing the calculation of the injected volumes, oil recovery efficiency, fractional flow, etc. into the time domain. Naturally, the flow velocity changes as the water front propagate within the layer (see e.g. equation 4-1), but this change is not that significant, and so the velocity estimate at $x^*=0.5$ is reasonably good enough. The accuracy of this assumption will be confirmed in section 4.3.4

B. Extending to the constant rate case.

   The constant pressure drop workflow can be easily extended to the constant rate case. The approximate layer rates are estimated by calculating the flow rates for an arbitrary pressure drop at the time when $x_j^*=0.5$ using equations 4-11, 4-12, 4-13. Their sum gives the total well rate. An optimizer is then used to find the pressure drop required for this well production rate. This pressure drop is then used as usual in the workflow described above. This extra step during the model set-up is included in our spreadsheet. The extra operation takes a fraction of a second.

It is worth mentioning that, in point B above, the well's approximate flow rate, used to match the reservoir pressure drop, was estimated before water breakthrough. If there is a significant post-breakthrough action (e.g. zonal isolation by an ICV), then the flow rate will change significantly at the given pressure drop. The integration therefore has to be

split into smaller intervals related to the periods before and after each zonal action. The appropriate changes must also be made to the flow rates, pressure drops, and FCC coefficients.

4.3.4 Model Verification and Example Applications

Model Verification

The oil recovery and fractional flow (or well watercut) predicted by the above model was compared with the results from of a commercial reservoir numerical simulator. A box-shaped reservoir model (Figure 4-8), composed of 5 non-communicating layers whose properties are described in Table 4-1 was prepared. The model dimensions are 10m x 500m x 30m, i.e. the distance L between the vertical wells, located on the opposite sides of the reservoir, was 500 m. (*The small width of 10m is chosen because we are considering a* reservoir cross-section problem. *The 10m width ensures the areal sweep efficiency is 100% since we are only considering the vertical sweep efficiency*).

Table 4-1. Layer properties in the test reservoir

Layer	**k**	**h**	**Φ**	**μ_w**	**μ_o**	**S_{wi}**	**S_{or}**	**k_{we} (end-point)**	**k_{oe} (end-point)**	**Area**
Unit	mD	m		cP	cP					m^2
1 (top)	5000	5	0.45	1	1.5	0.2	0.1	0.5	1	50
2	1000	7	0.25	1	1.5	0.2	0.25	0.4	1	70
3	300	9	0.2	1	1.5	0.2	0.4	0.6	1	90
4	2000	6	0.3	1	1.5	0.2	0.3	0.7	1	60
5	4000	3	0.4	1	1.5	0.2	0.15	0.5	1	30

The wells are controlled at a bottom-hole pressure selected to keep the pressure difference between the injection and production wells at 20 bars. The relative permeability curves used in this model are straight lines connecting the end-point values listed in Table 4-1. Note, the analytical solution derived above also to applies to any shape of relative permeability curves as long as the following conditions apply: a) The minimum oil –Sor- and water –Swc- saturation can be achieved; b) the flood front spread within a layer is smaller than within the whole reservoir i.e. the displacement is piston-like. The simulation

time is chosen to make sure that the sufficient amount (here around 2 pore volumes) of water is injected to flood the reservoir. The following well completion options are modelled (Table 4-2):

Table 4-2. Well completion options modelled in the test case

	Layer FCC strength a*before breakthrough	**Layer FCC strength a*after breakthrough**
Case	**bar/(rcm/d)^2**	**bar/(rcm/d)^2**
a* 0 0	0 (open-hole completion)	0 (open-hole completion)
a* 0.008 0.008	0.008 (medium strength FCC)	0.008 (medium strength FCC)
a* 0.016 0.016	0.016 (high strength FCC)	0.016 (high strength FCC)

The number and restriction of FCDs in the reservoir model were designed to add a reasonable pressure drop across the completion in front of each layer (note that "reasonable strength" in the ICD technology is understood as the strength causing the FCC pressure drop to be comparable to the drawdown across the reservoir). The chosen values for drawdown, flow rates, and FCC restriction levels are all realistic. The zonal FCC strength a* (i.e. combined performance of FCCs in both the injection and production wells for a given layer, see the comments made on equation 4-9) does not change after water breakthrough, even though the production well starts producing water. This corresponds to the performance of a fluid-property-tolerant ICD completion (or 'hybrid' ICDs). Also note that the FCC was designed to have the equal FCC strength for each layer. This was done to simplify the comparison and analysis of the model predictions to help ensure a robust model verification.

The case nomenclature (left hand column, Table 4-2) is "[a* (the FCC strength for every layer)] [strength before breakthrough in bar/(rcm/d)^2] [strength after breakthrough in bar/(rcm/d)^2]". For example, the case "a* 0.008 0.008" implies that the combined FCC strength for each layer before and after water breakthrough is 0.008 bar/(rcm/d)^2. The base case with no FCC (the original DP case) is denoted by "a* 0 0".

Figure 4-7 shows the Recovery Efficiency (RE) vs Injected Water volume (IW) measured in reservoir Pore Volumes (PV) predicted by both the numerical simulation and the semi-analytical model derived in this paper. The match is very good, verifying the extended DP model.

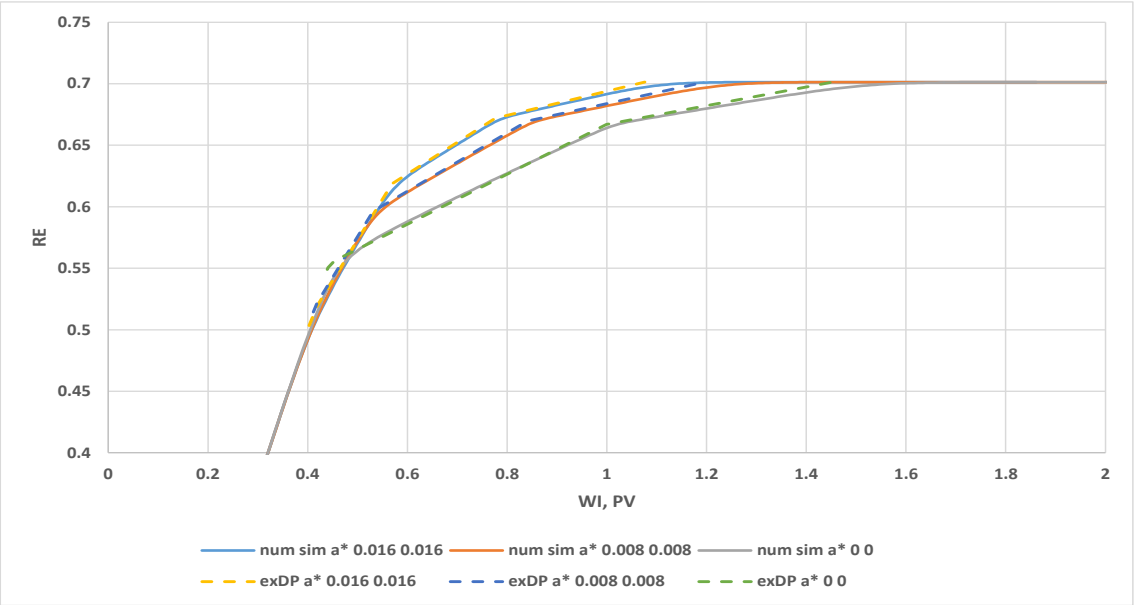

Figure 4-7. Numerical simulation ("num sim") and AWC-extended Dykstra-Parsons (exDP) model prediction results

As expected, a higher recovery is achieved for a given injected volume with a stronger FCC. The more productive layers are restricted more strongly resulting in a more uniform water propagation front, and a better sweep (Figure 4-8, Figure 4-9). This effect is non-linear: there is a clear gain in RE once the FCC strength is increased from 0 to 0.008 bar/(rcm/d)^2, but the gain caused by the change of strength from 0.008 to 0.016 bar/(rcm/d)^2 is less pronounced.

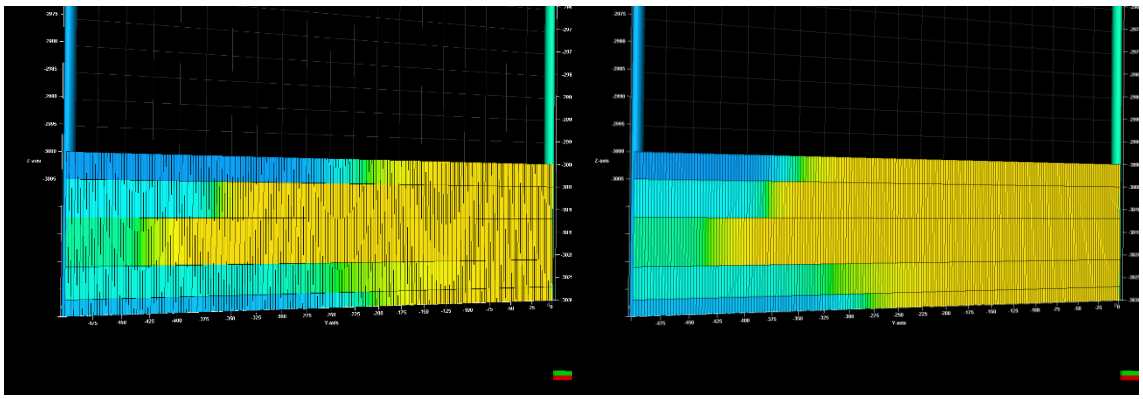

Figure 4-8.Water Saturation after 4 months, case "a* 0 0". Injection is from left to right.

Figure 4-9. Water saturation after 4 months, case "a* 0.016 0.016". Injection is from left to right.

Further Example Applications

We will now illustrate the use of the extended DP model for modelling and designing AWCs. The reservoir model used is the same as described in the section 4.3.4 above. (The numerical simulation results are also shown in several plots for background comparison.)

a) ICD completion modelling and design

Consider the case with the objective to find the FCC strength a^* to improve oil recovery. As explained in earlier, a reservoir numerical simulation is the best tool for evaluating and comparing different FCC design options. However, the most commonly used software due to its simplicity, method is to use a stand-alone wellbore model – either analytical or numerical - to find a trade-off between balancing zonal inflow and well productivity loss. Figure 4-10 is the (initial) oil inflow rate distribution along the production well is plotted on a layer-by-layer basis for the FCC options listed in Table 4-2 are modelled numerically in a wellbore model:

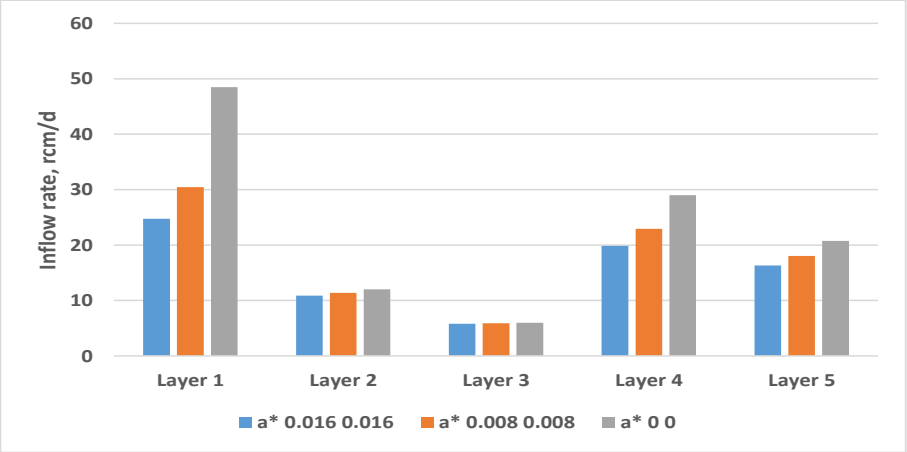

Figure 4-10. Inflow rate from each layer at the start of production

Naturally, the stronger the FCC, the smaller and more uniform, is the zonal inflow rates. It's hard to say which FCC strength is optimal. While there are several methods (Prakasa *et al.*, 2015, Birchenko *et al.*, 2011) speculates on the benefit of the reduced inflow variation and lower the well productivity, but they do not predict the actual, long-term recovery or economic gain from installing an AWC. The extended DP method presented here can do this:

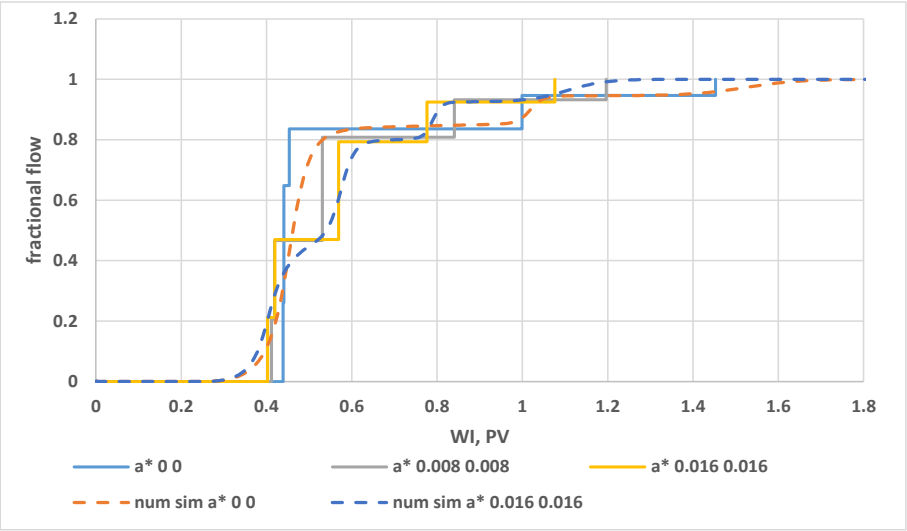

Figure 4-11. Fractional flow rate (i.e. watercut at bottomhole conditions) vs WI for several FCC strength options calculated by the extended DP method

Figure 4-7 and Figure 4-11 show that the stronger the FCC, the lesser WI is required to sweep the reservoir. Note the step-like shape of the fractional flow rate – each change is caused by the piston-like water breakthrough to each subsequent layer; while the smoother performance of the numerical simulator is due to the propagation front within each layer being more gradual and not piston-like.

It is sometimes useful to quantify how well the FCC reduces flow heterogeneity by adjusting the layer flow rates to achieve a more uniform sweep. The Lorenz plot is traditionally used for this. Here, the fraction of the total flow capacity (i.e. flow rate per net-pay interval) is plotted with respect to either the fraction of the total 'static' storage capacity (i.e. pore volume per interval) or the fraction of the total 'dynamic' storage capacity (i.e. streamline's pore volume per interval). The net-pay intervals are normally ordered so that the curve is strictly convex. The static and dynamic Lorenz plots for the modelled cases are presented as Figure 4-12 and Figure 4-13. Notice how the stronger FCC moves the curve towards the 'ideal', balanced flow (i.e. flow rate is proportional to the storage capacity) case.

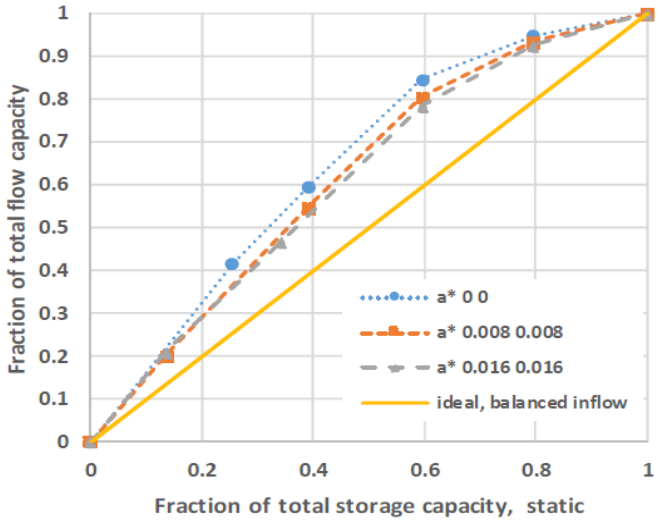

Figure 4-12. The 'Static' Lorenz plot illustrates how the stronger FCC balances the inflow (i.e. the curves move closer to the 'ideal' straight line).

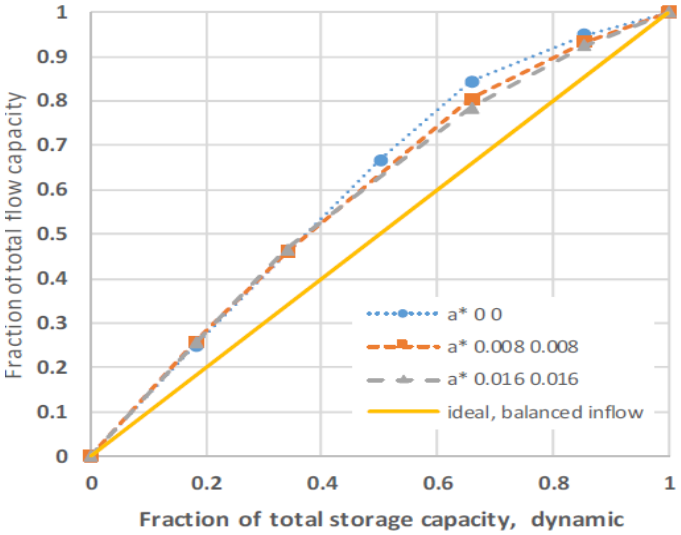

Figure 4-13. The Dynamic' Lorenz plot illustrating how the stronger FCC balances the inflow profile, i.e. the curves move closer to the 'ideal' straight line.

The area between the curve on the Lorenz plot and the orange 'ideal', 45^0 slope straight line is a measure of the heterogeneity known as Lorenz coefficient Lc. Figure 4-12 and Figure 4-13, show that both the static and dynamic Lorenz coefficients decrease with increasing the FCC strength from 0 through 0.008 bar/(rcm/d)^2 to 0.016 bar/(rcm/d)^2 : the static Lc takes the values of 0.29, 0.23 and 0.22 respectively, while the dynamic LC takes the values of 0.21, 0.19 and 0.17 respectively.

The volumetric efficiency of the waterflood increases with the stronger FCC. However,

the constant pressure drop between the wells' BHPs implies there will be a smaller reservoir pressure drop and production rate for the stronger FCC. The stronger FCC thus needs less WI to achieve the target sweep efficiency, but it will also take longer to inject volume of water. This will be examined by extending the AWC analysis to the time domain:

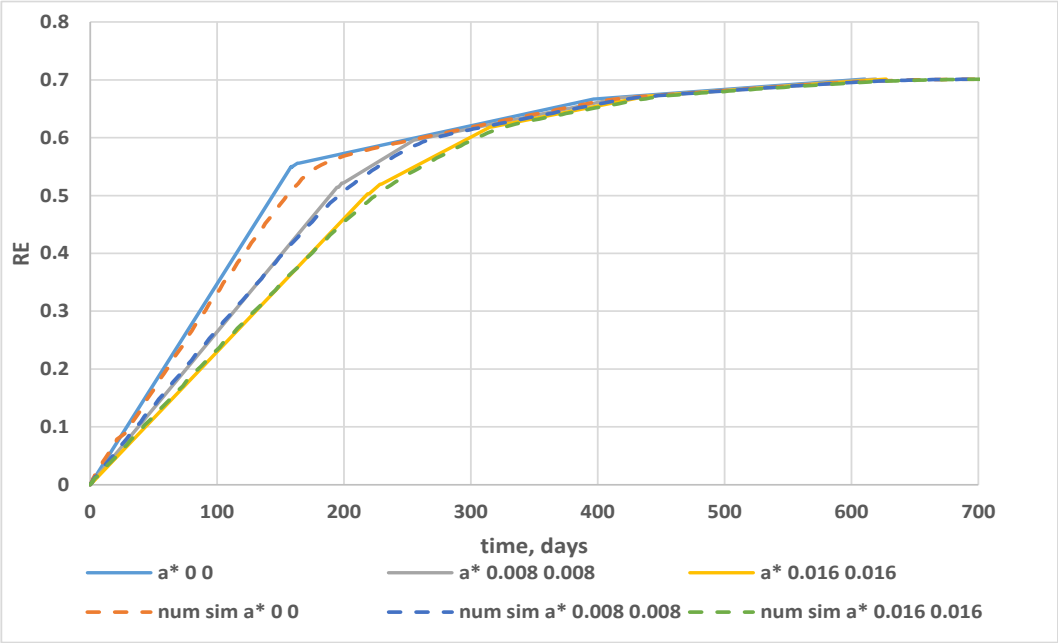

Figure 4-14. RE vs time for several FCC strength options

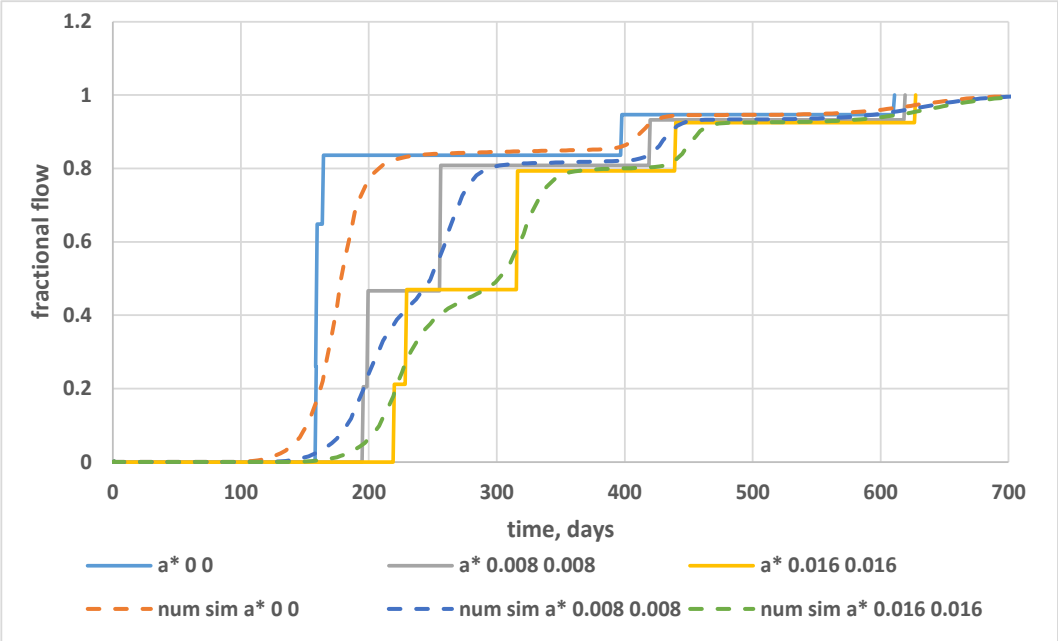

Figure 4-15. Fractional flow vs time for several FCC strength options

Fig. 4-14 and 4-15 show the production forecast versus time. It is clear that the less

restrictive FCC accelerates both oil and water production, while the more restrictive one constraints them. Option "a* 0.008 0.008" now looks reasonable giving a relatively fast increase in RE while significantly delaying water production. The analysis can be continued by calculating economic parameters for further quantification of the difference between the three completions.

b) Example of AFCD completion modelling and design

The second example evaluates the potential gain from an AFCD completion. Note that the value of this completion cannot be assessed with stand-alone wellbore simulators because they consider initial inflow state (as was explained above), while the major contribution of an AFCD is its response to the water breakthrough that happens in the well's life. This prediction requires access to a dynamic reservoir simulator. However, the extended DP method can be used reliably as will be shown below.

The blue solid line in Figure 4-16 and Figure 4-17 show how an AFCD completion performs, whose strength doubles from 0.008 to 0.016 bar/(rcm/d)^2 upon water breakthrough. It is compared with the reservoir simulation model and the single-strength ICD cases presented earlier:

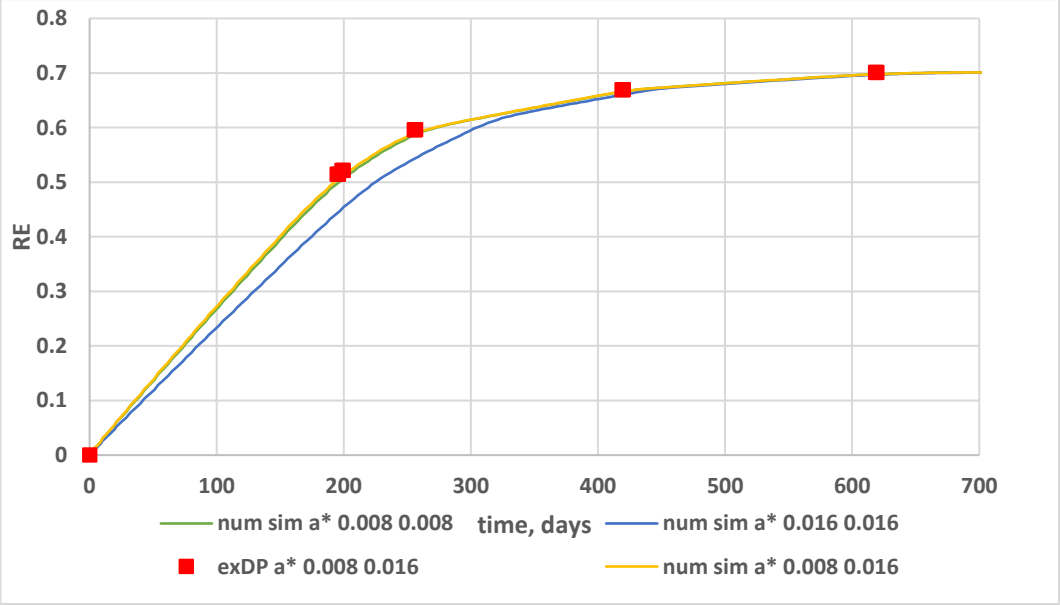

Figure 4-16. RE vs time for an AFCD completion compared with previous ICD completions

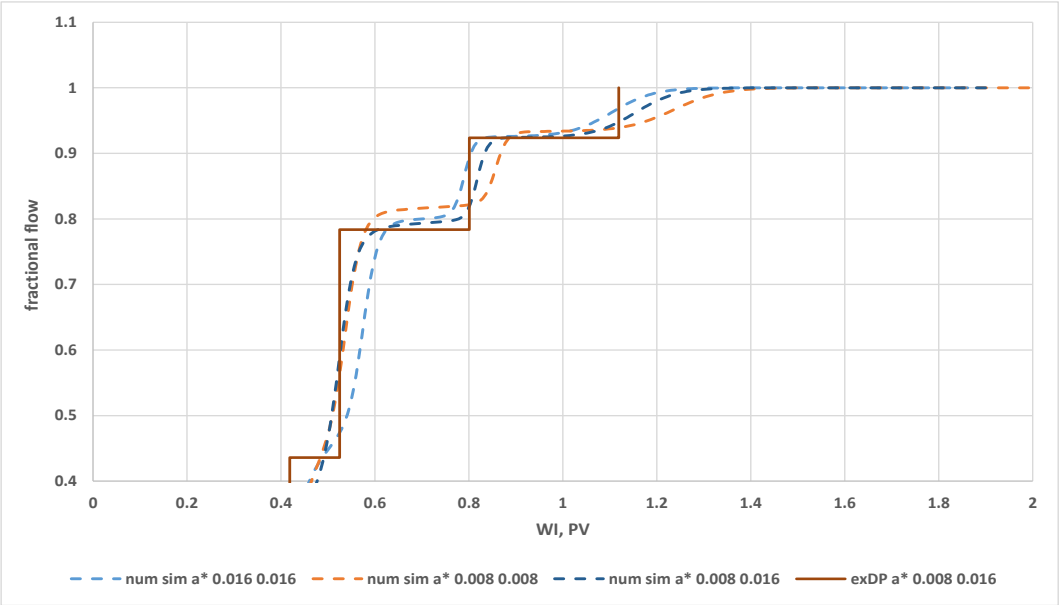

Figure 4-17. Fractional flow vs time for an AFCD completion compared with previous ICD completions

Note how well the extended DP model prediction matches the numerical simulator. The AFCD "a* 0.008 0.016" recovery efficiency overlays that for the ICD "a* 0.008 0.008" case. This is expected – the AFCD water response affects only the water production rate, while the oil production rate stays the same as for ICD case "a* 0.008 0.008". The impact of the increased AFCD strength to water is clearly seen in Figure 4-15 – the fractional flow rate (and so watercut) curve is between the medium and strong ICD cases.

It is clear that the AFCD completion offers the oil recovery efficiency as good as its response to oil, and the water control as good as its response to water. Eltaher *et al*., 2014 independently came to the same conclusion and recommended the AFCD design for maximum production efficiency is relaxed to oil while being restrictive to water.

4.4 Modelling performance of waterflood by vertical wells with AWCs using modified BL method

The validation of DP method in AWC is only valid when a 'piston-like displacement' of oil occurs. A "non-piston like" displacement, as occurs when the mobility ratio is unfavourable (M>1), and the relative permeability curve does not follow a linear plot, required a new method. This section explains the overview of BL method and its development to incorporate the non-linear pressure drop from the FCC. Compared to DP method, this method add more complexity, and solution will be firstly tested in single-

layer system before extending it to the multi-layer model. The solutions presented in this work are for the case of constant pressure difference between the injection and production wells. Note that in the original form, Buckley-Leverett equation was presented assuming constant rate and does not calculate pressure. Our BL method, used constant pressure differences to make a simple comparison with the DP method presented (which assumes constant pressure difference) previously.

4.4.1 BL method and non-piston like displacement

BL method assumes material balance, i.e. the volume of liquid entering the system is equal to the volume of liquid that has left. Consider a case where the injected water is displacing oil in a reservoir with porosity Φ (Figure 4-18). Mass conservation over the volume element of length, *dx*, dictates that the mass flow rate in – mass flow rates out = rate of increasing mass in the volume (equation 4-24).

$$(q_w\rho_w)_x - (q_w\rho_w)_{x+\Delta x} = A\,\Phi\,dx\,\frac{\delta}{\delta x}(\rho_w S_w) \qquad (4\text{-}23)$$

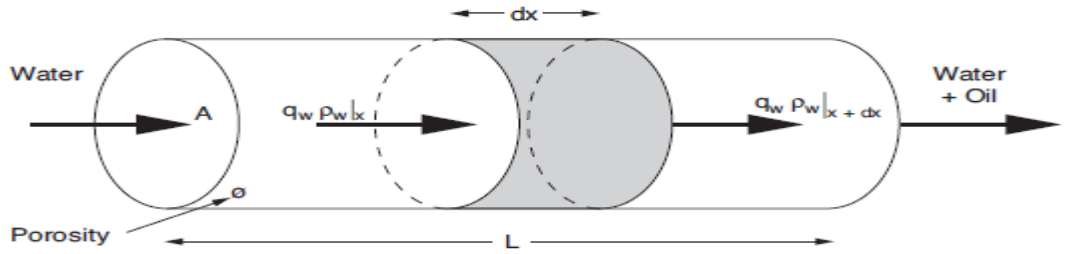

Figure 4-18. Mass flow through core (1D displacement) (Todd, 2012)

The frontal displacement solution or Buckley-Leverett (BL) equation for incompressible flow and a constant injection rate is:

$$V_{Sw} = \frac{q_t}{A\Phi}\frac{\delta f_w}{\delta S_w}\bigg|_{Sw} = \frac{q_t}{A\Phi} f_w{}'\big|_{Sw} \qquad (4\text{-}24)$$

Where f_w is the fractional flow, or ratio of water flow rate to the total flow rate; and V_{Sw} is the velocity of the place of a specific saturation, S_w.

The BL equation calculates S_w as a function of time and distance. It indicates that the velocity of a specific, water saturation front is directly proportional to the derivative of its fractional flow curve, $f_w{}'$. The fractional flow can be described as:

$$f_w = \frac{1}{1+\left(\frac{Kr_o \mu_w}{Kr_w \mu_o}\right)} \qquad (4\text{-}25)$$

Chierici, 1995 presented a systematic fractional flow analysis for three types of displacement:

Light Oils

This displacement type occurs when the displaced phase has a lower viscosity and higher relative permeability, when compared with the displacing phase. This fluid will have a concave upward fraction flow curve. Figure 4-19 illustrates this type of displacement. On the left side, the $f_w{}'$ curve decreases from when $S_w = 1\text{-}\ S_{or}$ (residual oil saturation) to its minimum value at $S_w = S_{wi}$ (irreducible water saturation). The front will thus have its highest velocity, when $S_w = 1\text{-}\ S_{or,}$ the lowest water saturations value. This analysis replicates a piston-like displacement. See Figure 4-19, where A is a concave upwards fractional flow curve, B shows the corresponding velocity of water saturation, and the C, the characteristic of water saturations (*Sw*) movement in the light oils displacement.

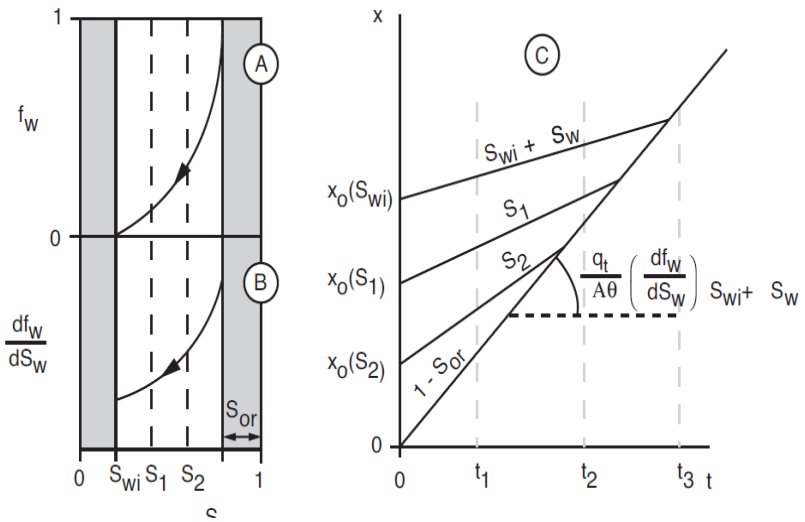

Figure 4-19. Displacement of oil by water for a concave upwards fractional flow curves (light oil displacement) (Todd, 2012)

Medium Viscosity Oils

Displacement of a medium viscosity oil by water results in an S-shaped f_w curve and a $f_w{}'$ curve in the form of an inverted "U". The rate of change of the fractional flow(f_w), reaches a maximum value of $f_w{}'$ at the peak of the inverted "U" at S_{wf}, where $S_w <$

$S_{wf} < (1 - S_{or})$. The front velocity would decrease, with increasing front S_w above this value. This implies that a shock front, where the water saturation has the highest velocity, S_{wf}, will develop. The water saturation behind this front will steadily increase, but at an ever-decreasing velocity. 100% oil will be produced until the shock front saturation reaches the production well with the fraction of water gradually increasing until all the mobile oil is completely displaced. Figure 4-20 summarise the above explanation, A is the S shaped fractional flow curve, B is the velocity of water saturation, and C is the characteristic of water saturations (*Sw*) movement for the medium oils.

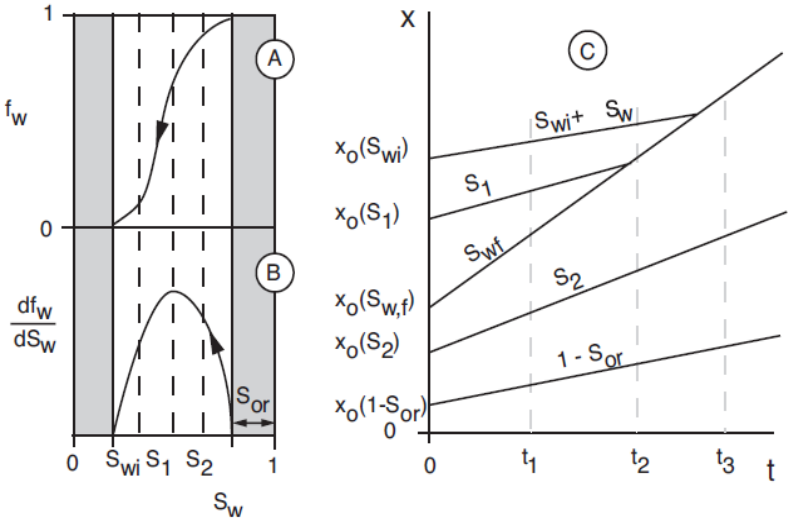

Figure 4-20. Displacement of a medium viscosity oil by water with an S-shaped fractional flow curve. (Todd, 2012)

Heavy Oils

The displaced phase for this case has a significantly greater viscosity than the displacing phase. The fractional flow curve has a concave downward shape (Figure 4-21), resulting in its derivative continually increasing in value, from the initial condition, $S_w = 1 - S_{or}$. The highest velocity is at the saturation value slightly higher than the irreducible water saturation (S_{wi}). This is the water saturation value when the flood front breaks through, followed by a steady increase in the water saturation which is moving at decreasing velocity - See Figure 4-21 where figure A is the Concave downwards fractional flow curve, figure B is the velocity of water saturation, and figure C is the characteristic of water saturations (S_w) movement for the heavy oils.

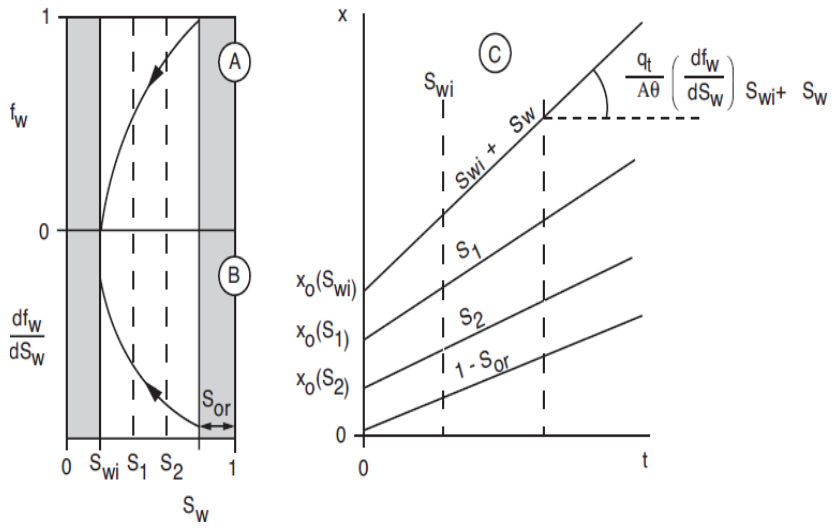

Figure 4-21. Displacement of a viscous oil by water (heavy oil displacement) (Todd, 2012)

The modelling of AWC for light oils which replicate piston-like displacement was discussed in the previous section. The latter two non-piston like displacement types are analysed in the next section.

4.4.2 Predicting front saturation and average saturation behind front

The saturation and the average saturation behind the flood front for light oil displacement are both assumed to be equal to 1-S_{or}. By contrast, the front saturation for medium oil displacement is a function of the fractional flow curve derivative, $f_w{}'$. Welge, 1952 provides an elegant method to estimate these values by integrating the saturation over the distance from the point of injection to the flood front. The integration formulated that the saturations of flood front is the inverse slope of average water saturation at breakthrough ($\overline{S_{wbt}}$) minus irreducible water saturations(S_{wi}).

$$\left(\frac{\delta f_w}{\delta S_w}\right)_{S_{wf}} = \frac{1}{\overline{S_{wbt}} - S_{wi}} \qquad (4\text{-}26)$$

He suggested drawing a tangent to the f_w curve originating at the irreducible water saturation of (*1-S_{or}*). The intersection point with the S_w axis defines the water saturation at the flood front and the reciprocal of the slope is the front velocity (Figure 4-22). In the fractional flow the average saturations behind this front is found by extrapolating this line to $f_w = 1$, or by finding the Sw value when tangent f_w is at maximum.

$$S_{wf} = max\left(\frac{fw - fw_{swi}}{sw - swi}\right) \quad (4\text{-}27)$$

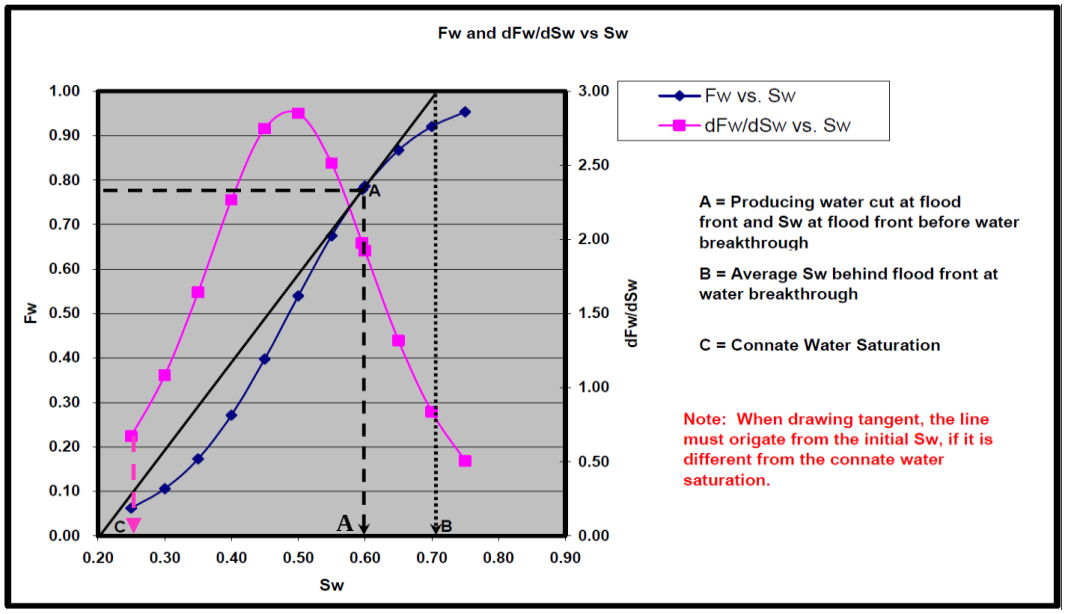

Figure 4-22. Fractional flow curve

The same method is adopted to find the average water saturations post-breakthrough. The sequence is to calculate the water saturations, S_{we}, and thereafter, draw a tangent line to $f_w = 1$ to find the average water saturation (Figure 4-23).

$$S_{avg} = \overline{S_w} = S_{wf} + \left(\frac{1 - fw}{\frac{\delta f_w}{\delta S_w}}\right) \quad (4\text{-}28)$$

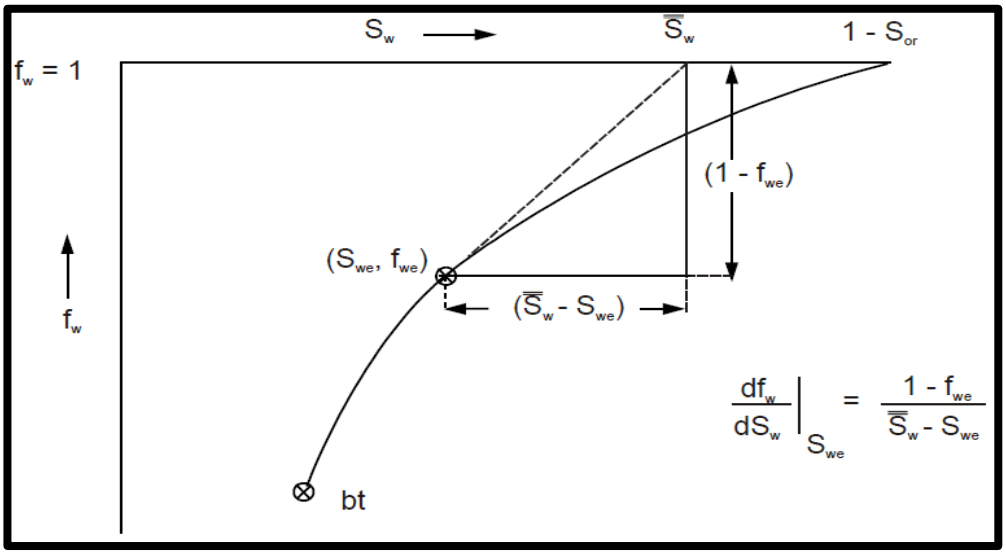

Figure 4-23. Welge's graphical determination of average water saturation. $\overline{S_w}$ after breakthrough.

This workflow was originally developed to determine the oil recovery and the water fraction as a function of cumulative volume of water injected. It implied that the water saturation of the formation behind the flood front was homogeneously saturated with water (equal to $\overline{S_w}$). The water behind the flood front can thus be considered to have a "pseudo" permeability based on this saturation value. The analytical prediction of the front's displacement follows this routine i.e. by finding the Kr value from relative permeability curve corresponding to the average water saturation calculated by Welge's method. This practice is only applicable to some types of relative permeability curves, i.e. liner ones. For non-piston like displacement, i.e. for medium and heavy oil displacement, there are layers of different oil and water saturations behind the flood front, moving with different permeability (Figure 4-24).

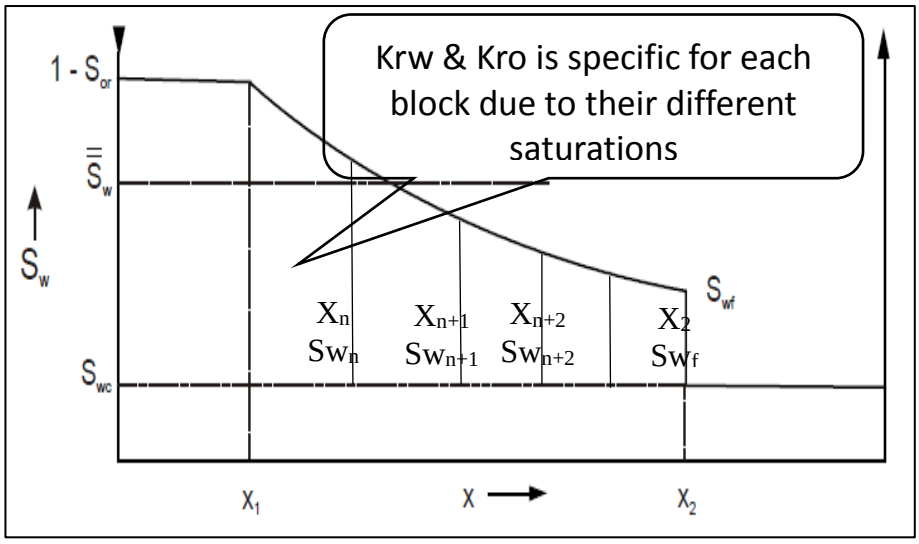

Figure 4-24. Dividing the formation water behind the front into blocks

Consider P1 is the upstream pressure, i.e. at the injector, while P2 is the pressure downstream, at the saturation front. It is possible to break the formation between these points into blocks with different water saturations and relative permeability values (see also figure 4-25). The aggregate differential pressure of each of these blocks is P1-P2.

$$P1 - P2 = (\Delta P_n + \Delta P_{n+1} + \Delta P_{n+i}) \quad (4\text{-}29)$$

Now consider this flooded region to be a homogeneous layer with a single pseudo-relative permeability value for each phase, Krw_{avg} and Kro_{avg}. As per Figure 4-25 notation, the sum of pressure drops across the flooded region is:

$$Vw\frac{\mu_w X_2}{krw_{avg}} = \left(Vw\frac{\mu_w\,(X_n - X_1)}{krw_n} + Vw\frac{\mu_w\,(X_{n+i} - X_n)}{krw_{n+i}} + \cdots + Vw\frac{\mu_w\,(X_2 - X_{n+i})}{krw_{n+i}}\right)$$

$$\frac{1}{Vw\mu_w}\frac{krw_{avg}}{X_2} = \frac{1}{Vw\mu_w}\left(\frac{krw_n}{(\Delta x_n)} + \frac{krw_{n+i}}{(\Delta x_{n+1})} + \frac{krw_{n+i}}{(\Delta x_{n+i})}\right)$$

$$krw_{avg} = \frac{X_2}{\sum_n^i \frac{\Delta x_n}{krw_n}} = \frac{X_2}{\sum_{1-Sor}^{Swf} \frac{\Delta x_{Sw}}{Krw_{Sw}}} \tag{4-30}$$

Where X_2 is the distance of the displacement from the injector. kro_{mix} Is calculated using the same concept:

$$kro_{avg} = \frac{X_2}{\sum_n^i \frac{\Delta x_n}{kro_n}} = \frac{X_2}{\sum_{1-Sor}^{Swf} \frac{\Delta x_{So}}{Kro_{Sw}}} \tag{4-31}$$

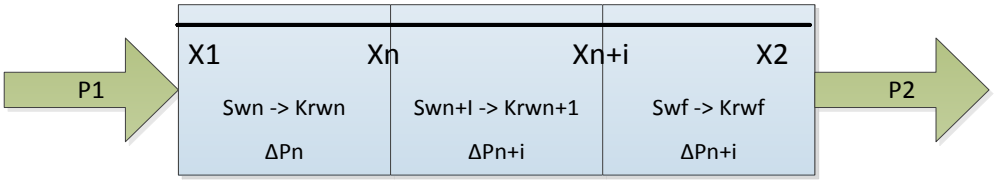

Figure 4-25. Behind the water front, there may be assumed several blocks with different relative permeability.

Note: The harmonic averaging formulae have been widely used in reservoir simulations for finding the average relative permeability for different block/cells. To the author's knowledge, this technique has not previously been applied to the semi-analytical model calculation.

It was now possible to evaluate the average mobility ratio in front of and behind the flood front (equations 4-32 and 4-33).

$$\lambda_{mix} = \frac{\bar{k}_{rw}}{\mu_w} + \frac{\bar{k}_{ro}}{\mu_o} \tag{4-32}$$

$$Mobility\ Ratio = \frac{M_{Displacing}}{M_{Displaced}} = \frac{\lambda_{mix}}{\lambda_o} \tag{4-33}$$

4.4.3 Extension of the BL method to the case of wells with AWC

We can model the non-pistonlike displacement for two systems (displacing and displaced) in manner similar to the application of DP method in AWC wells. The non-linear pressure drop from flow devices is added to the system using of equation 4-8. Note

that the modified BL method can work with either constraint of pressure difference or well's flow rate. To maintain consistency with the previously explained modified DP method, we will explain in detail the displacement under the constraint of pressure difference (as opposed to the flow rate constraint that the original BL method used). As a consequence, the constant pressure drop would not give a constant production rates, and the flow rates as well as the properties of the reservoir saturated with the displacing phase are evaluated for different flood front positions and saturations (as will be described in section 4.4.4).

$$B_j = \dot{x}(1 - M_{mix}) + M_{mix} \tag{4-34}$$

$$C_j = \frac{k\lambda_{avg}}{L} \tag{4-35}$$

$$Q_{inj} = \frac{\left(-B_j + \sqrt{B_j^2 + 4a_j^* A_j C_j^2 \Delta P}\right) \cdot A_j}{2a_j^* A_j^2 C_j} \tag{4-36}$$

4.4.4 Workflow for the modified BL method with an AWC

The following workflow has been designed:

Before Breakthrough

Step 1. Perform the fractional flow analysis using relative permeability values. Calculate and draw the f_w and $f_w{}'$ curves, find the value of flood front saturation and average water saturation with equations 4-27 and 4-28. The saturation front (S_{wf}) and average water saturation($\bar{S}_w$) behind the front are constant prior to breakthrough. Kro_{avg} and Krw_{avg} of the displacing front will also be constant during this period.

Step 2. For each layer, divide the distance between producer and injector into *n* blocks and evaluate displacement from every incremental of X, to X_n. Where X is the ratio of the front distance from the injector to the total distance (L) between the injector and producer wells. X_0 is the initial condition and $X_{0.2}$ is when the flood front has reached 0.2 L and X_1 is when the water has arrived at the producer. The injection rate (Q_{inj}) can be calculated using equations 4-34, 4-35, and 4-36. The displacement efficiency (E_d) behind this front is obtained using equation 4-37 before finding the total cumulative water injection with equation 4-38.

$$E_d = \frac{\bar{S}_w - S_{wi}}{1 - S_{wi}} * X \tag{4-37}$$

$$W_{inj} = (1 - S_{wi}) * E_d * PV \tag{4-38}$$

The cumulative water injection volume equals injection time * injected water rate: $W_{inj} = t * Q_{inj}$, hence the required time for every evaluated X is calculated with equation 4-39:

$$t = \sum \Delta t = \sum \frac{W_{inj}}{Q_{inj}} \tag{4-39}$$

The above is repeated for each of layers that make up the completion. The layers are ordered in terms of increasing line to breakthrough. The first layer that experiences breakthrough is the reference (*layer R)*. The time required to saturate block in layer R, is calculated. All other layers' displacement properties, e.g. front position and velocity are calculated at the total displacement time (t) to reach the injector. The front position in these layers (*layer j*) is obtained from equation 4-33 as follows:

$$t_J\big|_{X_n} = t_R \tag{4-40}$$

$$\frac{\left(W_{inj,X_n} - W_{inj,X_{n-1}}\right)_J}{\left(Q_{inj,n} - Q_{inj,n-1}\right)_J} = \frac{\left(W_{inj,X_n} - W_{inj,X_{n-1}}\right)_R}{\left(Q_{inj} - Q_{inj,n-1}\right)_R} \tag{4-41}$$

$$\frac{\left((\bar{S}_w - S_{wi}) * (X_n - X_{n-1}) * PV\right)_J}{\left(Q_{inj,n} - Q_{inj,n-1}\right)_J} = \frac{\left((\bar{S}_w - S_{wi}) * (X_n - X_{n-1}) * PV\right)_R}{\left(Q_{inj,n} - Q_{inj,n-1}\right)_R} \tag{4-42}$$

$$\frac{(X_n - X_{n-1})_R}{\left(Q_{inj,n} - Q_{inj,n-1}\right)_R} = \frac{1}{\left((\bar{S}_w - S_{wi}) * PV\right)_R} \frac{\left((\bar{S}_w - S_{wi}) * (X_n - X_{n-1}) * PV\right)_J}{\left(Q_{inj,n} - Q_{inj,n-1}\right)_J} \tag{4-43}$$

Note that $Q_{inj}{}_R$ is a function of X_R (equation 4-43), X_R cannot therefore be expressed explicitly, however using gradient-based, non-linear solver in Excel may be used to obtain this value in a fraction of a second.

Step 3. Repeat the step 2 until layer j experiences breakthrough (i.e. x_j = 1). Note that $Q_o = Q_{inj}$ at all time since flow into system equals flow out of it.

<u>After the water breakthrough in layer j</u>

Step 4. Use the second layer (x_{j+1}) to experience breakthrough as the reference layer. Use x_{j+1} = 1 as the corresponding time to calculate the front positon, injection and producing rates for all the remaining layers which have not yet experienced breakthrough, i.e. follow steps 2 and 3 to calculate the front's relative position and velocity in the other layers.

Step 5. Layer j had already experienced break through when water breaks through in layer x_{j+1}. Evaluate layer j as *m* number of incremental S_w starting from the current flood front saturation (S_{wf}) to when oil is not produced anymore, i.e. at (*1* - S_{or}). Multiphase flow occurs in layer j: $Q_{inj,j} = (Q_o + Q_w)_{prod,j}$ thus oil and water flow rates at the producer well can be obtained with equation 4-44 and equation 4-45.

$$Q_{o,prod} = \frac{Q_{inj}}{f_w} - Q_{inj} \tag{4-44}$$

$$Q_{w,prod} = Q_{inj} - Q_{o,prod} \tag{4-45}$$

The fractional flow is used to calculate the cumulative injected water:

$$W_{inj} = \frac{1}{{df_w}/{dS_w}} * PV \tag{4-46}$$

Since the cumulative water injection = time * injected water rate: $W_{inj} = t * Q_{inj}$, hence the required time for every evaluated S_W can be calculated using equation:

$$t = \sum \Delta t = \sum \frac{W_{inj}}{Q_{inj}} \tag{4-47}$$

By equating equation 4-40 and 4-47, we can calculate the water saturation of layer j at the time breakthrough occurs at the layer j+1.

$$t_{J+1} = t_J\big|_{Sw_m}$$

$$\frac{\left((\bar{S}_w - S_{wi}) * (X_n - X_{n-1}) * PV\right)_{J+1}}{\left(Q_{inj,n} - Q_{inj,n-1}\right)_{J+1}} = \frac{\left(\frac{1}{{df_w}/{dS_w}}\Big|_{S_w} * PV\right)_J}{\left(Q_{inj,m} - Q_{inj,m-1}\right)_J} \tag{4-48}$$

Note that the average water saturation behind the front changes with the increasing value of Sw during the period after breakthrough. Kro_{avg} *and* Krw_{avg} *for the system also will change for the different Sw.*

Q_{inj} is a function of Sw (equation 4-48). Gradient based, non-linear Excel Solver can be used to approximate S_w in layer J to solve equation 4-48.

Step 5a. The flow control strength, a^*_{abt} will vary as a function of watercut (WC) if Autonomous Flow Control Devices (AFCDs) are installed in the producer. This value is traditionally assumed to be governed by equation 4-49 (Halvorsen, Elseth and Nævdal, 2012; Mathiesen, Werswick and Aakre, 2014), where WC values are obtained from the fractional flow analysis (*fw*).

$$a_{ICD}{}^{*}_{abt} = \left[\frac{[(wc*\rho_w)*((1-wc)*\rho_o)]^2}{\rho_{cal}}\right] \cdot \left[\frac{\mu_{cal}}{[(wc*\mu_w)*((1-wc)*\mu_o)]}\right]^{y} \cdot a_{AICD} \quad (4\text{-}49)$$

Step 6. Repeat step 5, 5a until all layers have experienced the water breakthrough. Afterwards, consider the last layer as the reference (layer R), and the other layers as layers j. Calculate the displacement performances in layers J until layer R, using equation 4-50, has reached 100% production water cut, i.e. $Sw_j = 1 - S_{or}$. The waterflood of the reservoir is now complete.

$$\frac{\left(\frac{1}{df_w/dS_w}\Big|_{S_w} * PV\right)_{J+1}}{(Q_{inj,m} - Q_{inj,m-1})_{J+1}} = \frac{\left(\frac{1}{df_w/dS_w}\Big|_{S_w} * PV\right)_{R}}{(Q_{inj,m} - Q_{inj,m-1})_{R}} \quad (4\text{-}50)$$

Step 7. Reservoir flow performance can be evaluated as a summation of each layers performance at a given time.

$$N_p = \sum_{t=0}^{n} Q_{oil}|_t \cdot \Delta t \quad (4\text{-}51)$$

$$W_p = \sum_{t=0}^{n} Q_{water}|_t \cdot \Delta t \quad (4\text{-}52)$$

$$W_{inj} = \sum_{t=0}^{n} Q_{inj}\Big|_t \cdot \Delta t \quad (4\text{-}53)$$

A. Extending the workflow to the constant rate case

Extension of this workflow to the constant rate case is analogous to that used for the extended DP method's workflow. The approximate layer rates are estimated for an arbitrary pressure drop by calculating the flow rates at every X using equations 4-34, 4-35, 4-36 during the period prior to the breakthrough,. Their sum gives the total well rate. An optimizer (a gradient-based one in Excel or any non-linear optimisation in MATLAB)

is then used to find the pressure drop that gives the required well production rate. This process repeated for each incremental X. The same ideas applied for the period after breakthrough, and the process repeated for each incremental Sw. Our Excel's calculation completes this operation in a fraction of a second.

B. An Alternative workflow

The flood prediction is treated independently for each layer. The flow performances for each layer before breakthrough has been tabulated after step 2. Continue generating each layer's flow performances for the period after breakthrough with equations 4-36, 4-44, and 4-45. Once Q_{inj}, Q_{oil} and Q_w as a function of time have been acquired for each layer, a non-linear approximation (e.g. using LINEST command in Excel) could be applied to smooth the curves. To find the reservoir injection and producing rates, the flow rates from each layer are added together at the equal time step, i.e. cumulative flow rate from all the layers. It is now possible to find the total reservoir cumulative production/injection as a function of time using eq. 4-51 to 4-53.

4.4.5 Verification and Example Applications for the modified BL model with an AWC

A. Verification for a single layer displacement

The analytical model for waterflood performance of a medium and a heavy oil reservoirs for an AWC with flow control devices has been validated against a model in the ECLIPSE numerical simulation software. Both the medium viscosity oil and the heavy oil cases were evaluated in the bottom layer of the box-shaped reservoir model used previously (Figure 4-8 and Figure 4-9). The cross-section area perpendicular to flow is 30 m^2 (10m x 3m), and the distance between the wells, L, is 500 m. The mobility ratio of the medium and heavy oil is 5 and 125 respectively. The production well's AFCD completion had a strength prior to breakthrough (a^*_{bbt}) of 0.008 bar/(rcm/d)^2, which increased gradually after water reached the well until the maximum strength (a^*_{abt}) of 0.064 bar/(rcm/d)^2 is at 100% WC. The drawdown was 20 and 200 bars respectively. The above properties are summarised in Table 4-3.

Table 4-3. Well completion options modelled in the test case

Parameters	K	W	h	ϕ	S_{wi}	S_{or}	k_{we}	k_{oe}	μ_w	μ_o	n_o	n_w	a^*_{bbt}	a^*_{abt}	ΔP
Units	mD	m	m						cP	cP			$\frac{bar}{(rcm/day)^w}$		bar
Medium Oil Displacement	4000	10	3	0.4	0.2	0.15	0.5	1	0.4	4	2	3	0.008	0.064	20
Heavy Oil Displacement									0.4	100	3	4			200

Brooks-Corey type relative permeability curves are assigned for oil and water phase using Equations 4-54 and 4-55.

$$k_{ro} = k_{roe}\left(\frac{(S_o - S_{or})}{(1 - S_{wc} - S_{or})}\right)^{n_o} \quad (4\text{-}54)$$

$$k_{rw} = k_{rwe}\left(\frac{(S_w - S_{wc})}{(1 - S_{wc} - S_{or})}\right)^{n_w} \quad (4\text{-}55)$$

Where n_o and n_w are the Brooks-Corey exponents for oil and water and k_{roe} and k_{rwe} are the end points of the relative permeability curves. The example relative permeability curves are illustrated in Figure 4-26 with relative permeability for light oil (linear) compared against the heavy and medium oil (curve).

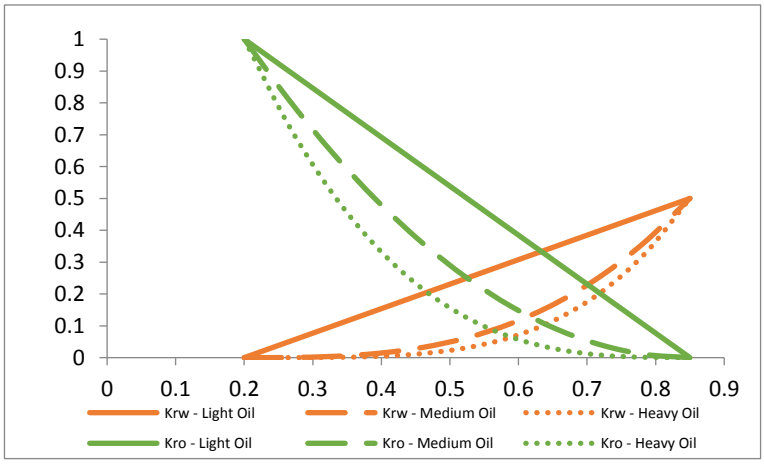

Figure 4-26. Corey type relative permeability curves for Layer 1

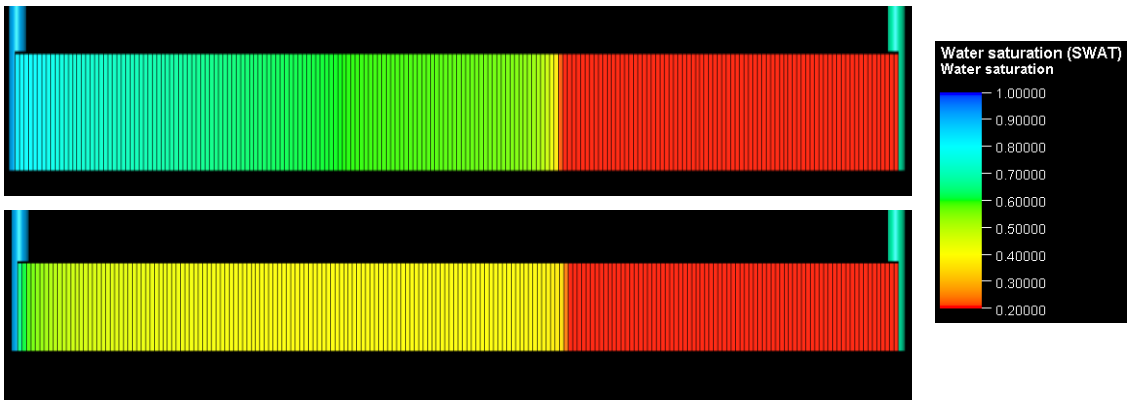

Figure 4-27. Water flood behaviour for different oils. Colours are representing saturation: red – oil, yellow – two-phase (oil and water), blue – water. Medium viscosity oil displacement (top). Heavy oil displacement (bottom).

The difference between medium oil displacement (Figure 4-27-top) and heavy oil displacement (Figure 4-27-bottom) is clearly seen. The sharp contrast of water saturation, between yellow and the greenish/blueish colour indicates the flood front. The position of this front relative to the distance between the wells is designated as X in the workflow step 2. The saturation distribution behind the front is noticeably different than in the piston-like case presented in the previous section (Figure 4-8 & Figure 4-9). In the non-piston like displacement, there is a distinctively sharp boundary (front) between flooded and unflooded parts of the layer, which is not present in the case of linear permeability curves.

This scenario will be illustrated by a 1 layer model. This simplification avoids the need to order the layers based on the breakthrough time since this essentially involves repetition of the same workflow.

Perform the fractional flow analysis is performed by drawing the f_w and $f_w{}'$ curves using the relative permeability curves. As previously, the Brooks-Corey relative permeability curves are used, allowing the f_w and $f_w{}'$ values to be calculated explicitly as:

$$f_w = \frac{1}{\left(1+\frac{\frac{\mu_w}{\mu_o}\frac{k_{roe}}{k_{rwe}}\cdot(S_o-S_{or})^{n_o}\cdot(1-S_{wc}-S_{or})^{n_w}}{(S_w-S_{wc})^{n_w}(1-S_{wc}-S_{or})^{n_o}}\right)} \tag{4-56}$$

$$f_w{}' = \frac{df_w}{dS_w} = (f_w - f_w^2)\left(\frac{n_o}{(1-S_w-S_{or})} + \frac{n_w}{(S_w-S_{wc})}\right) \tag{4-57}$$

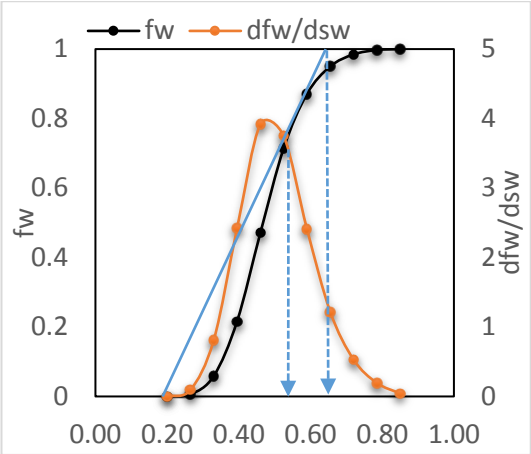

Figure 4-28. Fractional flow analysis for the medium oil displacement.

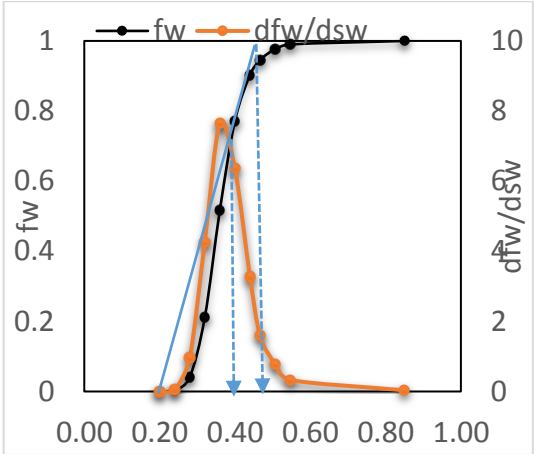

Figure 4-29. Fractional flow analysis for the heavy oil displacement.

Saturation at the flood front and the average saturation behind the front is calculated using equations 4-27 and 4-28, giving Sw_f = 0.57 and Sw_{avg} = 0.65 for medium oil displacement and Sw_f = 0.42, Sw_{avg} = 0.47 for heavy oil displacement.

The displacement length is divided into 10 block between the injector (X_0) and the producer (X_1). The average permeability of the front is calculated using the proposed harmonic averaging method, equation 4-30 and 4-31, followed by estimating the Qinj and Qo for each block. The calculation result is Kro_{avg} = 0.01, Krw_{avg} = 0.15 and Kro_{avg} = 0.13, Krw_{avg} = 0.01 for the medium and heavy oil cases respectively. For comparison, we checked if the method uses the relative permeability correlated directly from the Sw_{avg} using Welge method, i.e. Kro_{avg} and Krw_{avg} is obtained (using Figure 4-26) based on Sw_{avg} = 0.65 and Sw_{avg} = 0.47, for medium and heavy oil respectively. The mismatch clearly shows that choosing the right method to calculate the average rel-perm for the model is critical: our, discretized method is better. The contrast of our results with the calculation using the Welge method is displayed in table 4-4.

Table 4-4. The difference of Kr average between using the harmonic average method and using relative permeability table for Sw_{avg} Welge method.

Medium Oil Displacement			**Heavy Oil Displacement**		
	Kro-avg	**Krw- avg**		**Kro-avg**	**Krw- avg**
Proposed Method	**0.01**	**0.15**	Proposed Method	**0.13**	**0.01**
Welge	**0.09**	**0.17**	Welge	**0.20**	**0.01**

The fluid production rates both before and after breakthrough has been validated against the results of an Eclipse reservoir simulation. The proposed analytical model is in the excellent agreement with the numerical simulation for both medium and heavy oil displacement cases (Figure 4-30 and Figure 4-31).

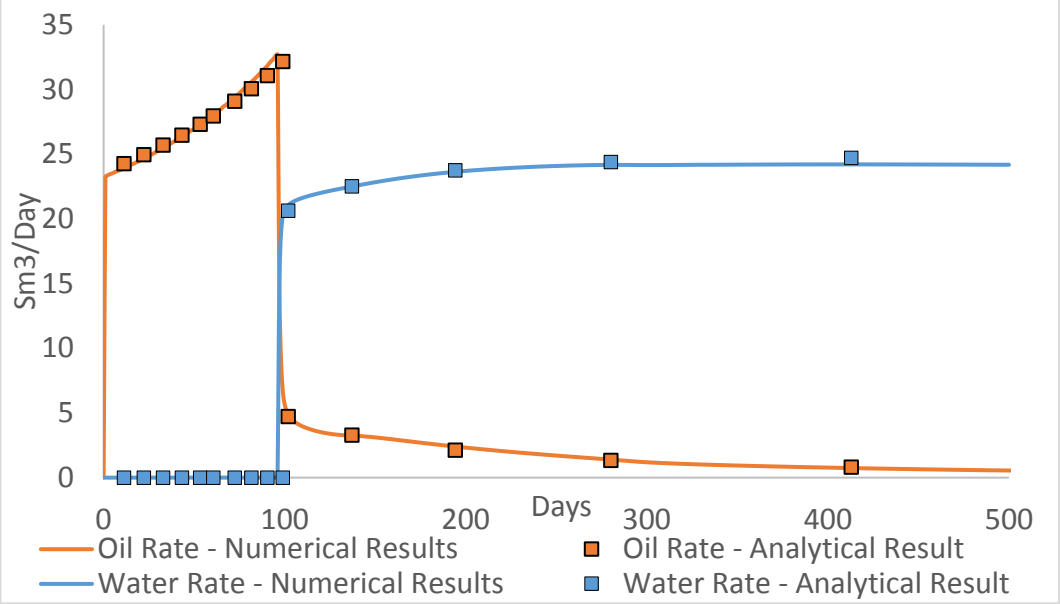

Figure 4-30. Water and oil production rates for medium oil displacement.

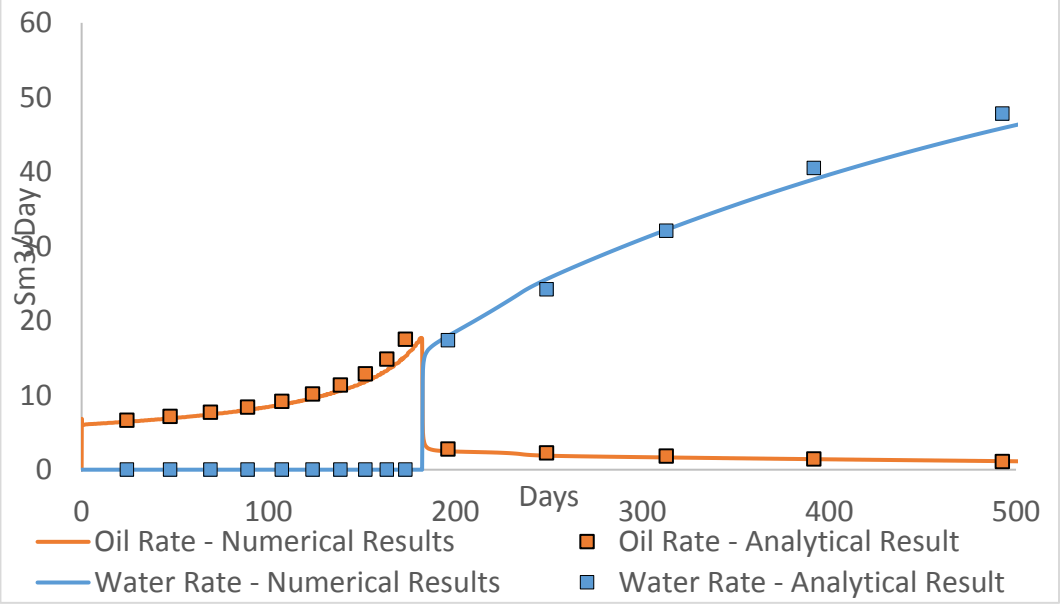

Figure 4-31. Water and oil production rates for heavy oil displacement.

B. Verification for the multi-layer displacement case

The box-shaped model (Figure 4-33 & Figure 4-34) with the table 4-5, a Brooks-Corey

function for medium oil was chosen to describe the relative permeability. A medium oil displacement case was chosen with a mobility ratio 10, the water viscosity μ_w, is 0.4 cP and the water exponent number, n_w, is 3. The oil viscosity μ_o is 4 cP and the oil exponent number, n_o, is 2. The production well's AFCD completion has a strength of 0.008 bar/(rcm/d)^2 when exposed to oil, and 0.064 bar/(rcm/d)^2 for the unwanted water.

Table 4-5. Properties of the reservoir with medium oil displacement.

Parameters	**K**	**h**	**ϕ**	**μ_w**	**μ_o**	**S_{wi}**	**S_{or}**	**k_{we}**	**k_{oe}**	**Area**	**n_o**	**n_w**
Units	**mD**	**m**		cP	cP					m^2		
1 (top)	5000	5	0.45	1	1.5	0.2	0.1	0.5	1	50	2	3
2	1000	7	0.25	1	1.5	0.2	0.25	0.4	1	70	2	3
3	300	9	0.2	1	1.5	0.2	0.4	0.6	1	90	2	3
4	2000	6	0.3	1	1.5	0.2	0.3	0.7	1	60	2	3
5	4000	3	0.4	1	1.5	0.2	0.15	0.5	1	30	2	3

Table 4-6. Properties of the AFCD completion

Drawdown (ΔP)	**a*before breakthrough**	**Maximum a*after breakthrough (single-phase)**
Bar	**bar/(rcm/d)^2**	**bar/(rcm/d)^2**
50	0.008	0.064

The AFCD strength for the unwanted fluids is 4 times the initial strength. This value is considered sufficient to choke the "bad-water" while still allowing a reasonable amount of oil production. As previous, it has been assumed that wells outflow is not restricted by the AFCD's additional performance. This either requires sufficient reservoir pressure or installation of artificial lift. A 50 bar pressure difference was maintained across the reservoir and completion between the injection and production wells. i.e. ΔP between the flow bottom-hole injection pressure (FBIP) and flow bottom-hole production pressure (FBHP) is always 50 bar.

Steps 1 to 7 of the extended BL workflow (section 4.4.3) were followed to investigate the layer and well performance of this reservoir. The layers were ordered from layer 5 (the

fastest) to layer 3 (the slowest) - See Figure 4-32.

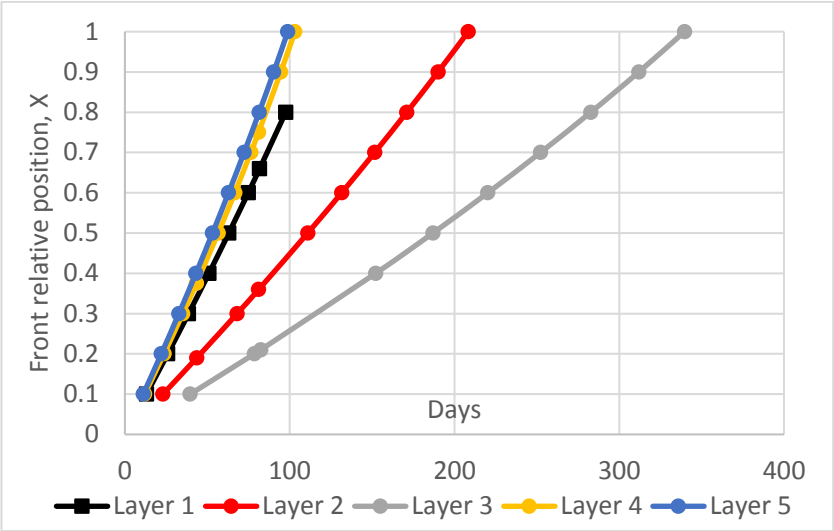

Figure 4-32. The layer front position vs time for each layer calculated with the analytical BL model

Figure 4-33 and Figure 4-34 are snapshots of the water saturation front at x_R = 0.4 and x_R = 0.8 in the (bottom) reference layer (the first one to be flooded), calculated by a numerical simulation. These numerical simulation results can be compared with the analytical flood (Figure 4-35) front predictions at the same x_R values

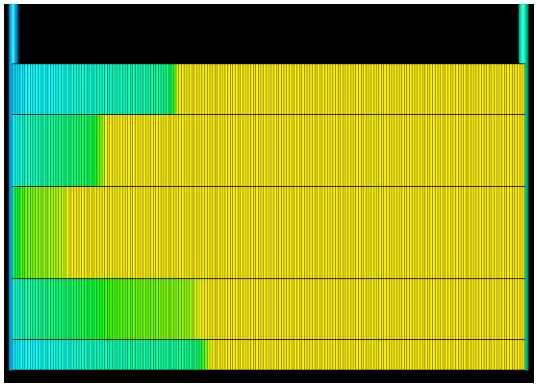

Figure 4-33. Displacement at x_R = 0.4

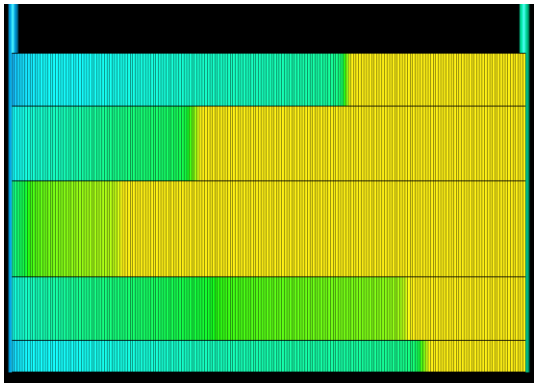

Figure 4-34. Displacement at x_R = 0.8

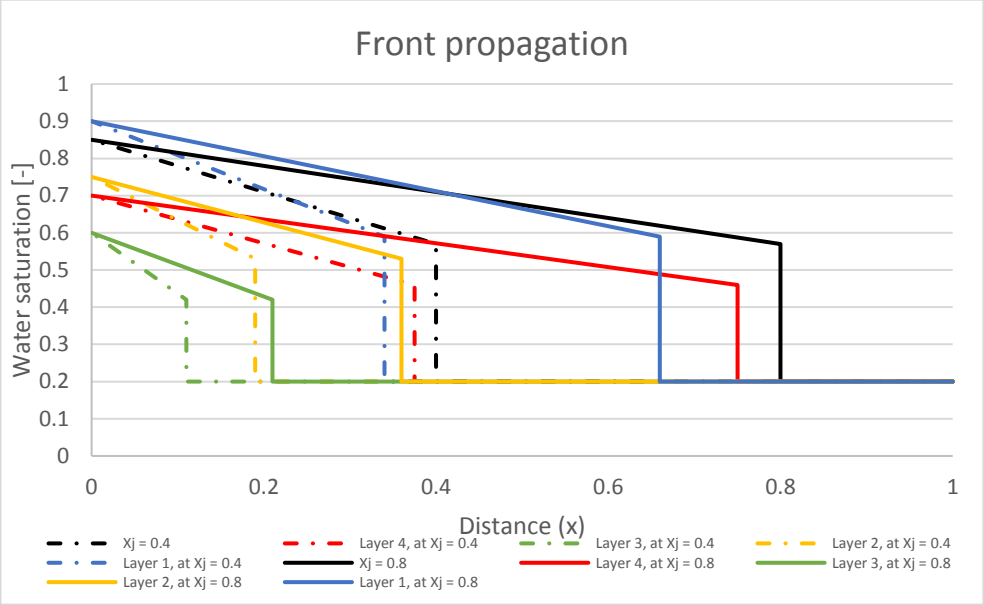

Figure 4-35. Water saturation as a function of distance

The calculation before breakthrough will find varying Q_{inj} for each increasing, evaluated X. Subsequently, workflow after breakthrough will also find varying Q_{inj} for each evaluated K_{rw}, K_{ro} average. This method thus captures and translates the front rate prediction into the time domain (Figure 4-36). The injection rate in layer 5 will increase over 25% from its initial values after 100 days (40 - 50 Sm^3/day), while the least prominent layer rate does not change significantly. The ratio between PI of the layer with the highest permeability to PI of the layer with the lowest permeability layer is increased from 6.5 to 7.5 fold after 100 days of production time.

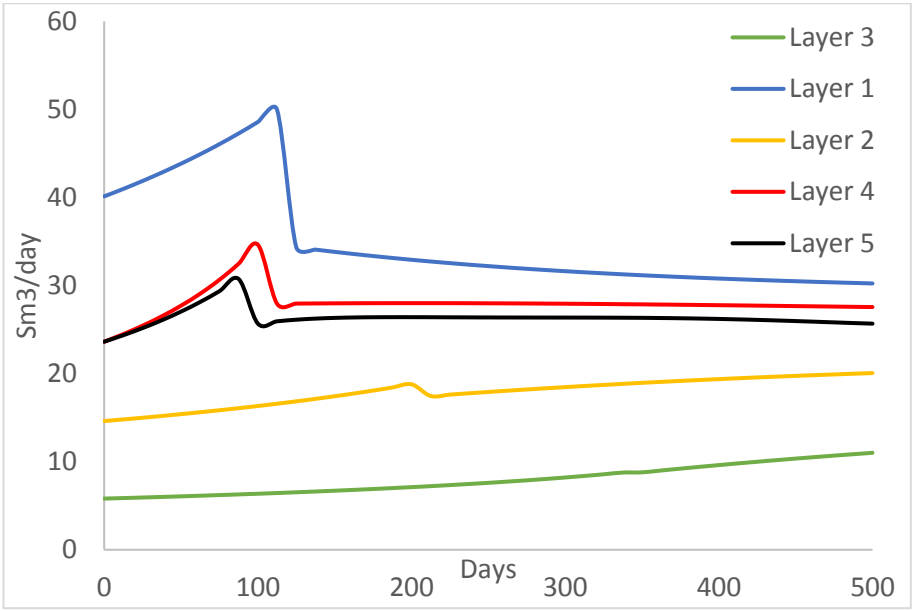

Figure 4-36. Layer's flow rate prediction over time

Figure 4-37 shows the well's oil and water production rate vs time, while Figure 4-38 shows the total cumulative oil and water production. Agreement between numerical and analytical work is clear and confirms the validity of the proposed method.

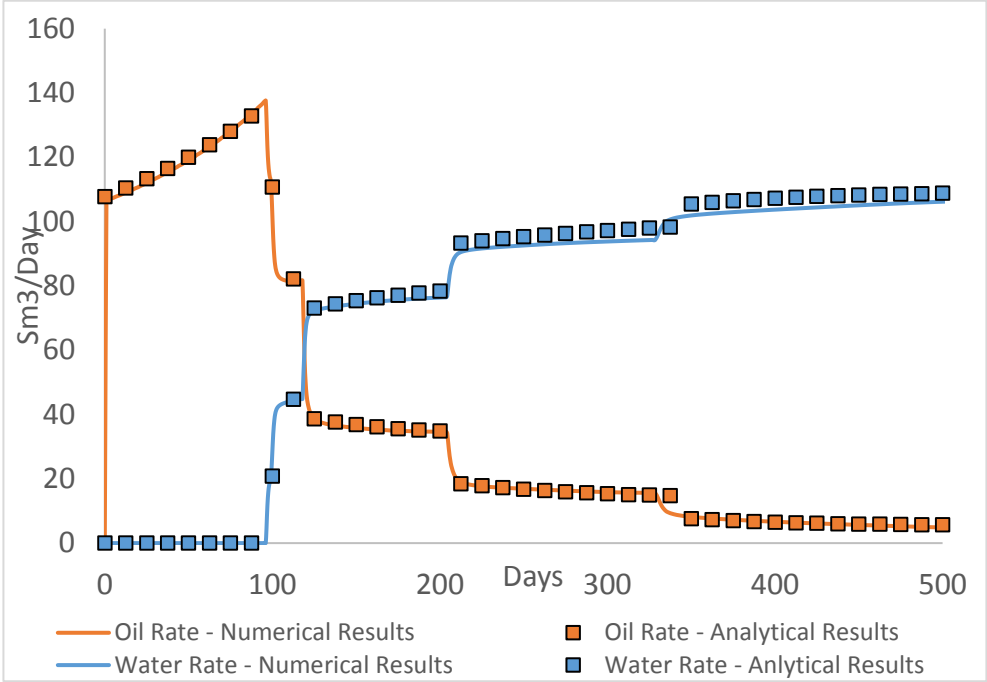

Figure 4-37. Numerical and analytical prediction of oil & water production rates

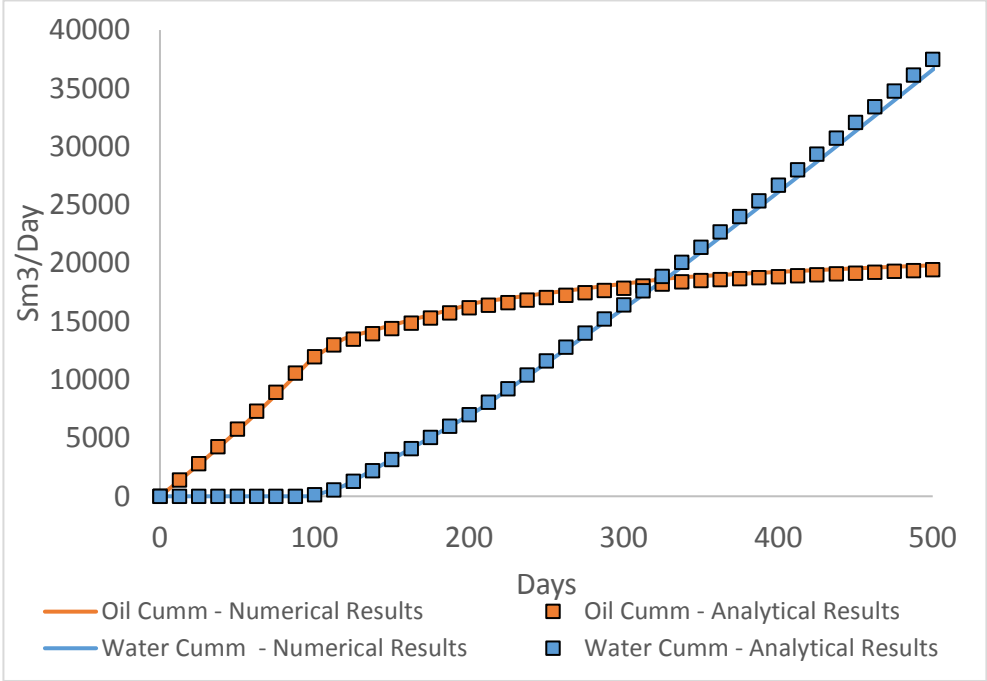

Figure 4-38. Numerical and analytical prediction of the cumulative oil and water production.

C. Example Applications

Whether a project will be sanctioned or not is ultimately dictated by its economics. Most companies use Net-Present-Value (NPV) as a measure to evaluate project economics (based on the time value of money) for comparing several possible scenarios. The scenario with the highest foreseen NPV will be the priority. Since the BL method can transform the waterflood performance into time-function based parameters (time domain), economic analysis becomes feasible.

This section evaluates the economics of several AFCD sizes. The application uses the same multi-layer model tabulated in Table 4-5. Consider scenario to search for a^*_{bbt} and a^*_{abt}values resulting in the highest NPV. The evaluation thus needs to calculate the explicit values of oil and water rate per month/days, before converting them into monthly revenue vs. cost results.

The scenario options we are going to check are listed in table 4-7:

Table 4-7. AFCD completion scenarios

	a^*_{bbt}	a^*_{abt}	**remarks**
Scenario number	**bar/(rcm/d)^2**	**bar/(rcm/d)^2**	
1	0	0	Screen
2	0	0.008	AFCD
3	0	0.016	AFCD
4	0	0.064	AFCD
5	0.008	0	AFCD
6	0.008	0.008	ICD
7	0.008	0.016	AFCD
8	0.008	0.064	AFCD
9	0.016	0	AFCD
10	0.016	0.008	AFCD
11	0.016	0.016	ICD
12	0.016	0.064	AFCD
13	0.064	0	AFCD
14	0.064	0.008	AFCD
15	0.064	0.016	AFCD
16	0.064	0.064	ICD

Evaluating all of these scenarios using reservoir simulation would require time and resources. There are also available guidelines developed to optimize AFCD using 'heat' maps (Eltaher *et al.*, 2014). However, they still need a number of reservoir numerical simulations to be run. The BL method for AWC developed here would replace the numerical reservoir simulation, at least for the rough optimisation of the vertical sweep. The workflow from section 4.4.4 is applied to all scenarios listed in Table 4-7. Oil and water production rates for each case are estimated (figure 4-39 and 4-40), similar to the process described to obtain Figure 4-37 and 4-38.

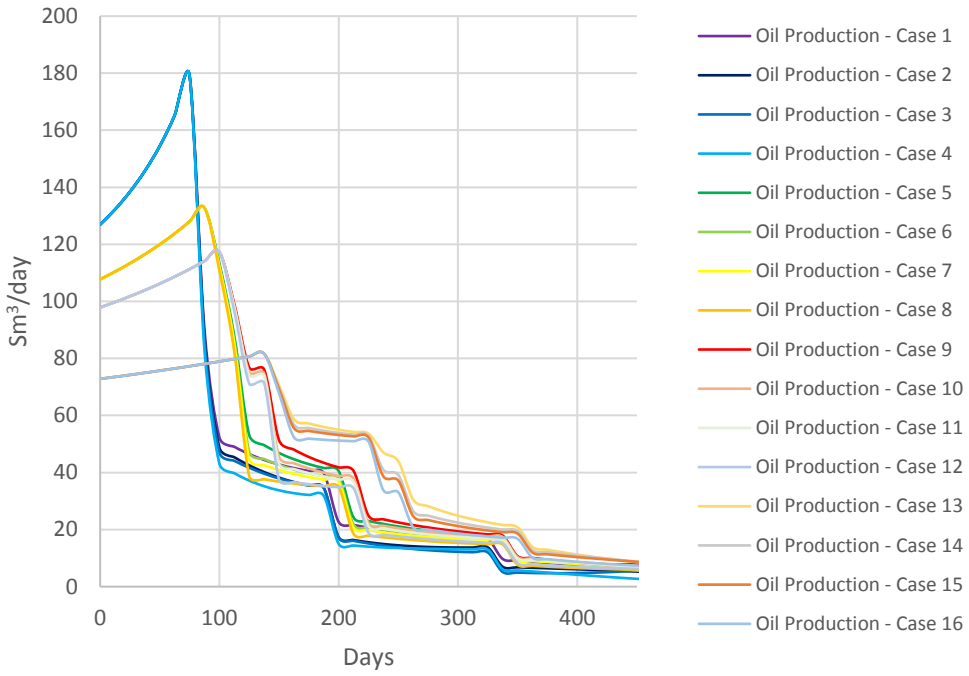

Figure 4-39. Comparison of oil production for scenario 1 - 16

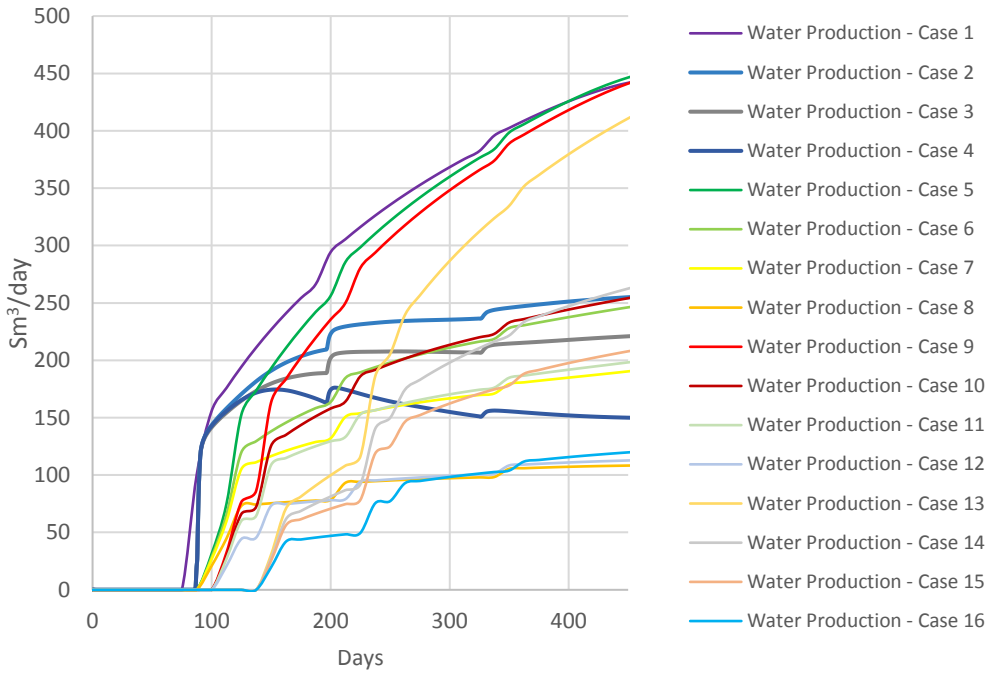

Figure 4-40. Comparison of water production for scenario 1 – 16

The workflow can also compare the fractional flow (*fw*) and recovery efficiency (*RE*), as a function of the volume of water injected expressed in reservoir pore volumes (*WI**), (figure 4-41, 4-42, 4-43).

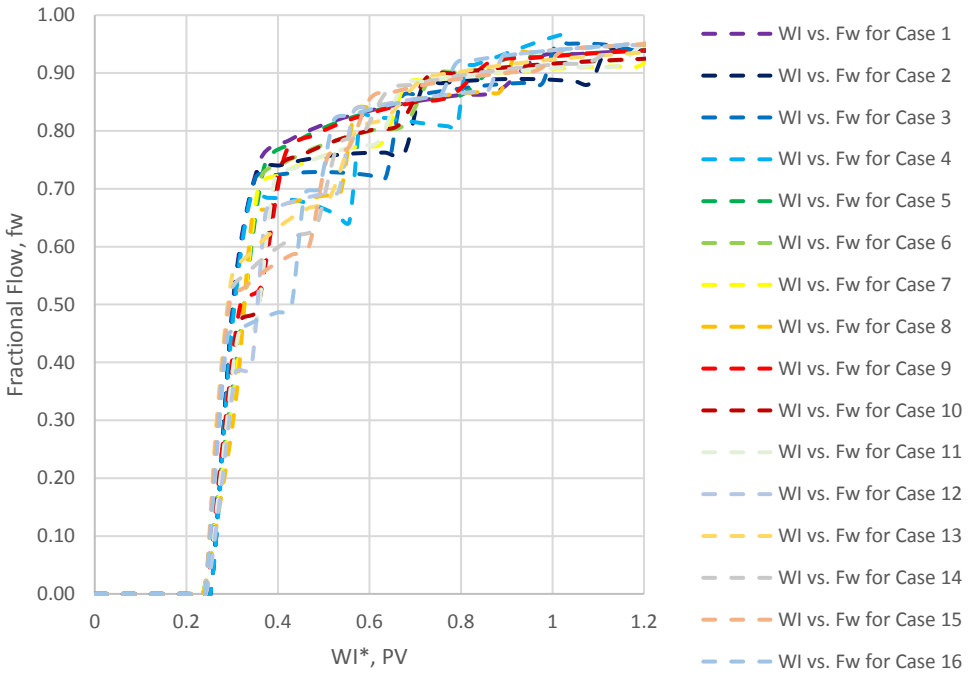

Figure 4-41. Comparison of *fw* vs. *WI** results for scenario 1 - 16

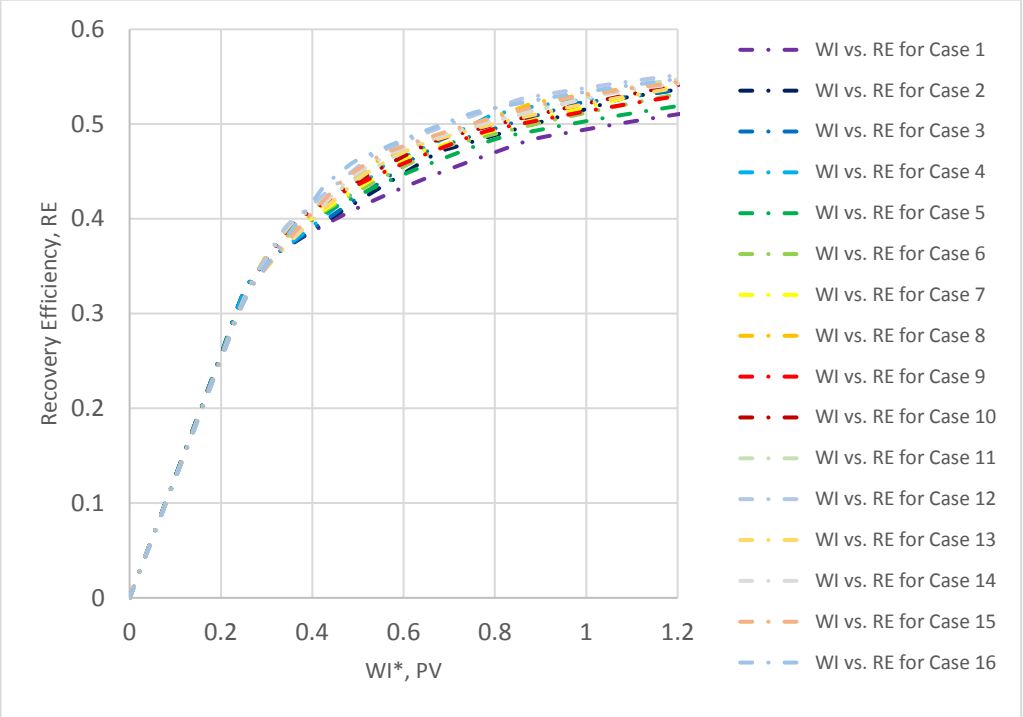

Figure 4-42. Comparison of RE vs. WI* results for scenario 1 - 16

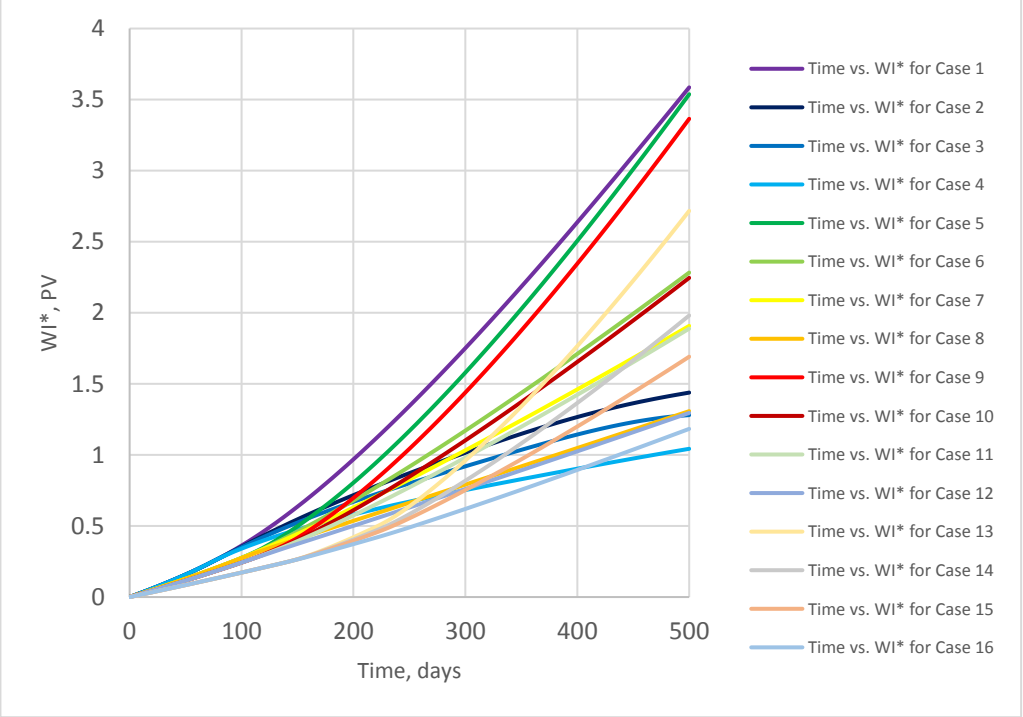

Figure 4-43. Comparison of WI* vs. time results for scenario 1 - 16

These figures demonstrated a few examples of long-term evaluation that is more meaningful for AWC performance analysis. For example, we illustrate this analysis by evaluating the long-term parameters of scenario 1 to 16, at 500 days from the start of production. The practice to select the optimum AWC completion by comparing the long-

term parameters such as FOPT, FWPT, NPV of different scenario at a specific time is a conventional routine as reported by Twerda *et al.*, 2011, Eltaher *et al.*, 2014, Least *et al.*, 2013, Stone *et al.*, 2015. Based on our workflow, we calculate the cumulative oil and cumulative field water production total (FOPT and FWPT) as depicted in Figure 4-44 and Figure 4-45.

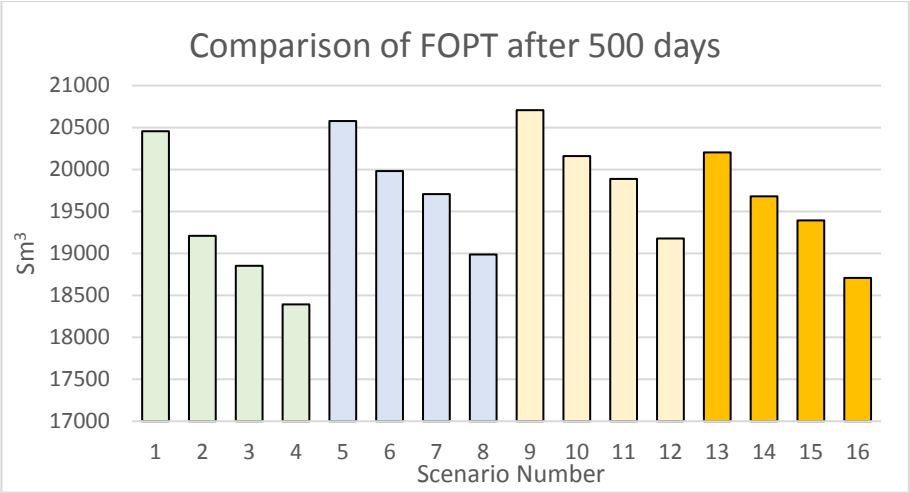

Figure 4-44. Comparison of FOPT results for scenarios 1 - 16

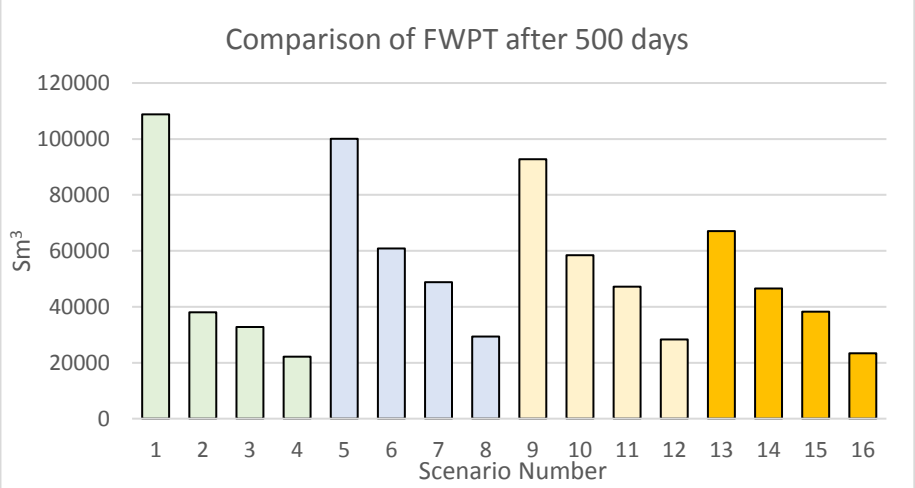

Figure 4-45. Comparison of FWPT results for scenarios 1 - 16

The better flow distribution increased the cumulative oil production as the FCC strength before breakthrough (a^*_{bbt}) is increased (scenario 1, 5, 9 in figure 4-39). The trend will be observed until a threshold, where the restriction due to FCC exceeds the "energy" provided by the pressure difference between injector and producer (50 bar). Beyond this threshold value, increasing the a^*_{bbt} would only decrease the cumulative oil production. Increasing a^*_{bbt} would also reduce the cumulative water production (scenario 1, 5, 9 in

figure 4-40), and the net of these results would improve the production performance of such well. This observation goes in line with the issue of trade-off between the well productivity and flow equalisation in ICD completion optimisation as has been described in chapter 3.

On the other hand, increasing FCC strength after breakthrough (a^*_{abt}) would significantly reduce the water production as well as the oil production, as observed when comparing scenario with the same colour. This observation is in contrast with the observation for "piston-like displacement (or M < 1)" where increasing a^*_{abt} would reduce the cumulative water production without much affecting the oil production (Eltaher, 2017). We observed that the general trends of Figure 4-44 is practically similar with the trends in Figure 4-45. Note that as seen in Figure 4-44 & Figure 4-45, adding higher a^*_{bbt} strength will reduce water faster than it reduces oil. This behaviour would not always be the same. Increasing a^*_{bbt} for fluids with high mobility ratio (M >>1) would reduce oil production more than it reduce water production (Eltaher, 2017).

Consider the following scenario now:

Table 4-8.Assumptions for economic calculation

Oil Price	**Water Handling Cost**	**Operational Cost**	**CAPEX**	**Discount factor**	**Discount factor**
$/m3	**$/m3**	**$/m3**	**$/10^{3}m^3**	**%/Year**	**%/month**
314.47	6.29	9.43	0.00	15.00	1.17
$/stb	**$/stb**	**$/stb**	**$/10^{3}stb**		
50	1.00	1.50	0		

Results depicted by Figure 4-44 & Figure 4-45 can be extended to a quick project economic prediction (Figure 4-45) and the economics will change the priority of those scenarios. *Note that the assumption of zero capex in table 4-8 may encourage some readers to judge the Net-Present-Value evaluation presented in the following section as a Present-Value. However, since the focus of this study is to evaluate the reliability of the BL method instead of the details of specific economic parameter, the term NPV is hence still used.*

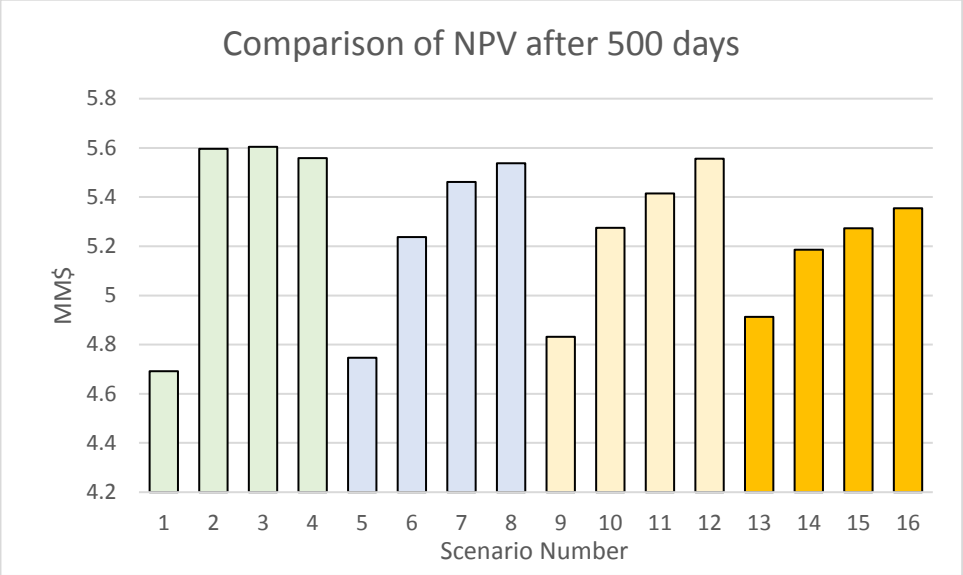

Figure 4-46. Comparison of NPV results for scenario 1 - 16

First, the most obvious observation is that scenario 1, 5, 9, 13, those with high cumulative oil, (corresponding to the weak FCC strength before breakthrough (a^*_{bbt})), does not translate to better economic results.

Second, the economic benefit of adding stronger AWC for control of the unwanted fluids, i.e. to increase a^*_{bbt}, is doubted by scenario 16, i.e. when the well is completed with aggressive a^*_{bbt} and a^*_{abt}. As indicated by its overall cumulative production, the added pressure drop from FCC has re-allocated the available energy (50 bar) needed to produce and inject the fluids. This excessive strength turns out to reduce the aggregate production as well as the aggregate NPV.

Third, scenario 2, 6, 10, 14 has a fluctuating trend although they are completed with equal a^*_{abt}. Each of this scenario has a different recovery before breakthrough which translated to different economic evaluation (due to the time dependence of money). Each scenario will have different shock front's properties that will be responded differently by the (same value of) post-breakthrough's restriction. It emphasises that the effect of a^*_{abt} depends on the restriction before breakthrough (a^*_{bbt}).

Fourth, unlike the conclusion for the section 4.3.4, the best results are not for the AFCD design open to oil and very restrictive to water. The scenario with an optimized opening to oil and optimized opening to water, e.g. scenarios 2, 3, 8 & 12 result in the most economic project. The needs to find the "optimum" strength AFCD thus echo the needs for rapid long-term goals calculation.

Another method to evaluate these completions is by comparing the maximum and the time when it is obtained. We understand that value of money is a function of time, and hence the profiles would differ. And since these completion options would have different production vs. time shape (figure 4-39 and 4-40), maximum NPV can be obtained at a different time. This is reflected by the various shape of curves in figure 4-47. The decline in NPV at later times indicates the project is losing money.

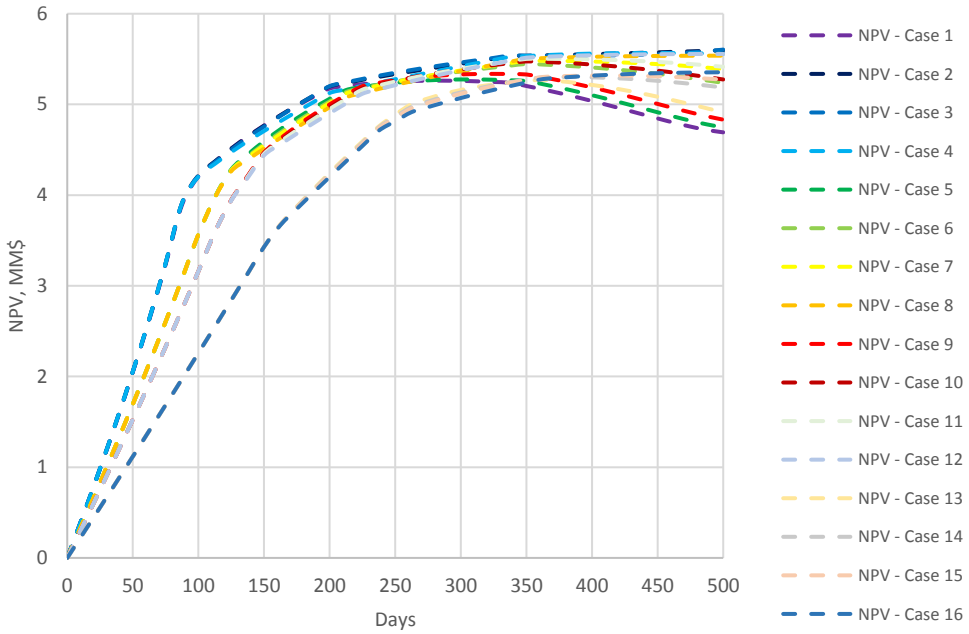

Figure 4-47. Comparison of NPV over time for scenario 1-16

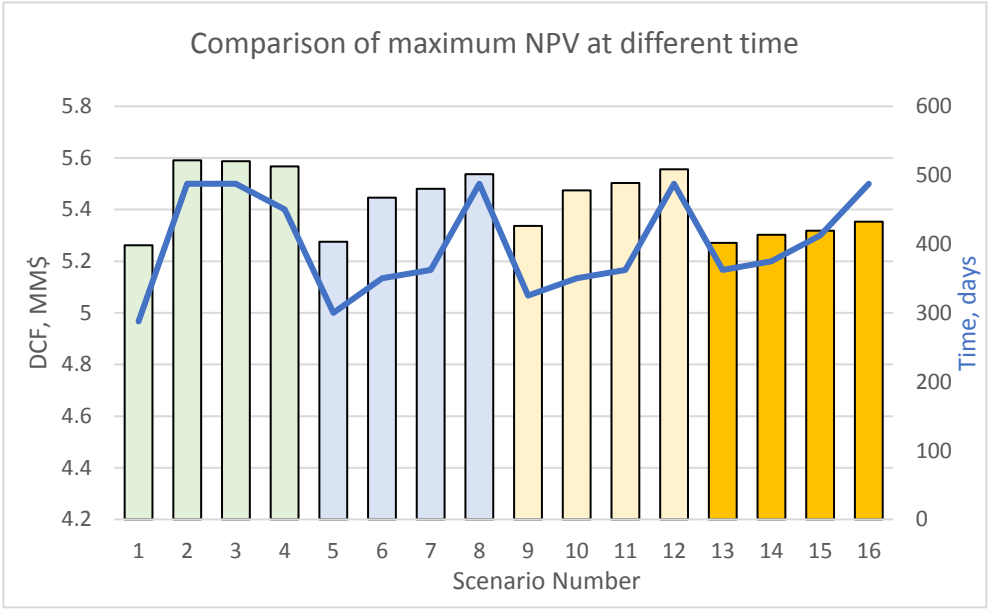

Figure 4-48. Comparison of maximum at different time for scenario 1-16

Such project evaluations would favour the scenarios with most accelerated project economics i.e. fast capital return. Completions that are less aggressive to water, scenario 1, 5, 9, 13 would accelerate production (including water) which generate the maximum earlier. These cases become more attractive when compared to previous comparisons at 500 days. On the contrary, scenario that were results in the NPV compared at 500 days, would be less attractive due to the longer period for getting the maximum NPV.

This evaluation is adopted by operators by producing the field until it reach the maximum NPV, and sell the asset once the NPV is considered highly declined. For instance, if the reservoir is licensed for 10 years and the highest NPV is obtained at 5 years of production, the license can be tendered to other (typically smaller) operators.

4.5 Modelling a horizontal well's AWC in a heterogeneous reservoir

4.5.1 AWC rapid modelling in a horizontal well for a heterogeneous reservoir with a large, active aquifer

So far, the presented technique for FCC rapid modelling has only been applied to vertical wells in horizontal, non-communicating reservoirs. In these cases, the distance between injectors and producers is relatively long, and the Darcy law entirely governs the fluids flow without considering the effect of gravity. On the other hand, many of the passive FCC completions are installed in horizontal wells, in the reservoirs where the distance to the aquifer or gas cap is relatively short, and the displacing fluids are moving in the vertical direction, i.e. the role gravity can no longer be neglected.

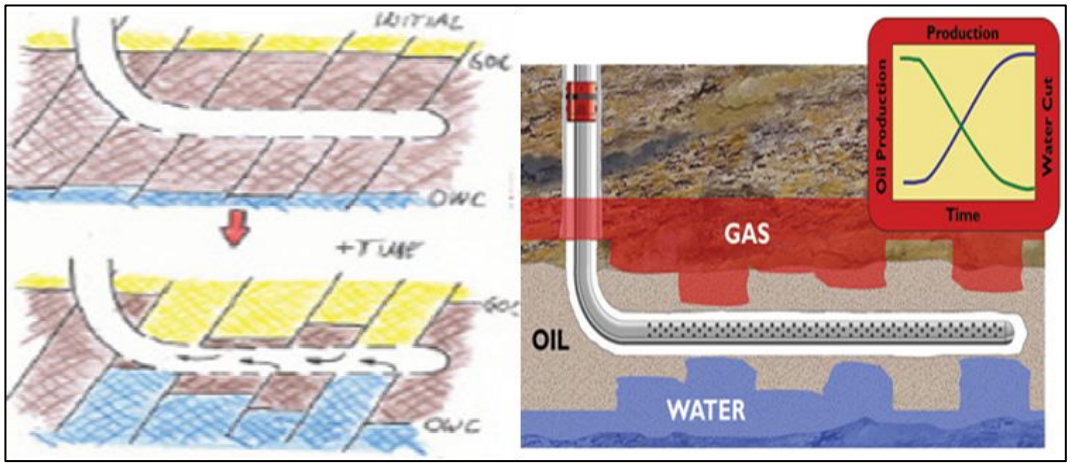

Figure 4-49. Illustration of vertical displacement around a horizontal well (Vela, 2011)

This section describes the implementation of the previously described, modified BL methods for an AWC installed in perfectly horizontal well. The reservoir-well-aquifer interaction replicates a fractional flow displacement model of aquifer which acts as the injector well. Thus the stand-off (H) between aquifer to the horizontal well is equivalent to the previously modelled inter-well distance (l). The previously derived equations are extended to include the role of gravity force is incorporated into the solutions. The remaining assumptions such as no capillary pressure: $\Delta P_o = \Delta P_w$; volumetric replacement or steady-state flow.

Consider the vertical displacement depicted in Figure 4-50:

$$Q_o = Q_w$$

Similarly to the horizontal displacement case, the system of pressure equations can be discretised into the pressure drop in water-phase, the pressure drop in oil-phase and the pressure drop in the flow control completion.

$$P_1 - P_2 = \Delta P_{water} + \Delta P_{oil} + \Delta P_{FCC}$$

The first and the second component in the right side of this equation is expanded based on the Darcy law, and the pressure drop in the completion (third component) is substituted based on the equation 2-6.

$$\Delta P_{12} = \left(\frac{Q_{mix}}{AK\lambda_{mix}} + \gamma_{mix}\right)x + \left(\frac{Q_o \mu_o}{AKK_{ro}} + \gamma_o\right)(H - x) + aQ_o^2$$

Note that this equation is similar to equation 4-9. The main difference is that now there is a correction for the gravity term, γ.

Finally, such displacement system can expressed as a quadratic equation:

$$Q_{inj} = \frac{-B_j + \sqrt{B_j^2 + 4.a^*.A_j^2.C_j^2.D_j}}{2a_j^* A_j C_j} \quad (4\text{-}58)$$

Where coefficients B, C, and D are defined as

$$B_j = \dot{x}(1 - M_{mix}) + M_{mix} \quad (4\text{-}59)$$

$$C_j = \frac{K_j.\lambda_{mix,j}}{L} \tag{4-60}$$

$$D_j = \left(\Delta P - \left(\left[\gamma_{mix,j} - \gamma_o\right].\dot{x}_j + \gamma_o\, H\right)\right) \tag{4-61}$$

Where γ_o and γ_{mix} is the specific gravity for oil and mixed fluids behind the front, and $M_{mix} = \frac{\lambda_{mix}}{\lambda_{oil}}$

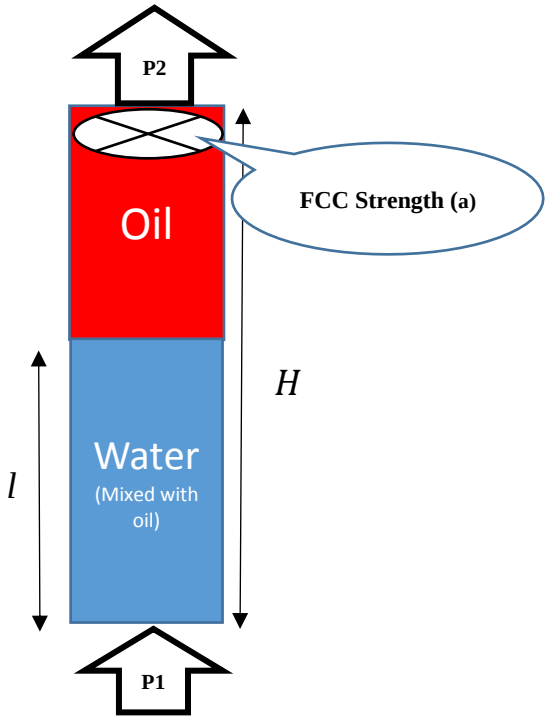

Figure 4-50. 1D column vertical layer displacement

Note that the strong movement of the earth that rotated these sediments (from a series of horizontal layers to become vertically alligned columns) would typically break the sealing capabiliy of these layers/columns. Such a system would find difficulty to trap oil migration and hence, it is less-likely to encounter a reservoir with perfect vertical, stratified layers depicted by figure 4-50. The more common geological realism is to have a steeply dipping reservoirs and the gravity terms in equation 4-61 will be corrected by the angle of the dip.

4.5.2 Verification of the horizontal well model in a heterogeneous, box-shaped reservoir model

The horizontal well is completed in a heterogeneous stratified heterogeneous reservoir, with communicating layers. A large aquifer underlying the reservoir supports the

reservoir pressure and preserves steady-state flow during production, and the oil recovery is driven by bottom-up water displacement. However, reservoir heterogeneity results in inefficient recovery as the water flows faster in the more permeable layers, and consequently, the layers with lesser permeability will be unswept.

The horizontal well completion contains 50 reservoir layers with log-normal permeability distribution (Table 4-9). The size of the layers is 50m x 2m, and the horizontal well is segmented across each of these layers, i.e. Segment length = 50 m, (the small width of 2m is chosen to ensure the 100% areal sweep efficiency). The stand-off (h) (the distance between the well and the aquifer) is 70 m. The same Brook-Corey medium oil relative permeability correlations are used.

Table 4-9. Reservoir properties along the horizontal well completion

Parameters	**K**	**Width**	**Length**	**Area**	**Φ**	**μ_w**	**μ_o**	**S_{wi}**	**S_{or}**	**k_{we}**	**k_{oe}**	**n_o**	**n_w**
Layers	**mD**	**m**	**m**	**m^2**		**cP**	**cP**						
1 - 50	12 (min) 80 (Max)	2	50	100	0.25	1	4	0.2	0.1	0.5	1	2	3

Each reservoir layer resembles the event in system described by Figure 4-50, and is treated as an individual displacement. The section 4.4.4 workflow is applied to this scenario.

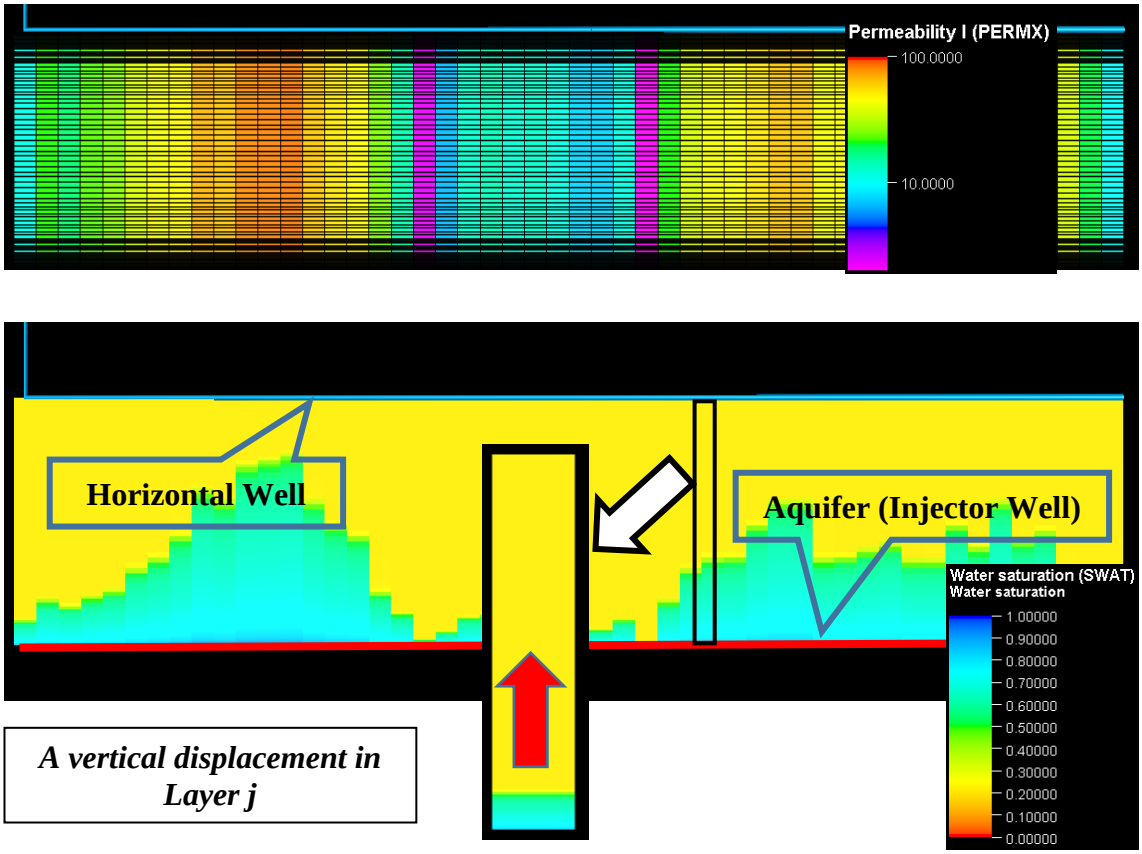

Figure 4-51. Illustration of horizontal well swept by vertical water displacement from the aquifer. Top-figure is the permeability distribution and bottom-figure is the water saturation distribution. Each layer is treated as an individual system and analysed with the modified BL method for an AWC completion.

The well is produced with BHFP 200 bar, and the aquifer pressure is 243 bars, making a 43 bar drawdown. The flow variation along a screen completion is clearly seen as illustrated by the height of water encroachment in Figure 4-51. The water has invaded the more permeable layers, leaving the lower permeability layers unswept. An advanced completion, such as ICD or AFCD is required to improve the sweep efficiency of this well. Completions with the table 4-10 strength were evaluated

Table 4-10. Completion properties for the box-shaped model, for non-pistonlike displacement

	a^*_{bbt}	Maximum a^*_{abt} (single-phase)
Case name	**bar/(rcm/d)^2**	**bar/(rcm/d)^2**
Screen	0 (open-hole completion)	0 (open-hole completion)
ICD	0.008 (medium strength FCC)	0.008 (medium strength FCC)
AFCD	0.008 (medium strength FCC)	0.016 (high strength FCC)

Figure 4-52 and 4-53 shows the oil and water production rates, respectively for these completions. The analytical results showed an excellent agreement with the numerical results from ECLIPSE Reservoir simulation.

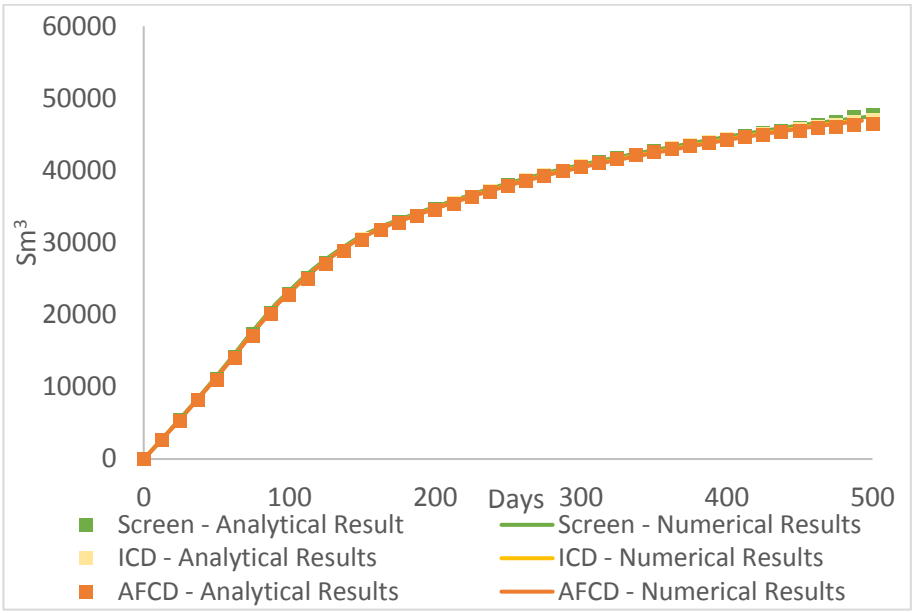

Figure 4-52. Comparison of horizontal well's cumulative oil production for the screen, ICD, and AFCD completion.

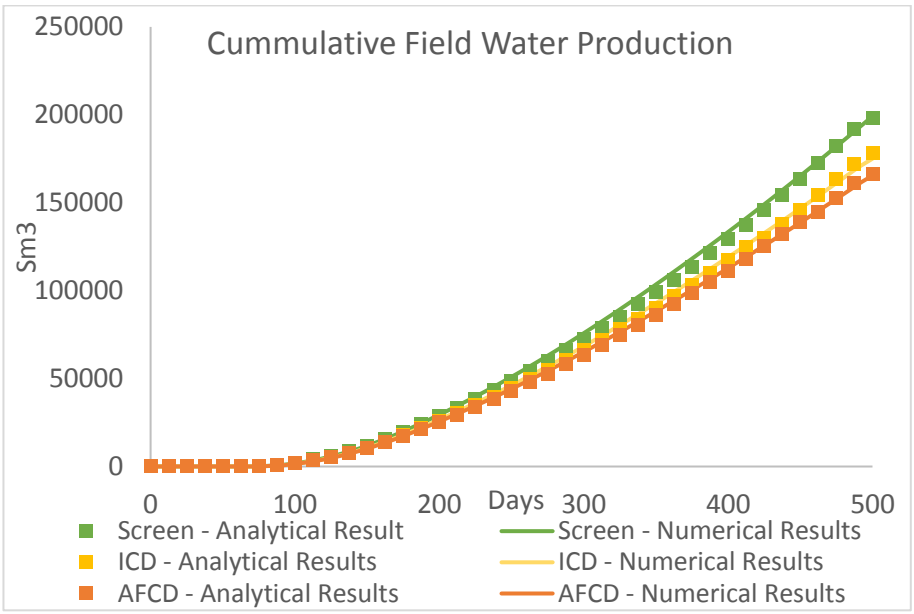

Figure 4-53. Comparison of horizontal well's cumulative water production for screen, ICD, and AFCD completion.

Figure 4-52 shows that installing flow control devices did slightly reduce the cumulative oil production after 500 days because of a reduction in the wells total fluid production.

This can be seen more clearly in figure 4-53 where, particularly, the AFCD's cumulative water production was reduced compared to the screen completion. The Table 4-10 economic assumptions (base case) parameters were used to calculate the NPV of the well's production. Figure 4-56 indicated that installing an FCC increase the NPV at 500 days between 2 to 3%. The small incremental changes are most likely due to the relatively weak choking strength imposed by the FCC. We suggest for future researcher to test our workflow with stronger (e.g. 2 or 3 times higher) FCC strength.

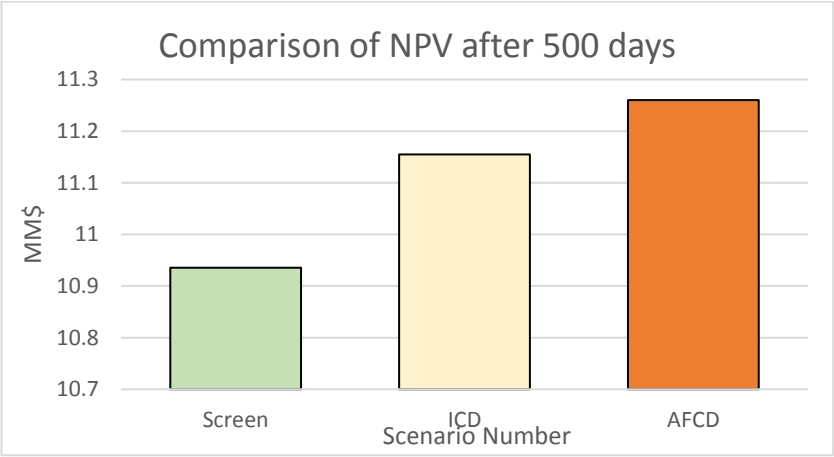

Figure 4-54. Comparison of NPV after 500 days for screen, ICD, and AFCD completion.

Similar to the previously explained horizontal displacement, when we plot the NPV against time, the maximum NPV will be achieved at different times (figure 4-55). If an operator would like to incorporate the rate of how fast the maximum NPV can be obtained, then screen completion may be more attractive since it accelerates the production faster than the FCC completion (figure 4-56).

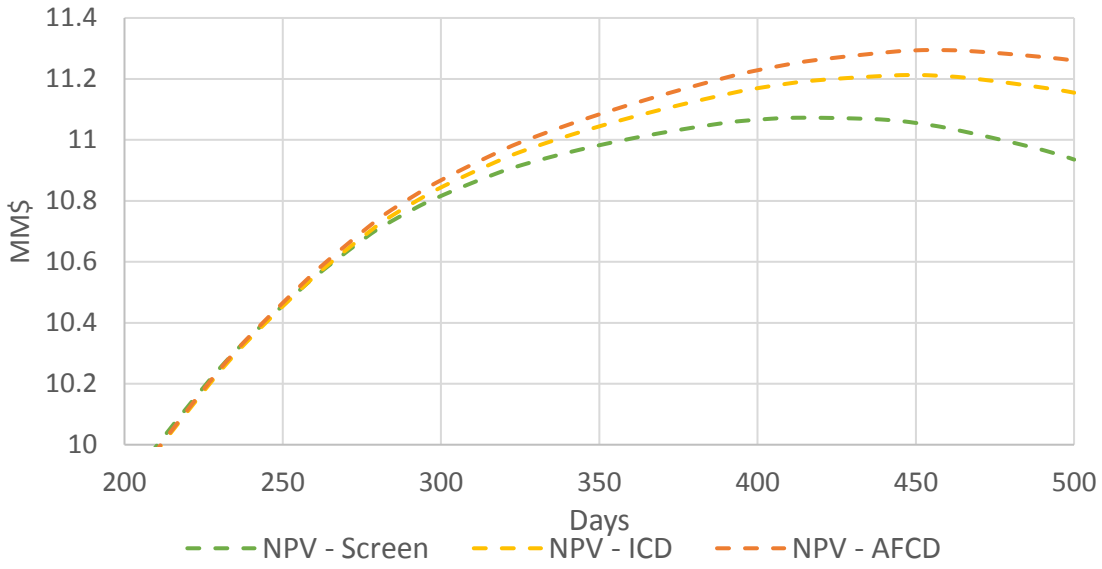

Figure 4-55. NPV over time for screen, ICD, and AFCD completion.

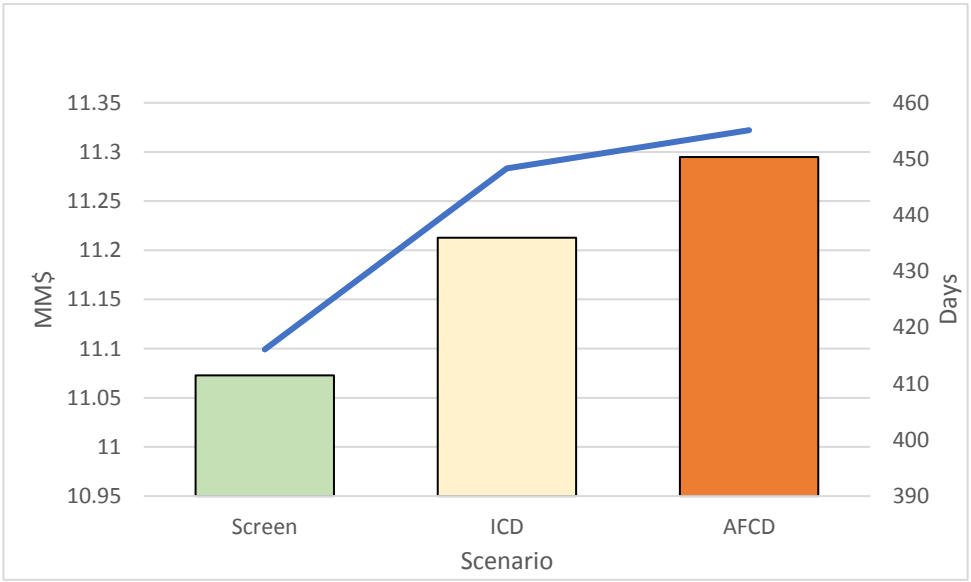

Figure 4-56. NPV comparisons for different type of completions.

Relating the long-term and the short-term strategy

Chapter 4 of this thesis has been concerned with the development of analytical methods for quantifying the long-term production performance of an advanced well completion. These methods can be coupled with the type-curve method presented in chapter 3, to develop a short-term "snapshot" of the well's performance. The following is a long- and short-term analysis for an ICD completion in a heterogeneous reservoir. For example, Table 4-11, the properties of the horizontal well AWC that was previously designed using the type-curve method by Prakasa, Muradov and Davies, 2015 and tabulated in Table 4-

11.

Table 4-11. The properties of the horizontal well in Figure 4-51, and Table 4-9.

Reservoir Properties			
Input Data			
Reservoir Heterogeneity	*IVoh*	**0.67**	
Drawdown	ΔP	**43**	bar
Permeability Distribution		**Log-normal**	
Well length		**2500**	m
Well's max PI	J_1	**0.0004**	Sm3/day/bar
Well's average PI	J_m	**0.0013**	Sm3/day/bar
Well's min PI	J_2	**0.0040**	Sm3/day/bar
Segment Length (layer)	l_{icd}	**50**	m
In-situ fluid density	ρ	**85**	kg/m3
In-situ fluid viscosity	μ	**4.0**	cp

The Inflow Variation when a screen completion is installed {i.e. no flow control devices (IV_{oh})} is 0.67. This value is obtained with equation 3-29. The (short-term) performance of the ICD completion is plotted by the red curve in figure 4-57. The type-curve method's, target is to install an inflow control with an IV_{ICD} value smaller than IV_{oh} provided the required well PI is still honoured. The IV_{ICD} value is translated into the required ICD strength by using equation 3-29, calculating (a) the nozzle diameter (nozzle type ICDs, equation 2-8) or (b) channels strength (channel type ICDs, equation 2-9). IV_{ICD} can be further translated to the long-term strategy with the modified BL method. IV_{ICD} become a representative for a parameter such as oil recovery, water cumulative production, NPV for a given set of scenarios. By combining these techniques, a "quick-look" evaluation incorporating long-term parameters is thus available. *Note that this coupling of strategies method assumes that ICD is installed with constant strength along the completion length.*

As an example, we use the previous scenario as in Figure 4-51 and Table 4-9. Economic parameters are listed in Table 4-8 and treated as the base case. Economic sensitivity run is applied to oil prices, discount rates, and water handling costs. The results, as presented in Figure 4-57, allow a quick judgment to choose the most desirable IV_{ICD} based on the project economic evaluation.

The IV_{ICD} value of 0.60 shows the best project result. This is equivalent to installing the ICD with strength, a = 1.75 bar/(rcm/d)^2 or equivalent the 0.85 mm diameter nozzle type ICDs or 1.377 bar/(rcm/d)^2 (channel type ICD) for every 50m segment along the well. Figure 4-57 also shows that reducing flow variations does not necessarily mean more valuable projects. This is observed when evaluating NPV results for the scenario with IV_{ICD} < 0.6 resulting in a lower economic gain.

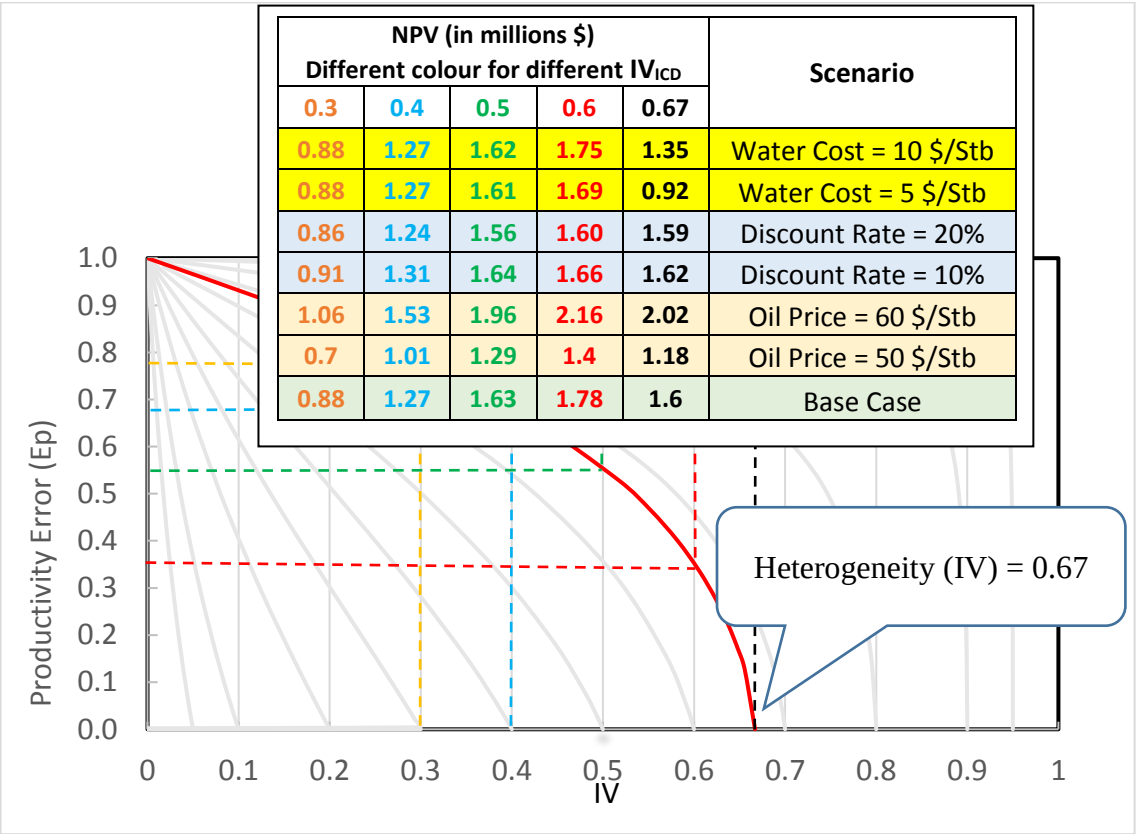

Figure 4-57. Type-Curve method for the heterogeneous reservoir, coupled with the modified BL method for AWC modelling. The economic sensitivity check is attached to the corresponding IVICD result.

4.6 Discussion and conclusion

Advanced Well Completions (AWCs) control the fluid flow at the reservoir sandface. They have become a proven, widely used technology (particularly in waterflooded reservoirs) for modifying a production or injection well's inflow/outflow rate profile along the well. On top of this, new AWC designs that react to water breakthrough have recently become available.

Incorporating a description of the AWC's performance into the waterflood analysis

models allows fast forecasting of the production profile and oil recovery, as well as help optimising the AWC configuration and control at the well design stage. The proposed methods are particularly useful for predicting, analysing, and designing an advanced well's and/or controlling the well's performance to maximize oil recovery or other means e.g. of economic gain – a task that is rarely done in reality due to the complexity of the existing modelling tools. The method's transparency and ease of implementation of its algorithms can make it a useful tool for well and reservoir engineers.

We built a tool to model and predict the long-term value added from AWC, and serve as a bridge between simple inflow snapshot evaluation and full dynamic reservoir simulation to enable quick screening of AWC. The tools will be realised in Excel spreadsheets allowing their easy and widespread use. The reservoir sweep models forming the basis of these tools have been recently, uniquely developed and successfully verified.

Preference will be for the tool to consider the drainage radius/area associated with a single well to determine cumulate oil from area over time (i.e. as per pressure depletion). Amongst others, the tool should be able to take following inputs into consideration:

- Permeability profile (e.g. md at depth)
- PVT information
- Saturation profile
- Reservoir Pressures
- Well/completion dimensions
- Typical boundary constrains, BHP, WHP, rate etc.

The engineers could be well served by a tool that can produce long-term parameters associated with a completions type without always depending on complete reservoir simulation tools, such as:

- Cumulative oil produced
- Cumulative water produced
- Cumulative gas produced
- Fluids distribution along horizontal segments

General observations from this chapter on extending the waterflood analyses to AWC

completions are:

- The solutions presented in this work are for the case of constant pressure difference between the injection and production wells. Note that in the original form, Buckley-Leverett equation was presented assuming constant rate and does not calculate pressure. Our BL method used constant pressure differences to make a simple comparison with the DP method presented (which assumes constant pressure difference) previously. The solution can be translated into the constant rate case. Note that, if a strong response in the production well to water breakthrough (e.g. zonal shut-in or increased AFCD strength) is observed, this results in a significant change in the reservoir pressure drop. The equation 4-6 integrals now need to be split into parts.
- Many publications emphasize in the impact of inflow uniformity, and its consequently delayed breakthrough objectives for AWC design. This work has discussed how long-term parameters such oil recovery, value creation, etc., should also be considered. Remember also that the unhindered well outflow performance is also required.
- It is also worth mentioning that the waterflood analysis methods for communicating layers in vertical wells were briefly discussed in introduction. These methods assume vertical pressure equilibrium for all layers, i.e. the local pressure derivative at a given distance from the well is the same for every layer. They cannot be extended to the AWC wells where a significantly different pressure drops is created across each layer.

The new models achieved a good match with the results of a numerical simulation. They provide a simplified, fast, analysis of the impact of various well completion and control options on the development of a waterflood and its efficiency. These models provide a missing link between the various AWC design workflows available today and the long-term value evaluation of an AWC when a commercial numerical simulation software is either not available or is too time consuming.

4.7 Summary

The advantages and limitations of the extended of the classical waterflood analysis for non-communicating layers to the situation when the reservoir is developed with an AWC are:

a) *The light oil displacement* is being replicated by a sharp waterfront, resulting in a "piston-like" displacement, modelled using Dykstra-Parsons method. The sandface,

flow control completion in an AWC well adds either a non-linear pressure drop across each layer or the option of zonal closure. The resulting DP method could be modelled analytically, though a numerical solution was required since the front position could not be expressed explicitly. This extended DP method is thus applicable to waterflood performance analysis for wells with arbitrary completion or control.

The important observations to note that:

- The parameters related to the fractional flow rate of water (or watercut) in the extended DP method have step-like performance. By contrast, an accurate numerical simulation will predict a smoother change (see e.g. Figure 4-7, Figure 4-11).
- This piston-like behaviour allows a fixed value of (A)FCD strength, ($\boldsymbol{a}^*_{\boldsymbol{bbt}}$ & $\boldsymbol{a}^*_{\boldsymbol{abt}}$), for each corresponding period. By contrast, these values for non-piston like (varying WC) displacements will be a function of the average water-cut (see below).
- Equation 4-17. An explicit analytical expression for the waterfront x is not possible for these extended DP methods. Modifications developed by various researchers to the conventional, layer-by-layer DP method that can no longer be applied to fields developed with AWCs. These include:
    1) Introducing a statistical description of the reservoir permeability distribution into the solution.
    2) Accurate translation of the waterflood performance prediction into the time domain by integrating the waterfront x over the layer. However, the alternative approach presented here using the approximate injection rates was showing to be acceptably accurate (e.g. Figure 4-14).
    3) Osman and Tiab, 1981 presented a DP method for composite layers (i.e. layer permeability changes laterally) with conventional production and injection wells. Their solution has the same quadratic form as the DP model, so it may well be possible to extend our AWC-DP model to composite layers. Further investigation is required.

b) *Medium or heavy oil displacement*, is "non-pistonlike" and requires use of non-linear or more realistic relative-permeability curves. This type of displacement follows the two-phase front movement described by Buckley-Leverett. The modified DP method

alone is not suited to such fluids. The displacement system is best described by splitting it into 3 different components.

1. The non-linear pressure drops across the installed flow control completion
2. The displaced phase as an oil with homogeneous properties
3. The displacing, mixed fluids: composed of oil and water. Its properties, e.g. make up the mixture mobility, velocity, etc. are modelled as the average of the individual fluid properties behind the front.

This averaging method follows the Welge method. Front saturation is predicted by classical fractional flow analysis, and the displacing phase's average properties are the harmonic average for the multiple layers with different fluid saturations behind the front. Tracking the front position in the time domain is possible since x is evaluated simultaneously with the corresponding front velocity. This allows the time to be found numerically using appropriate algorithms e.g. gradient based, non-linear Excel's Solver or any optimisation in MATLAB. The results were validated against a numerical simulation (Figure 4-30, Figure 4-31, Figure 4-37, Figure 4-38). The importance of this is outlined by:

- Economic evaluation, requiring the time value of money, is now possible.
- The step-like performance of the DP method is avoided and the predicted flow rates show more realistic results.
- The optimum AFCD design for a reservoir exhibiting piston-like displacement, is to install an AFCD with low restriction to oil production and aggressive restriction to water. This is not the case for reservoir with "non-pistonlike" displacement. There is an optimum restriction for each that achieves the best results. Eltaher, 2017 introduced the concept of "bad-water" and "good-water" production when designing an AFCD, emphasizing further the importance of achieving the correct FCC strength.

It is also worth to note that the optimum FCC strength is intrinsically a function of WC. Thus the ideal AFCD completion requires the FCC strength (a^*_{bbt}) to vary during the post breakthrough period. This is a consequence of multi-phase flow. Strictly speaking, the a^*_{abt} will progressively increase once breakthrough has occurred, until the maximum a^*_{abt} value is reached, when WC = 100 % (equation 4-49). The produced WC can be predicted using fractional flow analyses, hence the progressively increasing a^*_{abt} trajectory can be

calculated (see Figure 4-30, Figure 4-31, Figure 4-37, Figure 4-38). The BL method for AWC can also be extended to horizontal wells with vertical displacement, a common scenario for installing AWC. Gravity needs to be incorporated into equation 4-58, 4-59, 4-60, and 4-61. The workflow is otherwise identical to the workflow for vertical well.

4.8 Nomenclature

All values are in SI units and at reservoir conditions, unless otherwise stated.

A – effective area perpendicular to flow	RE – oil recovery efficiency (recovery factor)
a – flow control completion strength defined by eq. 4-8, 2-8, 2-9, 2-10, 2-11	S - saturation
t - time	S_{or} – residual oil saturation
b – formation volume factor	S_{wi} – irreducible water saturation
φ - porosity	u – fluid flow velocity
f_w – fraction flow rate of water (watercut at downhole conditions)	WI – volume of Water Injected
F – constant defined below equation $\frac{dx_j}{dt} \Big/ \frac{dx_R}{dt} = \frac{dx_i}{dx_R} = F_{j,R} \frac{x_R^* + M_R(1-x_R^*)}{x_j^* + M_j(1-x_j^*)}$	$\frac{df_w}{ds_w}$ = Fractional flow derivative
h – layer height	x – lateral coordinate of the water front
k – horizontal permeability	ΔP – pressure difference
L – distance between wells	ΔS – movable saturation ($1-S_{or}-S_{wi}$)
M – mobility ratio	λ – fluid mobility (i.e. rel.perm./viscosity)
P - pressure	μ – viscosity
n – exponent for modified Brooks-Corey functions	H – height (standoff) between well and aquifer
ρ - density	γ – Specific Gravity
q – flow rate	

4.8.1 Subscripts

abt – after breakthrough	or – residual oil (saturation)
bbt – before breakthrough	r – relative (permeability)
bt – breakthrough	w – water

j, k, R – referes to Layer j, k, or R respectively	wi –irreducible water (saturation)
o – oil	wf - waterfront
avg - average	oh – Openhole
1 – one standard deviation smaller median values	ICD – Inflow Control Devices
2 – one standard deviation larger than median values	m –median values

4.8.2 Superscripts

a^* - total FCC flow restriction coefficient for a layer, defined as $a^*=a_{producer}+a_{injector}$
WI* - volume of water injected expressed in reservoir pore volumes
x* - relative water front position defined as x* = x/L
λ’ - end-point mobility

4.8.3 Abbreviations

AICD	Autonomous Inflow Control Device (a class of FCDs)
AFCD	Autonomous Flow Control Device (a class of FCDs)
AWC	Advanced Well Completion: an arbitrary combination of FCDs in a well or a well’s zone
DP	Dykstra-Parsons
BL	Buckley-Leverett
FCC	Flow Control Completion. Same as FCDs
ICD	Inflow control device (a class of FCDs)
ICV	Inflow (interval) control valve (a class of FCDs)
JIP	Joint Industry Project
PI	Productivity Index
PV	(reservoir) pore volume
Rcm	Reservoir cubic meters (units)
NPV	Net Present Values
FOPT	Field Oil Production Total (Cumulative oil production)
FWPT	Field Water Production Total (Cumulative water production)
IV	Inflow Variation

Chapter 5 – Reservoir Characterisation and Production Optimisation of Advanced Well completion using Capacitance-Resistance Model

5.1 Introduction

Numerical reservoir simulation is a valuable, though computationally expensive, tool for the design, evaluation and operation of hydrocarbon fields. Such reservoir models are complex, time consuming to build, yet uncertain; being based on limited information. The use of alternative models based on the field's production history data to reliably quantify inter-well connectivity and support well control decisions is preferred. This chapter extends their application to a field with Advanced Well Completions (AWCs) equipped with downhole monitoring and flow control. A field with AWCs is a natural candidate for closed-loop, reservoir model update and field optimisation.

The Capacitance-Resistance Model (CRM), one type of data-driven models, has proved to be effective for making well production optimisation decisions in a single-layer, mature, water flooded reservoirs. This study extends the application of CRMs to a multiple-layer, heterogeneous reservoir being developed by AWCs. The optimisation strategy was further extended to include both injection and production control at the level of an AWC zone. The resulting, CRM-based, proactive optimisation strategy using zonal production/injection history data proved to be capable of delaying water breakthrough and increasing recovery.

This chapter proposed a new CRM solution which incorporates the non-linear pressure drop of flow control devices (e.g. ICVs). The solution will be described in synthetic, single- and multi-layer, reservoir models. CRM calculated inter-well, layer connectivity and time-storage results can be used to suggest changes to the operation of one or more AWC zone's injection or production rate. The CRM can be updated once sufficient further injection and production data has accumulated.

Furthermore, these calibrated parameters can be used to form a model of reservoir flow-capacity storage (modified $\hat{F} - \hat{\phi}$ graph) which reveal the flooding (or drainage) efficiency of each well/layer. The analysis of this graph provides data driven, feedback control strategies, and lay out a new guideline for production optimisation based on the degree of disparity of a well (or layer's) flow-capacity compared to its associated drainage

volume. The Lorenz Coefficient is used to quantify the degree of disparity. *Note that the term disparity is used instead of heterogeneity, since disparity measure the relationship between two different parameters (rate and drainage volume), while heterogeneity is typically used for comparing the same parameter (e.g. permeability of layer j compared to average permeability).*

A comprehensive CRM-based, closed-loop workflow for data gathering, history matching, and optimisation is described. The workflow, programmed as a spreadsheet, is a complementary tool to numerical reservoir simulation. It provides insights into both reservoir characterisation and production control for both intelligent and conventional field developments.

5.2 Capacitance-Resistance Model

Numerical reservoir simulation is the standard approach for modelling fluid flow in the reservoir. It provides the production forecast as well as informing reservoir management decisions. It is a computationally-expensive process that requires large volumes of frequently uncertain data that describes the reservoir's properties. This paper discusses an alternative approach that captures the reservoir-to-well system interactions with a reduced-physics model. The Capacitance-Resistance Model (CRM) (Yousef, Lake and Jensen, 2006) was chosen since it treats the pressure support from injection wells and/or the aquifer as an input signal and the production rates as the output signal. CRM provides an estimate of the values of the parameters controlling the relationship between the input-output signals; i.e. the properties of the medium (reservoir rock and fluid saturations) between the wells (the measurement points). CRM quantifies the inter-well connectivity and the associated drainage volume similarly to the parameters that are equivalent to the "resistance" and the "capacitance" of an electrical circuit. Further analysis of these parameters gives an insight into some key reservoir information with much reduced-computational time. It thus acts as a scoping tool, providing initial guidance prior to the more complex calculation of numerical, reservoir simulation.

Case studies have confirmed the utility of CRMs to turn basic, production history data (well production and injection rates and pressures) into field-performance information by simple and quick calculations. Sayarpour, Kabir and Lake, 2009 reported CRMs provide insights into the Reineke field's waterflood overall performance and pattern-allocation factors. The estimation of allocation water from each injectors and the time take for the

injection signal to reach a produces are the key elements in performance assessment. Izgec *et al.*, 2010 published a paper on how to use aquifer analytical model coupled with CRMs to quantifying and discerning variable aquifer influx for individual producers. Moreno and Garriz, 2014 reported a case study of channelling detection using CRMs in Chiuido de la sierra Negra field. They also reported successful injection leakage detection in this mature field using CRMs.

There many other cases where CRMs have been successfully applied to various fields, reservoirs and production conditions (Sayarpour, Kabir and Lake, 2009; Nguyen *et al.*, 2011; Jahangiri *et al.*, 2014; Kansao *et al.*, 2017) with research continuing to extend their application to even more complex cases. For example, BP applied the approach to waterflood performance management for a North-Sea asset (Jahangiri *et al.*, 2014). Their "Top-Down Waterflood Diagnostics and Optimisation" workflow successfully combined a CRM with their event-detection algorithms. The study emphasises the relative simplicity of the method compared to numerical, reservoir simulation. It allows non-specialist engineers to quickly identify the relative importance of all inter-well connections; allowing "Top-Down Waterflood" calculations to provide valuable analysis and understanding of the reservoir's performance.

This study extends the application of CRMs to a multiple layer, heterogeneous reservoir being developed by AWCs completed with zonal downhole sensors and flow-control equipment. The optimisation strategy was further extended to include both injection and production control at the level of an AWC zone. The rapid, production optimisation of an AWC enabled field will be demonstrated with synthetic, reservoir history data.

Strictly speaking, CRM is a material balance, data-driven model that measures the communication between wells in a waterflooded reservoir. The necessary reservoir information is obtained from the analysis of the wells' production and injection history without the need for detailed geological information. CRM has received much attention in the recent years since, unlike many other data-driven methods, it honours the fundamental reservoir engineering concepts of material balance and fluid front propagation. CRM characterises the reservoir as a 'proxy' model consisting of multiple, inter-well, control units. Each unit is described by parameters related to its connectivity and capacity; terms that represent the local, inter-well reservoir properties averaged over space and time. "Connectivity", analogous to 'resistance' in an electric circuit, represents the formation's conductivity to fluids flowing from an injector to a specific producer. The

drainage volume, or "capacitance", is a measure of the fluid storage volume between the wells.

CRM solutions have been developed for different levels of reservoir complexity. CRM solutions for complex reservoirs, those with multiple layers and a large number of wells, require a large number of fitting parameters and a corresponding increase in the volume of production history data to calibrate the CRM. Non-linear, gradient-based solver in Excel proved to be sufficiently powerful to perform the CRM calibration for a reservoir completed with few wells. However, a more robust platform (e.g. MATLAB) is required for a reservoir with multiple wells requiring calibration for numerous variables. We describe the reservoir waterflood performance by estimating the connectivity between injectors and producers using several CRM solutions in synthetic models of varying complexity. The production history data was generated by numerical, reservoir simulation. The inter-well connectivity calculations from the CRM were validated by comparison with a streamline reservoir simulation. It was shown that CRM can be used in this study to optimise the performance of AWC wells.

5.3 Available CRM solutions

5.3.1 CRM for a given Producer (CRMP)

This is the most widely used CRM (Sayarpour *et al.*, 2009; Holanda *et al.*, 2015) that separately solves for the drainage volume for each production well and its surrounding injectors Figure 5-1. The model investigates all the inter-well interactions between each specific injector-producer well pair. There is one connectivity value (f_{ij}) for each injector(i)-producer(j) pair and the total number of variables is kept relatively low by having only one capacitance value for each producer (i.e. one characteristic time-constant (τ_j) describing the time of water front propagation between wells). Equation 5-1 is the solution for the case of constant productivity and injectivity indices with changing injection rates (discretized into steps). It describes flow between N_i injectors I_i and the producer J_j. f_{ij} is the connectivity between Injector i and Producer j while τ_j is the capacitance value of producer j.

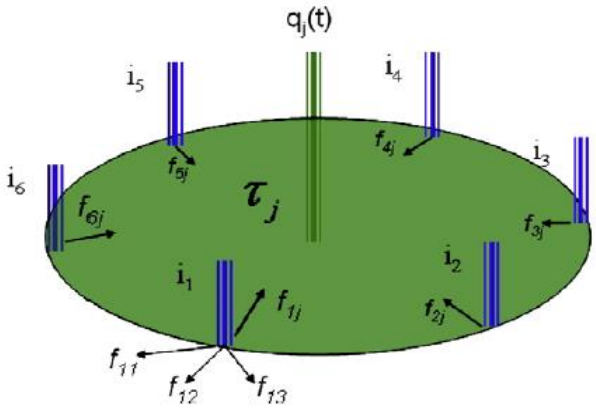

Figure 5-1. Control Schematic of volume of producer j in a single-layer reservoir, CRMP (Sayarpour, 2009). The green circle depicts the drainage volume of producer j, while the arrows depict the inter-well interactions between injector i and producer j.

$$q_j(t_n) = q_j(t_0)e^{\frac{-(t_n-t_0)}{\tau_j}} + \sum_{k=1}^{n}\left\{e^{\frac{-(t_n-t_k)}{\tau_i}}\left(1-e^{\frac{-\Delta t_k}{\tau_i}}\right)\left[\sum_{i=1}^{N_i}\left[f_{ij}I_i^{(k)}\right] - J_j\tau_j\frac{\Delta P_{wf,j}^{(k)}}{\Delta t_k}\right]\right\} \qquad (5\text{-}1)$$

Equation 5-1 can be integrated by parts for constant-injection rate case (Sayarpour et al., 2009) and re-formulated as (Equation 5-2) to illustrate that the well's production rate is a response to three signals. The first term is the production well's cumulative response to the previous/initial production rate history or the effect of inter-well reservoir depletion. The second term defines its response to injection rate changes for all injection wells that influence its production while the last term is the response to a change in the flowing bottom-hole pressure of the production wells.

$$q_j^{(n)} = \left[q_j^{(n-1)}e^{\frac{-(\Delta t_n)}{\tau_j}}\right] + \left[\left(1-e^{\frac{-\Delta t_n}{\tau_i}}\right)\sum_{i=1}^{N_i}\left[f_{ij}I_i^{(n)}\right]\right] + \left[\left(e^{\frac{-\Delta t_n}{\tau_i}}-1\right)J_j\tau_j\frac{\Delta P_{wf,j}^{(n)}}{\Delta t_n}\right] \qquad (5\text{-}2)$$

5.3.2 CRM for a given pair of Producer-Injector (CRMIP)

CRMIP is a refined version of CRMP. It exclusively solves the drainage volume (additional time constant) for production and injector well pair(Sayarpour et al., 2009; Holanda et al., 2015)]. This formulation, equation 5-3, being more sensitive to high reservoir heterogeneity (Holanda et al., 2015) is suited to when the geology or permeability changes with time {e.g. formation of Thermal Induced Fracture (TIF)}.

$$q_{ij}^{n} = \left[q_{ij}^{n-1} e^{\frac{-(\Delta t_n)}{\tau_{ij}}} \right] + \left[\left(1 - e^{\frac{-\Delta t_n}{\tau_{ij}}} \right) f_{ij} I_i^n \right] + \left[\left(e^{\frac{-\Delta t_n}{\tau_{ij}}} + 1 \right) J_{ij} \tau_{ij} \frac{\Delta P_{wf}^{(n)}}{\Delta t_n} \right] \quad (5\text{-}3)$$

Figure 5-2 explains the CRMIP parameters describing the flow between an injector, subscript i, and a producer, subscript j. f_{21} is thus the connectivity between Injector 2 and Producer 1. The production rate in producer j at time-step n, is a summation of producing rates from all injector-producer pairs that include producer, thus $q_j^n = \sum_{i=1}^{N} q_{ij}^n$.

$$q_j^n = \sum_{i=1}^{N} \left[q_{ij}^{n-1} e^{\frac{-(\Delta t_n)}{\tau_{ij}}} \right] + \sum_{i=1}^{N} \left[\left(1 - e^{\frac{-\Delta t_n}{\tau_{ij}}} \right) f_{ij} I_i^n \right] + \sum_{i=1}^{N} \left[\left(e^{\frac{-\Delta t_n}{\tau_{ij}}} + 1 \right) J_{ij} \tau_{ij} \frac{\Delta P_{wf}^{(n)}}{\Delta t_n} \right] \quad (5\text{-}4)$$

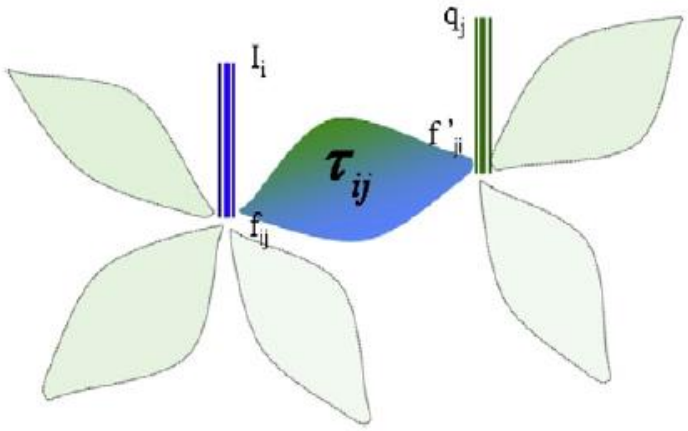

Figure 5-2. CRMIP Model of Flow between an Injection and a Production Well

5.3.3 CRM for a given Producer - Multi-Layered reservoir, no cross-flow (CRMP-ML)

CRMP assumes a single-layer reservoir where the completion's properties are described by an effective, average value. A multi-layer, heterogeneous reservoir requires layer-by-layer data (Figure 5-3), as provided by the zonal monitoring capabilities of AWCs with their continuous measurement of pressures and indirectly derived flow rates. CRM-ML (Mamghaderi, Bastami and Pourafshary, 2012) extends CRM to represent volumetric balance over the effective pore volumes in each layer (Equation 5-5). CRMP-ML's parameters are defined for each layer (l) instead of being averaged over the whole completion i.e. there is one time-constant (τ_j) and one connectivity constant (f_{ijl}) for each

layer of each injector(i)-producer(j) pair. $\left(f'_{i,l}\right)$ is treated as a parameter to be determined when the injection rate into each layer is not monitored, i.e. the fraction of the total well injector into each layer is not available. CRMP-ML assumes non-communicating layers i.e. there is no crossflow. This allows the data fitting for each layer to be computed separately.

$$q_{j,l}^{n}=\left[q_{j,l}^{(n-1)}e^{\frac{-(\Delta t_n)}{\tau_{j,l}}}\right]+\left[\left(1-e^{\frac{-\Delta t_n}{\tau_{i,l}}}\right)\sum_{i=1}^{N_i}\left[f_{ijl}\left(f'_{i,l}\,I_i^{(n)}\right)\right]\right]+\left[\left(e^{\frac{-\Delta t_n}{\tau_i,l}}+1\right)J_{j,l}\tau_{j,l}\frac{\Delta P_{wf,j,l}^{(n)}}{\Delta t_n}\right] \qquad (5\text{-}5)$$

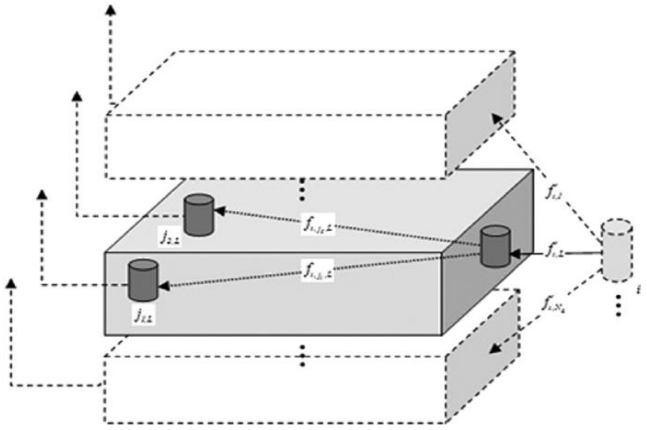

Figure 5-3. Control volume of producer j in a non-communicating multi-layer reservoir, CRMP-ML (Mamghaderi, 2012)

Installation of sandface monitoring in both injection and producing wells allows the injection rate into each layer to be directly observed. The fitting parameter $\left(f'_{i,l}\right)$ is no longer required. This will allow equation 5-5 to be simplified into equation 5-6.

Note that equation 5-6 is similar to equation 5-1 and 5-2, the difference being that parameters in equation 5-6 are measured for each layer (l) rather than on the full well basis as in equation 5-1 and 5-2.

$$q_{j,l}^{n}=\left[q_{j,l}^{(n-1)}e^{\frac{-(\Delta t_n)}{\tau_{j,l}}}\right]+\left[\left(1-e^{\frac{-\Delta t_n}{\tau_{i,l}}}\right)\sum_{i=1}^{N_i}\left[f_{ijl}\left(I_{i,l}^{(n)}\right)\right]\right]+\left[\left(e^{\frac{-\Delta t_n}{\tau_i,l}}+1\right)J_{j,l}\tau_{j,l}\frac{\Delta P_{wf,j,l}^{(n)}}{\Delta t_n}\right] \qquad (5\text{-}6)$$

5.3.4 CRM for a given Producer - Multi-Layered reservoir with Crossflow (CRMP-MLCr)

Mamghaderi and Pourafshary, 2013; Zhang, Li and Zhang, 2015 extended CRM-ML with

an added crossflow term between communicating layers (Figure 5-4). The added term allows the layer production rate to respond to crossflow from other layers. CRM-MLCr's more accurate description of a crossflow reservoir, adds the additional computational cost of needing to match significantly more parameters. The optimisation process can be speeded up by splitting the calculation into two steps. The CRM-ML scenario is initially solved by assuming no crossflow between layers, and the results used as the initial guess to solve CRM-MLCr (Mamghaderi and Pourafshary, 2013).

For monitoring system installed only in producing wells:

$$q_{j,l}^{n}=\left[q_{j,l}^{(n-1)}e^{\frac{-(\Delta t_n)}{\tau_{j,l}}}\right]+\left[\left(1-e^{\frac{-\Delta t_n}{\tau_{i,l}}}\right)\sum_{i=1}^{N_i}\left[f_{ijl}\left(f'_{i,l}\,I_i^{(n)}\right)\right]\right]+\left[\left(e^{\frac{-\Delta t_n}{\tau_{i,l}}}+1\right)J_{j,l}\tau_{j,l}\frac{\Delta P_{wf,j,l}^{(n)}}{\Delta t_n}\right]+\left[q_{cr,j,l}^{n}-q_{cr,j,l}^{(n-1)}e^{\frac{-(\Delta t_n)}{\tau_{j,l}}}\right] \tag{5-7}$$

For monitoring system installed in injection and producing wells:

$$q_{j,l}^{n}=\left[q_{j,l}^{(n-1)}e^{\frac{-(\Delta t_n)}{\tau_{j,l}}}\right]+\left[\left(1-e^{\frac{-\Delta t_n}{\tau_{i,l}}}\right)\sum_{i=1}^{N_i}\left[f_{ijl}\left(I_{i,l}^{(n)}\right)\right]\right]+\left[\left(e^{\frac{-\Delta t_n}{\tau_{i,l}}}+1\right)J_{j,l}\tau_{j,l}\frac{\Delta P_{wf,j,l}^{(n)}}{\Delta t_n}\right]+\left[q_{cr,j,l}^{n}-q_{cr,j,l}^{(n-1)}e^{\frac{-(\Delta t_n)}{\tau_{j,l}}}\right] \tag{5-8}$$

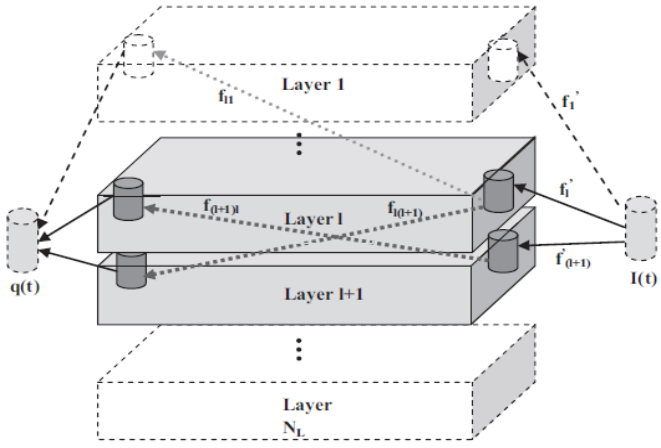

Figure 5-4. Control volume of producer j in a communicating multi-layer reservoir, CRMP-MLCr (Mamghaderi and Pourafshary, 2013)

5.3.5 Data Processing

The conventional CRM parameter fitting workflow consists of three steps: prediction,

validation and optimisation (Figure 5-5 and Figure 5-6). The prediction step is begun by inputting the injection and production data into a CRM coded as an Excel/MATLAB spreadsheet. The fitting routine's objective function (Equation 5-9) minimises the mismatch between the calculated and the observed production history. Non-linear, gradient-based solver in Excel or MATLAB's optimizer was used to derive the unknown parameters by non-linear regression after training on the production history data prior water breakthrough. (Izgec and Kabir, 2010 explain why the resulting inter-well connectivity before breakthrough is a viable parameter).

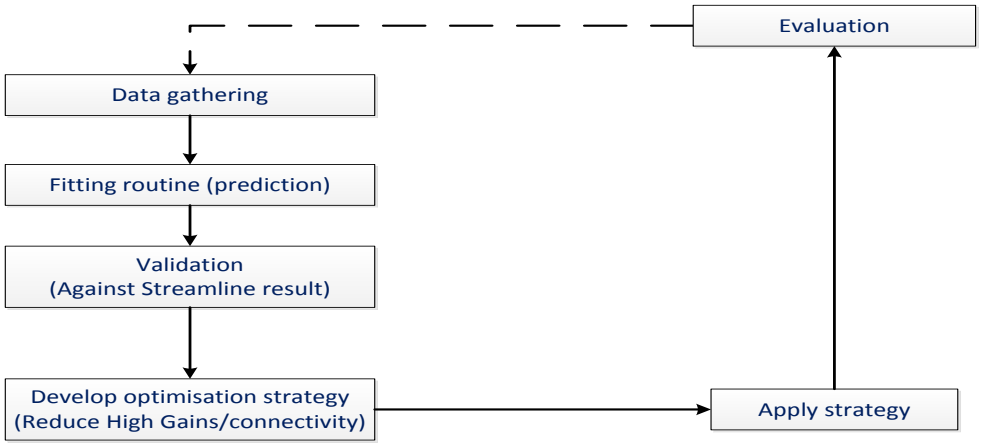

Figure 5-5. Workflow for CRM application in I-Wells

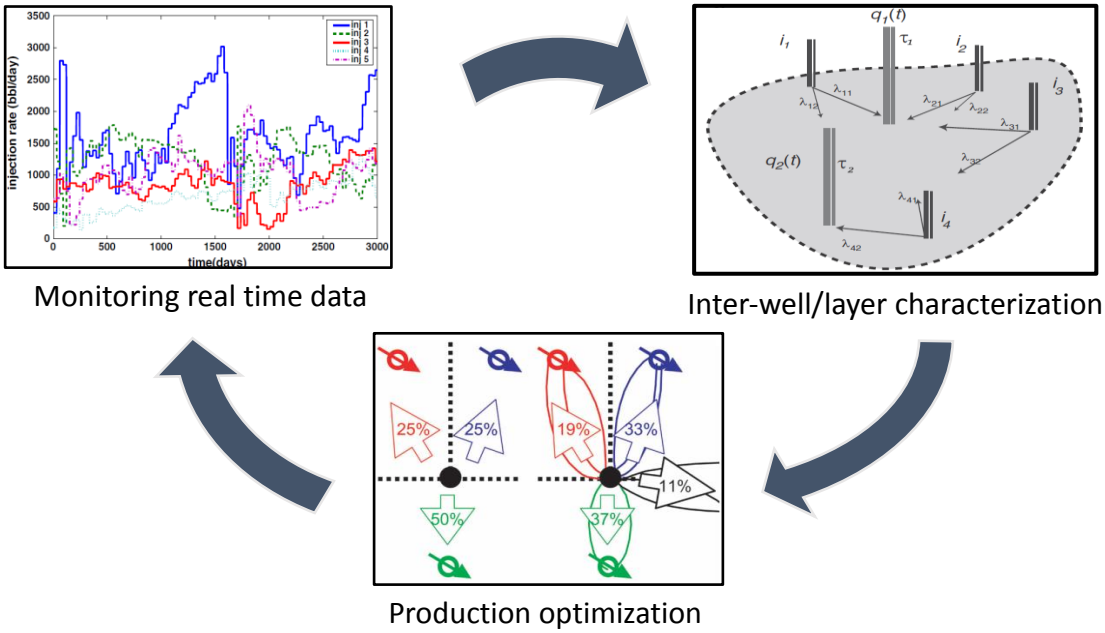

Figure 5-6. Illustration of CRM Workflow

The data-fitting process must also satisfy the equation 5-10 constraints that:

1. The water volume fraction flowing towards each layer (the injection fraction, f'_{il}), the time-constant, (τ_{jl}) and the connectivity constant (f_{ijl}) has to be a positive number or zero.
2. The sum of all the connectivity constants (f_{ijl}) should be unity for a closed system (voidage replacement), or it can be less than unity for an open system (i.e. a sector model or a reservoir with a poorly described aquifer). The sum of water rate fractions flowing towards each layer from an injector (f'_{il}) has to be unity.

Objective function for nonlinear regression:

$$Obj.function = \min \sum_{n}^{N_n} \left(q^n_{real,j,l} - q^n_{CRM,j,l} \right)^2 \quad (5\text{-}9)$$

Constraints for nonlinear regression:

$$f'_{i,l}, f_{ijl}, \tau_{j,l} \geq 0$$
$$\sum_{i=1}^{N_i} f_{ijl} \leq 1 \; ; \sum_{l=1}^{N_L} f'_{i,l} \leq 1 \quad (5\text{-}10)$$

The CRM fitting results were compared with the numerical reservoir model streamline results in the validation step. A proxy, inter-well connectivity map that illustrates the inter-well interactions was prepared from the CRM results and validated by comparison with the results of the streamline simulation results (Izgec and Kabir, 2010; Jahangiri *et al.*, 2014). This validation step increases confidence in the CRM. Further, the connectivity map can also be used to make informed production/injection optimisation decisions. This is particularly valuable for I-wells where zonal flow control in real time is possible.

Note the above description is for a multilayer reservoir. The workflow for single-layer is simpler with the parameters referring to the well instead of per layer basis. Subscript l is no longer applied.

5.4 CRM for a field with dynamic well control or changing permeability (fracture) with time.

Most publications on CRM assume the parameters are time-independent (Yousef, Lake and Jensen, 2006; Liang *et al.*, 2007; Sayarpour *et al.*, 2009; Kim, Lake and Edgar, 2012; Mamghaderi and Pourafshary, 2013). This can be inaccurate when analysing the performance of AWC since a change in the control of one well will affect the drainage area, and hence the inter-well connectivity, of all connected wells. Changing CRM

connectivities has been proposed for similar events, e.g. for: changes in relative permeability after water breakthrough (Jafroodi and Zhang, 2011), injection rate fluctations (He *et al.*, 2017), and transmissibility changes due to thermally induced fractures (Almarri *et al.*, 2017).

Figure 5-7 considers the case of one Injector (I1) and two producers (P1 and P2) which are both operated at a fixed Bottom Hole pressure (BHP). The formation layer between I1-P1 (Block K1) has greater permeability than that between I2-P2 (Block K2). Table 5-1 summarise the reservoir data for case 1.

Note that data-driven modelling method such as CRM, is highly dependent on the richness and the diversity of the available data points. Perturbing this scenario (fluctuating the well's control by 10% from its original values) is aimed to reduce the likelihood of having non-unique solutions and enhance the confidence of data-calibration.

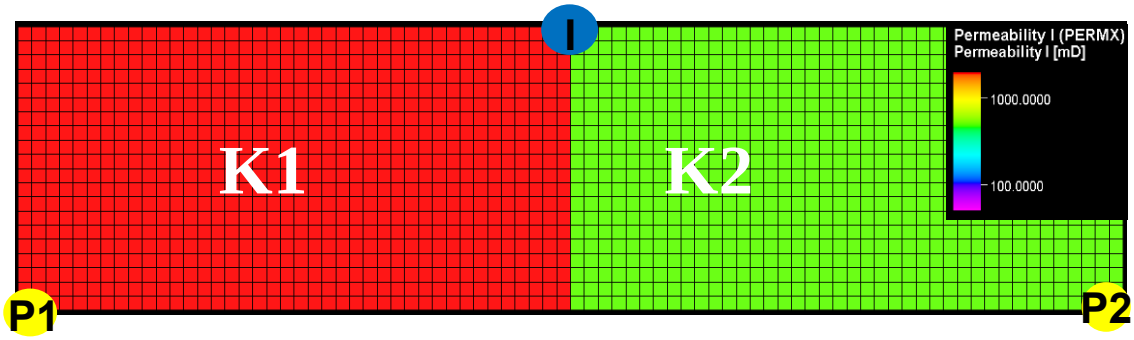

Figure 5-7. A simple reservoir model with 1 Injector supporting 2 Producers. Located in reservoir blocks with different permeabilities.

Table 5-1. Properties for the fig. 5-7 production system (Case 1).

Reservoir Properties			
Input Data			
Injection Control	I1	**350**	Sm3/Day
Production Control	P1	**175**	Bar
Production Control	P2	**175**	Bar
Permeability I1 – P1	Block K1	**2000**	mD
Permeability I1 – P2	Block K2	**500**	mD
Perturbation		**10**	%

The better connectivity between I1-P1 than for I1-P2 is illustrated by the greater number of streamlines between them. The streamline calculated connectivity's of f_{11}~0.80 and f_{12}~0.20 (Figure 5-8), is represented by the relative length of the two, green, CRM calculated arrows in the proxy-connectivity map (Figure 5-9). The validation from streamline model is also verified by the agreement between the observed production history and estimated production from CRM in P1 & P2 (Figure 5-10 and Figure 5-11). The water flood front will propagate faster in the direction of P1, resulting in a reduced sweep efficiency towards P2. The water saturation map calculated by a numerical simulator corroborates the CRM calculation (Figure 5-12).

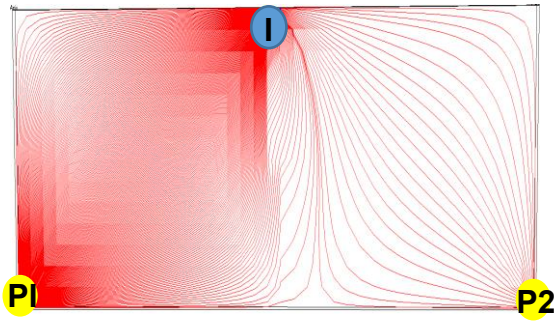

Figure 5-8. Streamline map (Case 1)

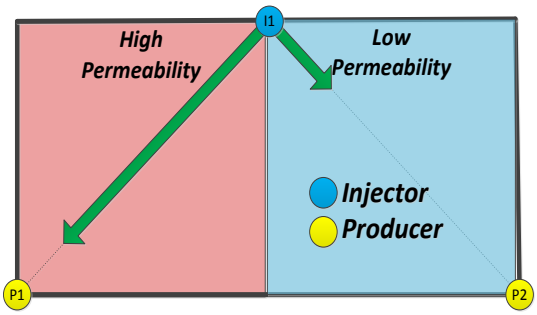

Figure 5-9. Connectivity map of reservoir (Case 1)

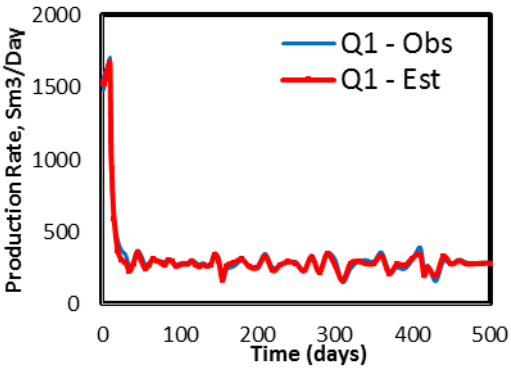

Figure 5-10. Comparison between the case 1 CRM results (Est.) against the production history data in P1 (Obs.)

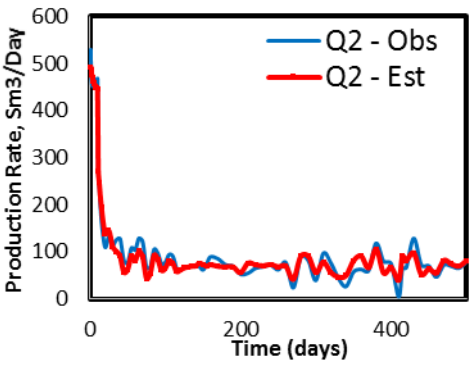

Figure 5-11. Comparison between the case 1 CRM results (Est.) against the production history data in P2 (Obs.)

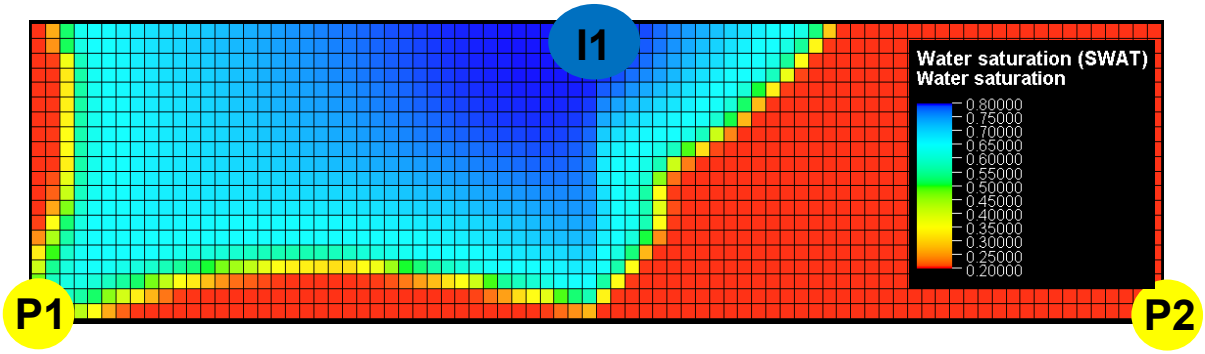

Figure 5-12. Field saturation map (Case 1)

Choking well P1 (Case 2) reduces the P1 well's production rate, alters the streamlines distribution (Figure 5-13). This increased the CRM-calculated connectivity between I1-P2 (f_{12}~0.45) with a corresponding decrease for I1-P1 (f_{11}~0.55). This is reflected in the relative size of the two green arrows in figures 5-14 which are now almost the same length. The new connectivity values can be expected to result in a more-uniform flood front (figure 5-15), delaying first water breakthrough and improving efficiency the sweep (Figure 5-19). The new production history also verified by the CRM prediction.

Note that an MS Excel solver was chosen to do data-fitting for this scenario. The fitting results can be improved given a more sophisticated optimization platform, such as Genetic Algorithm in MATLAB. (Mamghaderi, Bastami and Pourafshary, 2012).

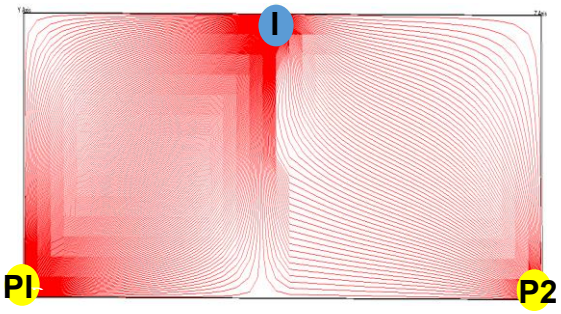

Figure 5-13. Streamline map (Case 2)

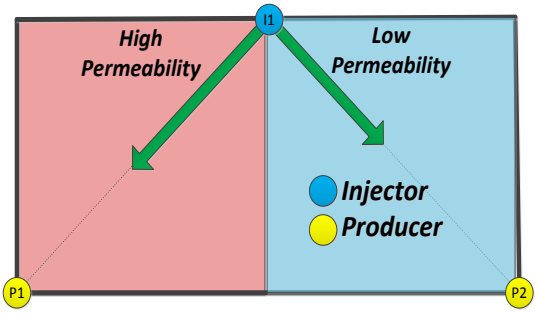

Figure 5-14. Connectivity map of reservoir (Case 2)

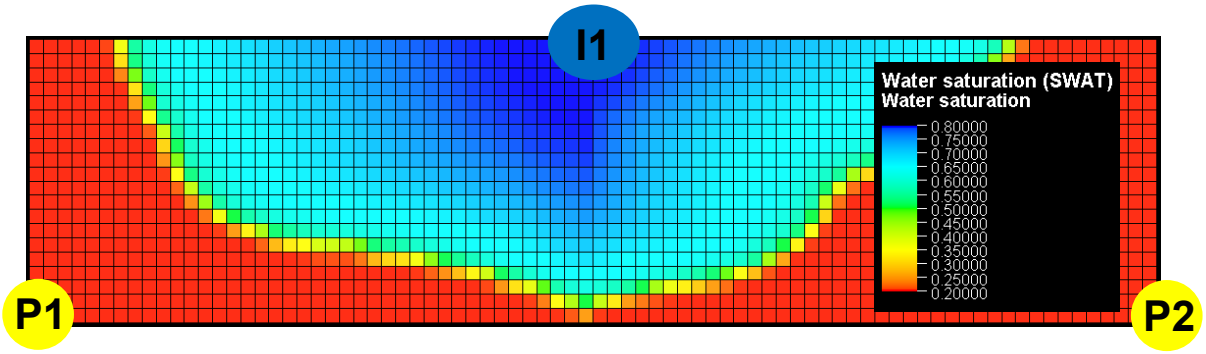

Figure 5-15. Field saturation map (Case 2)

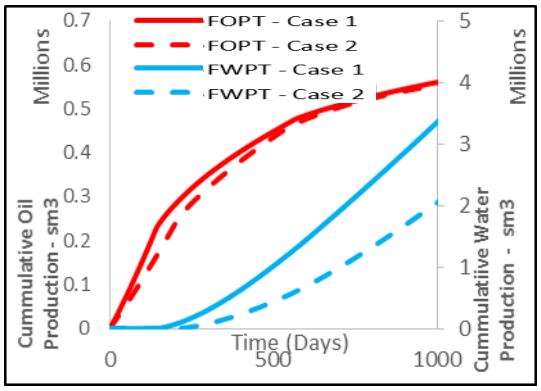

Figure 5-16. The case 1 and 2 comparison of cumulative oil and water

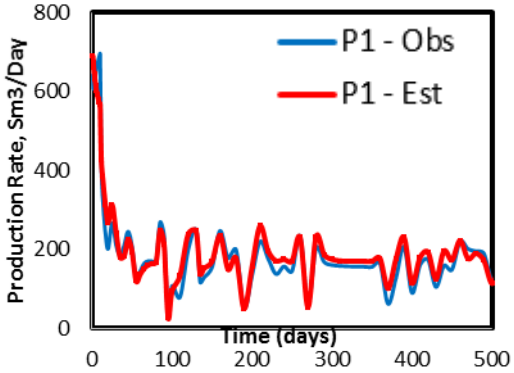

Figure 5-17. Comparison between the case 2 CRM results (Est.) against the production history data in P1 (Obs.)

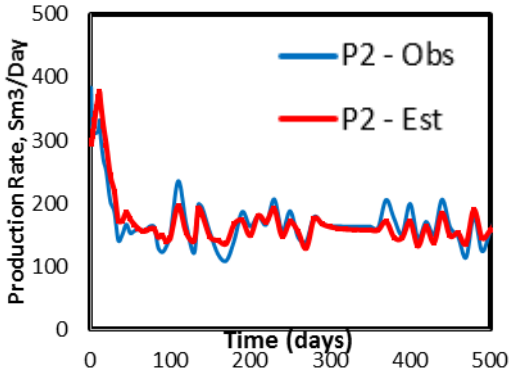

Figure 5-18. Comparison between the case 2 CRM results (Est.) against the production history data in P1 (Obs.)

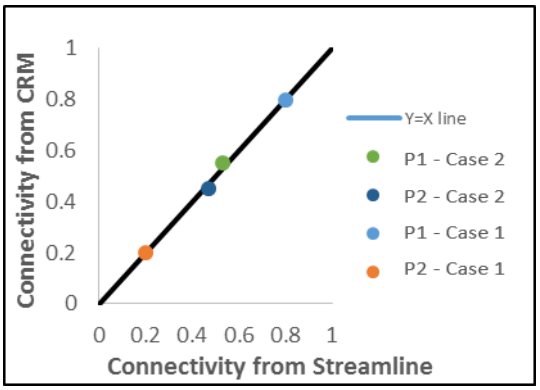

Figure 5-19. CRM and Streamline connectivities compared

5.4.1 Case history for reservoir with Thermal Induced Fractures

(For the following sub-section, I thank my colleague, Dr. Misfer Almarri, for his contribution to the study of analysis of thermally induced fractures using modern

analytical techniques). Thermally Induced Fractures (TIFs) are common in waterflooded fields where the injection of (relatively) cold water leads to a cooling front that reduces the formation's in-situ stresses. TIF initiation and growth can thus occur when the previously measured, fracture propagation pressure is not exceeded. The presence of TIFs severely distorts the flood front, decreasing sweep efficiency.

A field case study is used to demonstrate the value of integration of the recently developed analytical model, the Modified Hall Integral (MHI), with a semi-analytical model, the Capacitance Resistance Model (CRM). The MHI first identified the onset of TIF, its propagation properties, followed by CRM to quantify the change in inter-well communication due to TIF, the likely TIF direction and its subsequent impact on the well connectivity and flood efficiency. TIF initiation and propagation events were clearly identified, even when their existence was much less certain with the other techniques.

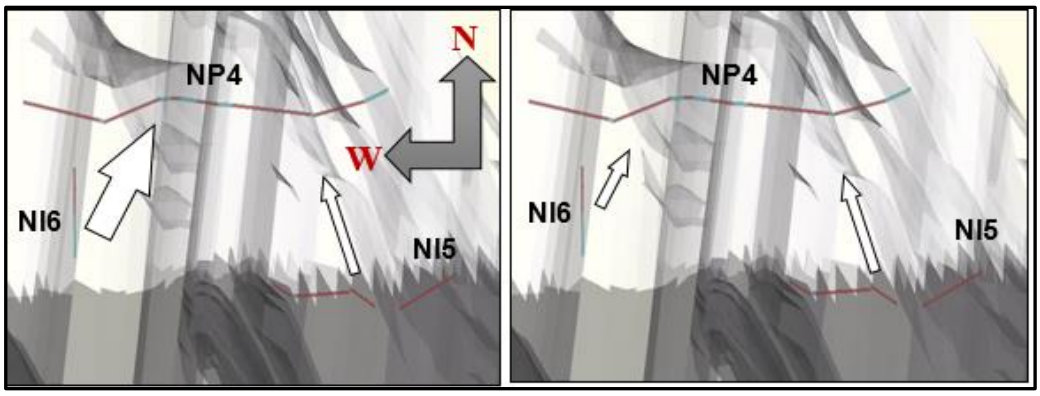

Figure 5-20. Illustration of TIF in N-field. (Left: connectivity pre-TIF); (right: connectivity post-TIF)

A sector of reservoir N has been developed by a total of three wells: two horizontal wells, Producer "NP4" and injector "NI5", and the vertical injection well, "NI6". The production and injection history of these two injection wells was analysed. The implemented workflow identified the TIF onset, the facture propagation period, and post TIF period. (Almarri *et al.*, 2017 details all the calculation entailing this case, this section will only describe the CRM calculation). The CRMIP solution is fist applied to the time-interval of 200 days before TIF initiation for the Pre-TIF period. The Post-TIF data was selected from the 200-day period after TIF initiation, when the TIF had seemingly stopped propagating after its initial growth. The comparison between CRMIP calculated rates agrees reasonably with production history match as depicted in figure 5-21 and 5-22. The root-mean square error (equation 5-9) for these comparisons is below 20%, the maximum

error rule-of-thumb suggested by Sayarpour, 2009.

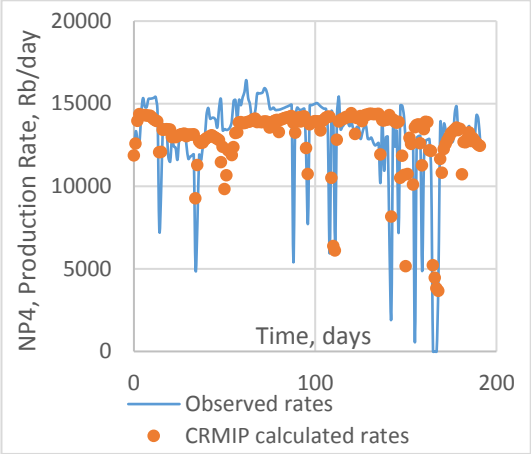

Figure 5-21. Comparison of CRM estimated flow rate and observed rate for NP4 production well for pre-TIF.

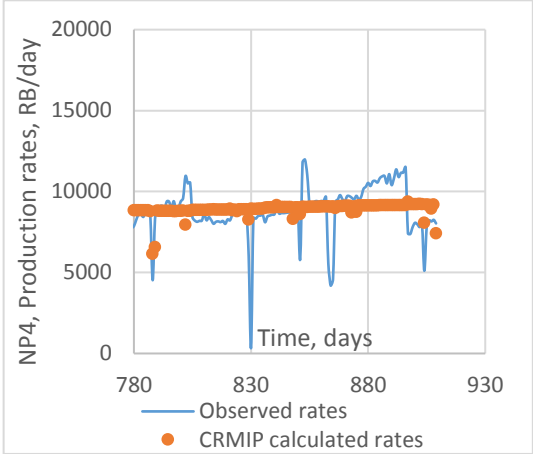

Figure 5-22. Comparison of CRM estimated flow rate and observed rate for NP4 production well for Post-TIF.

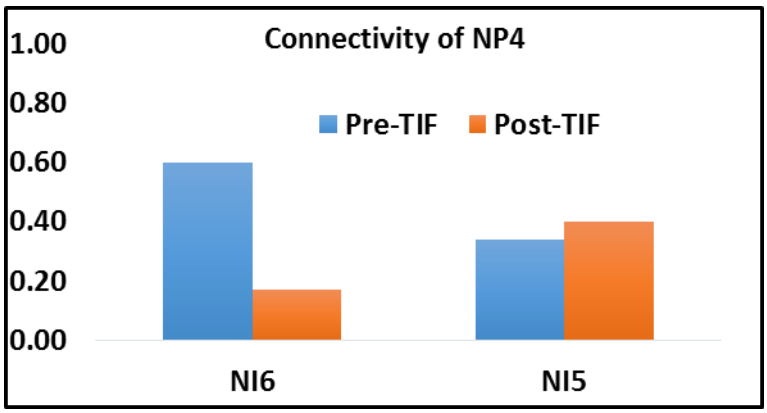

Figure 5-23. Pre- and Post-TIF Connectivity of Well NP4 with NI6 and NI5

Figure 5-23 presents the connectivity between well NP4 with the NI6 (f_{64}) and NI5 (f_{54}) injection wells in the Pre- and Post-TIF time intervals. f_{64} is significantly smaller in the Post-TIF period, implying the pressure support to NP4 by NI6 has considerably reduced even though the total volume of water injected has increased, as shown by Figure 5-24

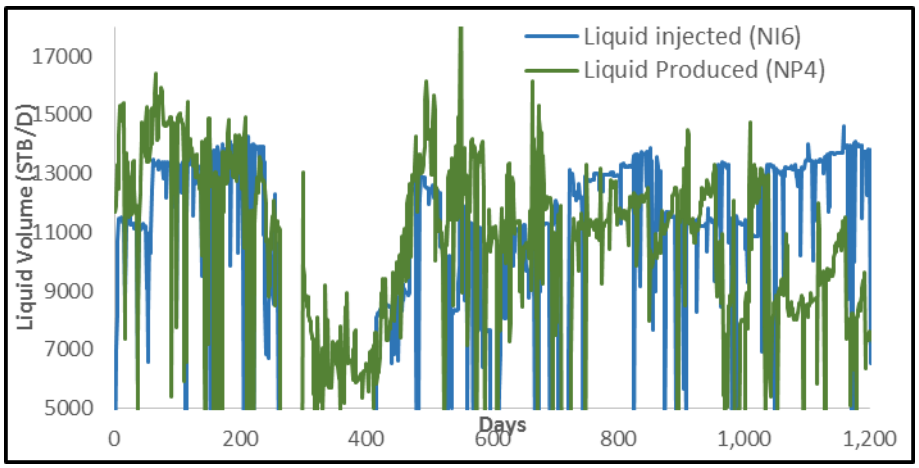

Figure 5-24. History data for injection well NI6 and production well NP4

The Post-TIF reduction in connectivity implies that the NI6 TIF propagated away from NP4 in an East-Westerly direction (Figure 5-25). This conclusion is supported by direction of tensile fractures observed by the Formation Micro Imager (FMI) log recorded after drilling another well in the same field. The NI6 TIF is thus expected to propagate approximately parallel to NP4's well path (Figure 5-25), the direction of the reservoirs maximum horizontal stress.

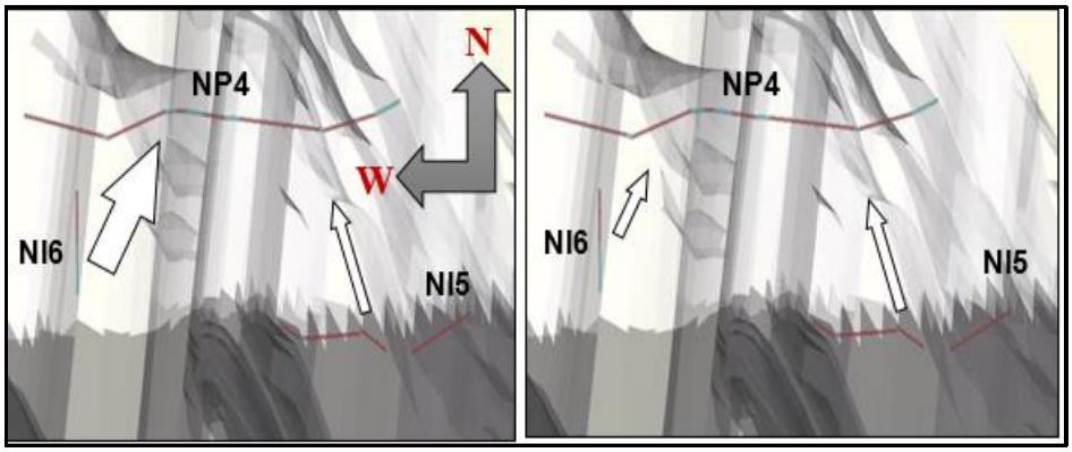

Figure 5-25 (left). Connectivity pre-TIF; (right). Connectivity post-TIF. The size of white arrows represent degree of connectivity between wells (red lines).

The CRM findings of a zone of reduced sweep efficiency between wells NI6 and NP4 were supported by Figure 5-24, a plot of the History Data for Injection Well NI6 and Production Well NP4. This figure shows that the injected and produced liquid volumes was reasonably similar before 690 days, the Pre-TIF time, but decreased thereafter, indicated TIF initiation and a reduced volumetric sweep efficiency between the well pair.

The produced liquid also increased slightly when TIF propagation ceased between 850 and 1000 days (Figure 5-24). The flood front propagated in a more radial direction during this period, confirming TIF has a significant impact on the sweep efficiency.

5.5 CRM for a Field with AWC completions

Figure 5-26, a schematic view of an open-hole, production completion with two zones is a case study of an AWC providing zonal, real-time, monitoring and production control without the need for well intervention by the means of Interval Control Valves (ICVs) or other types of Flow Control Devices (FCDs). FCDs can generally be classified as passive (a fixed restriction), active (the restriction can be controlled such as ICV) and autonomous (no control, but an autonomous reaction to the presence of an unwanted fluid). One or more passive FCDs are installed on every tubing joint opposite the completion, amounting to hundreds of FCDs per well. By contrast, the number of installed ICVs is limited to a maximum of around five (hydraulic control) or around 30 (electric control). Each ICV normally has between two and ten possible flow positions. A gravel pack or multiple packers at specified locations may also be installed to provide the level of annular isolation required to optimise the AWC's performance. Faisal Al-Khelaiwi (2013) and Eltaher (2017) provide a good overview of the evolution of AWC technology, including commercially available types and their applications. In this chapter we will focus on ICVs.

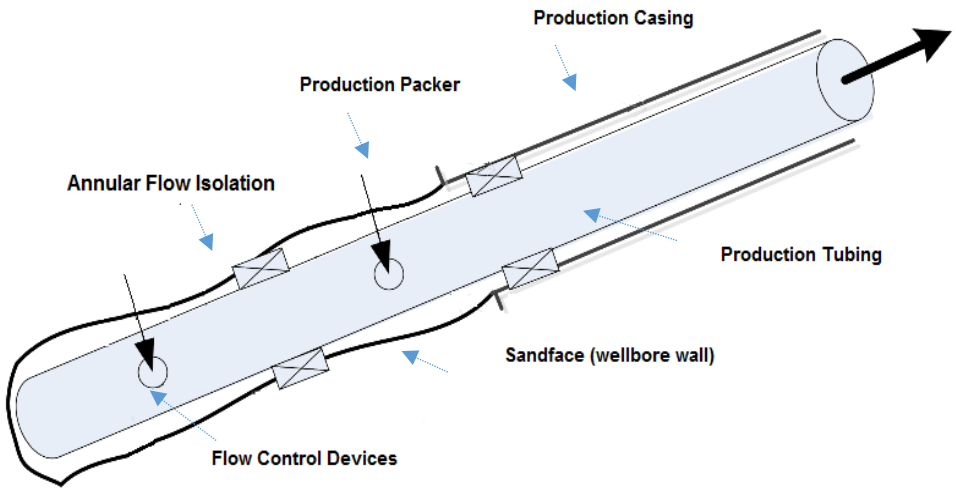

Figure 5-26. Schematic view of a well with Intelligent Well Completion

5.5.1 New analytical solution for CRM in wells with AWC

Normally all ICVs are initially in the fully open position and production is controlled by the surface choke. The AWC's production is frequently controlled by using the ICVs in a reactive manner after a water breakthrough. One or more ICVs are partly or completely shut to maximise the well's total oil production rate (Grebenkin and Davies, 2012). A real-time parameter reaction-based (e.g. to production WC) optimisation strategy (Dilib *et al.*, 2012; Grebenkin and Davies, 2012), although intuitive, may not be able to deliver long-term production optimisation. The alternative, proactive control (Alghareeb *et al.*, 2009; Almeida, Vellasco and Pacheco, 2010; Sefat, 2016), involves the early restriction of one or more ICVs in order to manage the well's inflow to maximise long-term oil recovery and/or its ultimate value. Such proactive, optimisation control strategy using numerical reservoir simulation is a complex, high-dimensional, mathematical and computational problem (Sefat, 2016). CRM provides a simple, fast and insightful workflow for developing a proactive ICV control strategy at a reduced cost in terms of the required data, computational resources and engineering time.

Modelling a well with FCDs, requires incorporation of the FCD's non-linear pressure drop into the CRM equation (i.e. CRM-AWC). The derivations process is detailed in Appendix C. Equation 5-11 is the general CRM-AWC solution.

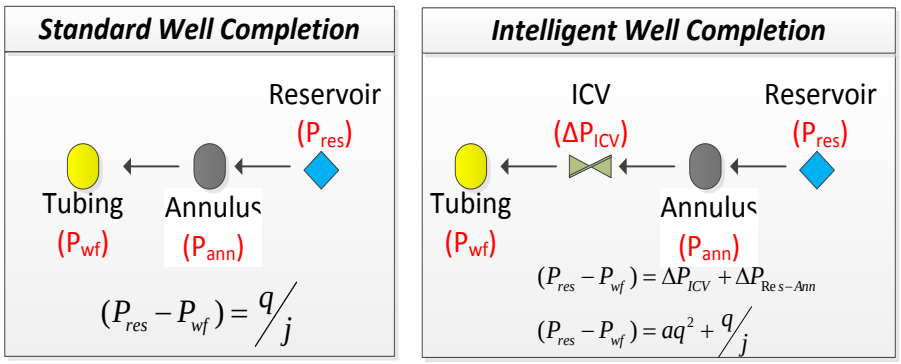

Figure 5-27. Nodal pressure analysis for a standard well (left) and an intelligent well completion (right). The FCD's pressure drop is not linearly related to the flow velocity

$$q_n = \frac{\left[\left(1-e^{-\left(\frac{\Delta t_k}{\tau}\right)}\right)\frac{Ja2\tau q_{n-1}}{\Delta t_k}-1\right]+\sqrt{\left\{\left[1-\left(1-e^{-\left(\frac{\Delta t_k}{\tau}\right)}\right)\frac{Ja2\tau q_{n-1}}{\Delta t_k}\right]^2\right\}+\left\{4q_{k-1}e^{-\left(\frac{\Delta t_k}{\tau}\right)}\left[\left(1-e^{-\left(\frac{\Delta t_k}{\tau}\right)}\right)\frac{Ja2\tau}{\Delta t_k}\right]\right\}-\left\{\left(1-e^{-\left(\frac{\Delta t_k}{\tau}\right)}\right)\left(i(t_k)-J\tau\frac{\Delta P_{wf}\Delta t_k}{\Delta t_k}\right)\right\}}}{4\frac{Ja\tau}{\Delta t_k}\left(1-e^{-\left(\frac{\Delta t_k}{\tau}\right)}\right)}$$

(5-11)

Equation 5-11 can be extended considering different drainage volumes for single and multi-layered wells {i.e. CRMP-AWC (equation 5-12), CRMIP-AWC (equation 5-13), CRMP-ML-AWC (equation 5-14), CRMP-MLCr-AWC (equation 5-15)}.

1. <u>CRM for a given producer with Advanced Well Completion (CRMP-AWC)</u>

$$q_j^n = \frac{\left[2\frac{Ja\tau q_{n-1}}{\Delta t_k}\left(1-e^{-\left(\frac{\Delta t_k}{\tau_j}\right)}\right)-1\right]+\sqrt{\left[1-2\frac{Ja\tau q_{n-1}}{\Delta t_k}\left(1-e^{-\left(\frac{\Delta t_k}{\tau_j}\right)}\right)\right]^2+\ldots}}{4\frac{Ja\tau}{\Delta t_k}\left(1-e^{-\left(\frac{\Delta t_k}{\tau_j}\right)}\right)}$$

$$\frac{\sqrt{\ldots+8\frac{Ja\tau}{\Delta t_k}\left(1-e^{-\left(\frac{\Delta t_k}{\tau_j}\right)}\right)\left(q_{n-1}e^{-\left(\frac{\Delta t_k}{\tau_j}\right)}+\left(1-e^{-\left(\frac{\Delta t_k}{\tau_j}\right)}\right)\left[\sum_{i=1}^{Ni}[f_{ij}I_i^n]-\mathrm{J}\,\tau\frac{\Delta P_{wf}\Delta t_k}{\Delta t_k}\right]\right)}}{4\frac{Ja\tau}{\Delta t_k}\left(1-e^{-\left(\frac{\Delta t_k}{\tau_j}\right)}\right)} \quad (5\text{-}12)$$

This equation is analogous to equation 5-2. It evaluates all the inter-well interactions between each specific injector-producer well pair, where there is one connectivity value for each pair, and one capacity value for each producer. This solution will require additional input parameter, a (or ICV strength), for each production well.

2. <u>CRM for a give pair of Injector-Producer with Advanced Well Completion (CRMIP-AWC)</u>

$$q_j^n = \sum_{i=1}^{N} q_{ij}^n$$

$$q_{ij}^n = \frac{\left[2\frac{aJ_{ij}\tau_{ij}q_{ij}^{n-1}}{\Delta t_k}\left(1-e^{-\left(\frac{\Delta t_k}{\tau_j}\right)}\right)-1\right]+\sqrt{\left[1-2\frac{aJ_{ij}\tau_{ij}q_{ij}^{n-1}}{\Delta t_k}\left(1-e^{-\left(\frac{\Delta t_k}{\tau_{ij}}\right)}\right)\right]^2+\ldots.}}{4\frac{aJ_{ij}\tau_{ij}}{\Delta t_k}\left(1-e^{-\left(\frac{\Delta t_k}{\tau_{ij}}\right)}\right)}$$

$$\frac{\sqrt{\ldots+8\frac{aJ_{ij}\tau_{ij}}{\Delta t_k}\left(1-e^{-\left(\frac{\Delta t_k}{\tau_{ij}}\right)}\right)\left(q_{ij}^{n-1}e^{-\left(\frac{\Delta t_k}{\tau_j}\right)}+\left(1-e^{-\left(\frac{\Delta t_k}{\tau_{ij}}\right)}\right)\left[\sum_{i=1}^{Ni}[f_{ij}I_i^n]-J_{ij}\tau_{ij}\frac{\Delta P_{wf}\Delta t_k}{\Delta t_k}\right]\right)}}{4\frac{aJ_{ij}\tau_{ij}}{\Delta t_k}\left(1-e^{-\left(\frac{\Delta t_k}{\tau_{ij}}\right)}\right)} \quad (5\text{-}13)$$

This equation is analogous to equation 5-3. It is a refined version of CRMIP-AWC, and

exclusively solves the drainage volume (additional time constant) for production and injection pair. This solution requires additional input parameter, a (or ICV strength), for each production well.

3. CRM for a given Producer with Advanced Well Completion, Multi-Layered reservoir, no cross-flow (CRMP-ML-AWC).

$$q_{j,l}^{n}=\frac{\left[2\frac{aJ_{j,l}\tau_{j,l}q_{j,l}^{n-1}}{\Delta t_k}\left(1-e^{-\left(\frac{\Delta t_k}{\tau_{j,l}}\right)}\right)-1\right]+\sqrt{\left[1-2\frac{aJ_{j,l}\tau_{j,l}q_{j,l}^{n-1}}{\Delta t_k}\left(1-e^{-\left(\frac{\Delta t_k}{\tau_{j,l}}\right)}\right)\right]^2+\ldots}}{4\frac{aJ_{j,l}\tau_{j,l}}{\Delta t_k}\left(1-e^{-\left(\frac{\Delta t_k}{\tau_{j,l}}\right)}\right)}$$

$$\frac{\sqrt{\ldots+8\frac{aJ_{j,l}\tau_{j,l}}{\Delta t_k}\left(1-e^{-\left(\frac{\Delta t_k}{\tau_{j,l}}\right)}\right)\left(q_{j,l}^{n-1}e^{-\left(\frac{\Delta t_k}{\tau_{j,l}}\right)}+\left(1-e^{-\left(\frac{\Delta t_k}{\tau_{j,l}}\right)}\right)\left[\sum_{i=1}^{Ni}\left[f_{ijl}I_{l,l}^{n}\right]-J_{ij}\tau_{ij}\frac{\Delta P_{wf\,\Delta t_k}}{\Delta t_k}\right]\right)}}{4\frac{aJ_{j,l}\tau_{j,l}}{\Delta t_k}\left(1-e^{-\left(\frac{\Delta t_k}{\tau_{j,l}}\right)}\right)} \qquad (5\text{-}14)$$

This equation is analogous to equation 5-6. The solution evaluate the interactions between layers, where the connectivity and drainage volume are calibrated for each layer. The solution would also require the ICV strength input for each layer.

4. CRM for a given Producer with Advanced Well Completion, Multi-Layered reservoir, with cross-flow (CRMP-MLcr-AWC).

$$q_{j,l}^{n}=\frac{\left[2\frac{aJ_{j,l}\tau_{j,l}q_{j,l}^{n-1}}{\Delta t_k}\left(1-e^{-\left(\frac{\Delta t_k}{\tau_{j,l}}\right)}\right)-1\right]}{4\frac{aJ_{ij}\tau_{ij}}{\Delta t_{k-1}}\left(1-e^{-\left(\frac{\Delta t_k}{\tau_{ij}}\right)}\right)}+\frac{\sqrt{\left[1-2\frac{aJ_{j,l}\tau_{j,l}q_{j,l}^{n-1}}{\Delta tn}\left(1-e^{-\left(\frac{\Delta t_k}{\tau_{j,l}}\right)}\right)\right]^2+\ldots}}{4\frac{aJ_{j,l}\tau_{j,l}}{\Delta t_k}\left(1-e^{-\left(\frac{\Delta t_k}{\tau_{j,l}}\right)}\right)}$$

$$\frac{\sqrt{\ldots+8\frac{aJ_{j,l}\tau_{j,l}}{\Delta t_k}\left(1-e^{-\left(\frac{\Delta t_k}{\tau_{j,l}}\right)}\right)\left(q_{cr,j,l}^{n}+\left(q_{cr,j,l}^{n-1}-q_{j,l}^{n-1}\right)e^{-\left(\frac{\Delta t_k}{\tau_{j,l}}\right)}+\left(1-e^{-\left(\frac{\Delta t_k}{\tau_{j,l}}\right)}\right)\left[\sum_{i=1}^{Ni}\left[f_{ijl}\,I_{l}^{n}\right]-J_{ij}\tau_{ij}\frac{\Delta P_{wf\,n}}{\Delta t_k}\right]\right)}}{4\frac{aJ_{j,l}\tau_{j,l}}{\Delta t_k}\left(1-e^{-\left(\frac{\Delta t_k}{\tau_{j,l}}\right)}\right)}$$

(5-15)

This equation is analogous to equation 5-8, and principally an extended version of CRMP-ML-AWC which incorporated crossflow between layers.

5.5.2 CRM-AWC in a single-layer reservoir

The scenario in Section 5.4, where a surface choke to raise the flowing Bottom Hole Pressure (BHP), could also have use of an ICV choke (figure 5-25, right). The new CRM-AWC solution (equation 5-12) may be used to evaluate the results of different choke strengths for zone 1. The ICV restriction will reduce the connectivity with the associated wells or layers. These will be a corresponding increase in the connectivity values to the other wells or layers. A stronger restriction will magnify the effect.

The case study uses an infinitely variable ICV in P1 with three fixed ICV open position (Table 5-2). The same reservoir used previously was modelled and reservoir parameters (Figure 5-7). The ICV restriction strength is calculated using equation 2-11.

Table 5-2. ICV strength and the associated ICV flow area of scenario 1-3

Scenario	**ICV Strength** bar/(rcm/d)^2	**ICV flow area** m^2
1	0.00034	0.00004
2	0.0014	0.00002
3	0.0545	0.00001

Scenario 1 (low ICV strength) only slightly improves the flow distribution the CRM-AWC calculated connectivity for P1 has reduced from 0.80 (original connectivity) to 0.70. Figure 5-28 shows the comparison between the CRM results against the observed production rates.

Note that the bumps in figure 5-28 were not caused by the noise that we normally see in the typical field measurements. In this figure, the large-bump during the initial time refer to the production data during transient times, whilst the small-bumps or rate fluctuations over the fitting windows are the results from the perturbations imposed to the production and injection control in this scenario, i.e. numerical perturbations. Without perturbations, the production rate are expected to be very flat and the data points needed for calibration are monotonous. Such results are undesirable since fitting the parameters can be easily yielded to non-unique results. By introducing numerical perturbation we will increase the data-point's diversity and consequently our confidence for our CRM fitting parameters.

The excellent production history's matching for this scenario is clearly seen in figure 5-

28, and the connectivity map is illustrated in Figure 5-29.

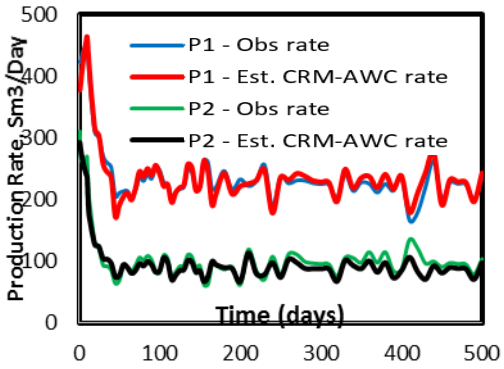

Figure 5-28. Scenario 1 comparison between CRM results against the history data for P1 and P2

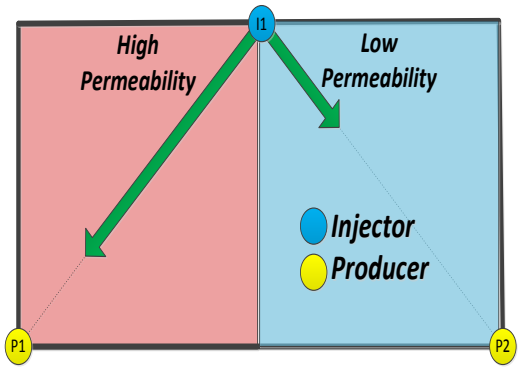

Figure 5-29. Scenario 1 connectivity map of single-layer reservoir

Scenario 2, where PI's moderate ICV strength equally distributes the injector 1 flow between the production connectivity to P2 improves to 0.45, while that to P1 reduces to 0.55 (Figure 5-29). This agrees with production history match in Figure 5-30 and the connectivity map is in Fig 5-31.

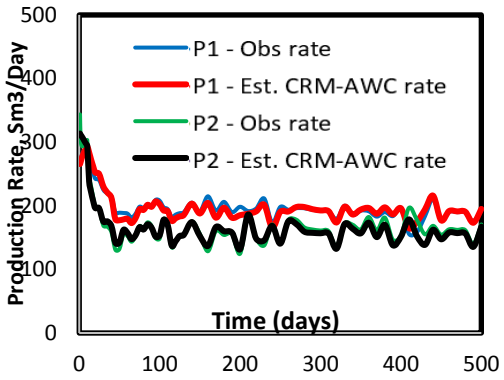

Figure 5-30. Scenario 2 comparison between CRM results against the history data in P1 and P2

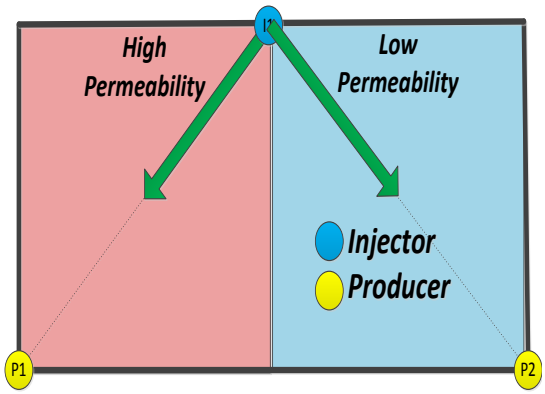

Figure 5-31. Scenario 2 connectivity map of reservoir

The very aggressive P1 ICV choke operates in scenario 3 result in an unbalanced injection profile in scenario 3. The CRM-AWC calculated connectivity to P2 increases to 0.65, while that to P1 reduces to 0.35 (Figure 5-33). This agrees with the production history match (Figure 5-32).

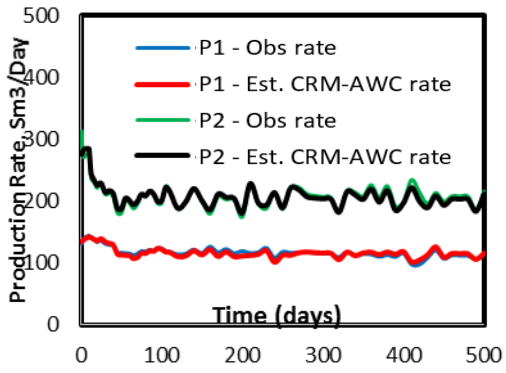

Figure 5-32. Scenario 3 comparison between CRM results against the history data in P1 and P2

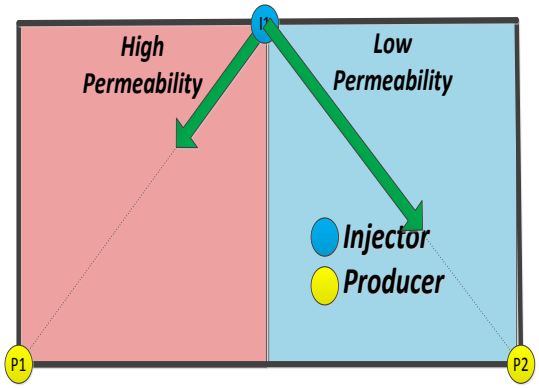

Figure 5-33. Scenario 3 connectivity map of reservoir

5.5.3 CRM-AWC in a multi-layer reservoir

Figure 5-34, a simpler case of one injector (I1) and two producers (P1 and P2), where all wells are now completed on two layers separated by an impermeable shale. A flow monitoring system is installed in both the production and injection wells. The reservoir parameters in this reservoir are summarised in Table 5-3, while Figure 5-34 illustrates the greater permeability different between K1-top and K1-bottom between K2-top and K2-bottom.

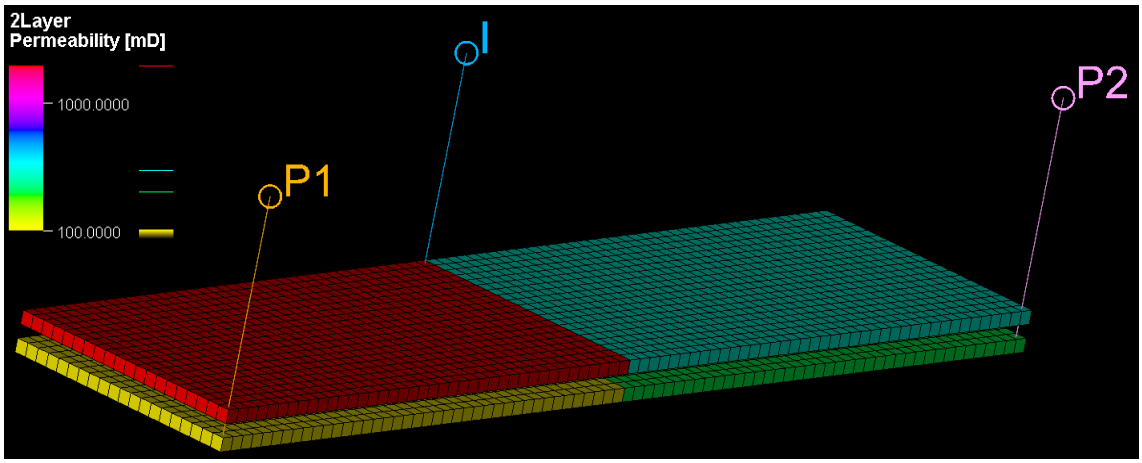

Figure 5-34. Schematic of the simple reservoir case, completed with one injector and two producers (testing-bed for CRM for AWC).

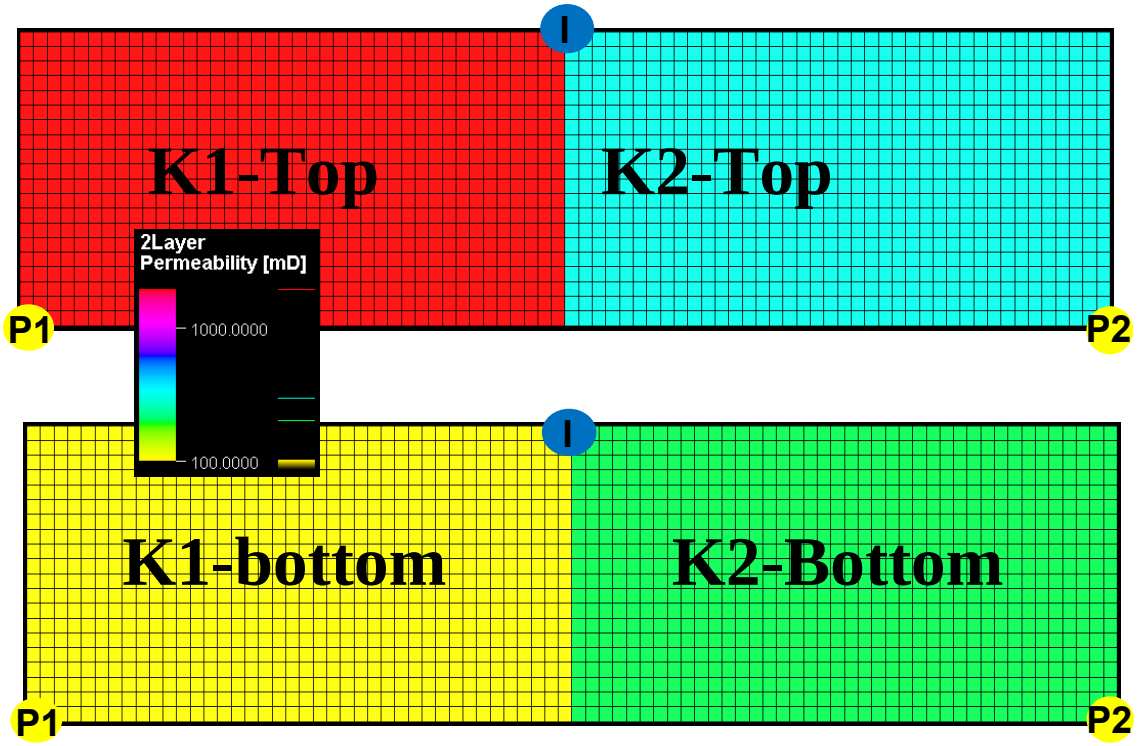

Figure 5-35. Aerial view of the permeability map of the top and bottom reservoir layers in Figure 5-32

Table 5-3. Properties of reservoir illustrated in Figure 5-35

Reservoir Properties			
Input Data			
Injection Control	I1	**350**	Sm3/Day
Production Control	P1	**175**	Bar
Production Control	P2	**175**	Bar
Permeability I1 – P1 Top Layer	Block P1 – Top	**2000**	mD
Permeability I1 – P2 Top Layer	Block P2 – Top	**300**	mD
Permeability I1 – P1 Bottom Layer	Block P1 – Bottom	**100**	mD
Permeability I1 – P2 Bottom Layer	Block P2 – Bottom	**200**	mD
Perturbation		**10**	%

The injector operated at injection rate control 350 sm^3/day, while both producers operated at operating pressure 175 bar. These parameters are 10% perturbed from the base values every 10 days in order to get varying production/injection profiles to feed the data-fitting optimisation. The ICV fully open for the first four months (i.e. equivalent to an open-hole completion). Hence the CRM-ML-AWC model (i.e. equation 5-14) simulates this scenario with a restriction strength equal to zero. Figure 5-37 shows the connectivity of $f_{11\,(Top)} = 0.87$ between I1-P1 in the top layer (Block P1 – Top) is greater than that for I1-

P2 (Block P2 – Top), $f_{12\ (Top)}$ = 0.13. The water saturation map (Figure 5-34) and the relative connectivities are illustrated in Figure 5-37 (on the left). The water flood in the top layer has hardly propagated in the direction of P2 during this period. Also, there is virtually no injection into the lower zone (on the right).

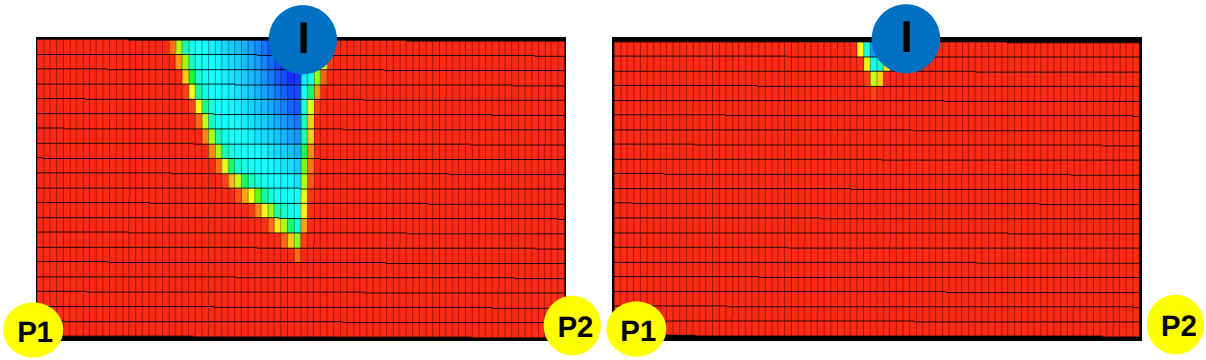

Figure 5-36. Water saturation map after 120 days for top layer (left) and bottom layer (right). Blue = water; red = oil

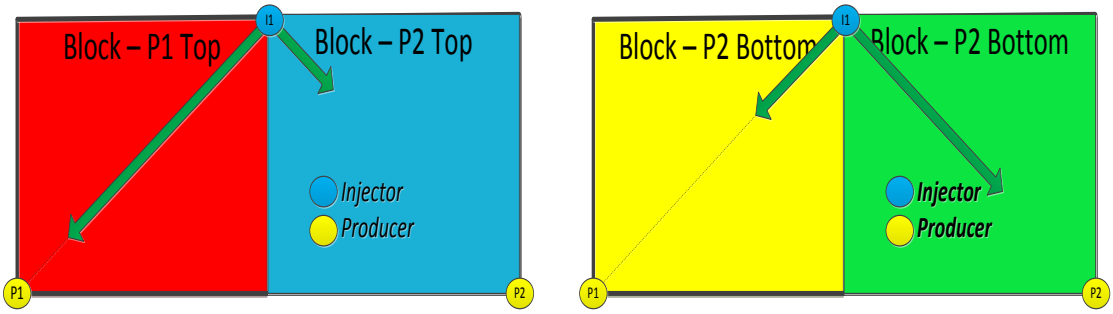

Figure 5-37. Connectivity map (stage 1) after 120 days.

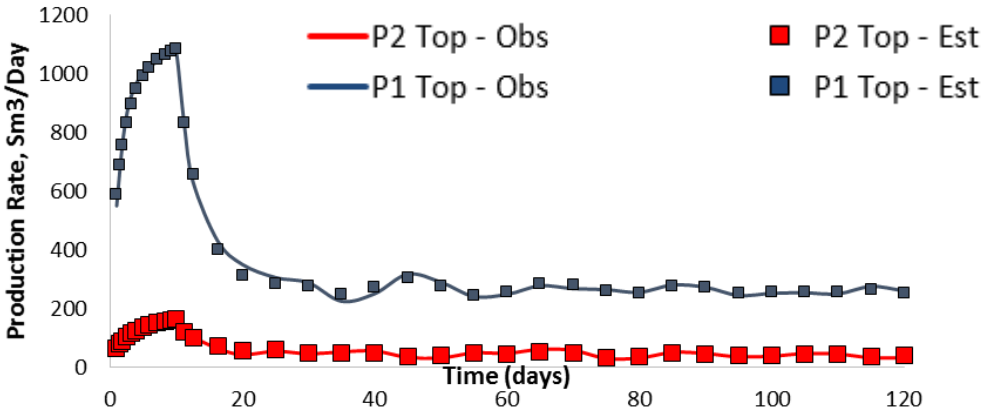

Figure 5-38. Comparison of CRM estimated flow rate and observed rate for P1 and P2 top layers

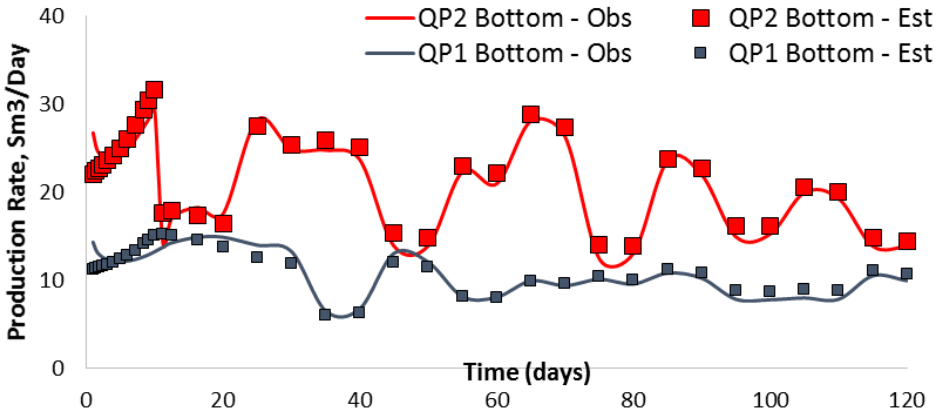

Figure 5-39. Comparison of CRM estimated rate and observed rate for bottom P1 and P2 bottom layers

The top layer of P1 is choked to re-distribute the injected water by increasing the ICV restriction strength of the P1-top layer to 0.001675 bar/(rcm/d)^2 after 120 days. This valve setting is changed in an "ad-hoc" way i.e. the ICV specific strength is fixed without optimisation. This new date is for CRMP-AWC calibration. After 245 days of production (from days 120 to 365), the CRM-ML-AWC calculation is applied to this reservoir at day 365 and the connectivity map is revised (Figure 5-38). The connectivity for the bottom layer does not change, $f_{11\,(Bottom)} = 0.32$ and $f_{12\,(Bottom)} = 0.68$, while the ICV restriction in the top layer reduces $f_{11\,(Top)}$ from 0.87 (stage 1) to 0.61 (stage 2), with $f_{12\,(Top)}$ increasing from 0.13 (stage 1) to 0.38 (stage 2).

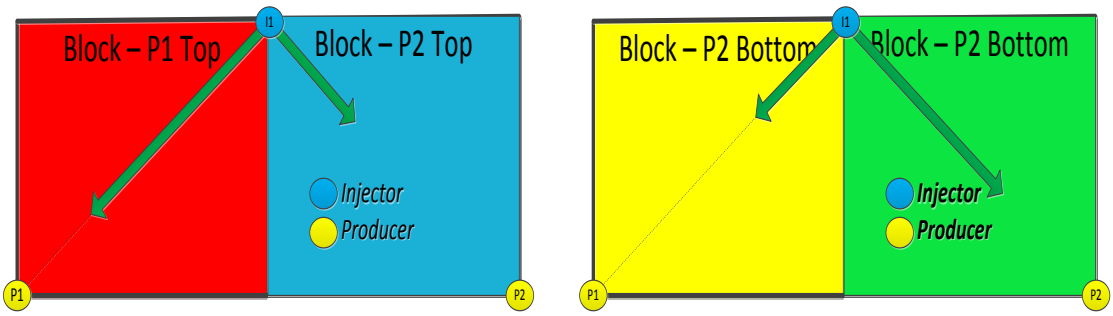

Figure 5-40. Connectivity map (stage 2) after 245 days

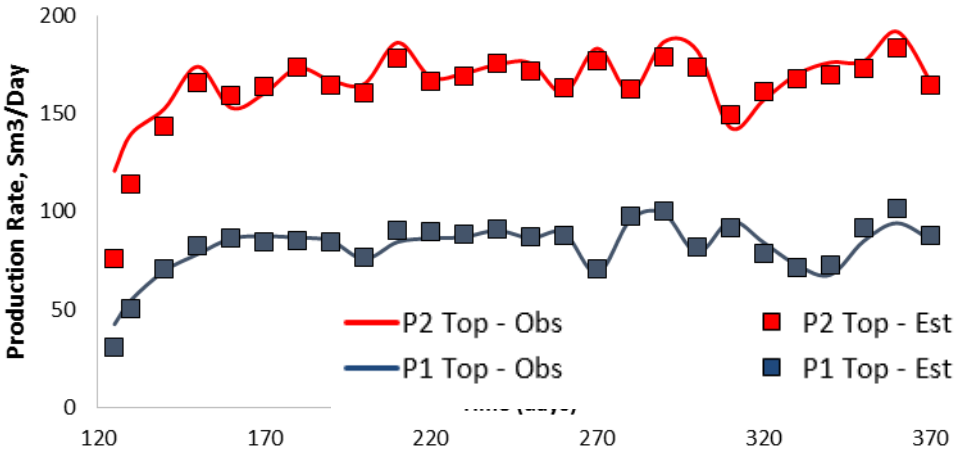

Figure 5-41. Comparison of CRM estimated flow rate and observed rate for P1 and P2 top layers between 120 and 365 days

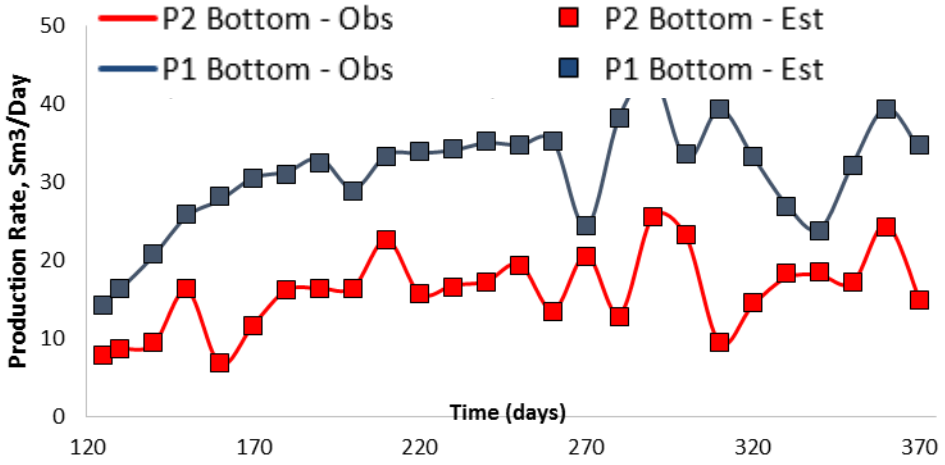

Figure 5-42. Comparison of RM estimated flow rate and observed rate for P1 and P2 bottom layers between 120 and 365 days.

After 365 days, the choke strength of P1-top is increased to 0.0067 bar/(rcm/d)^2 in order to improve the flow distribution in the top layer. The data (stage 3) collected between 365 to 800 days. CRM-ML-AWC (equation 5-14) is applied with the new FCC strength in P1-top is 0.0067 bar/(rcm/d)^2. Fig. 5-43 show no change in the connectivity of the bottom layer, while the extra ICV restriction in the top layer reduces the $f_{11\,(Top)}$ from 0.62 (stage 2) to 0.47 (stage 3), and re-distributes it to $f_{12\,(Top)}$ from 0.38 (stage 1) to 0.53 (stage 3).

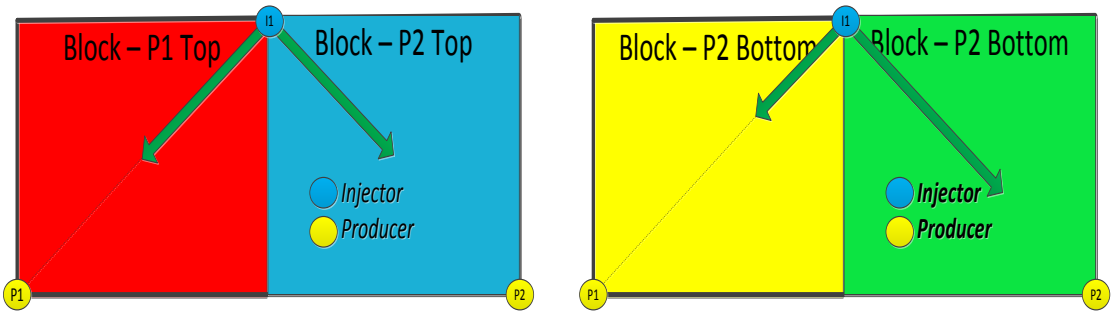

Figure 5-43. Connectivity map (stage 2) after 370 days.

The perfect agreement between the observed and estimated results from the CRM calculation is displayed in Fig. 5-44 and 5-45, and the production history from stage 1 to stage 3 is shown in Fig. 5-46 and 5-47 where the gradual improvement of flow uniformity is observed on the top layer where the ICV is operated.

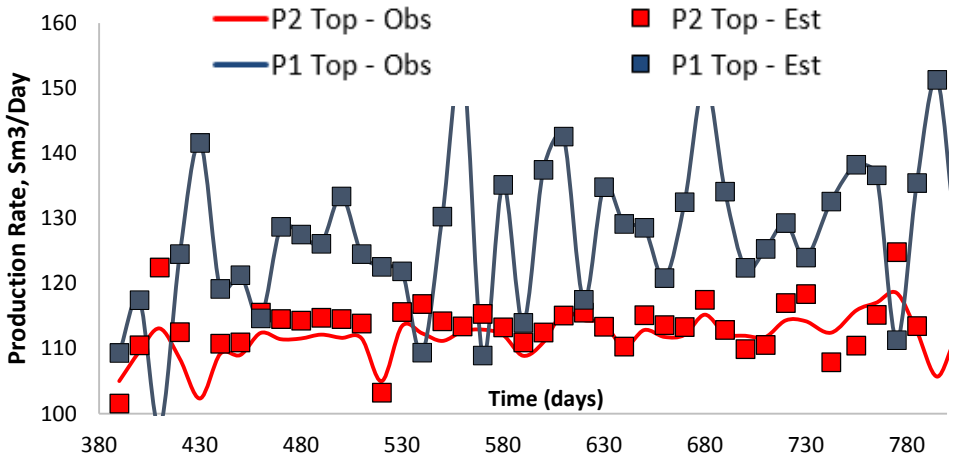

Figure 5-44. Comparison of the CRM estimated flow rate and the observed rate for the P1 and P2 top layer from 365 to 800 days production

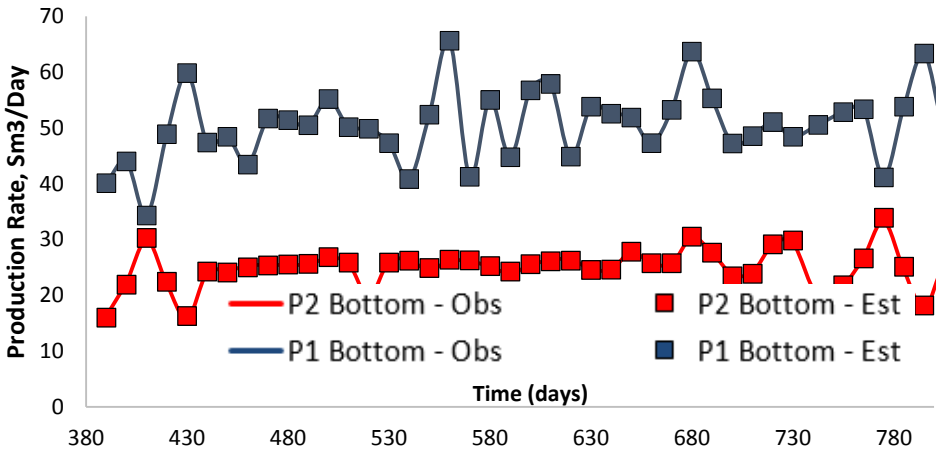

Figure 5-45 Comparison of CRM estimated flow rate and the observed rates for the P2 and P2 bottom layers after 365 to 800 days of production

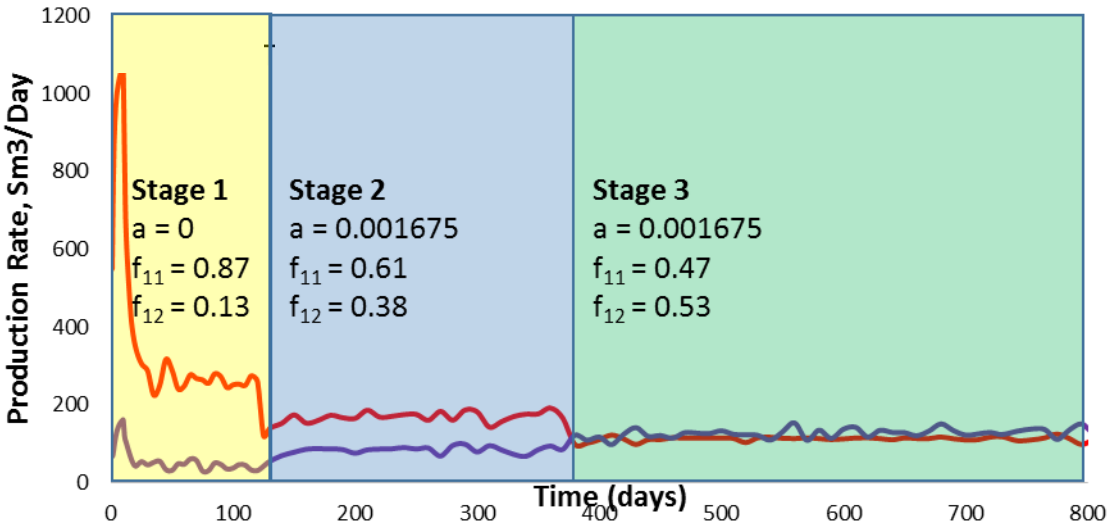

Figure 5-46. CRM estimated rate for the P1 (red line) and P2 (purple line) top layers from 0 to 800 days

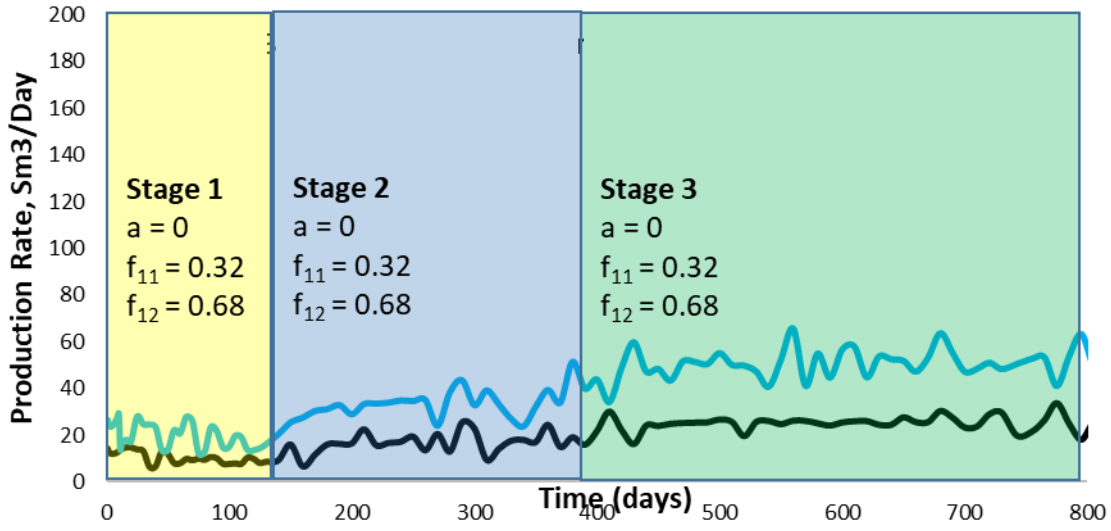

Figure 5-47. CRM estimated flow rate for the P1 (black line) and P2 (blue line) bottom layers from 0 to 800 days

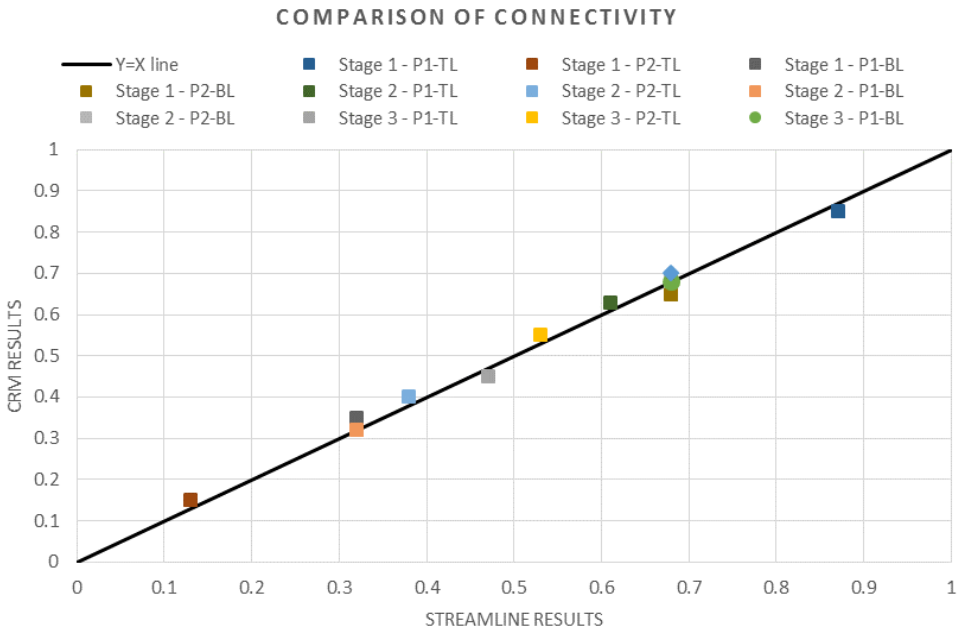

Figure 5-48. Comparison of the connectivity values from CRM and Streamline simulation for stage 1 to stage 3

Modelling AWC in a multi-layered reservoir by streamline simulation

The calibrated parameters from CRM data-fitting are analogous with parameters that can be calculated from a streamline simulator. The CRM's well connectivity (fij) and individual layer connectivities is comparable to the streamline well's allocation factor. Furthermore, the CRM's time-storage is comparable with the streamline well's pore volume allowing us to verifiy our calculation. The CRM's inter-well connectivity and the CRM's time-storage are comparable with streamline's allocation factor and streamline's drainage volume.

Well segmentation and multi-layered reservoir are not available for streamline simulation in available commercial simulators. AWC in streamline simulation was therefore modelled by creating each segment within the AWC well as an individual well. For example, the three wells (two producers and one injector) in Figure 5-34 were modelled in the two layer reservoir as six different wells (i.e. I_1_{STR} & 1_2_{STR} as proxy wells for I top layer and I bottom layer; $P1\_1_{STR}$ & $P1\_2_{STR}$ as proxy wells for P1 top layer and P1-bottom layer; and $P2\_1_{STR}$ & $P2\_2_{STR}$ as proxy wells for P2 top layer and P2-bottom layer).

Furthermore, the pressure drop created by the ICV restriction is not linearly related to the

flow velocity. Unfortunately, this feature is not available in streamline simulation. The ICV well's performance was therefore mimicked by controlling the well in the simulator by the Pannulus (Figure 5-49).

Stage 1 (Days 0 to 120) is the period when the ICV is not operated on. Within this period, all production wells in streamline simulator ($P1\_1_{STR}$, $P1\_2_{STR}$, $P2\_1_{STR}$ & $P2\_2_{STR}$) are controlled with BHP 175 bar (it is the same with the well control in the standard reservoir simulator). On the other hand, injection wells in the streamline simulator were controlled by the injection rate (Figure 5-50) (i.e. I_1_{STR} is controlled with 330 Sm^3/day and I_2_{STR} is controlled with 20 Sm^3/day). The stage 2 (days 120 to 370) is a period when the ICV in P1-top operates with restriction strength (a) = 0.001675 bar/(rcm/d)^2. Within this period, the additional pressure drop from the ICV result makes the Pann higher than the Pwf (Figure 5-49). At this stage, the $P1\_1_{STR}$ is controlled with a BHP 226 bar (which follows the Pann in the standard reservoir simulator). Operating the ICV in the P1-top changes the dynamic of the reservoir so that the I_1_{STR} is controlled with 285 Sm^3/day and I_2_{STR} is controlled with 65 Sm^3/day. Stage 3 (day 370 onward) is the period when the ICV in the P1-top operates with restriction strength (a) = 0.0067 bar/(rcm/d)^2. Within this period, the stronger choke from ICV results in an even higher Pann (Figure 5-49). At this stage, the $P1\_1_{STR}$ is controlled with a BHP 258 bar while the rest of the production wells are still controlled with the BHP 175 bar. At stage 3, the I_1_{STR} is controlled with 265 Sm^3/day and the I_2_{STR} is controlled with 85 Sm^3/day.

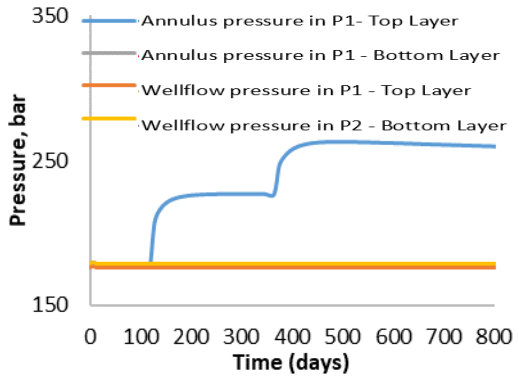

Figure 5-49. Well flow and Annulus pressure of the top & bottom layer in Producer 1

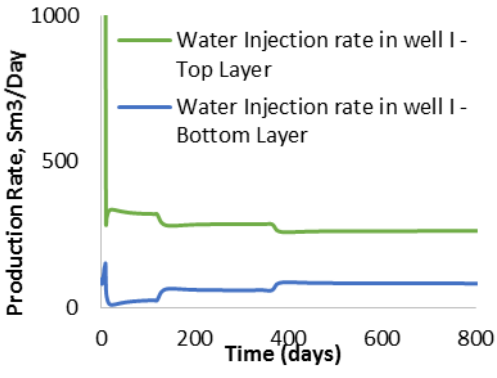

Figure 5-50. ICV restriction change the allocated injection water of the I's top and bottom layers

Finally, the observed production history for stage 1, 2 and 3 are verified against the

streamline simulator as depicted in figure 5-51 and 5-52.

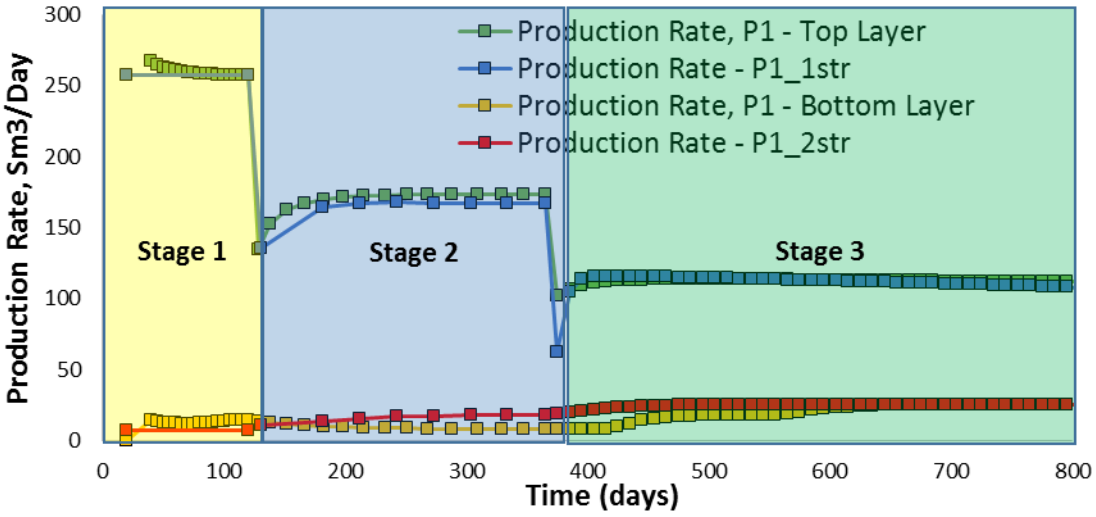

Figure 5-51. Comparison between the conventional reservoir simulator (ECLIPSE) and Streamline simulator (Streamline) for the top layer

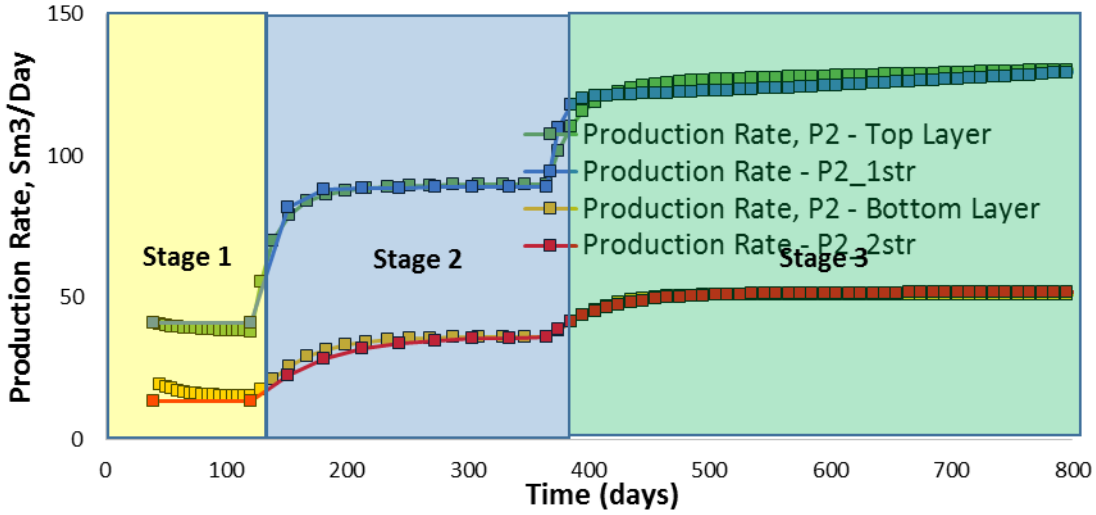

Figure 5-52. Comparison between the conventional reservoir simulator (ECLIPSE) and Streamline simulator (Streamline) for the bottom layer

5.6 Proactive optimisation in AWC using CRM

This study develops a new production optimisation method based on the relationship between flow-capacity vs. storage (F-C curves). This curve was developed from the Lorenz plot in early 1990 to relate wealth (flow-capacity) to population (storage capacity). A measure of wealth distribution across people (Corbett, 2012). Petroleum engineering uses F-C curves to measure heterogeneity, and as indicator of double porosity behaviour

(Corbett, 2012).

The (modified) flow-capacity vs storage relationship can be constructed using CRM's derived parameters (Izgec, 2012). An F- ϕ graph for injection well can be generated by

$$F_i = \frac{\sum_{j=1}^{m} f_{ij}}{\sum_{j=1}^{N_p} f_{ij}} \tag{5-16}$$

$$\phi_i = \frac{\sum_{j=1}^{m} \tau_j J_j}{\sum_{j=1}^{N_p} \tau_j J_j} \tag{5-17}$$

Where *F* is the flow-capacity, *f* is the CRM inter-well connectivity, ϕ is the capacity, τ is the CRM capacitance, and J is the CRM Productivity-Index. While the subscript i and j are respectively the indices of the injector and producer. The workflow of this graph follows the workflow for drawing Lorenz plot as explained previously, where data are ordered prior to calculation.

Note that the F- ϕ curve is derived based on production data (dynamic parameters). Izgec, 2012, considered it to be a better reflection of flow-path and the geological features of the reservoir than the static parameters. This is important because the F–Φ curve discloses information about both degree and type of the communication (through channel, high permeability streak, or matrix) within an injector–producer pair. Also, note that this relationship can be extended to multi-layer wells by simply refining the parameter into the layer's properties. The gradient of the curve is larger than 45^0 when F_i is larger than ϕ_i. This indicates that the injection stream is flowing through a formation with a relatively low pore volume, for example when the connection is a high permeability channel. By contrast, F_i being smaller than ϕ_i, and the gradient of the curve is below 45^0 is an indication that there is a relatively low injection rate into a high pore volume; for example, when the connection has a low conductivity/connectivity. The F- ϕ curve thus gives insight into whether a layer/zone is 'underflooded' or 'overflooded'. Note that conductivity is a function the permeability of the associated regions as well as the pressure difference of each injector-producer pair.

This curve has been used to examine the performance of injector wells in a waterflooding operation (Izgec, 2012). The curves (Figure 5-53 and 5-53) relate the fractional rate from the injector wells (LI1 & LI2) to the pore volume associated with the supported producer wells (LP2, LP3, LP4, LP5, LP6, LP7 were connected to LI1; and LP1, LP2, LP4, LP7,

LP8, LP9 were connected to LI2). Izgec (2012) concluded that LI1 is over-supporting the LP3 (Figure 5-53 left), and LP7 requires more energy from LI2.

The level/degree of heterogeneities captured by the F- ϕ curve is slightly different with the static model (figure 5-54); however, the qualitative interpretation was the same that is the permeabilities region around LP3 is relatively high, and the permeabilities region around LP7 is relatively low. This example thus signifies the importance of having a dynamic (CRM) evaluation to compare with the static model (or vice versa).

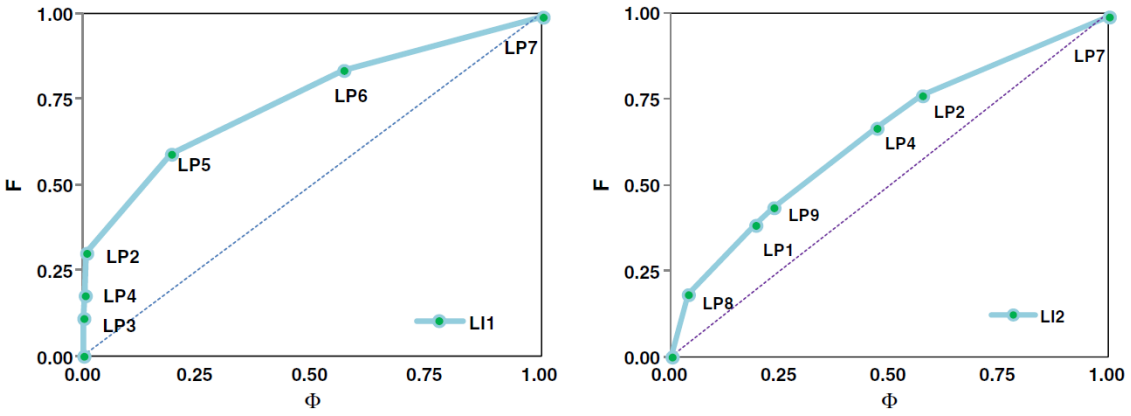

Figure 5-53. F- ϕ graph for injector LI1 & LI2 (Izgec, 2012)

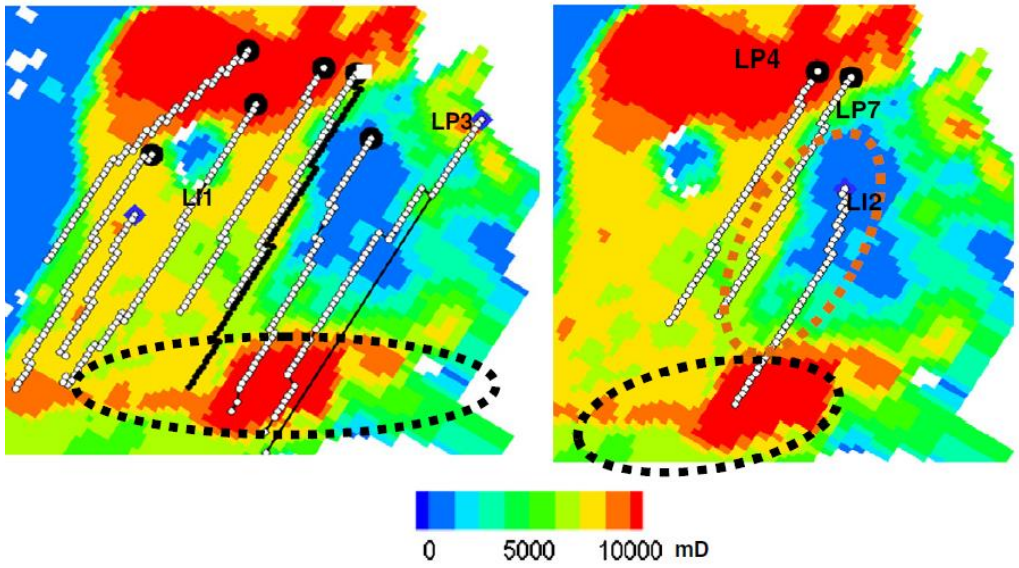

Figure 5-54. Static permeability map for area nearby well LI1(left) and LI2 (right) (Izgec, 2012). This map is compared to dynamic heterogeneity captured by figure 5-53

5.6.1 F- ϕ graph

A more refined layer (or well) performance evaluation can be formulated by normalising the parameters (equations 5-18 and 5-19). The modified F- ϕ graph $\left(\hat{\mathrm{F}} - \hat{\phi}\right)$ can provide guidelines for ICV (or well) proactive optimisation, since the CRM parameters respond to alterations in the well's or layer's control settings. A $\hat{\mathrm{F}} - \hat{\phi}$ graph for a production well completed in multi-layers can be generated by:

$$\widehat{F_j} = \frac{\sum_{j=1}^{m}\sum_{l=1}^{n}\bar{q}_{j,l}}{\sum_{j=1}^{Np}\bar{q}_{j,l}} \tag{5-18}$$

$$\widehat{\phi}_j = \frac{\sum^{m}\sum_{l=1}^{n}\tau_{j,l}\,J_{j,l}}{\sum_{j=1}^{Np}\tau_{j,l}J_{j,l}} \tag{5-19}$$

The main difference with the original F- ϕ graph are :

1. Equation 5-18 and 5-19 are calibrated for multi-layers reservoir (the second sum referred to layer, l = layer number).
2. Instead of comparing the connectivity values, the new graph directly evaluates (average) production contribution for each layers
3. In the original $\hat{\mathrm{F}} - \hat{\phi}$ graph, the connectivities were evaluated on well's basis while in the equation 5-18, each layer's production rate is normalized against the whole observed rate in the system. By doing so, we can have neutral comparison to evaluate contribution of each layer's.

Figure 5-55 is the modified $\hat{\mathrm{F}} - \hat{\phi}$ curve for the reservoir illustrated in Figure 5-34. The data were taken from table 5-3, and CRM calibration results illustrated in figure 5-46, 5-47. The development of this was split into three stages. Stage 1 when the completion had no restriction and stage 3 when an aggressive restriction was applied in the completion.

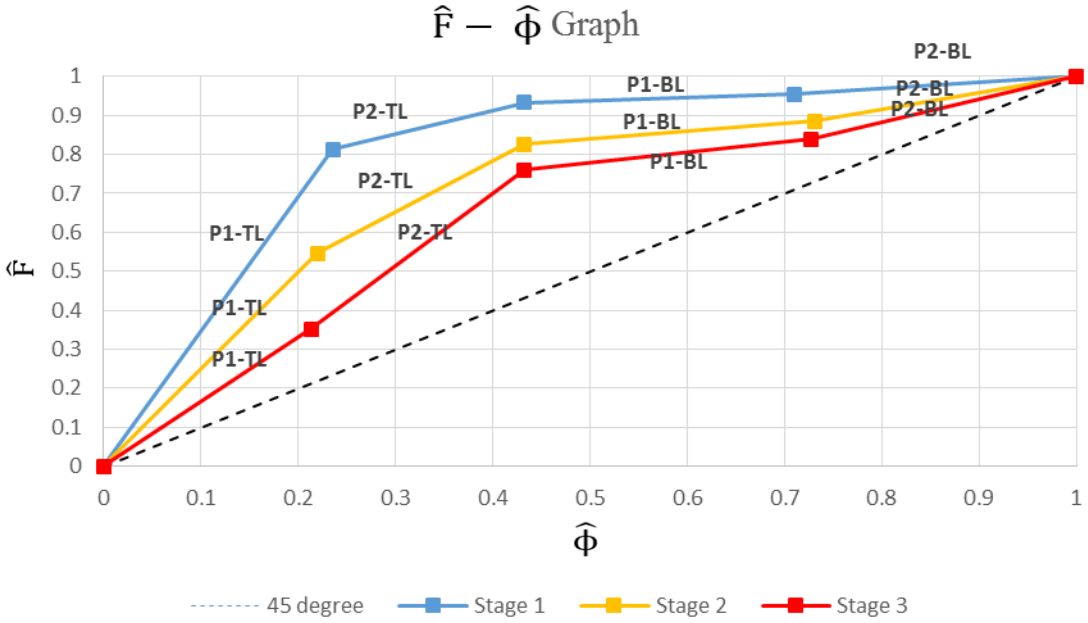

Figure 5-55. Modified $\hat{F} - \hat{\phi}$ curve for stage 1 to stage 3 for the reservoir depicted in Figure 5-34

Stage 1, the open-hole completion (i.e. no restriction) is represented by then blue line. It is clearly indicated that the P1 top layer (P1-TL) is excessively produced (the large positive-deviation from the 45^0 line) and the P1 bottom layer (P1-BL) is sub-optimally produced. This layer behaviour will encourage early water breakthrough. The $\hat{F} - \hat{\phi}$ graph can be used to reveal the most important layers or wells to be controlled (i.e. the ICV control priority). This is exemplified by comparing the performances of the top and bottom layer layers in Figure 5-55. The $\hat{F} - \hat{\phi}$ graph reveals that the degree of flow variation in the bottom layer is less severe compared to the flow variation in the top layer. The reservoir's behaviour is illustrated more clearly than when the conventional $F - \phi$ or typical CRM's connectivity maps were employed.

When a restriction is applied to the P1-TL during Stage 2. The choke reduces the deviation and encourages other layers to advance their drainage capacity (increased $\hat{F} - \hat{\phi}$ gradient). However, the mismatch of P1-TL against 45^0 line is still relatively large, and further restriction is required to achieve "ideal" control of this layer's production.

Stage 3 is a scenario where a more aggressive restriction is applied to the P1-TL, and the deviation from the 45^0 line is further reduced.

$\hat{F} - \hat{\phi}$ can be plotted into the histogram to compare the gradient of each layer

quantitatively. In Figure 5-56, stage 3 confirms the flow variation in the top layer is minimised, and an additional restriction only in P1-TL would not further improve the field performance. Using this figure, the appropriate control strategy for the next stage would be to simultaneously control both P1-TL & P2-TL to encourage production from P1-BL & P2 BL.

The Lorenz coefficient (Lc), can also be used to quantify the inequality index of the well's (or layer's) production compared to its drainage volume (see Chapter 3 Section 3.3.2). Lc is measure of the area between the $\hat{F} - \hat{\phi}$ line(s), and the diagonal line in Figure 5-55.

The Lc value (Figure 5-55) decreases from Stage 1 (no ICV restriction) to stage 3 (largest ICV restriction). Note that as explained previously these ICV specific strength are selected in an ad-hoc way, i.e. without optimisation.

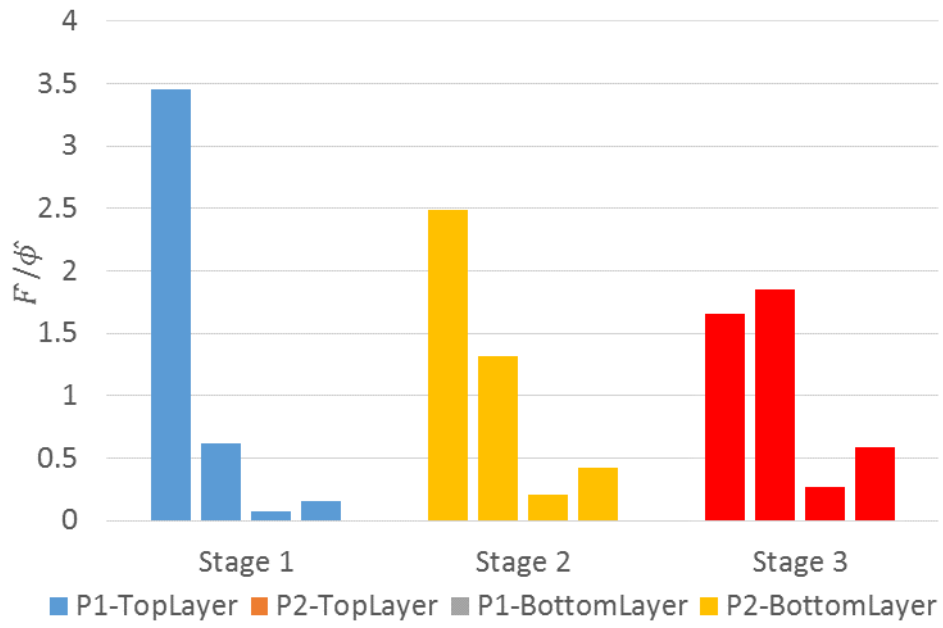

Figure 5-56. Modified $\frac{\hat{F}}{\hat{\phi}}$ for each producer at different stages for the reservoir depicted in Figure 5-34.

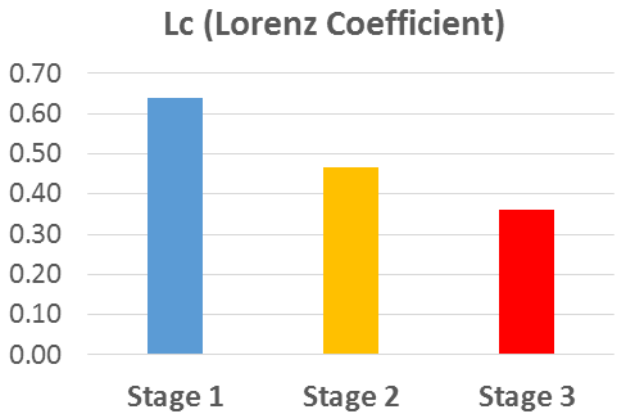

Figure 5-57. Lorenz coefficient for stages 1, 2 and 3 for the reservoir depicted in Figure 5-34.

5.6.2 The workflow for closed-loop production optimisation of AWC wells using CRM-AWC and a modified $\hat{F} - \hat{\phi}$ graph

The integration of CRM-AWC and the modified $\hat{F} - \hat{\phi}$ graph forms the basis of a new production optimisation guideline for a reservoir completed with AWC wells. The CRM-AWC provides an insight into the dynamic inter-well connectivity and the drainage volume of each layer. The modified $\hat{F} - \hat{\phi}$ graph indicates the reservoir heterogeneity and reveal the disparity between the rates and its associated pore volumes; hence, it can be used to highlight which layers (or wells) might benefit from an ICV restriction, in order to ensure a more uniform recovery profile.

A control strategy that is designed to reduce the disparity between the rate and its associated drainage volume which can be based on the Lc value. The strategy is that the highest rate contribution should originate from the layers (or wells) with the largest pore volumes, and vice versa. The objective is to achieve a more uniform waterflood and better sweep efficiency with a reduced Lc value, by extending the previous workflow (Figure 5-58).

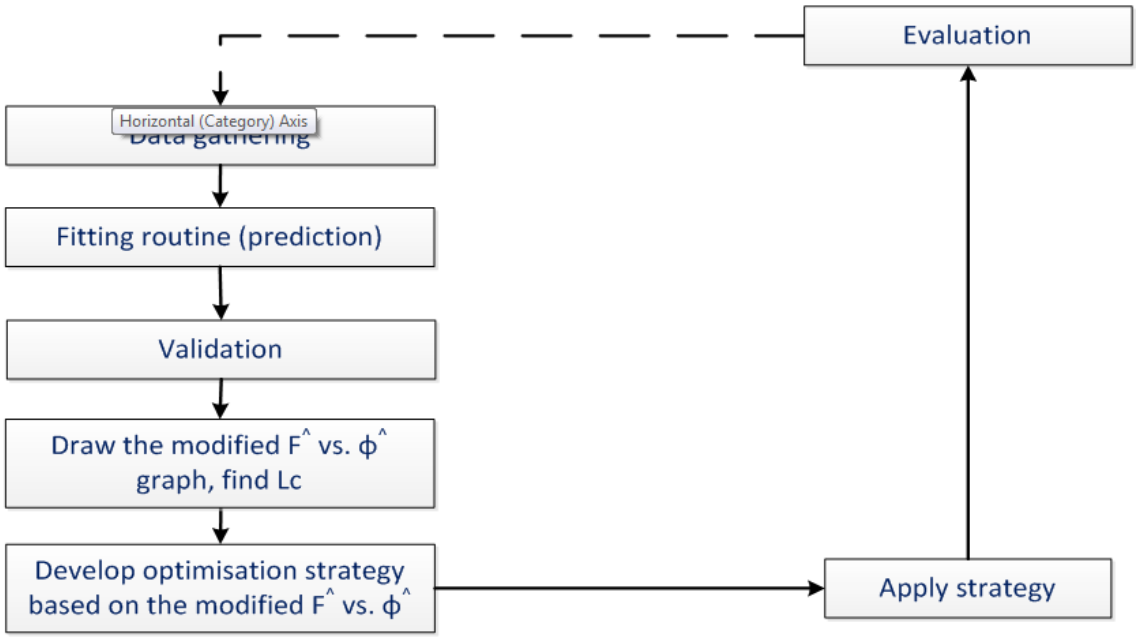

Figure 5-58. Workflow for production monitoring and optimisation using CRM-AWC and modified $\hat{F} - \hat{\phi}$

5.6.3 CRM-AWC Case study

The construction of a synthetic field model (Figure 5-59 and table 5-4) was inspired by a reservoir model used by Sayarpour *et al.* (2009). It is a two-layer system with 4 production and 5 injection wells equipped with a monitoring system (pressure gauges and flowmeter), and infinitely variable ICVs installed in each production well. The top layer is separated from the bottom layer by an impermeable layer. All four producers and five injectors are completed on both layers (zones) with, initially, fully open ICV production wells. A highly permeable channel exists in the top layer between the injector 1 (I1-TL) and producer 2 (P2-TL), (see Figure 5-60), with a second highly permeable channel in the bottom layer between injector 4 (I4-BL) and producer 4 (P4-BL) (see Figure 5-61). The four producers and five injectors achieve a field (liquid) total production rate of 3000 Sm^3/day at a minimum flowing wellbore pressure of 50 bar and a voidage replacement ratio of one. All producers are constrained to a well production rate of 750 Sm^3/day, while the injectors are constrained to a well injection rate of 600 Sm^3/day. CRM calibration and control optimisation are scheduled at 100 day intervals for the first 500 days. CRMP-AWC-ML (equation 5-14) was used to describe the dynamic properties at each stage. Note that a history-matching workflow is typically split into two subsets: a training set and a testing set. The focus of this case study is to observe and test the proposed optimisation framework, thus validation using RMSE (root mean–squared error, equation

5-9) is considered sufficient. Finally, the scenario will be evaluated after ten years (3650 days) of production. The information about Synfield is tabulated in Table 5-4. *This scenario has a large number of unknown variables and requires a Genetic Algorithm optimiser in MATLAB for data calibration.*

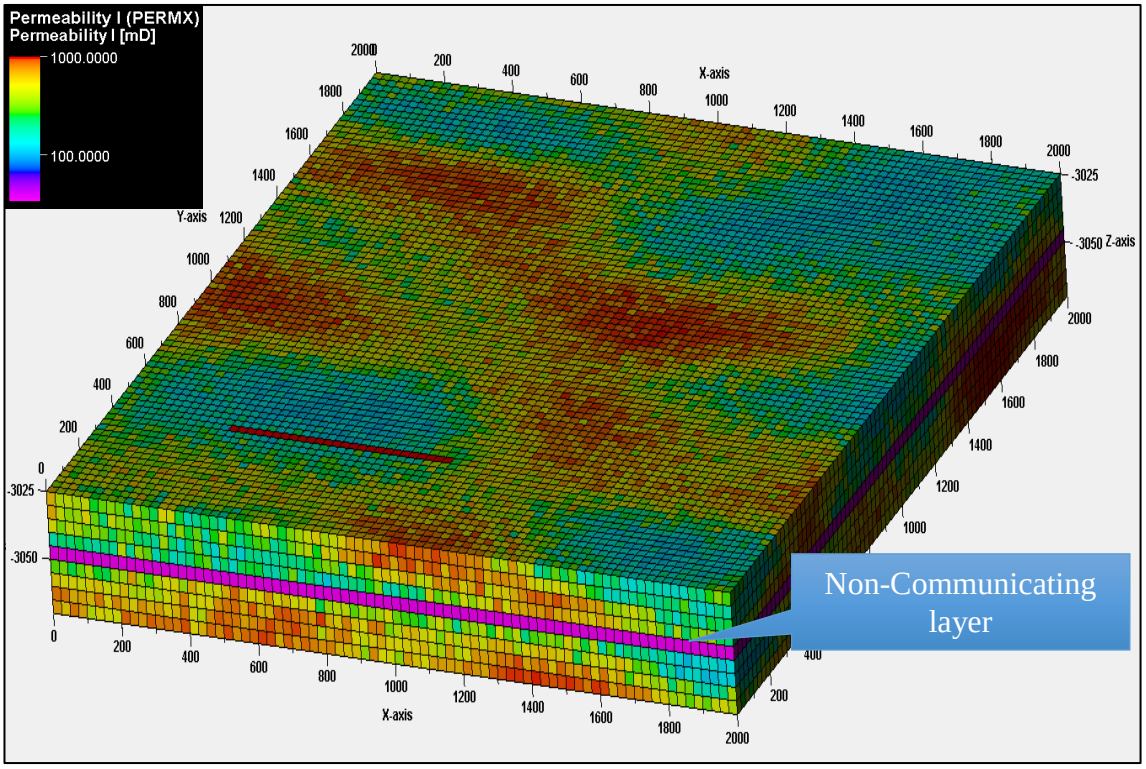

Figure 5-59. Synthetic field permeability map (multi-layer reservoir with non-communicating layer in between)

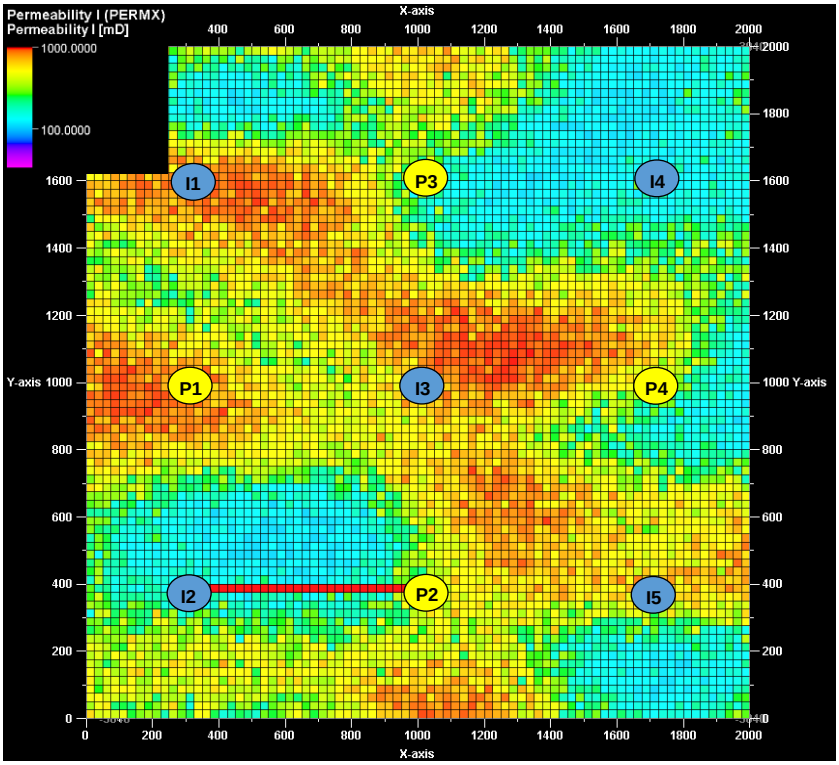

Figure 5-60. Top layer permeability map, with five injectors and four producers.

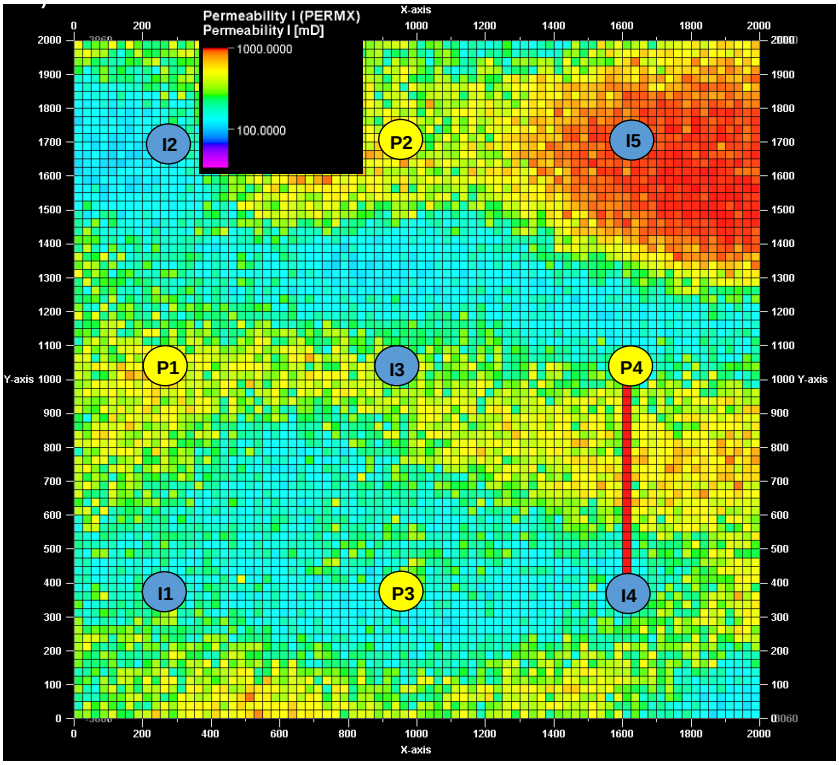

Figure 5-61. Bottom layer permeability map with five injectors and four producers.

Table 5-4. List of reservoir properties illustrated in Figure 5-59

Scenario Schedule			
Injection Control	I1, I2, I3, I4, I5	**600**	Sm3/Day
Production Control	P1, P2, P3, P4	**750**	Sm3/Day
Min Permeability		**0**	mD
Mean Permeability		**213**	mD
Max Permeability		**3000**	mD
Perturbation		**10**	%
Stage 1	Choke P2 top layer's (P2-TL) Choke P4 bottom layer's (P4-BL) Choke P1 top layer's (P1-TL)	**0 – 100**	days
Stage 2	Relax the restriction on P2-TL Relax the restriction on P4-BL Relax the restriction on P1-TL	**100 – 200**	days
Stage 3	Maintained the previous control in P1-TL, P2-TL, and P4-BL Choke P1 bottom layer's P1-BL	**300 – 400**	days
Stage 4	Choke P4 top layer's P4-TL	**300 – 400**	days
Stage 5	Maintained the ICV control in P1-BL and P4-TL. Relaxed the ICV restriction in P1-TL Relaxed the ICV restriction in P2-TL Choke P4 bottom layer's P4-BL	**400 – 500**	days

Base case or stage 1 evaluation

The predicted history was derived using the inter-well connectivity network (Fig. 5-62). The length and direction of the green arrows represents the volume of injection water that is supporting each producer. They highlighted the highly permeable streak between I1-TL and I2-TL and between the I4-BL and P4-BL. The match is verified by the comparison of the actual and predicted production data for the first 100 days (Figure 5-63).

P2-TL, with its high connectivity to I2-TL (f_{221}) {and to a lesser extent I5-Tl (f_{521})}, can be expected to experience early water breakthrough. Excessive injection towards P2 also implies that the other producers are relatively poorly supported. A similar observation is seen in the bottom layer, where P4-BL, with its high connectivity to I5-BL (f_{452}), will also be likely to experience early water breakthrough.

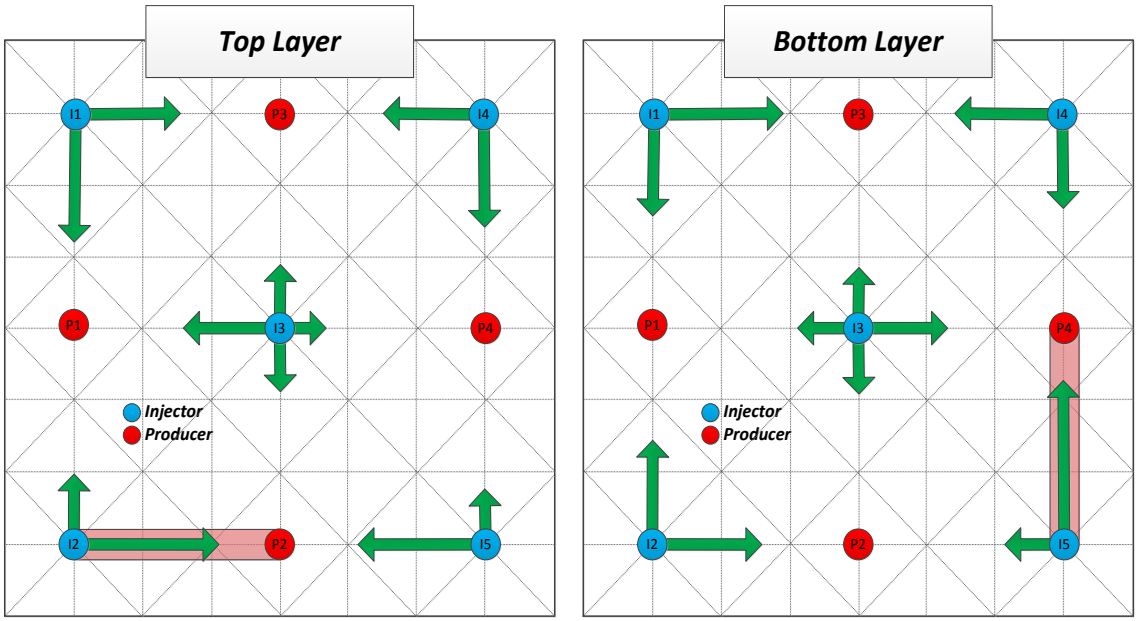

Figure 5-62. Connectivity network between injectors and producers for stage 1

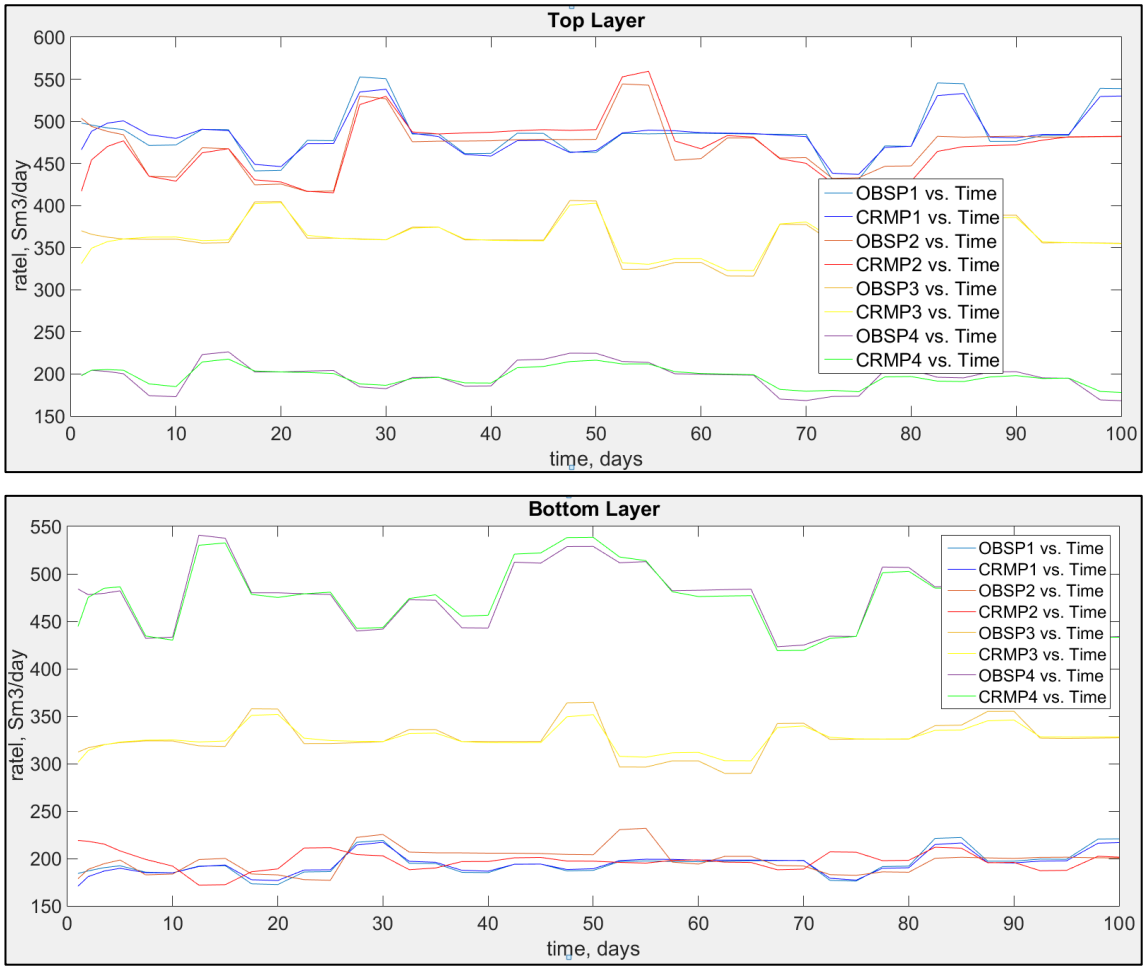

Figure 5-63. Comparison of the CRM-AWC estimated rate and the observed rate for the top and bottom layer from the start to 10 years. OBSPx is observed production rates, CRMPx is CRM calculated rates

$\hat{F} - \hat{\phi}$ plot for this scenario is illustrated in Figure 5-64. The gap between the stage 1's $\hat{F} - \hat{\phi}$ plot and the dashed diagonal line can be observed – the Lorenz coefficient (Lc^{Stage1}) is 0.19. The localised gradient of Figure 5-64 or $\frac{\hat{F}}{\hat{\phi}}$ plot (Figure 5-65) allows us to compare the mismatch of the normalised production rate for each layer compare to its normalised pore volume. Figure 5-65 suggests that P2-TL, P4-BL, and P1-TL are the layers with the highest disparity. Hence, the first suggested ICV control strategies to improve uniformity is:

1. Choke P2 top layer's (P2-TL) ICV to 20% of its original production rate.
2. Choke P4 bottom layer's (P4-BL) ICV to 20% of its original production rate.
3. Choke P1 top layer's (P1-TL) ICV to 20% of its original production rate.

The ICV strengths, recorded in Table 5-5, is to choke (i.e. operate the ICV) the above layers and encourage the drainage volume of the remaining layers with low $\hat{F}$ vs. $\hat{\phi}$ values.

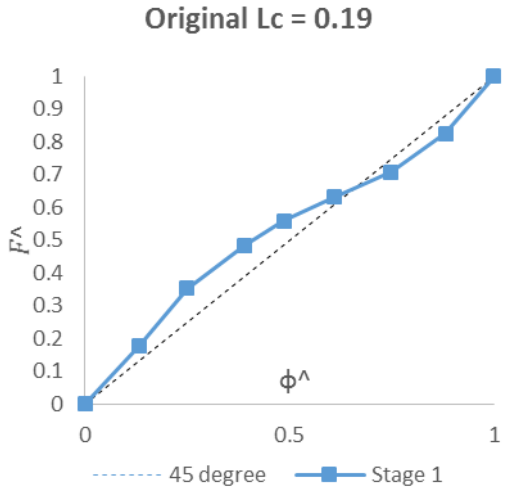

Figure 5-64. Modified $\hat{F} - \hat{\phi}$ graph of stage 1

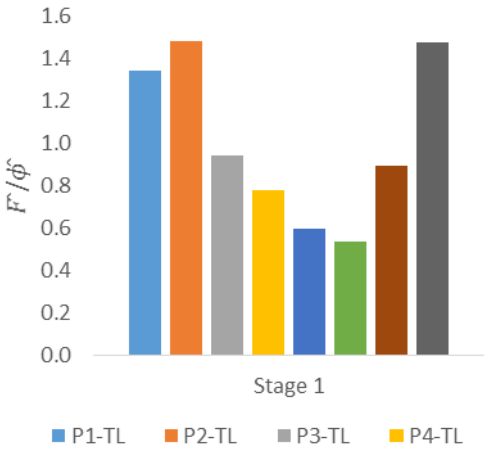

Figure 5-65. $\frac{\hat{F}}{\hat{\phi}}$ histogram of stage 1

Stage 2 evaluation

At stage 2, the injection water from the top layer of P1 and P2 has been re-allocated to the bottom layer, and the injection water from the bottom layer of P4 is re-allocated to the top layer. This action alters all other connectivity values, seen in Table 5-6. The

altered connectivity distribution (from bottom layer to top layer), is clearly seen in the network attributed to P4 (see the comparison of Figure 5-60 and 5-64). The similar event in P1 and P2, however, results in a relatively similar connectivity outcome (compared to the stage 1 in

This is because the P1-TL and P2-TL were the producers surrounding I2-TL, and the effect of the ICV that operated in these wells was cancelling each other out. The result was that the allocation rates from these injectors were not diverted to another producer (e.g. f_{211} to $f_{221;}$ f_{221} to f_{211}) but instead the injection rates were mostly re-allocated to the bottom layers (e.g. f_{211} to $f_{212;}$ f_{221} to f_{222}). It thus can be seen that altering the ICV control provides information on the reservoir connectivity between the injectors and producers. As the CRM's connectivity value is relative to the layer's injection rate, the connectivity values of I2-TL at stage 2 were similar when compared to stage 1. This good match is confirmed by the comparison of the actual and predicted production data for between 100 - 200 days (Figure 5-67).

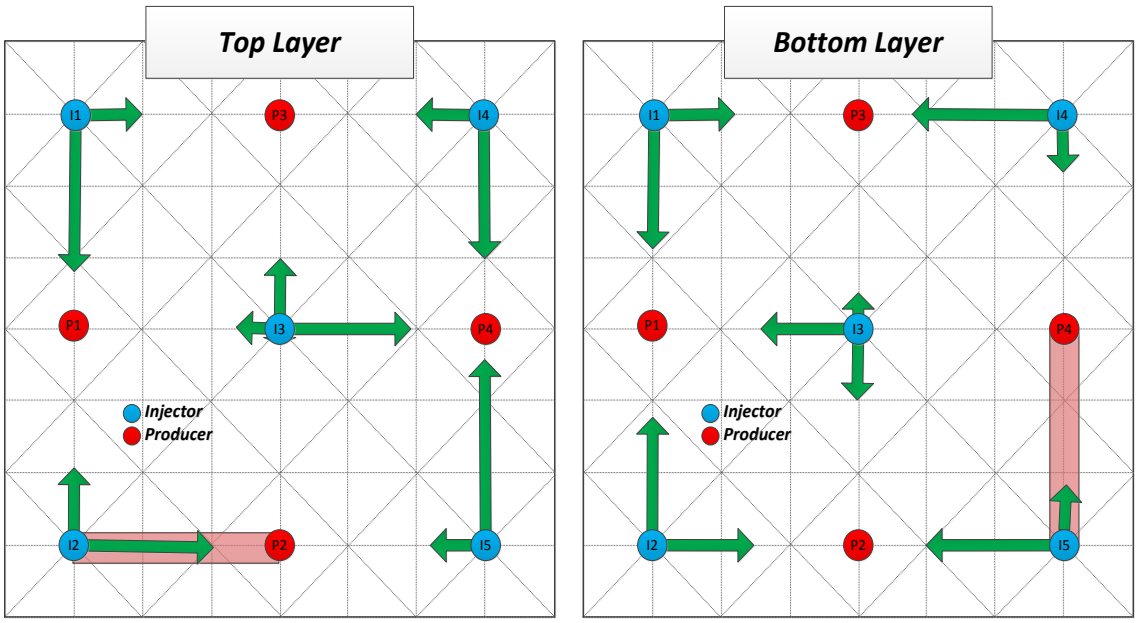

Figure 5-66. Connectivity network between injectors and producers for stage 2.

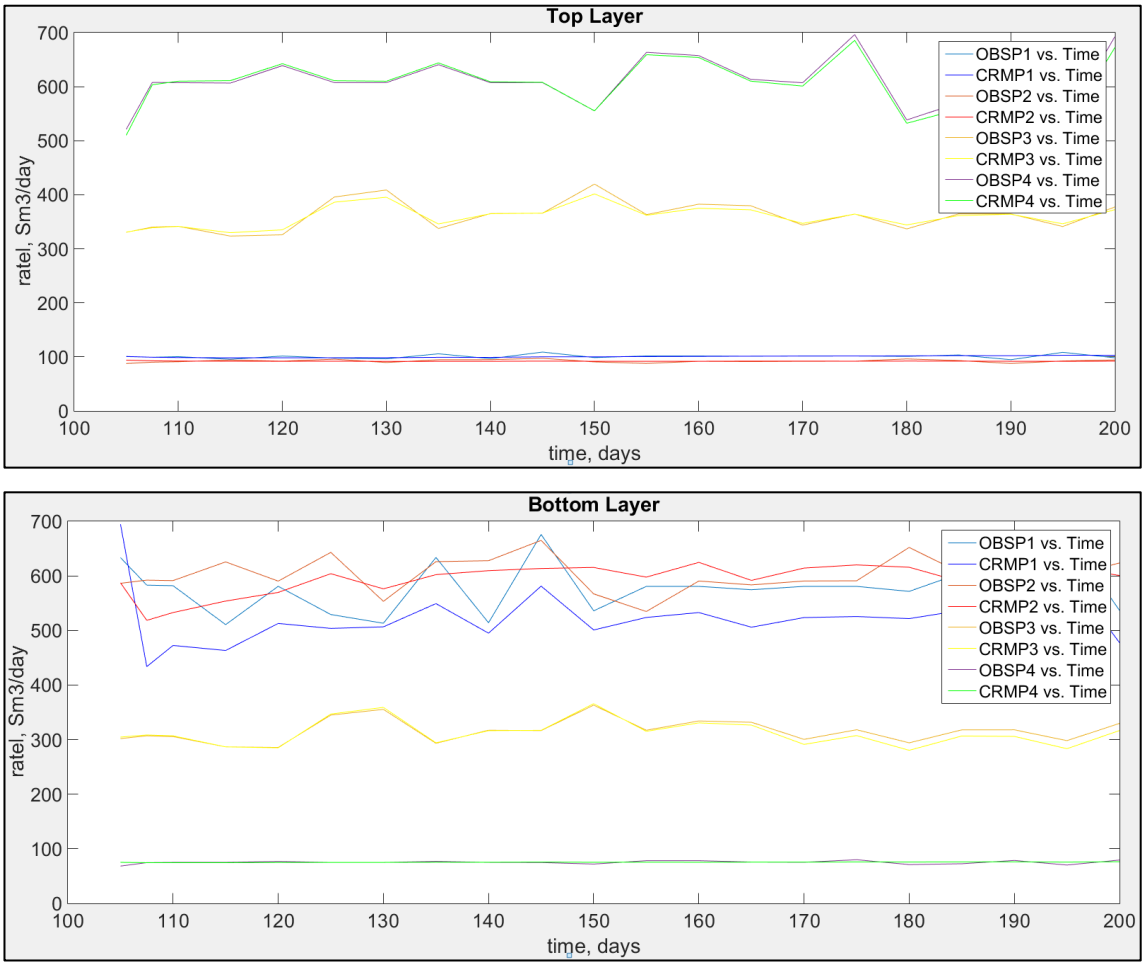

Figure 5-67. Comparison of estimated CRM-AWC rate and observed rate for top and bottom layers between 100-200 days. OBSPx is observed production rates, CRMPx is CRM calculated rates

The $\hat{F} - \hat{\phi}$ graph of stage 2 was a mirror like shape of stage 1's $\hat{F} - \hat{\phi}$ graph, with a slightly lower flow-storage disparity index {$Lc^{stage2} = 0.18$ (Figure 5-68)}. Stage 2 control strategy was successful in deterring the injection rates towards prominent layers; however, the layers where the injection was re-directed into, such as P4-TL, P1-BL, P2-BL are also likely to experience water breakthrough (Figure 5-69). *The relativity nature of connectivity values is rarely mentioned in CRM publications. A comparison of stage 2 vs. stage 1 exemplifies how more information is gained for reservoir characterisation and optimisation with each movement of the ICV's (or alteration of the well or layer control).*

Restricting ICV in those high-permeability streaks (stage 2 optimisation) should improve the oil production and reduce the water production, as confirmed by Figure 5-70 and 5-69. *In these figures, we compared the scenario of the reservoir that had been produced without any control (stage 1) and the scenario of the reservoir had been produced with*

ICV control as described above (stage 2 optimisation).

Examination of stage 2 field performance using Figure 5-68 and Figure 5-69 suggests that P2-TL, P4-BL, and P1-TL were excessively restricted during this period. The proposed, ICV control strategy for stage 3 optimisation is to:

1. Relax the restriction on P2 top layer (P2-TL) ICV to increase the stage 2 liquid production rate by 50%.
2. Relax the restriction on P4 bottom layer (P4-BL) ICV to increase the stage 2's fluid production rate by 100%.
3. Relax the restriction on P1 top layer (P1-TL) ICV to increase the stage 2's production rate by 100%.

The resulting ICV strength are recorded in table 5-5.

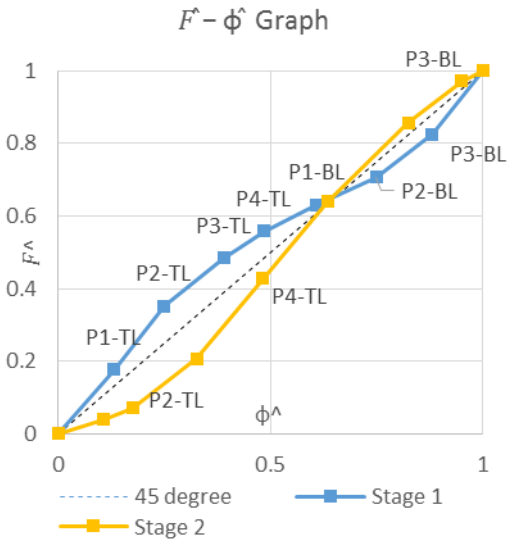

Figure 5-68. Modified $\hat{F} - \hat{\phi}$ graph for stage 1 and 2

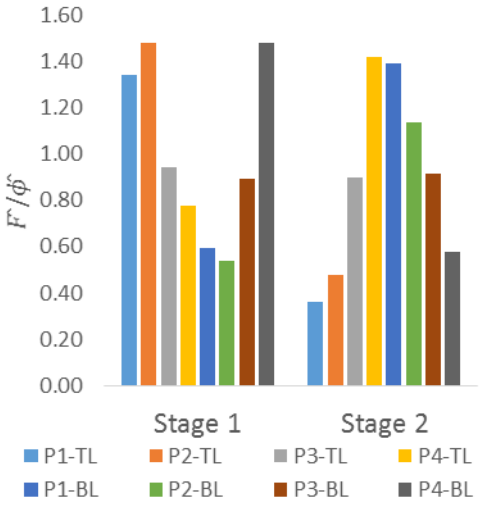

Figure 5-69. $\frac{\hat{F}}{\hat{\phi}}$ histogram for stage 1 and stage 2

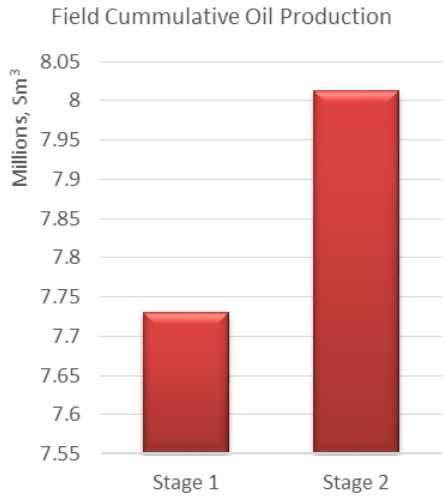

Figure 5-70. Stage 1 and 2 field oil cumulative production from the start until 10 years

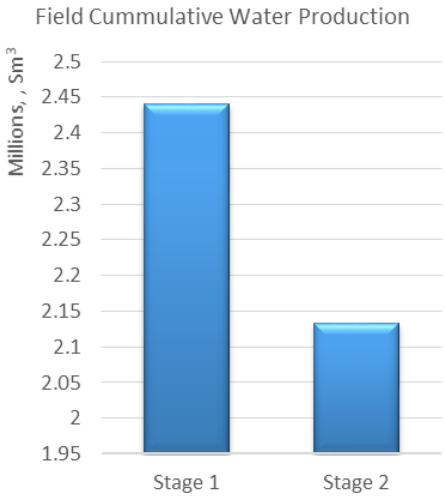

Figure 5-71. Stage 1 and 2 field water cumulative production from the start until 10 years

Stage 3 evaluation

Stage 3 derived connectivity values are tabulated in, and plotted in Figure 5-72. Evaluating the effect of ICV control based solely on this network diagram is difficult since the stage 3 network change is similar to that for stage 2 (Figure 5-66). As previously, there is a good match between the actual and CRM-AWC predicted production data for between 200 - 300 days (Figure 5-73). The required, greater insight into the layer performance can therefore be provided by the modified $\hat{F} - \hat{\phi}$ graph.

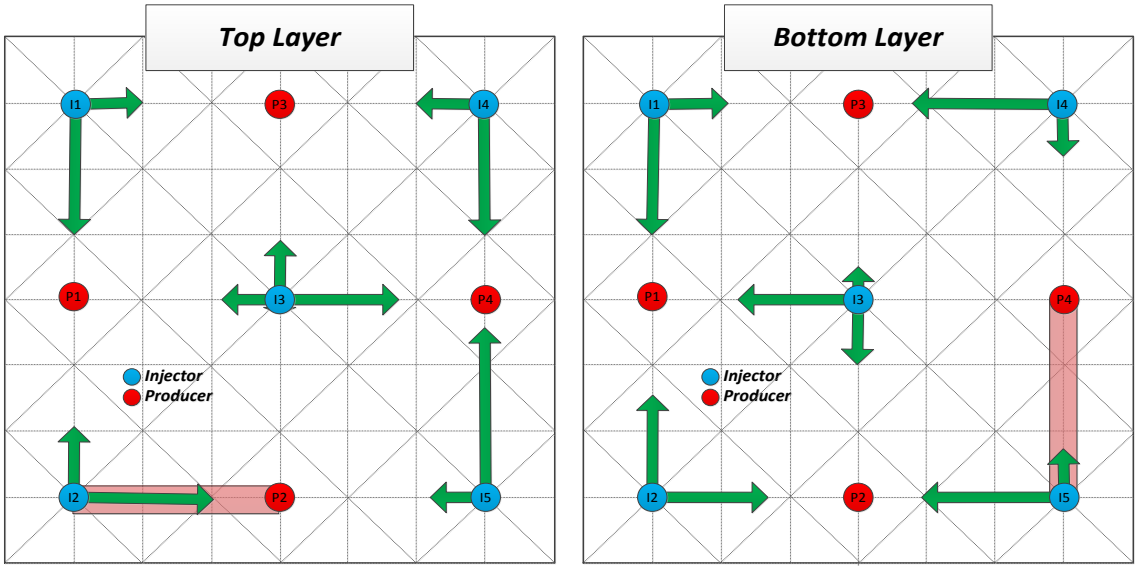

Figure 5-72. Connectivity network for stage 3

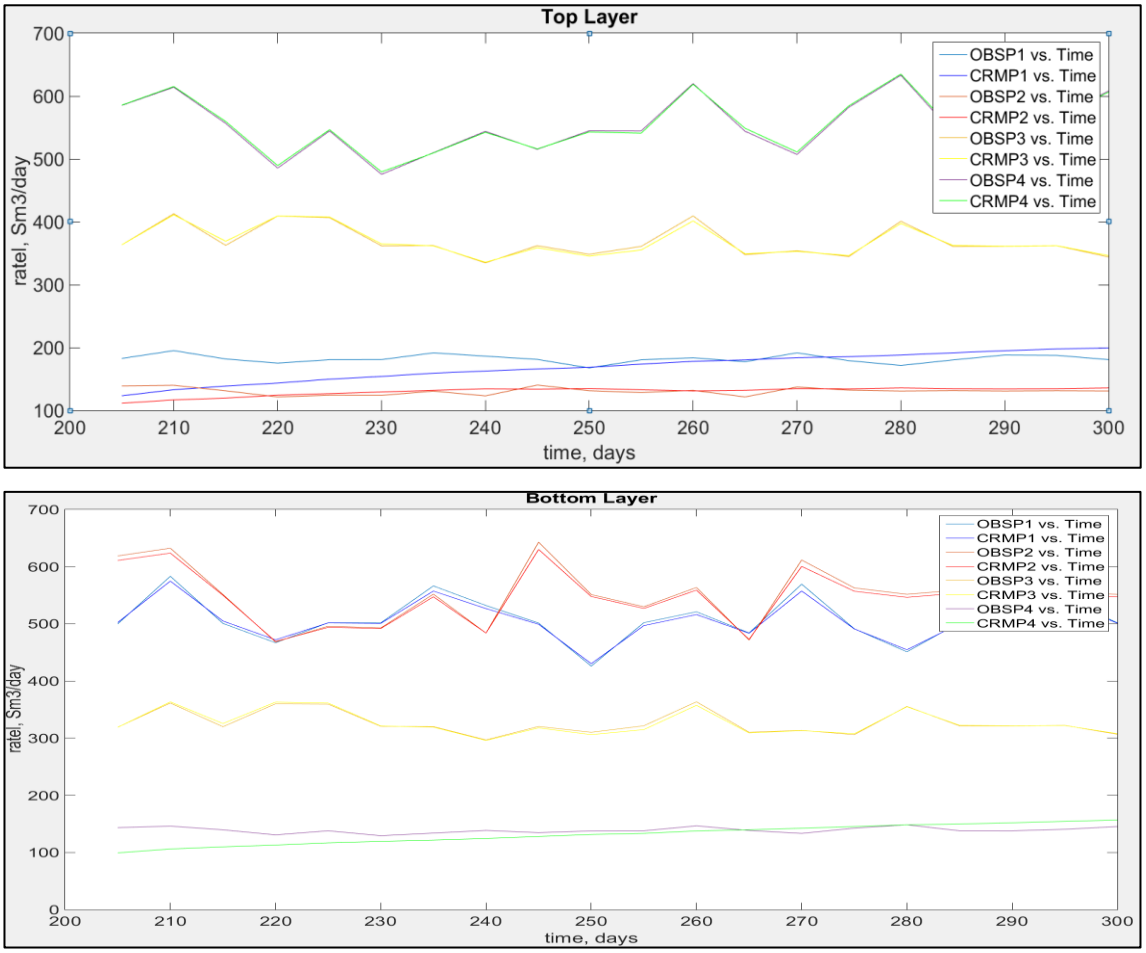

Figure 5-73. Comparison of estimated rate from CRM-AWC and observed rate for top and bottom layers between 200-300 days.

The stage 3's (red) line in Figure 5-74 is closer to the homogenous line, than the stage 2 (yellow) line, indicates a more uniform water flood, as confirmed by the reduction of the Lorenz coefficient (Lc^{stage3}) to 0.12.

If the reservoir resumes with this control (stage 3 optimisation), the cumulative oil will be improved, and the cumulative water will be reduced compared to stage 2 and stage 1 optimisation (Figure 5-76 Figure 5-77)

In stage 3, production data indicates that the restriction applied to P4-BL encouraged the P4-TL production to increase, in order to meet the well's rate control constraint. P4-TL had attracted most of the injected water from the surrounding injectors (I3-TL, I4-TL, I5-TL), reducing the waterflood support to the other producers. A similar analysis, to a lesser extent also applies for P1-BL. The (stage 2) restriction in P1-TL encouraged

the P1-BL to produce at a higher production rate, attracting water from its surrounding injectors (I1-BL, I2-BL, and I3-BL). The above analysis forms the foundation for stage 4 optimisation strategy:

1. Maintained the previous ICV control in P1-TL, P2-TL, and P4-BL.
2. Choke P1 bottom layer's (P1-BL) ICV to 20% of stage 3 production rate.
3. Choke P4 top layer's (P4-TL) ICV to 20% stage 3's production rate.

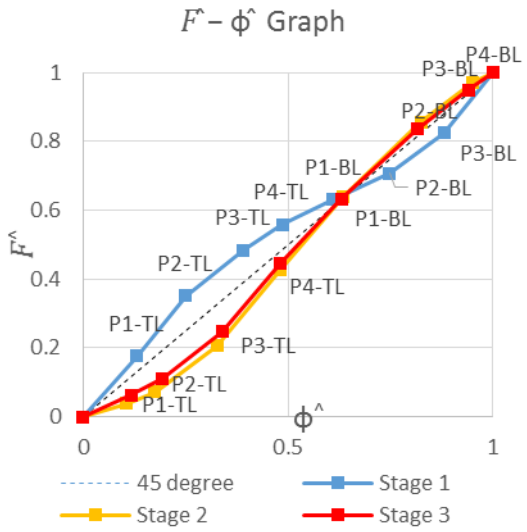

Figure 5-74. Modified $\hat{F} - \hat{\phi}$ graph of stage1, 2 and 3

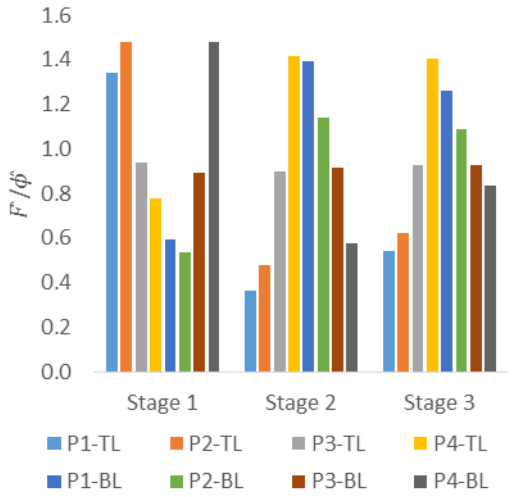

Figure 5-75. $\frac{\hat{F}}{\hat{\phi}}$ Histogram for stage 1, 2 and 3

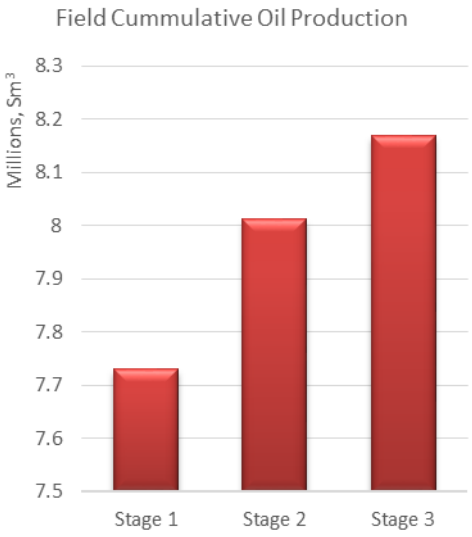

Figure 5-76. Stage 1, 2 and 3 field oil cumulative production from the start until 10 years

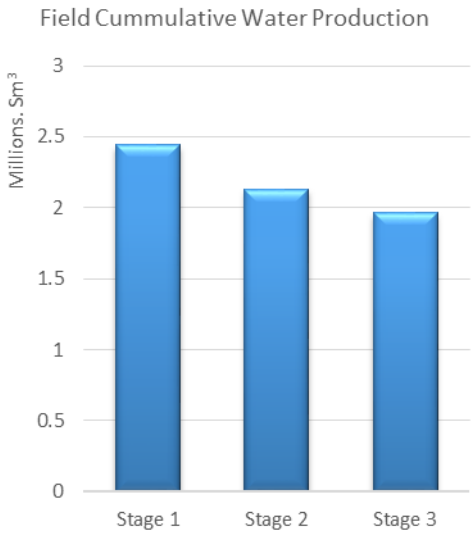

Figure 5-77. Stage 1, 2 and 3 field water cumulative production from the start until 10 years

Stage 4 evaluation

The stage 4 connectivity values are tabulated in Table 5-6 and plotted in Figure 5-78. The additional restriction applied to P4-TL and P1-BL, reallocated their excessive injection support to other layers (Figure 5-81). This control strategy created more uniform waterflooding (green line in Figure 5-80). The stage 4 coefficient (Lc^{Stage4}) was now 0.07.

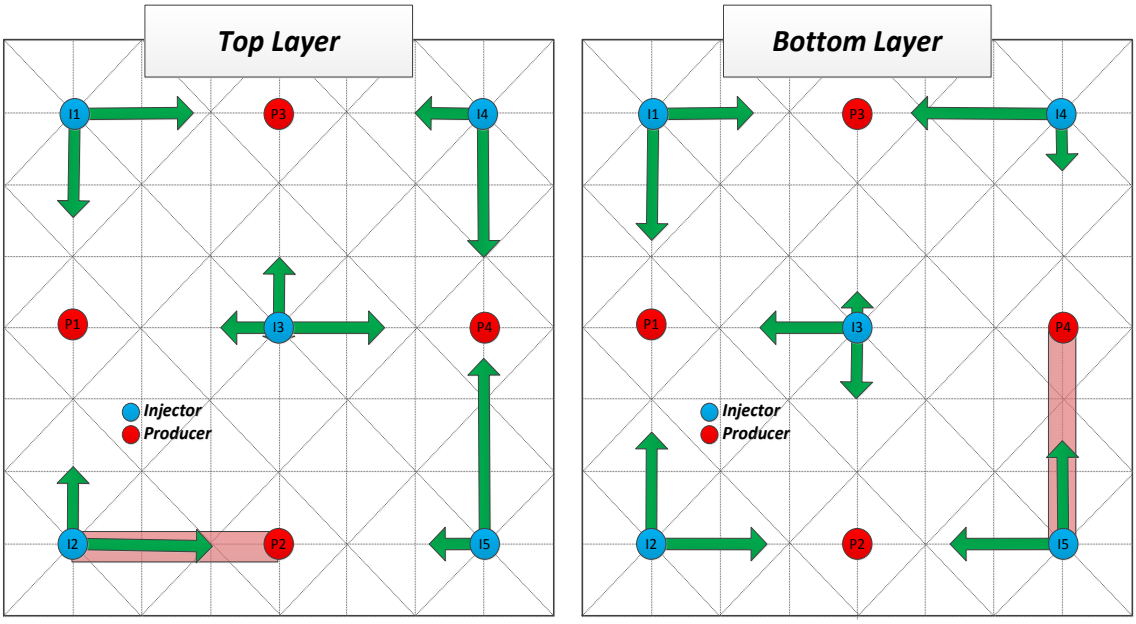

Figure 5-78. Connectivity network of stage 4

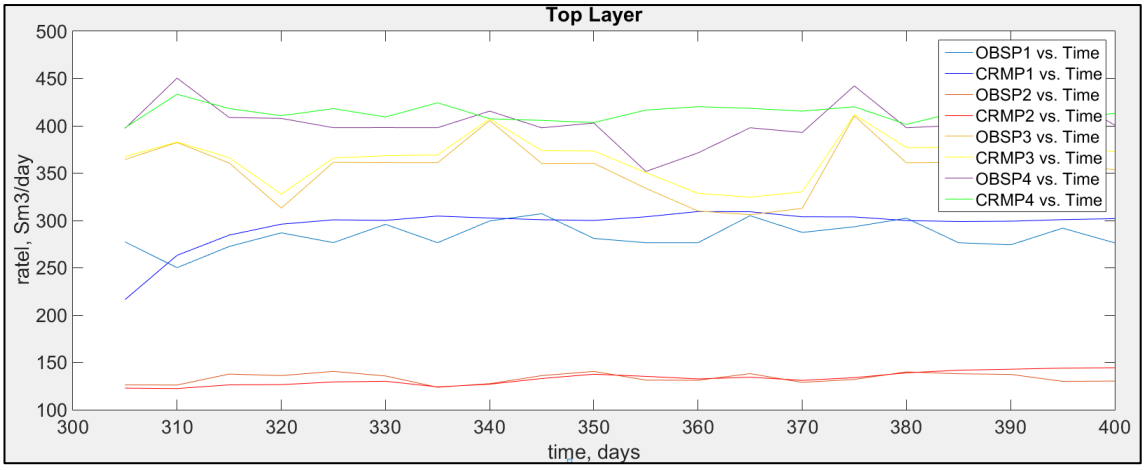

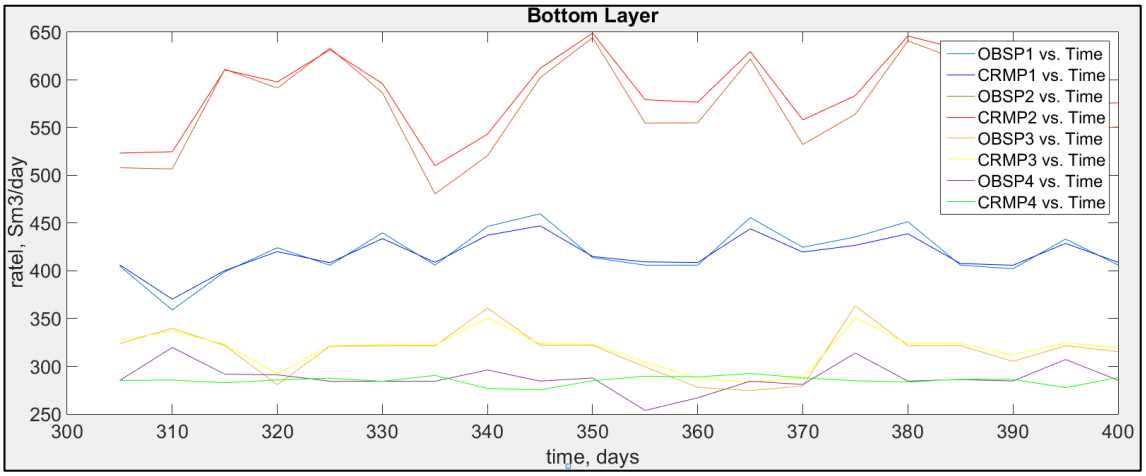

Figure 5-79. Comparison of the CRM-AWC estimated rate and the observed rate for the top and bottom layers between 300-400 days. OBSPx is observed production rates, CRMPx is CRM calculated rates

The stage 4 ICV control strategy further improved the cumulative oil and reduce cumulative water (Figure 5-82 and 5-81). This low Lorenz coefficient indicate a uniform waterflood. It would be difficult to achieve such a low value in a real field, but it is still possible to analyse the $\hat{F} - \hat{\phi}$ gradient for each layer (Figure 5-81) for a further optimisation stage in this synthetic field.

1. Maintained the ICV control in P1-BL and P4-TL.
2. Relaxed the ICV restriction in P1 Top layer (P1-TL) to increase the stage 4's production rate by 10%.
3. Relaxed the ICV restriction in P2-TL (P2-TL) to increase the stage 4's production rate by 15%
4. Choke P4 bottom layer's (P4-BL) ICV to 15% of the stage 4's production rate.

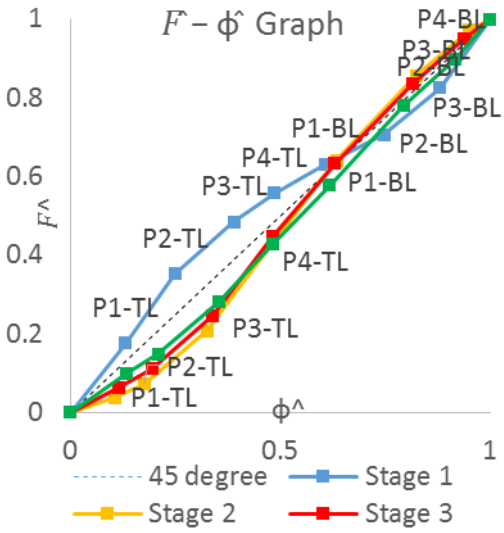

Figure 5-80. Modified $\hat{F} - \hat{\phi}$ graph for stage 1, 2, 3, and 4

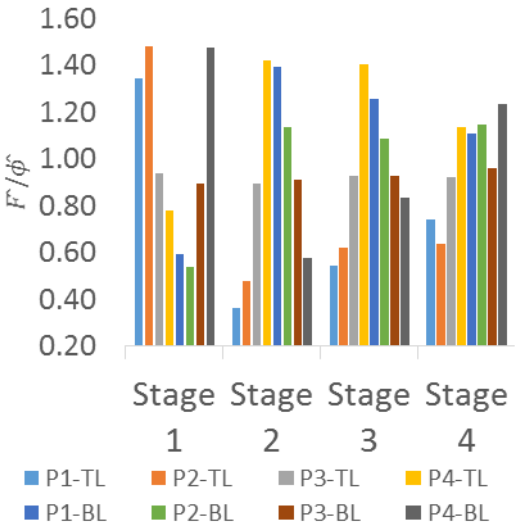

Figure 5-81. $\frac{\hat{F}}{\hat{\phi}}$ histogram of stage 1, 2, 3, and 4

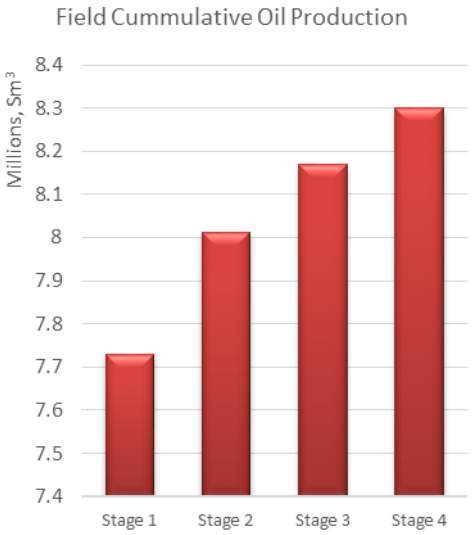

Figure 5-82. Stage 1, 2,3 and 4 field oil cumulative production from the start until 10 years

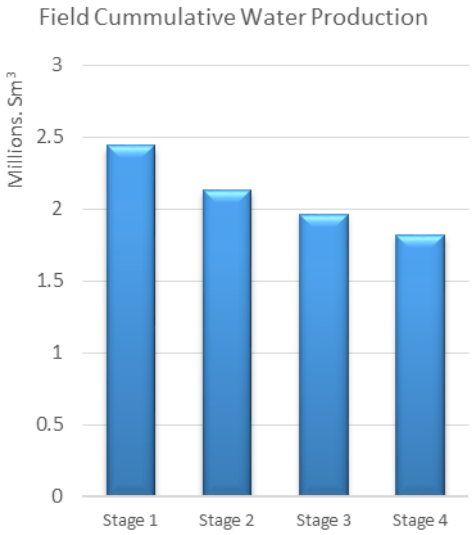

Figure 5-83. Stage 1, 2,3 and 4 field water cumulative production from the start until 10 years

Stage 5

The connectivity network of stage 5 (Figure 5-84) is very similar to that for connectivity network of stage 4 (Figure 5-76). The stage 5 (black) line of the modified $\hat{F} - \hat{\phi}$ plot is the closest to the "ideal" 45^0 line (Figure 5-86). The water flood uniformity at stage 5 has also slightly improved (Lc^{Stage5} = 0.06). The control applied to P4-BL reduced the flow-

storage of P5-BL; however, it encouraged disparity in P4-BL (Figure 5-87). Compared to stage 4, optimisation at stage 5 only slightly improve the cumulative oil production (Figure 5-88); without much affected the cumulative water (Figure 5-89).

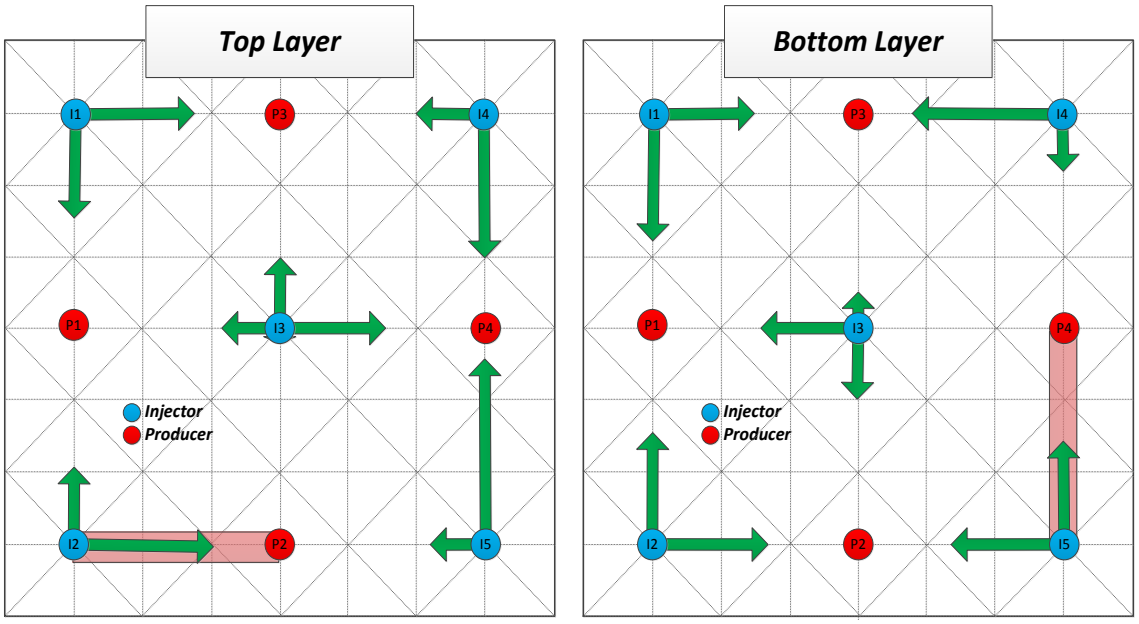

Figure 5-84. Connectivity network for stage 5

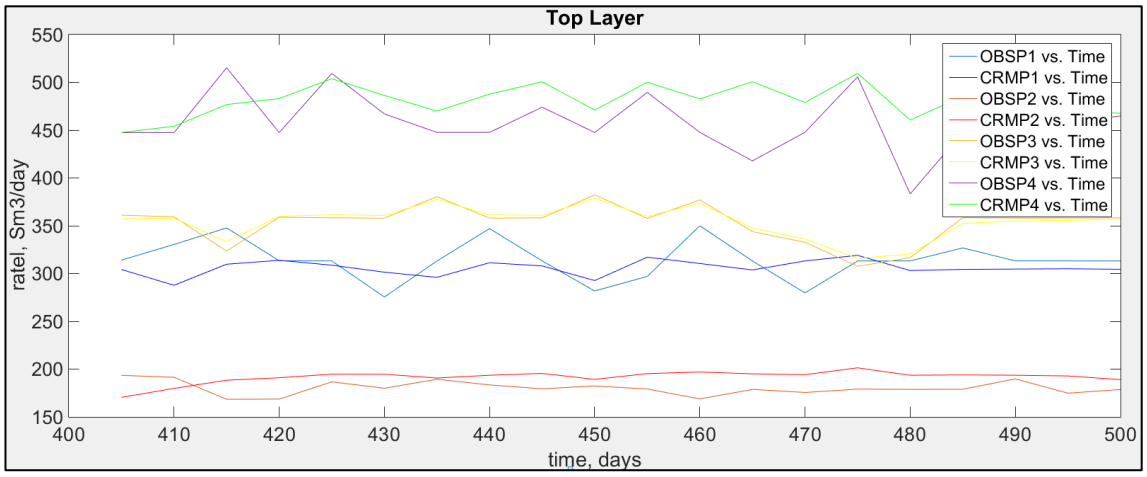

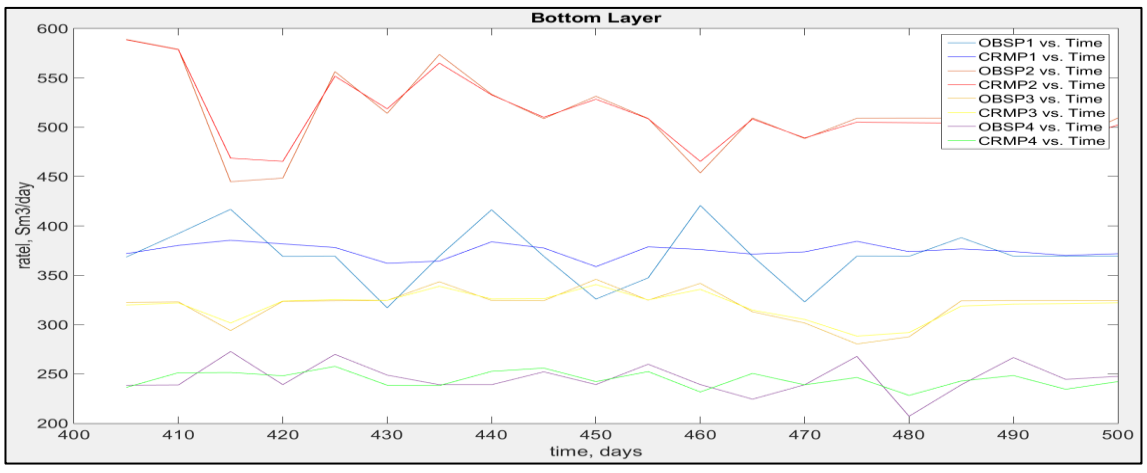

Figure 5-85. Comparison of estimated rate from CRM-AWC and observed rate for top and bottom layers between 400-500 days. OBSPx is observed production rates, CRMPx is CRM calculated rates

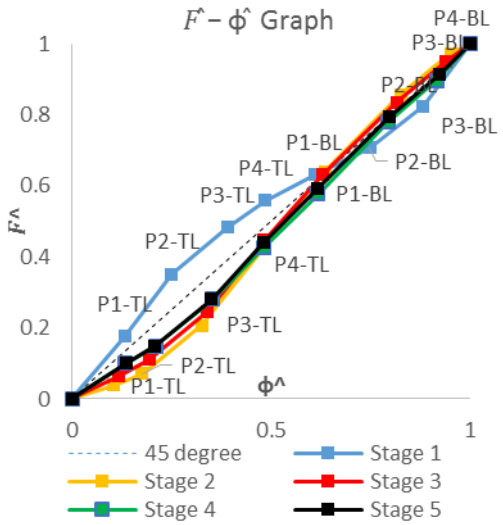

Figure 5-86. Modified $\hat{F} - \hat{\phi}$ graph of stage 1, 2, 3, 4 and 5

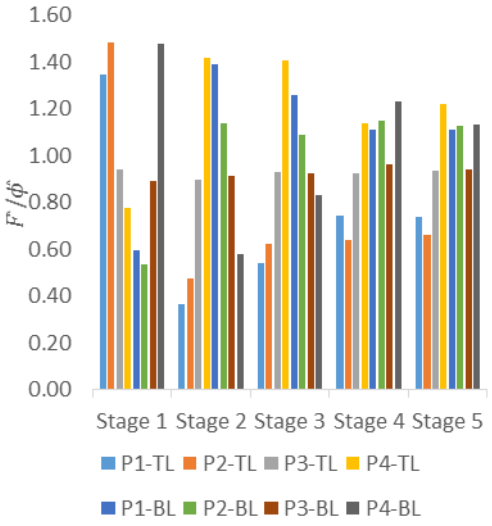

Figure 5-87. $\frac{\hat{F}}{\hat{\phi}}$ Histogram of stage 1, 2, 3, 4 and 5

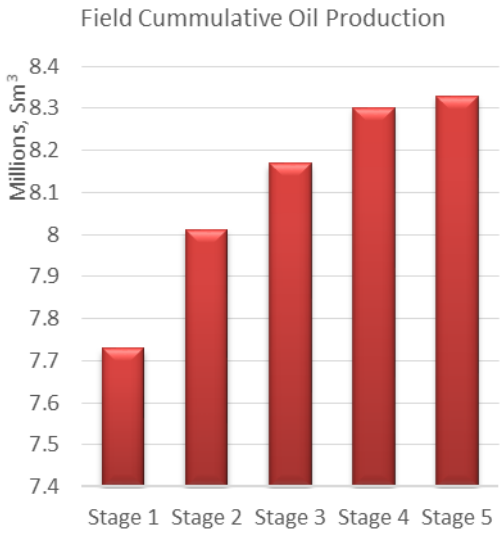

Figure 5-88. Stage 1, 2, 3, 4 and 5 field oil cumulative production from the start until 10 years

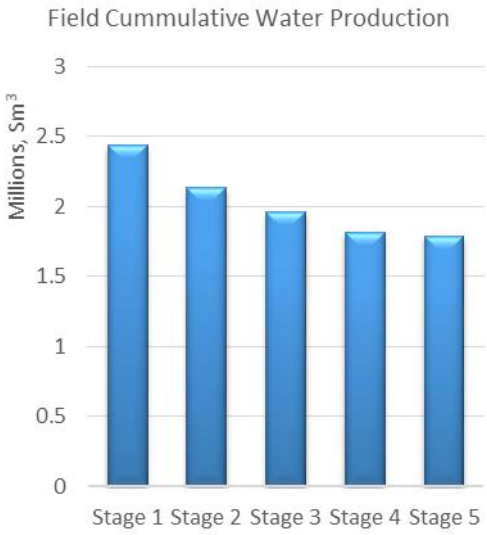

Figure 5-89. Stage 1, 2, 3, 4 and 5 field water cumulative production from the start until 10 years

Table 5-5. ICV strength for different stage

ICV Restriction strength (bar/(rcm/d)^2) – Top Layer					
	Stage 1	**Stage 2**	**Stage 3**	**Stage 4**	**Stage 5**
P-1	0	0.00546	0.00137	0.00137	0.00087
P-2	0	0.00546	0.00243	0.00045	0.00113
P-3	0	0	0	0	0
P-4	0	0	0	0.00061	0.00061
ICV Restriction strength (bar/(rcm/d)^2) – Bottom Layer					
P-1	0	0	0	0	0.00045
P-2	0	0	0	0	0
P-3	0	0	0	0	0
P-4	0	0.00546	0.00137	0.00137	0.00243

Table 5-6. CRM vs. Streamline results, comparison of connectivity and allocation factors

Top-Layer					
f	**Stage 1**	**Stage 2**	**Stage 3**	**Stage 4**	**Stage 5**
f_{111}	0.55	0.72	0.68	0.43	0.43
f_{121}	0	0	0	0	0
f_{131}	0.45	0.28	0.32	0.57	0.57
f_{141}	0	0	0	0	0
f_{211}	0.32	0.35	0.36	0.35	0.34
f_{221}	0.68	0.65	0.65	0.65	0.66
f_{331}	0	0	0	0	0
f_{441}	0	0	0	0	0
f_{311}	0.41	0.09	0.12	0.28	0.29
f_{321}	0.26	0.03	0.02	0.04	0.03
f_{331}	0.20	0.25	0.24	0.23	0.23
f_{341}	0.14	0.63	0.61	0.45	0.45
f_{411}	0	0	0	0	0
f_{421}	0	0	0	0	0
f_{431}	0.52	0.31	0.32	0.37	0.37
f_{441}	0.48	0.69	0.68	0.63	0.63
f_{511}	0	0	0	0	0
f_{521}	0	0	0	0	0
f_{531}	0.76	0.18	0.14	0.25	0.24
f_{541}	0.24	0.82	0.86	0.75	0.76
Bottom-Layer					
f	**Stage 1**	**Stage 2**	**Stage 3**	**Stage 4**	**Stage 5**
f_{112}	0.37	0.65	0.65	0.57	0.57
f_{122}	0	0	0	0	0
f_{132}	0.63	0.35	0.35	0.43	0.43
f_{142}	0	0	0	0	0
f_{212}	0.51	0.53	0.52	0.47	0.47
f_{222}	0.49	0.47	0.48	0.53	0.53
f_{332}	0	0	0	0	0
f_{442}	0	0	0	0	0
f_{312}	0.23	0.55	0.56	0.44	0.43
f_{322}	0.15	0.33	0.33	0.41	0.42
f_{332}	0.23	0.12	0.11	0.15	0.15
f_{342}	0.40	0	0	0	0
f_{412}	0	0	0	0	0
f_{422}	0	0	0	0	0
f_{432}	0.55	0.80	0.80	0.71	0.71
f_{442}	0.45	0.16	0.18	0.29	0.29
f_{512}	0	0	0	0	0
f_{522}	0	0	0	0	0
f_{532}	0.24	0.82	0.77	0.59	0.59
f_{542}	0.76	0.18	0.23	0.41	0.41

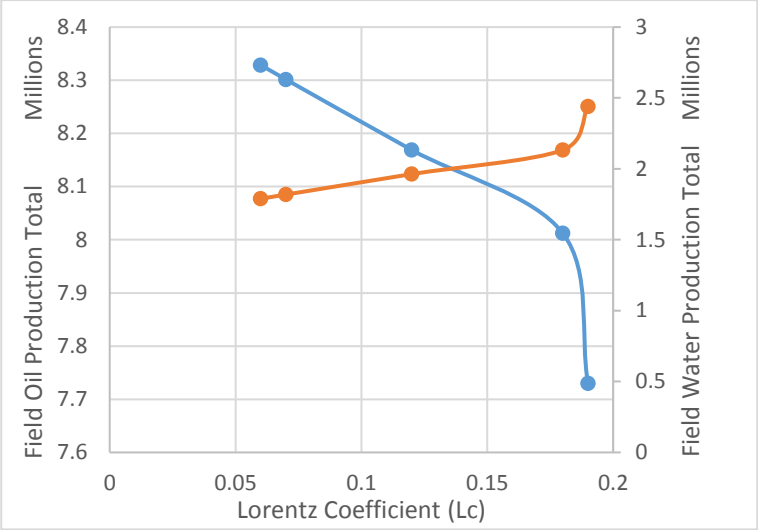

Figure 5-90. Cross-plot of oil and water production cumulative against the modified Lorenz coefficient

5.7 Discussion and conclusion

There are two essential steps of a closed-loop optimisation workflow discussed in this chapter:

1. The first step is to perform the history-matching using CRM-AWC. The calibration results will characterise fluid flow in the reservoir between the wells as a simpler, reduced-physics, system model. It provides a clear understanding of key reservoir features; such as inter-well connectivity, reservoir heterogeneity, flow barriers, etc. using minimal computational resources.
2. The parameters of a calibrated CRM-IW also provide a model similar to a Lorentz plot of the reservoir's flow and storage capacity. It clarifies the relationship between a well, zone or layer's flow-capacity and its connected drainage volume. The resulting insight into the recovery efficiency forms the basis of a feedback-control strategy for optimising the field's reserves by optimising the production and injection volumes at the level of a well, zone or layer, as appropriate.

This workflow is implemented as a spreadsheet or similar open-source software, providing a diagnostic tool for practicing engineers to analyse daily production data to optimize the recovery of hydrocarbon resources from all types (simple to complex) well and field design strategies. The accuracy of a constructed CRM depends on the sufficient amount of production/injection data (Q and BHP) to cross-correlate them for calibration. Note that well downtimes or non-variable injection/production history is less informative

for CRM as they carry little (new) interaction events. An event/history should also be long enough for the well rates/pressures to react to each other via their inter-well reservoir volume.

There are several observations we can draw from this chapter:

- The CRM workflow turns the routinely recorded data from production/injection wells into a 'proxy' model quantifying the inter-well interactions and capturing the major trends (or upscaled properties) of the reservoir system. The aim of the CRM approach is not to replace numerical reservoir simulation, but to be a simple and practical way of providing insights into the reservoir performance.
- Theoretically, CRM could also be used to propose an injection strategy that would enhance the information content of future production history data, specifically in terms of a CRM update. In addition, integration of CRM prediction studies with data from the injection of tracers, and the analysis of transient build-up tests provides fundamental information on reservoir compartmentalization; this is information that can be used to constrain the CRM calibration algorithm and improve its accuracy. However, this will not always be a practical strategy due to the need to wait for weeks or months before the reservoir's reaction to well rate changes becomes clearly interpretable.
- The workflow of the new CRM-AWC follows a conventional CRM workflow apart from the new parameter added to the model: the ICV restriction strength. The ICV strength (a) was predicted in advance (using equation 2-11) and was treated as the input parameter for the data calibration. In the scenario where the mechanical position of the ICV is difficult to locate, and the value of ICV strength (a) becomes arbitrary, such a procedure can be inverted and ICV strength (a) becomes one of the CRM-calibrated parameters (along with connectivity and time-storage). *This type of inverse analysis is also applicable for cases where the prediction of ICV strength using an explicit model (such as equation 2-11) is not recommended (e.g. eroded or plugged valve).*
- This work used data generated by reservoir simulator and thus a noise free experiment. In practical cases, the data required are measured in the field and may be noisy due to measurement errors or fluctuations. Such noise must be reduced, controlling the quality of the data used to model the reservoir. Cao, 2011; Weber,

2009; Kaviani *et al*, 2014; Holanda *et al*, 2015 suggest methods to deal with noise and measurement errors to better evaluate the CRM model.

- The modified flow-capacity storage ($\hat{F} - \hat{\phi}$) graph reveals the rate-drainage disparity and can be treated as a "guide" for selecting (or prioritising) which layer(s) are most needed to be controlled. However, the graph does not specify the required restriction for these layers. For example, in the case study of the 5I-4P synthetic field, stage 3 control (whereby ICV valve is "fine-tuned" for a more appropriate restriction strength) proved to be more effective than stage 2 control. Formulating the CRM-AWC into a 1D system (Lerlertpakdee, and Jafarpour, 2014) and integrating it with the Buckley-Leverett for the AWC solution, as explained in Chapter 3 might possibly address this issue. The integration between CRM-AWC and Buckley-Leverett could potentially translate the CRM's conductivity/connectivity into permeability, or parameters which practicing engineers commonly use. Such relationship is useful to avoid calibrating the permeability values during history matching or avoiding any inefficient history matching or optimisation tasks.
- The disparity of the well's (or layer's) flow-capacity storage can be measured quantitatively using the Lorenz coefficient (Lc). This parameter has a similar role with the Inflow Variation (IV) parameter in Chapter 2; that is, it indicates the long-term objectives of the reservoir management. Hence, the reduction of Lc becomes the objective of each optimisation. In our case study, control action (i.e. task to reduce the production and injection) for the otherwise inefficient layers is carried out without lowering the total well's productivity index. This can be done by maintaining the production and injection rates control for each well, e.g. reduced production from bottom-layer of a well will be compensated by its top layer.
- Our hypotheses is there is a perfectly balanced well/layers contribution which yields to optimal solution. We also showed in our case study that adjusting inflow to move the modified Lorenz curve towards the 45^0 degree straight line suggested it will improve the reservoir performance. However, without more robust testing such a production varies significantly with small variations in Lorenz curve; also diminishing its comparison to other optimisation method, etc. We hope to inspire future researcher to do more work to test the assertion that the optimal solution correlates with the modified Lorenz curve-based one.

In conclusion, this chapter has presented Capacitive Resistance Models in a new form for

reservoir characterisation and zonal, intelligent well control (i.e. CRM-AWC) that includes the non-linear pressure drop from FCDs. The new CRM solution can be extended to different levels of reservoir complexity such as single- or multi-layers with or without cross-flow. Furthermore, the CRM-AWC calibration generates the parameters for a production optimisation workflow based on the modified Lorenz plot. This chapter also propose a new way to optimise the ICV before a water breakthrough (proactive optimisation) using the CRM's derived parameters (connectivity and time-storage). The proposed technique adopted the ideas behind the classic Lorenz plot and translated it into water flood operations. Unlike most production optimisation strategies that are based on complex mathematical equations, this approach uses an engineering-based understanding of a relationship between a well's (or layer's) flow-capacity against its associated drainage volume. The workflow is employed as an intuitive, simple approach for AWC production optimisation.

5.8 Summary

This chapter reports the application of a new analytical solution for the CRM in the presence of AWC to manage the production and injection from a reservoir that provides a continuous data stream of sand face pressure measurements. This chapter also discusses the importance of considering the CRM's properties (connectivity and time-storage) as dynamic properties. We investigated a real field case of a thermal-induced-fracture (TIF) reservoir using the principle of a dynamic CRM to estimate the likely TIF growth impact and direction. When dealing with AWC, the ICV action (closing and opening the valve) altered the well/zone drainage control. This provides an opportunity to optimise the waterflood operations, such as reallocating the injection rate by choking ICVs.

In summary, we have presented:

- A review of the CRM.
- The application of a Capacitance-Resistance Model (CRM) to inform dynamic well control.
- A case history for a reservoir with Thermally Induced Fractures.
- Development of the CRM to the case of wells with AWC (i.e. CRM-AWC). Analytical solutions were presented for different form of CRMs.
- Example application of the CRM-AWC in a single-layer reservoir. The examples illustrated the method's value and potential.

- Example application of the CRM-AWC in a multi-layer reservoir. The examples illustrate the method's value and potential.
- Modelling a multi-layer reservoir completed with AWC wells in a streamline simulation.
- Development of an $\hat{F} - \hat{\phi}$ graph and modified $\hat{F} - \hat{\phi}$ graph.
- Introduction and steps to calculate the Lc of the modified $\hat{F} - \hat{\phi}$ graph.
- Production optimisation of AWC wells using CRM-AWC and a modified $\hat{F} - \hat{\phi}$ graph.
- Example application of closed-loop optimisation using CRM-AWC and modified $\hat{F} - \hat{\phi}$ graph in a synthetic multi-layer reservoir with five injector wells and four producer wells.
- Finally, the method's limitations and potential improvements were discussed.

5.9 Nomenclature

I – Water injection rate	N_p– Total number of production wells
ΔP – Change of flowing bottom-hole pressure	J - Productivity index of a producer pair
f – Connectivity	q - Fluid production rate
τ - Time-constant	q_{cr} - Fluid production rate of cross-flow
f' - Fraction injection into each layer from an injector	F – Flow capacity
t – injection time	Φ – Flow storage
N_i – Total number of injection wells	Lc – Lorenz coefficient

5.9.1 Subscripts and superscripts

i – Injector index	j – Producer index
k – Time-step index	k – Time-step index
n – Time-like variable	ij – Injector-producer pair index
^ - Normalized	STR - Streamline

5.9.2 Abbreviations

CRM	Capacitance-Resistance Model
AWC	Advanced Well Completion
PI	Productivity Index

TIF	Thermal Induced Fracture
CRMT	CRM for single tank representation of a field
CRMP	CRM for a given Producer
CRMIP	CRM for a given pair of Producer-Injector
CRM-ML	CRM for a given Producer - Multi-Layered reservoir, no cross-flow
CRMP-MLCr	CRM for a given Producer - Multi-Layered reservoir with Crossflow
CRMP-AWC	CRMP-ML for a given producer with Advanced Well Completion
CRMP-ML-AWC	CRMP-ML for a given producer with Advanced Well Completion
CRMP-MLCr-AWC	CRMP-MLCr for a given producer with Advanced Well Completion
BHP	Bottom Hole Pressure
MHI	Modified Hall Integral
FMI	Formation Micro Imager
ICV	Interval Control Valves

Chapter 6 – Conclusions and Future Work

6.1 Discussion

The advancement of well technology has enabled us to build wells which would not only intersect multiple reservoir layers (e.g. horizontal well, multi-lateral well), but also have means of controlling and monitoring the production performance with the advent of AWC. These completions typically incorporate permanent downhole sensors, active surface-controlled downhole inflow flow control valves (ICV), or autonomous and non-autonomous passive downhole inflow control devices ((A)ICD). These well's components will monitor, evaluate, and actively manage production (or injection) in real time without any well interventions. Controlling the production performance has been possible by installing the inflow control technology in the completion tubing to restrict the amount of influx coming to the well. The gauges or sensors mounted in the completion will measure the pressure and temperature of respected depth/layers which can be processed further to be interpreted as flow rate, pressure, skin, and many other important reservoir parameters.

There are three different topics in this thesis, dedicated to three main application areas of AWC technologies.

1. *ICD system.* This is mainly covered in chapter 3.
2. *AFCD system.* This is mainly covered in chapter 4.
3. *ICV and monitoring system.* This is mainly covered in chapter 5.

We described the development of our models separately to illustrate how they solve issues encountered by each system, such as: the lack of simple modelling to fine-tune the ICD design; predicting long-term parameters of AFCD completion using an efficient model, the necessity to extract meaningful information from pressure and rate data in the ICV and monitoring system. Bear in mind that, each of above systems have their specific operational differences, and thus it is important to evaluate the operational applicability of equations we presented in this thesis. For example, ICD and AFCD completions are modular that are typically installed with more than 20ea modules in a horizontal well. ICD and AFCD completions are often not supported with full-monitoring system, e.g. only one PT gauge is installed on the top of the lower completion. Due to these operational

limitations, CRM-ML-AWC may not be applicable for these systems. On the other hand, there is a number of scenario with monitoring and AWC technologies installed on one well. For example: a multi-lateral well with both ICV and monitoring system are operated in the upper completion, while ICDs and AFCDs are installed in the lower completion. This strategy is aimed to address multifaceted problems that require deeper analysis, and engineers should employ combination of various models. We briefly introduced a case where coupling of the type-curve design (chapter 3) and the extended BL-method for AWC (chapter 4) can address the short-term vs. long-term evaluation of an AWC well. In the future, more analysis can be done to test and analyse combination of all our developed models.

This thesis focuses on the development of the methods to model and design AWC flow performance, rather than using the conventional grid-based numerical simulation. The proposed illustrate the advantage of the reduced-physics models to capture the main-trends of the reservoir and access some key reservoir information with a much-reduced computational time. Complex numerical simulation is often over-detailed and uncertain. The methods developed in this thesis provide a good insight into the AWC's performance as well as being used to calibrate or verify a comprehensive numerical model if needed. It has been recognised as good practice to employ many models of varying complexity rather than depending only on a single model. The semi-analytical models developed are simple, transparent, and allow engineers to perform AWC evaluations in an easily understood form. The ideal workflow as suggested by (Hey, Tansley and Tolle, 2009) is to use all available models including analytical, statistical (data intensive), and numerical models to complement each other (Figure 6-1).

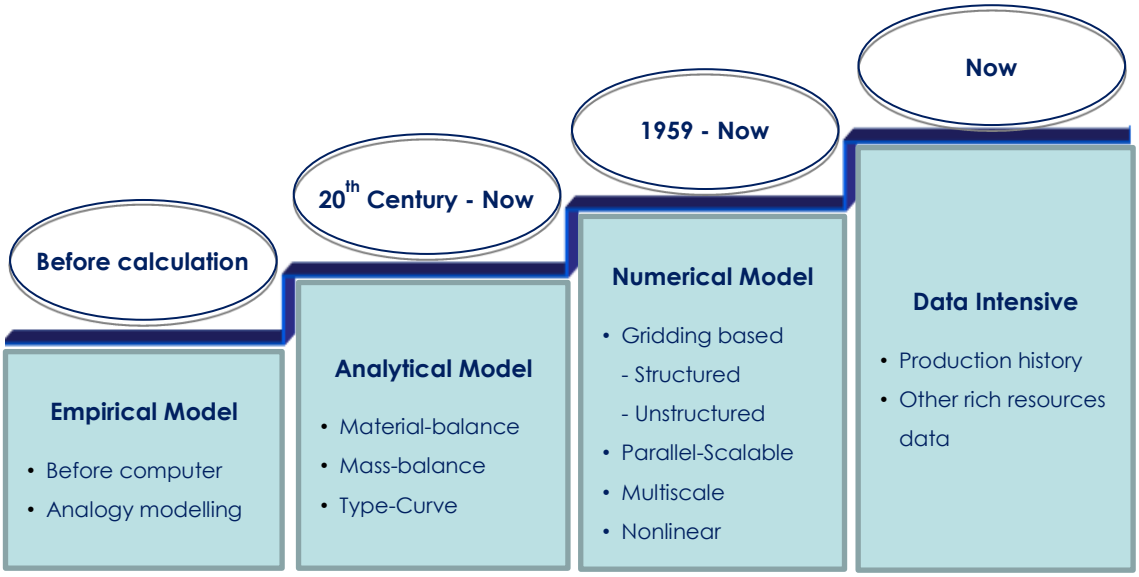

Figure 6-1. Hierarchy of reservoir modelling tools

It is important recognise that the accuracy of our models is still dependant on geological information that is often uncertain. The optimum completion size for one realisation may no longer be the optimum for other geological realisations. Our solutions, being a fast and simple calculation, would find optimum completion size based on reservoir built from the latest open-hole log measurement. The most recent information would update the reservoir model or ensemble of models to reduce uncertainty in the reservoir description.

In most cases, the common, most used engine for determining the uncertainty effect is a numerical, gridding based simulation model. However, relying solely on numerical simulation can be an obstacle in transferring best practices, it is also recognized that employing numerical simulation would require some level of experiences that is varies from company to company. It is also necessary to compare the numerical simulation with other methods of modelling as a means of validation, pre-cursor, complementary tools to enhance the robustness of reservoir modelling alone. Coarser model derived from analytical solution or data-intensive methods would be used in this study. The nature of these models is simpler, more transparent, and provides one with an insight into underlying physics in the reservoir in an easily understood form. The simplicity of these methods would enable engineers to perform various sensitivity studies of the main foreseen uncertainties without having to run those hours of computational calculation when using the grid based reservoir simulation. Utilizing these rapid methods, we could address the reality of business paradigm which is bias towards simpler and integrated process that is also favouring the breadth over depth at the outset of a study. The methods

introduced in this study are not an alternative for the established, common way or predicting reservoir performance via gridding-based simulator, but as a rough-sketch or blueprint of a reservoir model.

The new equations presented in this thesis to describe both the short- and long-term AWC performance. They are made possible by the flow performance of a standard FCD being described by a quadratic equation with the help of an empirical constant called FCD's strength (a). This parameter also allows approximating the published data from flow-loop testing which presents the relationship between the FCD's pressure drop and flow rate. In the past few years however, a new generation of AFCDs shows a different rate vs. pressure drop relationship. Hence, new AWC analytical equations that honour the type of non-linear pressure drop of such FCDs may be required. The key approach to derive these new equations is to incorporate the FCD's pressure drop as an additional element in the system of the equation, add together with other pressure drops in the specific observed system, e.g. pressure drop of Darcy's law, two-phase Buckley-Leverett's pressure drop, or CRM. We hope that future researchers will be inspired by our workflows to develop AWC performance models for the new generations of AWCs.

6.2 Conclusion

In summary, the achievements of this work are the development of analytical models and workflows that are able:

Chapter 3 examines the:

1. Short-term (a.k.a. 'snapshot') added values of installing AWCs in wells with dominating heel-toe effect.
2. Short-term added values of installing AWCs in wells in heterogeneous reservoirs with dominating inflow imbalance due to the heterogeneity.

Chapter 4 examines the:

3. Long-term AWC value derived by controlling the zonal flow rate in light oil (when the piston-like displacement assumption is valid) waterflood scenarios.
4. Long-term AWC value derived by controlling the zonal flow rate in medium/heavy oil (i.e. both piston and non-piston-like displacement) waterflood scenarios.

Chapter 5 characterises the reservoir and inter-well connectivities to:

5. Assess the effectiveness of both conventional and the zonal, intelligent well control.
6. Optimally control wells and/or ICVs for improved recovery.

6.3 Future work

The effort to advance the fast, transparent, data-driven modelling that capture (reduced) physics involved in Advanced Well Completion is far from complete. Many areas for research and improvements remain. Based on the work presented in this thesis, possible extensions for the future work include:

Chapter 3:

1. A comprehensive evaluation tool can be developed advising how to make a choice between installing constant or variable strength of flow control devices in an AWC.

   The motivation for this research is to investigate the prevalent assumption that installing constant size/strength AWC in wells is more robust against geological and operational uncertainty, than installing a variable strength one. The studies would review major aspects dictating the choice and quantify the value difference between two different methodologies.

2. Develop an analytical model for the reduction of flow imbalance in a heterogeneous reservoir in a long horizontal well when the heel-toe effect is no longer negligible.

   The main assumption for analytical model of the ICD performance in heterogeneous reservoir is that the pressure losses along the well are small compared to the reservoir drawdown. We observed that there are cases where this is no longer the case and adjustment for the new analytical formulation is needed.

Chapter 4:

1. Further investigation of the proposed methods in the presence of a strong gas-cap.

   We have presented robust investigation about extending the fractional flow model to include the response of non-linear pressure drop of the flow control devices. So far

the studies have been focused on the water-oil system, meanwhile there are many AWC application in the presence of a gas-cap. The study could start by assuming an immiscible gas-oil system, and then followed by the gas-water-oil system. The outcome of such study would be the basis for future immiscible system.

2. Implement the proposed methods where the areal sweep efficiency (Ea) is not 100%.

   Note that the oil recovery factor is the product of the efficiency of oil displacement by water and the volumetric sweep efficiency (the extent of the water front on the reservoir level). The latter is the product of the areal and vertical sweep efficiencies (Ea). Chapter 4's main assumption is that there is 100% Ea, while in reality this is often not the case since Ea is the function of rock and fluids properties. The Ea value can be found by other means, e.g. mathematical models of Dyes et al., 1954 or core flooding experiments respectively.

3. The proposed workflows in this chapter assume strong water drive which enables a perfect voidage replacement or steady-state conditions. Further model developments for non-steady state conditions are desirable.

   Such system would no longer follow the assumption of incompressible flow and this study may have to consider the alternatives of fractional flow model.

4. Further investigation when there is pressure communication between layers.

   Analytical solutions for vertical sweep efficiency in heterogeneous reservoirs require two assumed situations: the layers can either be non-communicating or are perfectly communicating (i.e. instantaneous, vertical, pressure equilibrium). The investigation presented in chapter 4 deals with the non-communicating layers assumptions and there is good opportunity to extend the findings for the situation where the layers have good communication. This future work should start from the condition where there is a perfect (instantaneous) equilibrium between layers. The available classical waterflood method for a gravity dominated flow can be coupled to include the advanced well completion.

5. Development of a semi-analytical model where the capillary pressure is non-trivial.

   The analysis so far has been focussing around the displacement where diffuse flow occurrs, and it is assumed that ahead of displacement interface, only oil is flowing

with water present at Swc. In reality, there would be a transition zone between these two phases, associated with the imbibition capillary curve, i.e. Pc is no longer negligible. Furthermore, this is especially important for AWC application where the horizontal wells are completed in the transition zone, close to water-oil contact. It is recommended to start this study from available studies of the classical waterflood method where Buckley-Leverett was applied to the reservoirs with some degree of capillary pressure. Such models can be extended to include the non-linear pressure drop from flow control devices.

Chapter 5:

1. Automating the CRM event detection using the Integration of CRM-AWC with ensemble Kalman-filter (EnKF).

   Using CRM-AWC as the driving dynamical system describing the reservoir, a future study can implement the ensemble EnKF procedure that estimates the CRM parameters (interconnectivity, time lag, etc.) to obtain a time dependent estimate for the parameters. These parameters can be automatically interpreted to detect events such as well control or changed ICV strength, and change of reservoir properties, due to a thermal induced fracture from cold water injectors. The uncertainty involved with interwell connectivities and time lags can be systematically reduced with the EnKF procedure (Jafroodi and Zhang, 2011).

2. Comparison between the optimal scenario based on $\hat{F} - \hat{\phi}$ graph and optimal scenario based on the proactive/reactive optimisation concepts by (Sefat, 2016) and (Grebenkin, 2013).

   Comparing the result from our proposed modified Lorenz plot – CRM-AWC with common production optimisation strategies production such as Genetic Algorithm, Simultaneous-Perturbation Stochastic Approximation (SPSA), etc. Additionally, this study can do more robust testing such as production varies significantly with small variations in Lorenz curve to test the assertion that the optimal solution correlates with the modified Lorenz.

3. Implementing CRM-AWC as a forward predictive model.

The modified flow-capacity storage (Fˆ- ϕ) graph does not specify the required restriction for layers. Formulating the CRM-AWC into a 1D system (Lerlertpakdee, and Jafarpour, 2014) and integrating it with the Buckley-Leverett for the AWC solution, is possible to quantify the required specific restriction and can be used as a forward predictive model. This solution may well possibly quantify the required restriction to optimize the recovery of hydrocarbon resources.

Bibliography

Abd Elfattah, M., Al-Yateem, K., Qahtani, H., & Rajabian, B. (2013) 'Variable Nozzle–Based Inflow Control Device Completion: Inflow Distribution Comparison, Analysis, and Evaluation', *International Petroleum Technology Conference*. Beijing, China: International Petroleum Technology Conference.

Addiego-Guevara, E., Jackson, M. D., & Giddins, M. A. (2008). Insurance Value of Intelligent Well Technology against Reservoir Uncertainty. SPE/DOE Symposium on Improved Oil Recovery, Tulsa, Oklahoma, USA, Society of Petroleum Engineers.

Aguilera, R. (1991). *Horizontal wells : [formation evaluation, drilling, and production, including heavy oil recovery]*, *Contributions in petroleum geology & engineering*. Gulf Pub. Co.

Ajayi A. A. (2007) 'Theory and Application of Probabilistic Method of Designing Customized Interval Control Valves Choke Trim for Multizone Intelligent Well Systems', *SPE Annual Technical Conference and Exhibition*. California, U.S.A: Society of Petroleum Engineers.

Akbari, M., Gonzalez, J. R. and Macklin, N. (2014) 'Considerations for Optimum Inflow Control Devices (ICDs) Selection and Placement in Horizontal Sections', *SPE Russian Oil and Gas Exploration & Production Technical Conference and Exhibition.* Moscow, Russia: Society of Petroleum Engineers.

Al-Khelaiwi, F. T., Birchenko, V. M., Konopczynski, M. R., & Davies, D. (2010) 'Advanced Wells: A Comprehensive Approach to the Selection Between Passive and Active Inflow-Control Completions', *SPE Production & Operations*. Society of Petroleum Engineers, 25(3), pp. 305–326.

Alghareeb, Z., Horne, R. N., Yuen, B. B. W., & Shenawi, S. H. (2009) 'Proactive Optimization of Oil Recovery in Multilateral Wells Using Real Time Production Data', *SPE Annual Technical Conference and Exhibition*. New Orleans, Louisiana, U.S.A: Society of Petroleum Engineers.

Alhuthali, A. H. H., Datta-Gupta, A., Yuen, B. B. W., & Fontanilla, J. P. (2008) 'Optimal Rate Control Under Geologic Uncertainty', *SPE/DOE Symposium on Improved Oil Recovery*. Tulsa, Oklahoma, U.S.A: Society of Petroleum Engineers.

Almarri, M., Prakasa, B., Muradov, K., & Davies, D. (2017) 'Identification and Characterization of Thermally Induced Fractures Using Modern Analytical Techniques', *SPE Kingdom of Saudi Arabia Annual Technical Symposium and Exhibition*. Dammam, Saudi Arabia: Society of Petroleum Engineers.

Al Marzouqi, A. A. R., Helmy, H., Keshka, A. A.-S., Elasmar, M., & Shafia, S. (2010) 'Wellbore Segmentation using Inflow Control Devices : Design and Optimisation Process'. *Abu Dhabi International Petroleum Exhibition and Conference*. Abu Dhabi, UAE: Society of Petroleum Engineers.

Almeida, L. F., Vellasco, M. M. B. R. and Pacheco, M. A. C. (2010) 'Optimization system for valve control in intelligent wells under uncertainties', *Journal of Petroleum Science and Engineering*. Elsevier B.V., 73(1–2), pp. 129–140.

Anklam, E. G. and Wiggins, M. L. (2005) 'A Review of Horizontal-Wellbore Pressure Equations', *SPE Production and Operations Symposium*, p. 7.

Babu, D. K. and Odeh, A. S. (1989) 'Productivity of a Horizontal Well', *SPE Reservoir Engineering*, 4(4), pp. 417–421.

Bailey, W. J. & Couet, B. 2005. 'Field OptimisationTool for Maksimising asset Value', SPE Reservoir Evaluation & Engineering, 8, 7-21.

Beliveau, D. (1995) 'Heterogeneity, Geostatistics, Horizontal Wells, and Blackjack Poker', *SPE Journal*.

Birchenko, V. M., Demyanov, V., Konopczynski, M. R., & Davies, D. R. (2008) 'Impact of Reservoir Uncertainty on Selection of Advanced Completion Type' *SPE Annual Technical Conference and Exhibition*, Denver, Colorado, U.S.A: Society of Petroleum Engineers.

Birchenko, V. (2010) '*Analytical modelling of wells with inflow control devices*', PhD Thesis, Heriot-Watt University.

Birchenko, V. M., Bejan, A. Lu., Usnich, A. V., Davies, D. R (2011a) 'Application of inflow control devices to heterogeneous reservoirs', *Journal of Petroleum Science and Engineering*, 78(2), pp. 534–541.

Birchenko, V. M., Muradov, K. M. and Davies, D. R. (2010) 'Reduction of the horizontal well's heel-toe effect with inflow control devices', *Journal of Petroleum Science and Engineering*. Elsevier B.V., 75(1–2), pp. 244–250.

Birchenko, V. M., Usnich, A. V. and Davies, D. R. (2010) 'Impact of frictional pressure losses along the completion on well performance', *Journal of Petroleum Science and*

Engineering. Elsevier B.V., 73(3–4), pp. 204–213.

Borisov, J. P. (1984) 'Oil Production Using Horizontal and Multiple Deviation Wells', *Translated into english by J. Strauss, edited by S. D. Joshi, Phillips Petroleum Co.*

Brekke, K. and Lien, S. C. (1994) 'New , Simple Completion Methods for', *SPE Drilling & Completion*, pp. 205–209.

Burda, B., Crompton, J., Sardoff, H. M., & Falconer, J. (2007) 'Information Architecture Strategy for the Digital Oil Field', *Digital Energy Conference and Exhibition*, Houston, Texas, U.S.A : Society of Petroleum Engineers.

Cheung, C. M., Goyal, P., Harris, G., Patri, O., Srivastava, A., Zhang, Y., … Prasanna, V. K. (2015) 'Rapid Data Integration and Analysis for Upstream Oil and Gas Applications', *SPE Annual Technical Conference and Exhibition.* Houston, Texas, U.S.A: Society of Petroleum Engineers.

Chierici, G. l. (1995) *Principles of Petroleum Engineering*. Vol 2. Berlin: Springer Verlag.

Cho, H. and Shah, S. N. (2002) 'Optimization of well length for horizontal drilling', *Journal of Canadian Petroleum Technology*, 41(5), pp. 54–62.

Corbett, P. (2012) *'Petroleum Geoscience'*, MSc. Petroleum Engineering Module, Heriot-Watt University.

Cullick A. S. and Sukkestad T. (2010). 'Smart Operations with Intelligent Well Systems. SPE 126246, SPE Intelligent Energy Conference and Exhibition', *Society of Petroleum Engineers.* Utrecht, The Netherlands, Society of Petroleum Engineers.

Daneshy, A. A., Guo, B., Krasnov, V., & Zimin, S. (2012) 'Inflow-Control-Device Design: Revisiting Objectives and Techniques', *SPE Production & Operations*, 27(1), pp. 44–51.

Davies, D. (2012) '*Production Technology'*, MSc. Petroleum Engineering Module, Heriot-Watt University.

Denney, D. (2012) 'Intelligent-Well-Monitoring Systems: Review and Comparison', *Journal of Petroleum Technology*, 64(09), pp. 27–29.

Dikken, B. J. (1990) 'Pressure drop in horizontal wells and its effect on production performance', *SPE Journal*, 42(11), pp. 1426–1433.

Dilib, F. A., Jackson, M. D., Mojaddam Zadeh, A., Aasheim, R., Årland, K., Gyllensten, A. J., & Erlandsen, S. M (2013) 'Closed-Loop Feedback Control for Production Optimization of Intelligent Wells Under Uncertainty', *SPE Production & Operations*, 28(4), pp. 345–357.

Dowlatabad, M. (2015) 'Novel Integrated Approach Simultaneously Optimising AFI Locations Plus Number and (A)ICD Sizes', *EUROPEC.* Madrid, Spain: Society of Petroleum Engineers.

El-khatib, N. A. F (2011) 'The Modification of the Dykstra-Parsons Method for Inclined Stratified Reservoirs', *SPE Middle East Oil and Gas Show and Conference.* Manama, Bahrain: Society of Petroleum Engineers.

Elgaghah, S. A., Osisanya, S. O. and Tiab, D. (1996) 'A Simple Productivity Equation for Horizontal Wells Based on Drainage Area Concept', *SPE Western Regional Meeting.* Anchorage, Alaska: Society of Petroleum Engineers.

Eltaher, E. (2017) *'Modelling and Applications of Autonomous Flow Control Devices'*, PhD Thesis, Heriot-Watt University.

Eltaher, E. M. K., Sefat, M. H., Muradov, K., & Davies, D. (2014) 'Performance of Autonomous Inflow Control Completion in Heavy Oil Introduction to Advanced Well Completions', *International Petroleum Technology Conference,* Kuala Lumpur, Malaysia: International Petroleum Technology Conference.

Faisal Al-Khelaiwi (2013) '*A Comprehensive Approach to the Design of Advanced Well Completions Faisal Turki Manee Al-Khelaiwi',* PhD Thesis, Heriot-Watt University.

Fu, X., Li, G., Huang, Z., & Chi, H. (2014) 'The Principle of Target Influx Selection and the Optimization Process of Variable-ICD Completion Design for Heterogeneous Reservoirs Reservoir model', *SPE Deepwater Drilling and Completions Conference*, Texas, U.S.A: Society of Petroleum Engineers.

Furui, K., Zhu, D. and Hill, A. D. (2005) 'A Comprehensive Skin-Factor Model of Horizontal-Well Completion Performance', *SPE Production & Operations*, 20(3), pp. 207–220.

Gao, C. H., Rajeswaran, R. T., & Nakagawa, E. Y. (2007) 'A Literature Review on Smart-Well Technology', *Production and Operations Symposium.* Oklahoma City, Oklahoma, U.S.A: Society of Petroleum Engineers.

Garcia, G. A., Coronado, M. P. and Gavioli, P. (2009) 'Identifying Well Completion Applications for Passive Inflow Control Devices', *SPE Annual Technical Conference and*

Exhibition, New Orleans, Louisiana, U.S.A: Society of Petroleum Engineers.

Gavioli, P., Vicario, R. and Hughes, B. (2012) 'The Evolution of the Role of Openhole Packers in Advanced Horizontal Completions : From Novel Technology to a Critical Key to Success', *SPE Asia Pacific Oil and Gas Conference and Exhibition*. Brisbane, Queensland, Australia: Society of Petroleum Engineers.

Giger, F. M. (1984) 'The Reservoir Engineering Aspects of Horizontal Drilling', SPE Annual Technical Conference and Exhibition, Houston, Texas, U.S.A: Society of Petroleum Engineers.

Grebenkin, I. and Davies, D. (2010) 'Analysis of the Impact of an Intelligent Well Completion on the Oil Production Uncertainty', *SPE Russian Oil and Gas Conference and Exhibition.* Moscow, Russia: Society of Petroleum Engineers.

Grebenkin, I. M. and Davies, D. R. (2012) 'A Novel Optimisation Algorithm for Inflow Control Valve Management', *SPE Europec/EAGE Annual Conference.* Copenhagen, Denmark: Society of Petroleum Engineers.

Grubert, M. A., Wan, J., Ghai, S. S., Livescu, S., Brown, W. B., & Long, T. A. (2009) 'Coupled Completion and Reservoir Simulation Technology for Well Performance Optimization', *SPE Annual Technical Conference and Exhibition*. New Orleans, Louisiana, U.S.A: Society of Petroleum Engineers.

Halliburton (2012), *NETool Reference Manual*. Halliburton

Halliburton (2017), *NETool List of publications*. Halliburton

Halvorsen, M., Elseth, G. and Nævdal, O. M. (2012) 'Increased oil production at Troll by autonomous inflow control with RCP valves', *SPE Annual Technical Conference and Exhibition*. San Antonio, Texas, U.S.A: Society of Petroleum Engineers.

Hasan, A. I., Echeverria-Ciaurri, D., Foss, B. A., & Kleppe, J. (2009) 'Discrete Optimization of Oil Production in Thin Oil Rim Reservoir under Geological Uncertainty', *SPE Asia Pacific Oil and Gas Conference & Exhibition*, Jakarta, Indonesia: Society of Petroleum Engineers.

He, Y., Cheng, S., Li, L., Mu, G., Zhang, T., Xu, H., (2017) 'Waterflood Direction and Front Characterization With Four-Step Work Flow: A Case Study in Changqing Oil Field, China', *SPE Reservoir Evaluation & Engineering*, 20(3), pp. 708–725.

Henriksen, K., Augustine, J. and Wood, E., "Integration of New Open Hole Zonal Isolation Technology Contributes to Improved Reserve Recovery and Revision in the ndustri Best Practices", *SPE International Improved Oil Recovery Conference in Asia Pacific*. Kuala Lumpur, Malaysia: Society of Petroleum Engineers.

Henriksen, K. H., Gule, E. I. and Augustine, J. R. (2006) 'Case Study: The Application of Inflow Control Devices in the Troll Oil Field', *SPE Europec/EAGE Annual Conference and Exhibition*. Vienna, Austria: Society of Petroleum Engineers.

Hill, A. and Zhu, D. (2008) 'The Relative Importance of Wellbore Pressure Drop and Formation Damage in Horizontal Wells', *SPE Production & Operations*, 23(2).

Hird, K., Setiawan, A., & Petler, J. S. (2011) 'Application of Real-Time Downhole Pressure Data for Assessing Initial-Gas- In-Place Uncertainty'. *SPE Asia Pacific Oil and Gas Conference and Exhibition*. Jakarta, Indonesia: Society of Petroleum Engineers.

Holanda, R. W. de, Gildin, E., & Jensen, J. L. (2015) 'Improved Waterflood Analysis Using the Capacitance-Resistance Model', *SPE Latin American and Carribbean Petroleum Engineering Conference*. Quito, Ecuador: Society of Petroleum Engineers.

Holmes, J., Barkve, T. and Lund, O. (1998) 'Application of a multisegment well model to simulate flow in advanced wells', *European Petroleum Conference*. The Hague, Netherlands: Society of Petroleum Engineers.

Izgec, O. (2012) 'Understanding waterflood performance with modern analytical techniques', *Journal of Petroleum Science and Engineering*. Elsevier B.V., 81, pp. 100–111.

Izgec, O., & Kabir, C. S. (2010) 'Quantifying Nonuniform Aquifer Strength at Individual Wells', *Direct*, (August 2008), pp. 296–305.

Izgec, O., & Kabir, C. S. (2010) 'Understanding reservoir connectivity in waterfloods before breakthrough', *Journal of Petroleum Science and Engineering*. Elsevier B.V., 75(1–2), pp. 1–12.

Jackson, M. D. and Addiego-Guevara, E. A. (2008) 'Insurance Value of Intelligent Well Technology Against Reservoir Uncertainty', *SPE Symposium on Improved Oil Recovery*. Tulsa, Oklahoma, U.S.A: Society of Petroleum Engineers.

Jafroodi, N. and Zhang, D. (2011) 'New method for reservoir characterization and optimization using CRM-EnOpt approach', *Journal of Petroleum Science and Engineering*. Elsevier B.V., 77(2), pp. 155–171.

Jahangiri, H. R., Adler, C., Shirzadi, S., Bailey, R., Ziegel, E., Chesher, J., & White, M. (2014) 'A Data-Driven Approach Enhances Conventional Reservoir Surveillance Methods for Waterflood Performance Management in the North Sea', *SPE Intelligent Energy Conference & Exhibition.* Utrecht, The Netherlands: Society of Petroleum Engineers.

Jensen, J. and Currie, I. (1990) 'A new method for estimating the Dykstra-Parsons coefficient to characterize reservoir heterogeneity', *SPE Reservoir Engineering*, (August), pp. 369–374.

Jensen, J. L. (2000) '*Statistics for petroleum engineers and geoscientists*. Elsevier.

Johnson, C. E. (1956) 'Prediction of Oil Recovery by Waterflood - A Simplified Graphical Treatment of the Dykstra-Parsons Method', *Journal of Petroleum Technology*, 8(11), pp. 55–56.

Joshi, S. D. (1988) 'Augmentation of Well Productivity With Slant and Horizontal Wells (includes associated papers 24547 and 25308)', *Journal of Petroleum Technology*, 40(6), pp. 729–739.

Joshi, S. D. (1991) '*Horizontal Well Technology*'. PennWell Corporation.

Junior, M. F. S., Muradov, K. M. and Davies, D. R. (2012) 'SPE 150195 Review , Analysis and Comparison of Intelligent Well Monitoring Systems', *SPE Intelligent Energy International*, (March), pp. 27–29.

Kabir, C. S., Haftbaradaran, R., Asghari, R., & Sastre, J. P. (2015) 'Understanding Variable Well Performance in a Chalk Reservoir', (September), pp. 8–11.

Kansao, R., Yrigoyen, A., Haris, Z., & Saputelli, L. (2017) 'Waterflood Performance Diagnosis and Optimization Using Data-Driven Predictive Analytical Techniques from Capacitance Resistance Models CRM'. *EUROPEC*. Paris, France: Society of Petroleum Engineers.

Karim, R. A., Goh, K. F. G., Nuriyadi, M. A., Ahmad, N. A., Leung, E., & Murison, J. A. (2010) 'Horizontal Well Optimization With Inflow Control Devices (ICDs) Application in Heterogeneous and Dipping Gas-Capped Oil Reservoirs', *SPE Annual Technical Conference and Exhibition*. Florence, Italy: Society of Petroleum Engineers.

Kim, J. S., Lake, L. W. and Edgar, T. F. (2012) 'Integrated capacitance-resistance model for characterizing waterflooded reservoirs', *IFAC Proceedings Volumes (IFAC-PapersOnline)*, 1(PART 1), pp. 19–24.

Lake, L. W. and Jensen, J. L. (1989) ‘A Review of Heterogeneity Measures Used in Reservoir Characterization’.

Least, B., Bonner, A. J., Regulacion, R. E., Penaranda, R., Sampedro, T. F., & Coloma, F. (2013). ‘Autonomous ICD Installation Success in Ecuador Heavy Oil: A Case Study‘, *SPE Annual Technical Conference and Exhibition*. New Orleans, Louisiana, USA: Society of Petroleum Engineers.

Lerlertpakdee, P., Jafarpour, B. and California, S. (2014) ‘Efficient Production Optimization With Flow-Network Models’, *SPE Journal*, (2006), pp. 1–13.

Levitan, M. M., Clay, P. L. and Gilchrist, J. M. (2001) ‘How Good Are Your Horizontal Wells ?’. *SPE European Formation Damage Conference.* Hague, Netherlands: Society of Petroleum Engineers.

Liang, X., Lake, L. W., Edgar, T. F., Al-Yousef, A., Sayarpour, M., & Weber, D. (2007) ‘Optimization Of Oil Production Based On A Capacitance Model Of Production And Injection Rates’, *SPE Hydrocarbon Economics and Evaluation Symposium*. Dallas, Texas, U.S.A: Society of Petroleum Engineers.

Lim, M. (2017) ‘ICDs for Uncertainty and Heterogeneity Mitigation: Evaluation of Best Practice Design Strategies for Inflow Control Devices’, *SPE/IATMI Asia Pacific Oil & Gas Conference and Exhibition*. Jakarta, Indonesia: Society of Petroleum Engineers.

Livescu, S., Brown, W. P., Jain, R., Grubert, M., Ghai, S. S., Lee, L.-B. W., & Long, T. (2010) ‘Application of a coupled wellbore/reservoir simulator to well performance optimization’, *SPE Annual Technical Conference and Exhibition*. Florence, Italy: Society of Petroleum Engineers.

Mamghaderi, A., Bastami, A. and Pourafshary, P. (2012) ‘Optimization of Waterflooding Performance in a Layered Reservoir Using a Combination of Capacitance-Resistive Model and Genetic Algorithm Method’, *Journal of Energy Resources Technology*, 135(1), p. 13102.

Mamghaderi, A. and Pourafshary, P. (2013) ‘Water flooding performance prediction in layered reservoirs using improved capacitance-resistive model’, *Journal of Petroleum Science and Engineering*. Elsevier, 108, pp. 107–117.

Mathiesen, V., Werswick, B. and Aakre, H. (2014) ‘The Next Generation Inflow Control, the Next Step to Increase Oil Recovery on the Norwegian Continental Shelf’, *SPE Bergen One Day Seminar*. Bergen, Norway: Society of Petroleum Engineers.

Moradidowlatabad, M., Muradov, K. and Davies, D. (2014) 'Novel Workflow to Optimise Annular Flow Isolation in Advanced Wells AFI Design and Annulus Pressure', *SPE Offshore Europe Conference and Exhibition.* Aberdeen, Scotland, UK: Society of Petroleum Engineers.

Moreno, G. A. and Garriz, A. E. (2014) 'Injection Leakage Detection in Mature Fields Using Data-Driven Models', *SPE Latin America and Caribbean Petroleum Engineering Conference.* Maracaibo, Venezuela: Society of Petroleum Engineers.

Muradov, K. M. and Davies, D. R. (2013) 'Prediction of Temperature Distribution in Intelligent Wells', *SPE Russian Oil and Gas Technical Conference and Exhibition.* Moscow, Russia: Society of Petroleum Engineers.

Newswire, P. (2009) *Tejas Completion Solutions Acquires the ICD Business of Ziebel AS*. Available at: https://www.prnewswire.com/news-releases/tejas-completion-solutions-acquires-the-icd-business-of-ziebel-as-62118337.html (Accessed: 20 November 2017).

Nguyen, A. P., Lasdon, L., Lake, L. W., & Edgar, T. F. (2011) 'Capacitance Resistive Model Application to Optimize Waterflood in a West Texas Field', *SPE Annual Technical Conference and Exhibition*. Denver, Colorado, U.S.A: Society of Petroleum Engineers.

Penmatcha, V., Arbabi, S. and Aziz, K. (1999) 'Effects of Pressure Drop in Horizontal Wells and Optimum Well Length', *SPE Journal*, 4(3), pp. 215–223.

Pinto, M. A. S., Barreto, C. E., & Schiozer, D. J. (2012). 'Optimization of Proactive Control Valves of Producer and Injector Smart Wells under Economic Uncertainty', *SPE Europec/EAGE Annual Conference*, Copenhagen, Denmark: Society of Petroleum Engineers.

Potiani, M., Eduardo, M. and Hughes, B. (2014) 'A Review of IC Installations: Lessons Learned from Electric-Hydraulic, Hydraulic and All-Electric Systems', *Offshore Technology Conference.* Houston, Texas, U.S.A: Society of Petroleum Engineers.

Prakasa, B., Shi, X., Muradov, K., & Davies, D. (2017) 'Novel Application of Capacitance-Resistance Model for Reservoir Characterisation and Zonal, Intelligent Well Control', *SPE/IATMI Asia Pacific Oil & Gas Conference and Exhibition*. Jakarta, Indonesia: Society of Petroleum Engineers.

Prakasa, B., Muradov, K. and Davies, D. (2015) 'Rapid design of an inflow control device completion in heterogeneous clastic reservoirs using type curves', *SPE Offshore Europe Conference and Exhibition*. Aberdeen, Scotland, UK: Society of Petroleum Engineers.

Renard, G., Frangais, I. and Dupuy, J. M. (1991) 'Formation Damage Effects on Horizontal Well Flow Efficiency', *SPE*, 2(19414).

Robinson, M. (2003) 'Intelligent Well Completions', *SPE Journal of Petroleum Technology*, 55(8), pp. 57–59.

Sayarpour, M., Kabir, C. S., & Lake, L. W. (2009) 'The use of capacitance-resistance models for rapid estimation of waterflood performance and optimization', *Journal of Petroleum Science and Engineering*. Elsevier B.V., 69(3–4), pp. 227–238.

Sayarpour, M., Kabir, C. S. and Lake, L. (2009) 'Field Applications of Capacitance-Resistance Models in Waterfloods', *SPE Reservoir Evaluation & Engineering*, 12(6), pp. 21–24.

Schlumberger (2014) *ECLIPSE Reference Manual*. Schlumberger.

Haghighat Sefat, M., Muradov, K. M., Elsheikh, A. H. & Davies, D. R. (2015) 'Proactive Optimisation of Intelligent Well Production Using Stochastic Gradient-Based Algorithms, *SPE Reservoir Evaluation & Engineering*, 24(9), pp. 239–252.

Haghighat, M., Prakasa, B., Khalid, E., Davies, D. Guidelines for Flow Control Completion Modelling and Design, Inflow Control Technology Forum, Houston 2015.

Sefat, M. H. (2016) *'Proactive Optimisation of Intelligent Wells under Uncertainty'*, (October). PhD Thesis, Heriot-Watt University.

Seines, K., Aavatsmark, I., Lien, S. C., & Rushworth, P. (1993) 'Considering Wellbore Friction in Planning Horizontal Wells', *Journal of Petroleum Technology*, 45(10), pp. 994–1000.

Shi, H., Zhou, H., Hu, Y., He, Y., Fu, R., & Ren, B. (2016) 'A New Method to Design and Optimize the ICD for Horizontal Wells'. *Offshore Technology Conference*. Houston, Texas, U.S.A: Offshore Technology Conference.

Skarsholt, L. T., Mitchell, A. F., & Bjørnsgaard, A. H. (2005) 'Use of Advanced Completion Solutions to Maximise Reservoir Potential – Experiences in The Snorre Field', *SPE/IADC Drilling Conference,* Amsterdam Netherlands: Society of Petroleum Engineers.

Stone, T. W., Moen, T., Edwards, D. A., Shadchnev, A., Rashid, K., Kvilaas, G. F., & Christoffersen, K. (2015) 'Optimized Design of Autonomous Inflow Control Devices for Gas and Water Coning', *SPE Reservoir Simulation Symposium*. Houston, Texas, U.S.A: Society of Petroleum Engineers.

Todd, A. (2012) '*Reservoir Engineering*'. MSc. Petroleum Engineering Module, Heriot-Watt University.

Twerda, A., Nennie, E. D., Alberts, G., Leemhuis, A. P., & Widdershoven, C. (2011). 'To ICD or not to ICD? A techno-economic analysis of different control strategies applied to a thin oil rim field case', *SPE Middle East Oil and Gas Show and Conference*. Manama, Bahrain: Society of Petroleum Engineers.

U.S Energy Information Administration (2016) *Oil Wells Drilled Horizontally Are Among the Highest-Producing Wells*, *The Energy Collective*. Available at: http://www.theenergycollective.com/todayinenergy (Accessed: 8 November 2017).

Van Den Berg, F. G., Perrons, R. K., Moore, I., & Schut, G. (2010) 'Business Value From Intelligent Fields', *SPE Intelligent Energy Conference and Exhibition*. Utrecht, The Netherlands: Society of Petroleum Engineers.

Van Essen, G., Zandvliet, M., Van Den Hof, P., Bosgra, O. & Jansen, J.-D. 2013. Robust Waterflooding Optimization of Multiple Geological Scenarios. *SPE Journal,* 14, 202-210.

Vela, I., Viloria-gomez, L. A., Caicedo, R., & Porturas, F. (2011) 'Well Production Enhancement Results with Inflow Control Device (ICD) Completions in Horizontal Wells in Ecuador', *SPE EUROPEC/EAGE Annual Conference and Exhibition*. Vienna, Austria: Society of Petroleum Engineers.

Wan, J., Dale, B. A., Ellison, T. K., Benish, T. G., & Grubert, M. (2008) 'Coupled Well and Reservoir Simulation Models to Optimize Completion Design and Operations for Subsurface Control', EUROPEC. Rome, Italy: Society of Petroleum Engineers.

Williams, G. J. J., Mansfield, M., MacDonald, D. G., & Bush, M. D. (2004) 'Top-Down Reservoir Modelling', *SPE Annual Technical Conference and Exhibition*. Houston, Texas: Society of Petroleum Engineers.

Williamson, J. R., Bouldin, B., & Purkis, D. (2000) 'The Development of an Infinitely Variable Choke for Intelligent Well Completions', *Offshore Technology Conference.* Houston, Texas: Offshore Technology Conference.

Yeten, B., Castellini, A., Guyaguler, B., & Chen, W. H. (2005). 'A Comparison Study on Experimental Design and Response Surface Methodologies', *SPE Reservoir Simulation Symposium*. Texas, U.S.A: Society of Petroleum Engineers.

Yousef, A. A., Lake, L. W. and Jensen, J. L. (2006) 'A Capacitance Model To Infer Interwell Connectivity From Production and Injection Rate Fluctuations', *SPE Annual Technical Conference and Exhibition*. Dallas, Texas: Society of Petroleum Engineers.

Zadeh, A., Slotte, P. A., Gyllensten, A. J., Aasheim, R., & Årland, K. (2012) 'Optimal Inflow Control Devices Configurations for Oil Rim Reservoirs', *Offshore Technology Conference*. Houston, Texas, U.S.A: Offshore Technology Conference.

Zhang, Z., Li, H. and Zhang, D. (2015) 'Water flooding performance prediction by multi-layer capacitance-resistive models combined with the ensemble Kalman filter', *Journal of Petroleum Science and Engineering*. Elsevier, 127, pp. 1–19.

Appendix A

Derivation to express ICD strength (a) as a function of the total drawdown (∆Pw) for ICD completions in wellbores with dominating Heel-Toe Effect

The ICD number for a pressure constrained well is:

$$I_p = \frac{C_f \rho f B^2 j^2 L^3 \Delta P_{ann}^{heel}}{\left(2aj^2 \Delta P_{ann}^{heel} + 1\right) D^5} \tag{A-1}$$

This equation can also be instead written in a form of ICD strength (a) as a function of the annulus drawdown in the heel (ΔP_{ann}^{heel}):

$$(2aj^2 \Delta P_{ann}^{heel} + 1) = \frac{C_f \rho f B^2 j^2 L^3 \Delta P_{ann}^{heel}}{Ip\ D^5} \tag{A-2}$$

$$2j^2 \Delta P_{ann}^{heel} a = \frac{C_f \rho f B^2 j^2 L^3 \Delta P_{ann}^{heel}}{Ip\ D^5} - 1 \tag{A-3}$$

$$a = \frac{1}{I_p} \frac{C_f \rho f B^2 j^2 L^3 \Delta P_{ann}^{heel}}{2j^2 \Delta P_{ann}^{heel} D^5} - \frac{1}{2j^2 \Delta P_{ann}^{heel}} \tag{A-4}$$

Or

$$a + \frac{1}{\Delta P_{ann}^{heel}} \frac{1}{2j^2} = \frac{1}{I_p} \frac{C_f \rho f B^2 L^3}{2D^5} \tag{A-5}$$

ΔP_{ann}^{heel} can be described by the quadratic equation by (Birchenko, 2010):

$$\Delta P_{ann}^{heel} = \Delta P_w - \left(\frac{\left(\sqrt{1 + 4aj^2 \Delta P_w} - 1 \right)^2}{4aj^2} \right) \tag{A-6}$$

Hence A-6 can be expressed as:

$$a + \frac{1}{\Delta P_w - \left(\frac{\left(\sqrt{1 + 4aj^2 \Delta P_w} - 1 \right)^2}{4aj^2} \right)} \frac{1}{2j^2} = \frac{C_f \rho f B^2 L^3}{2 I_p D^5} \tag{A-7}$$

This equation can be simplified into:

$$\frac{2a\sqrt{1+4aj^2\Delta P_w}}{\left(\sqrt{1+4aj^2\Delta P_w}-1\right)} = \frac{C_f \rho f B^2 L^3}{I_p D^5} \quad \text{(A-8)}$$

The right-hand side term is now for simplicity named β, with equation A-8 reduced to:

$$\left(2a\sqrt{1+4aj^2\Delta P_w} - \beta\sqrt{1+4aj^2\Delta P_w}\right) = -\beta \quad \text{(A-9)}$$

The quadratic form of equation A-9 is:

$$(1+4aj^2\Delta P_w)(4a^2 - 4a\beta + \alpha^2) = \beta^2 \quad \text{(A-10)}$$

By simplifying A-10, the solution for *a* can be expressed as a cubic equation:

$$(16j^2\Delta P_w)a^3 + (4 - 16j^2\Delta P_w\beta)a^2 + (4j^2\Delta P_w\beta^2 - 4\beta)a = 0 \quad \text{(A-11)}$$

Finally, the physical solution of A-11, applicable to our problem, is:

$$a = \frac{\left(4j^2\Delta P_w\beta - \sqrt{8j^2\Delta P_w\beta+1}\right)-1}{8j^2\Delta P_w} \quad \text{(A-12)}$$

Where $\beta = \frac{C_f \rho f B^2 L^3}{I_p D^5}$

Appendix B

Derivation to express ICD strength (a) as a function of the total drawdown (ΔPw) and the well's production rate (Qw) for ICD completion in wellbores with a strong inflow variation due for flow from a heterogeneous reservoir

The Inflow Equalisation (IE) is defined as:

$$IE = \frac{IV_{ICD}}{IV_{OH}} = \frac{\frac{(U_m - U_1)}{U_m}}{\frac{(J_m - J_1)}{J_m}} \quad \text{(B-1)}$$

Equation B-1 can be expressed as:

$$U_1 = \left[1 - \left(\left(IE - IE\ \frac{J_1}{J_m}\right)\right)\right] U_m \quad \text{(B-2)}$$

Following Birchenko, 2010, U_1 and U_m can be replaced by a solution of a quadratic equation for specific inflow rate.

$$\frac{-1+\sqrt{1+4\Delta P a J_1^2}}{2aJ1} = \left[1 - \left(\left(IE - IE\ \frac{J_1}{J_m}\right)\right)\right] \frac{-1+\sqrt{1+4\Delta P a J_m^2}}{2aJm} \quad \text{(B-3)}$$

Equation B-3 can be simplified to:

$$\sqrt{1 + 4\Delta P a J_1^2} = \left(-\Omega + \Omega\sqrt{1 + 4\Delta P a J_m^2}\right) + 1 \quad \text{(B-4)}$$

Where:

$$\Omega = \frac{J1}{Jm}(1 - IV_{ICD}) \quad \text{(B-5)}$$

The left and right hand sides of the equation B-4 are then squared and rearranged to yield:

$$\left(\sqrt{1 + 4\Delta P_w a J_m^2}\right) = \left(1 - \frac{\left(4\Delta P_w J_1^2 - \Omega^2 4\Delta P_w J_m^2\right)}{2\Omega(\Omega - 1)} a\right) \quad \text{(B-6)}$$

The left and right hand side terms of this equation are squared again and simplified as:

$$\left(\frac{\left(2\Delta P_w J_1^2-\Omega^2 2\Delta P_w J_{\bar{m}}^2\right)}{\Omega(\Omega-1)}\right)^2 a=\frac{-\left(4\Delta P_w J_1^2-4\Delta P_w \Omega^2 J_{\bar{m}}^2\right)}{\Omega(\Omega-1)}-4\Delta P_w\left(J_{\bar{m}}^2\right) \tag{B-7}$$

Finally, the solution for strength for a pressure constrained well is:

$$a=\frac{\left(\frac{\left(\Omega J_{\bar{m}}^2-J_1^2\right)}{(\Omega-1)}-J_{\bar{m}}^2\right)}{\left(\frac{\left(J_1^2-\Omega^2 J_{\bar{m}}^2\right)}{\Omega(\Omega-1)}\right)^2 \Delta P_w} \tag{B-8}$$

And since $\Delta P=\frac{q_w}{<J>L}\frac{1}{\left(1-E_p\right)}$, the solution can be translated to the case of a rate constrained well as:

$$a=\frac{\left(\frac{\Omega J_{\bar{m}}^2-J_1^2}{(\Omega-1)}-J_{\bar{m}}^2\right)<J>L\left(1-E_p\right)}{\left(\frac{\left(J_1^2-\Omega^2 J_{\bar{m}}^2\right)}{\Omega(\Omega-1)}\right)^2 q_w} \tag{B-9}$$

Inverting equations B-8 and B-9 further allows calculating Ep as a function of ICD strength (a) for a given IV_{OH}.

Appendix C

CRM Solution incorporating the non-linear pressure drop from flow control devices

The CRM equation was developed based on the following reservoir flow assumptions (Sayarpour, 2009):

- Constant temperature (isothermal)
- Instantaneous equilibrium
- Two immiscible phases
- Negligible capillary pressure effect
- Small fluid compressibility
- Darcy's law applies
- Constant productivity index

Material balance of a given system:

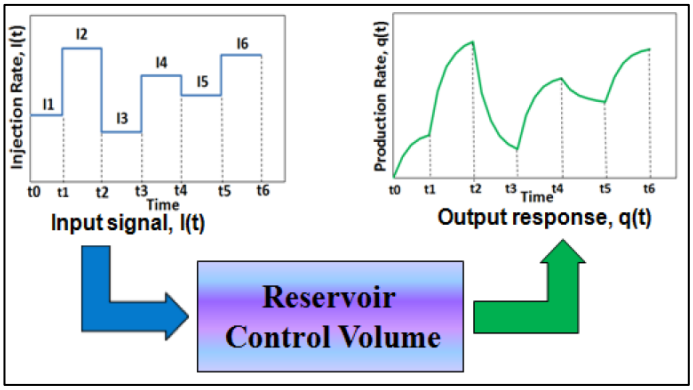

Figure C-1. Schematic representation of the impact of an injection rate signal on total production response for an arbitrary reservoir control volume in CRM (Kim, Lake and Edgar, 2012)

$$C_t V_p \frac{d\bar{P}}{dt} = i(t) - q(t) \qquad \text{(C-1)}$$

Meanwhile the pressure drops from an intelligent well completion or advance well completion (AWC) is governed by quadratic equation:

$$\bar{P} = aq^2 + \frac{q}{J} + P_{wf} \qquad \text{(C-2)}$$

We can couple the equation C-3 with C-1 and describe the material balance of an AWC system as:

$$C_t V_p \frac{d\left(aq^2+\frac{q}{J}+P_{wf}\right)}{dt} = i(t) - q(t) \quad \text{(C-3)}$$

Or

$$\frac{C_t V_p}{J}\frac{dq}{dt} + C_t V_p \frac{dP_{wf}}{dt} = i(t) - q(t) - aC_t V_p \frac{dq^2}{dt} \quad \text{(C-4)}$$

Where time-storage (τ) is defined as:

$$\tau = \frac{C_t V_p}{J} \quad \text{(C-5)}$$

Equation C-5 can be simplified as:

$$\frac{dq}{dt} + \frac{1}{\tau}q(t) = \frac{1}{\tau}i(t) - \mathrm{J}\frac{dP_{wf}}{dt} - \mathrm{J}a\frac{dq^2}{dt} \quad \text{(C-6)}$$

The right side of equation C-7 can be represented as the auxiliary parameter:

$$g(t) = \frac{1}{\tau}i(t) - \mathrm{J}\frac{dP_{wf}}{dt} - \mathrm{J}a\frac{dq^2}{dt} \quad \text{(C-7)}$$

Substituting equation C-7 into C-6 gives:

$$\frac{dq}{dt} + \frac{1}{\tau}q(t) = g(t) \quad \text{(C-8)}$$

Multiplying both side of C-8 with $e^{\frac{t}{\tau}}$ gives:

$$e^{\frac{t}{\tau}}\left[\frac{dq}{dt} + \frac{1}{\tau}q(t)\right] = e^{\frac{t}{\tau}}g(t) \quad \text{(C-9)}$$

Or:

$$\frac{d\left[e^{\frac{t}{\tau}}q\right]}{dt} = e^{\frac{t}{\tau}}g(t) \quad \text{(C-10)}$$

Integrate equation C-10 with respect to t:

$$e^{\frac{t}{\tau}}q = c + \int e^{\frac{t}{\tau}}g(t)dt \quad \text{(C-11)}$$

$$\int_{t_0}^{t} e^{\frac{t}{\tau}} q = \int_{t_0}^{t} e^{\frac{t}{\tau}} g(t)dt \tag{C-12}$$

$$e^{\frac{t}{\tau}} q = e^{\frac{t_0}{\tau}} q_o + \int_{t_0}^{t} e^{\frac{t}{\tau}} g(t)dt \tag{C-13}$$

The constant of the integration is evaluated by applying initial condition at time t_0,

$$q = q_o e^{-\left(\frac{t-t_0}{\tau}\right)} + e^{\frac{-t}{\tau}} \int_{t_0}^{t} e^{\frac{t}{\tau}} \left[\frac{1}{\tau} i(t) - \mathrm{J}\frac{dP_{wf}}{dt} - \mathrm{J}a\frac{dq^2}{dt}\right] dt \tag{C-14}$$

Writing equation C-14 in full:

$$q = q_o e^{-\left(\frac{t-t_0}{\tau}\right)} + e^{\frac{-t}{\tau}} \int_{\xi=t_0}^{\xi=t} e^{\frac{\xi}{\tau}} \frac{1}{\tau} i(\xi)d\xi - e^{\frac{-t}{\tau}} \int_{\xi=t_0}^{\xi=t} e^{\frac{\xi}{\tau}} \mathrm{J}\frac{dP_{wf}}{d\xi} d\xi - e^{\frac{-t}{\tau}} \int_{\xi=t_0}^{\xi=t} e^{\frac{\xi}{\tau}} \mathrm{J}a\frac{dq^2}{d\xi} d\xi$$

Where $t > t_0$ (C-15)

The output signal, $q(t)$, is composed of four elements on the right of Eq. C-15. Changes in rate at the producer are comprised of primary depletion, the injection input signal, the changing of the BHP at the producer, and the non-linear pressure drops of the flow control device. Note that apart of the fourth part of the right-hand side of the equation C-15, equation C-16 is identical with the solution proposed by Sayarpour, 2009.

We integrate the right-hand side of the equation C-15

2nd part of right-hand side of the equation C-15:

$$e^{\frac{-t}{\tau}} \int_{\xi=t_0}^{\xi=t} e^{\frac{\xi}{\tau}} \frac{1}{\tau} i(\xi)d\xi \tag{C-16}$$

Integrating by parts,

$$e^{\frac{-t}{\tau}} \left[e^{\frac{\xi}{\tau}} i(\xi)\right]_{\xi=t_0}^{\xi=t} \tag{C-17}$$

$$i(t) - e^{-\left(\frac{t-t_0}{\tau}\right)} i(t_0) \tag{C-18}$$

The most common approach to derive CRM is by assuming a liner variation of BHP, and a stepwise change in injection rate (SVIR), (see fig. C-3 and C-4). There are two time-step indices in this approach, k is the time-step index attached Δt, while n is time-step index is attached to q. This approach would allow us to simplify the equation C-

15 as:

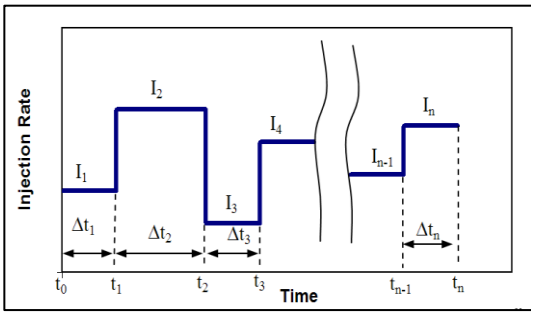

Figure C-2. Stepwise change of injection rate schedule from time t_0 to t_n (Sayarpour et al., 2009).

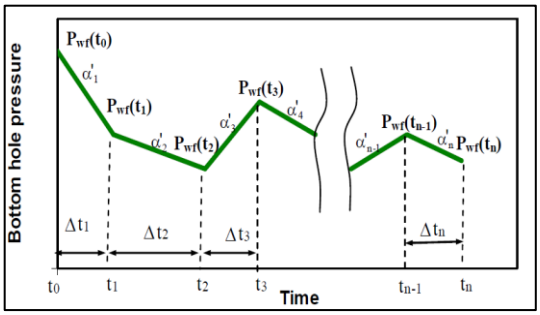

Figure C-3. Piecewise linear producer bottom hole pressure change schedule from time t_0 to t_n (Sayarpour et al., 2009)

$$\left(1 - e^{-\left(\frac{\Delta t_k}{\tau}\right)}\right) i(\Delta t_k) \tag{C-19}$$

3rd part of right-hand side of the equation C-15:

$$e^{\frac{-t}{\tau}} \int_{\xi=t_0}^{\xi=t} e^{\frac{\xi}{\tau}} \mathrm{J} \frac{dP_{wf}}{d\xi} d\xi \tag{C-20}$$

$$e^{\frac{-t}{\tau}} \mathrm{J}\, \tau \int_{\xi=t_0}^{\xi=t} e^{\frac{\xi}{\tau}} \frac{1}{\tau} \frac{\Delta P_{wf}}{\Delta \xi} d\xi \tag{C-21}$$

Yousef (2006) reported that the time constants between producer pairs (τ_{kj}) are very large. The integration of equation C-21 will yields to:

$$e^{\frac{-t}{\tau}} \mathrm{J}\, \tau \left[e^{\frac{\xi}{\tau}} \frac{\Delta P_{wf}}{\Delta \xi} \right]_{\xi=t_0}^{\xi=t} \tag{C-22}$$

$$\mathrm{J}\, \tau \frac{\Delta P_{wf}}{\Delta t} - e^{-\left(\frac{t-t_0}{\tau}\right)} \tau \frac{\Delta P_{wf}}{\Delta t} \tag{C-23}$$

And follows the assumption of SVIR as described above.

$$\left(1 - e^{-\left(\frac{\Delta t_k}{\tau}\right)}\right) \mathrm{J}\, \tau \frac{\Delta P_{wf_{\Delta t_k}}}{\Delta t_k} \tag{C-24}$$

4th part of right-hand side of the equation C-15:

$$e^{\frac{-t}{\tau}} \int_{\xi=t_0}^{\xi=t} e^{\frac{\xi}{\tau}} \, \mathrm{Ja} \frac{dq^2}{d\xi} d\xi \tag{C-25}$$

$$e^{\frac{-t}{\tau}} Ja2q \int_{\xi=t_0}^{\xi=t} e^{\frac{\xi}{\tau}} \frac{dq}{d\xi} d\xi \tag{C-26}$$

$$e^{\frac{-t}{\tau}} Ja2\tau \int_{\xi=t_0}^{\xi=t} e^{\frac{\xi}{\tau}} \frac{1}{\tau} \, q \frac{dq}{d\xi} d\xi \tag{C-27}$$

$$Ja2\tau e^{\frac{-t}{\tau}} \left[e^{\frac{\xi}{\tau}} q \frac{\Delta q}{\Delta t} \right]_{\xi=t_0}^{\xi=t} \tag{C-28}$$

$$Ja2\tau \, q \frac{\Delta q}{\Delta t} - e^{-\left(\frac{t-t_0}{\tau}\right)} Ja2\tau \, q \frac{\Delta q}{\Delta t} \tag{C-29}$$

And follows the assumption of SVIR as described above.

$$\left(1 - e^{-\left(\frac{\Delta t_k}{\tau}\right)}\right) Ja2\tau \, q_n \frac{\Delta q_k}{\Delta t_k} \tag{C-30}$$

or

$$\left(1 - e^{-\left(\frac{\Delta t_k}{\tau}\right)}\right) Ja2\tau q_n \frac{(q_n - q_{(n-1)})}{\Delta t_k} \tag{C-31}$$

The superposition principle allows replacing the effect of primary depletion (the first part of the equation C-16) with $q(t_{n-1})$ from the previous time interval's solution followed by repeating this process for all time intervals from t_0 to t_n. Sayarpour, 2009 provides a full explanation of superposition procedure. This allows the predicted rate at time n or the end of time interval Δt_k to be reduced by writing equation C-15 as:

$$q_n = q_{(n-1)} e^{-\left(\frac{\Delta t_k}{\tau}\right)} + \left(1 - e^{-\left(\frac{\Delta t_k}{\tau}\right)}\right) \left[i(\Delta t_k) - \mathrm{J}\,\tau \frac{\Delta P_{wf\,\Delta t_k}}{\Delta t_k} \right] - \left(1 - e^{-\left(\frac{\Delta t_k}{\tau}\right)}\right) Ja2\tau q_n \frac{\left(q_n - q_{(n-1)}\right)}{\Delta t_k} \tag{C-32}$$

Formulating equation C-32 as quadratic equation:

$$\left[\left(1 - e^{-\left(\frac{\Delta t_k}{\tau}\right)}\right) \frac{Ja2\tau}{\Delta t_k}\right] \boldsymbol{q_n^2} + \left[1 - \left(1 - e^{-\left(\frac{\Delta t_k}{\tau}\right)}\right) \frac{Ja2\tau q_{(n-1)}}{\Delta t_k}\right] \boldsymbol{q_n} - q_{k-1} e^{-\left(\frac{\Delta t_k}{\tau}\right)} - \left(1 - e^{-\left(\frac{\Delta t_k}{\tau}\right)}\right) \left[i(t_k) - J\,\tau \frac{\Delta P_{wf} \Delta t_k}{\Delta t_k} \right] = 0 \tag{C-33}$$

This will allow us to describe equation C-34 as: $[a]q_n^2 + [b]q_n + [c] = 0$, which can be solved for q_n as:

$$q_n = \frac{-b \pm \sqrt{b^2 - 4ac}}{2a}$$

Finally, the solution of C-34, i.e. general solution of CRM-AWC, is:

$$q_n = \frac{\left[\left(1-e^{-\left(\frac{\Delta t_k}{\tau}\right)}\right)\frac{Ja2\tau q_{n-1}}{\Delta t_k}-1\right]+\sqrt{\left\{\left[1-\left(1-e^{-\left(\frac{\Delta t_k}{\tau}\right)}\right)\frac{Ja2\tau q_{n-1}}{\Delta t_k}\right]^2\right\}+\left\{4q_{k-1}e^{-\left(\frac{\Delta t_k}{\tau}\right)}\left[\left(1-e^{-\left(\frac{\Delta t_k}{\tau}\right)}\right)\frac{Ja2\tau}{\Delta t_k}\right]\right\}-\left\{\left(1-e^{-\left(\frac{\Delta t_k}{\tau}\right)}\right)\left(i(t_k)-J\tau\frac{\Delta P_{wf}{}_{\Delta t_k}}{\Delta t_k}\right)\right\}}}{4\frac{Ja\tau}{\Delta t_k}\left(1-e^{-\left(\frac{\Delta t_k}{\tau}\right)}\right)}$$

(C-34)